Corso di Dottorato di Ricerca Ingegneria Industriale
Università Politecnica delle Marche

The Synthesis and Study of TiO_2/Aluminosilicate Composites as Components of Building Finishing Materials for Improvement of the Indoor Air Quality

Curriculum in Ingegneria di Materiale

Author:

Eng. Vladimir Bondarenko

Tutor:

Doctor Maria Letizia Ruello

Supervisor:

Professor Fabio Pollonara

Date: 15-07-2017

XXV cicles

Contents

Introduction …… **6**
Actuality……..……...…... **6**
The Goals and Objectives of the study…… **6**
Structure of the thesis…….…….. **7**
1. Literature review…….. **9**
1.1 Passive Degradation for Indoor Air Quality and new role of building materials.. **9**
1.2 Working principles of heterogeneous photocatalysis……... **13**
1.3 Photocatalytic materials. Titanium dioxide……..….. **15**
1.3.1 Impact of phase composition of TiO_2…… **16**
1.3.2 The Effect of particle size on the photocatalytic activity…….….. **16**
1.3.3 The impact of surface composition on the properties of TiO_2……. **17**
1.4 The synthesis of TiO_2 and TiO_2-containing material…….….. **18**
1.4.1 Preparation Methods of Powdered TiO_2 ……... **18**
1.4.2 The Preparation of Films……...…. **19**
1.4.3 Modified photocatalyst and Composite photocatalysts……. **20**
1.4.4 Clays as carriers of TiO_2…… **22**
1.4.5 The using of Fly Ash as TiO_2 carrier for possible waste utilization …… **24**
1.4.6 Nonmetal co-doping as a way of surface sensitization for visible light strategies. **25**
1.5 The modern applications of TiO_2-containing materials……. **28**
2. Characterization of materials and definition of methods…….. **32**
2.1. Introduction……...……...…… **32**
2.2. The method of producing the titanium-containing materials…… **32**
2.3. Materials……... **35**
2.4 Analytical control devices……. **35**
2.5 Surface morphology, average particle size, particle shape……..…… **36**
2.6 Preparations for the experiment…….…..…… **37**
2.6.1 The preparation of the samples for tests for water vapor and benzene vapor adsorption…….……. **37**
2.6.2 The preparation of the samples for tests of UV-sensitivity……... **37**
2.7 Adsorption activity…….……. **38**
2.7.1 Water vapor adsorption…… **38**
2.7.2. Benzene vapor adsorption, specific surface area and properties of the porous structure…….…… **39**
2.8. Testing methyl ethyl ketone (MEK) removal of the composite materials...….. **42**
2.8.1 The photosensitivity of the materials in the absence of UV-irradiation (reactor 43.6 mL)……...…… **42**
2.8.2 The photosensitivity of the materials and MEK removal kinetics in the presence of UV-irradiation (ULTRA-VITALUX E27 lamp, reactor 16 L)……...… **43**
2.8.3 The photosensitivity of the materials and MEK removal kinetics in the presence of UV-irradiation (UV and Daylight LEDs, reactor 0.45 L)……..…… **45**
2.8.4 Using the parameters of the kinetic equation for estimating UV-sensitivity of the TiO_2-containing materials……. **50**
3 Ageing, properties and optimal conditions for the preparation of composite materials…….. **54**
3.1 Introduction…….…….. **54**

3.2 Synthesis of the samples……. **54**
3.3 The analyses of water vapor adsorption isotherms……..…… **56**
3.4 The analyses of the kinetics of MEK adsorption……..…….. **62**
3.5 The effect of UV-radiation on TiO_2-containing materials ……..……. **66**
3.6 Conclusions for Chapter 3……..…….…… **70**
4. The synthesis and testing UV-sensitive materials on clay supports……. **72**
4.1 Introduction……..……...……. **72**
4.2 The clay materials characterization and the investigation of the thermochemical treatment influence……..……. **72**
4.2.1 Montmorillonite and its activated form……..……..…….. **72**
4.2.2 Kaolinite and its activated form ……..……..…… **77**
4.3 Composite materials: Synthesis, Structure and Properties…….…..…… **82**
4.3.1 The choice of technology for TiO_2-containing materials preparation……..……. **82**
4.3.2 The synthesis of composite materials…….…. **84**
4.3.3 The study of chemical composition and surface morphology of the samples……...…… **85**
4.3.4 Water vapor adsorption isotherms for TiO_2-containing material…….. **91**
4.3.5 Benzene adsorption isotherms, specific surface area and porous structure …….. **93**
4.3.6 The results of X-ray crystallography for the kaolinite-based materials…….. **97**
4.3.7 UV-sensitivity of the samples (MEK removal)…….…… **102**
4.4 The pilot plant for producing the TiO_2-containing composite additives for building materials: technological scheme……..……...… **110**
4.4.1 The consumption ratios for to produce…….…….…. **110**
4.4.2 The Process Flow Diagram…….…….…... **111**
4.5 Conclusions for Chapter 4…….…….……... **113**
5. The Development and Application of the Materials…….…….……... **115**
5.1 Introduction……..…… **115**
5.2 The testing of the photosensitive building materials, containing the K (1:6)-750 composite……..……...…… **115**
5.3 The nonmetal co-doped samples…… **119**
5.3.1 Examination of the chemical composition and surfaces…… **119**
5.3.2 The study of photo-catalytic activity of the samples…… **124**
5.3.3. Conclusion for Section 5.3……. **127**
5.4. The study of the properties of fly ash as a matrix for photoactive component… **128**
5.4.1 The study of the composition and adsorption characteristics of fly ash……. **129**
5.4.2 The preparation of TiO_2-contaned materials and investigation of their compositions…… **132**
5.4.3 The adsorption of water vapor by the TiO_2–FA materials ……. **136**
5.4.4 The kinetics of MEK-removal under UV-irradiation…….. **137**
5.4.6 Conclusion for Section 5.4 **139**
Conclusion…… **140**
References…….…... **142**

Nomenclature

A – thermodynamic potential $A=RT\ ln\ P_s/P$, J/mol

a – equilibrium adsorption capacity, g/g (mg/g)

a_s – maximum adsorption capacity at $P/P_s=1$, g/g (mg/g)

a_m – monolayer adsorption capacity , mmlol/g

E_0 – characteristic energy of benzene vapor adsorption, J/mol

$K_{C_t}^{ap}$ – apparent" kinetic constant

k_{ads} –kinetic constant, mg/(g* min)

m_t – the specific mass MEK adsorbed by 1 g of material at time t; mg/g

m_{lim} – limit value of adsorbed mass corresponding equilibrium monolayer capacity; mg/g

P – porosity (%)

P/P_s – relative pressure, relation of partial vapor pressure to saturated vapor pressure of adsorbate at the temperature of the experiment

S_{meso} – specific surface area of mesoporous, m^2/g

S_{BET} – specific surface area according theory of polymolecular adsorption of BET, m^2/g

t – duration of the process, min

V_{total} – total pore volume, cm^3/g

V_{fr} – base layer fenestration, cm^3/g

$V_{ме}$ – volume of mesopores, cm^3/g

V_S – limit adsorption volume, cm^3/g

x_0 – micro-pores width, it is calculated from the theory of the volume filling of micropores (TVFM), nm

W_0 – maximum micropore volume, cm^3/g

Δ – bulk density, g/cm^3

θ – the surface filling rate

ϱ_{true} – true density, g/cm^3

ϱ_{app} – apparent density, g/cm^3

ID of obtained materials

Chapter	ID	Notes
Chapter 3	K158, K109, K97, M316, M167, M49	Samples of the TiO_2-containing materials obtained under conditions described in Table 3.1. K, M – clay matrix. 158, 316 etc. – content of TiO_2, mg/g.
Chapter 4	M (1:3) act, K (1:3) act, K (1:6) act	Samples of kaolinite and montmorillonite after the thermo-acid treatment. (1:3), (1:6) – ratio clay matrix: acid solution 7.8% wt, g**:**ml.
Chapter 4	M(1:3)-600, M(1:3)-750, K(1:3)-600, K(1:6)-600, K(1:3)-750, K(1:6)-750	Samples of the TiO_2-containing materials obtained under conditions described in Table 4.6. K, M – clay matrix. (1:3), (1:6) – ratio clay matrix: reaction solution 7.8% wt, g:ml. 600, 750 – temperature of calcinations, ^oC .
Chapter 5	K-S, K-S-N, K-S-P, K-S-Cl	Samples of the co-doped materials obtained under conditions described in Table 5.1.
Chapter 5	FA FA (1:3) Act, FA (1:6)Act FA-(1:3); FA-(1:6)	Fly Ash. Fly Ash after the thermo-acid treatment . (1:3), (1:6) – ratio FA matrix: acid solution 7.8% wt, g **:** ml. Samples of the TiO_2-containing materials obtained under conditions described in Table 5.8.

Introduction

Actuality

The introduction of modern technologies in common life can affect people in both positive and negative ways. On the one hand, technologies improve the quality of life for billions of people in terms of health, nutrition, education, etc.; at the same time, it often makes hew hazards. While the environmental harm caused by industrial and agricultural activities on a global scale falls outside the scope of this study, using new materials (e.g. building materials, furniture, household chemicals) for domestic purposes causes pollution of the environment (this study focuses on chemical pollutants). A shift to only ecologically pure materials is impossible so far, apart from the fact that "ecologically pure" does not necessary mean "safe". Therefore, the strategy for providing safety environment is based on the reduction of the emissions and on depollution processes, including methods, which focus on Indoor Air Quality (IAQ).

Ensuring the IAQ management includes various technologies, in particular, the passive degradation of indoor air pollutants, which implies the use of construction components and finishing materials able to physical or chemical immobilization of pollutants and, ideally, be able to provide their decomposition to harmless compounds.

The development of construction materials able to adsorb the pollutants for a passive reduction process is one of the areas of interest for the Department of Materials, Environmental Sciences and Urban Planning of Università Politecnica delle Marche (SIMAU UNIVPM) [1]. However, the main disadvantages of the technologies based on the adsorption of pollutants is reversibility of the process and saturation of the material. Therefore, the chemical decomposition of pollutants is one of the most promising approaches. The process is usually based on photocatalytic oxidation and titanium dioxide is one of the most commonly used materials with such properties [2].

The photodegradation process was developed by SIMAU UNIVPM, both in terms of the development of reactors for the photocatalytic purification of indoor air [3,4], and the preparation of building materials containing photoactive components [5]. Application of low-cost materials or waste materials for preparation a component is important goal of environmental protection researches. This study describes the method of synthesis composites based on the technology of TiO_2 film deposition on finely powdered aluminosilicate suppport materials (hereinafter matrix). Titanium scrap was used as raw material for obtaining titanium dioxide, while clays (montmorillonite and kaolinite) and fly ash were proposed as carrier materials. The preparation method is based on high-temperature hydrolysis of the titanium-containing precursore.

The Goals and objectives of the study

The overall goals of the study were to develop the method for obtaining composite components for building materials with photoactive properties providing passive degradation process.

The following studies were carried out:

- The method of synthesis of TiO_2-based composites using cheap raw materials as titanium shavings and alluminoselicates was developed and tested;

- The samples were prepared under various conditions (e.g. matrix/precursor ratio, type of the support, temperature of calcination, etc.). Their composition, surface morphology, adsorption properties and photo-activity were investigated;
- The effects of aging on the materials after three years of storage were examined;
- A pilot scheme for the material industrial production is proposed;
- The technology of co-doping with non-metals (Cl, N, P) was proposed for further developing of the method. In addition, the potential of fly ash as a carrier material was investigated.

Structure of the thesis

The thesis includes the following chapters:

Chapter 1. Literature review
The chapter contains a literature review of the application of photoactive materials to ensure Indoor Air Quality, and in particular, review elaborates the following issues:
-the principles of photocatalysis and photoactive materials;
-the use of photo-sensitive components in construction materials for providing Indoor Air Quality;
-the properties of titanium dioxide and the impact of different factors on its efficiency;
-the methods of synthesis of TiO_2-containing composites;
-the use of clay and fly ash as supports, doping and co-doping of materials with anions for obtaining a composite active under visible-light;
-the main areas for practical application of titanium dioxide.

Chapter 2. Characterization of materials and definition of methods
The chapter describes in detail the technology of preparing the samples, the methodology of examining chemical and phase composition, surface morphology, an average particle size, specific surface area and adsorption activity and photosensitivity. The tools including the reactors, which were used to study the influence of UV- and daylight-irradiation on the obtained samples, were also described here.

Chapter 3. Ageing, properties and optimal conditions for the preparation of composite materials
The chapter investigates the stability of properties of the composites after 3 years of storage, in order to extend validity period of the composites [6, 7]. Based on the results obtained, the recommendations for method of synthesis of stable samples were describe [8].

Chapter 4. Synthesis and Testing of UV-sensitive Materials on Supports
This chapter focuses on the examination of new materials on montmorillonite and kaolinite supports, which were synthesized under various conditions, taking into account the results and recommendations described in Chapter 3. In addition, the influence of calcination temperature increasing were examined [9].
The obtained samples were examined by the methods, described in Chapter 2:

- Chemical contents;
- Characterisation of the surface structures;
- Adsorptive properties (water vapor capacity);
- Adsorptive properties (benzene vapor capacity);
- Determination of parameters of porous structures;

- X-ray phase analysis;
- Photosensitivity of the materials was examined UV-sensitivity was estimated by the method of methyl ethyl ketone (MEK) removal in the reactors of two different types (16 L & 0,45 L) with two types of UV-irradiation source: ULTRA-VITALUX E27 lamp and DFL-5013UVC-380.

Degussa P25 for LEDs irradiation sources was tested as reference material under the same to compare UV-sensitivity.
For the promising way of the material preparation, the scheme of pilot mini-plant is proposed.

Chapter 5. Development and Application of the Materials
This chapter presents the results of preliminary studies on the possible development of the proposed method for producing composite materials.
The few sorts of building materials without and with obtained TiO_2-containing component were tested by the method of methyl ethyl ketone (MEK) removal.
The co-doping for visible light strategy were preliminary used as second direction of the development of the technique. During the preparation of the samples, hydrochloric, phosphoric and nitric acids were singularly added to the Ti-containing precursor. The samples were tested under both UV (DFL-5AP4SC-400) and daylight (L54 PWC) LEDs irradiation. Titanium dioxide Degussa P25 was tested for comparison. All samples showed more or less the activity under daylight irradiation, but they were less effective than in the presence of ultra violet light. Encouraging results were achieved for Cl-containing materials.
Another issue was the possibility of the use of fly ash as a matrix for composites. The samples of obtained materials showed slight photoactivity under UV-irradiation. However, kaolinite matrix-based samples showed better results in the removal of MEK compared to the fly FA-samples [10].

1. Literature review

1.1 Passive Degradation for Indoor Air Quality and new role of building materials

Nowadays modern people spend 90% of their time in indoor environment, much more than years ago [11]. These environments correspond to e.g. buildings offices, school, public transports. That is why strategies for the improvement of Indoor Air Quality (IAQ) are particularly important: the levels of air pollution inside houses are often from two to five times higher than outdoor levels [2]. Pollutants are classified into three broad categories: physical, chemical and biological. Some examples are Volatile Organic Compounds (VOCs), the most present of which are formaldehyde, toluene, benzene; and carbon monoxide, nitrogen dioxide, ozone, particulate matter (PM), tobacco smoke, asbestos, other anhydrides (XO). The physical agents are radon, natural and artificial electromagnetic fields and noise. The biological agents are: molds, bacteria, fungi and pollens [12].

Taking into account that each person inhales about 22 m^3 of air per day [13], an inhalation of indoor air is potentially the major determinant of human exposure to many pollutants [14]. Some harmful compounds are associated with sick building syndrome (SBS) including mucous membrane irritation, headache, allergies and respiratory problems; others are known as carcinogens, mutagens, or teratogens [13] Millions of people are currently suffering from the consequences of poor indoor air quality.

Figure 1.1 [2] shows the air point sources of pollution in a house. As can be seen, a significant part of them is related to building materials (such us paint, varnishes, caulks, composite wood products, upholstery, foam) and domestic products (cleaning products, gasoline, and cosmetic).

In general, three methods are suggested to improve the indoor air quality, namely source control, increase ventilation, and air purification [15]. Source control is often ungovernable and unacceptable, especially when it comes to the limitation of household items and materials. Increased ventilation is an effective way when there is a high quality outdoor air. Otherwise, it might even transport more pollutants from the outdoor environment. Thus, air cleaning remains the most feasible option to improve the indoor air quality [15].

While conventional techniques of air purification are effective, they often can be either energetically and operationally intensive or suitable only for large systems (e.g. adsorption or filtration systems). Moreover, the residuals coming from intensive chemical treatments (such as ozone-based methods), can add to the problems of contamination. This is the reason why Passive Degradation technology attracts the particular attention of researchers. And along with ventilation and special devices for air purification [3,16,17], the technology of Passive Degradation of pollutants with the use of building materials that have a special structure and components becomes very important [18,19].

There are two main approaches in technology of Passive Degradation of indoor pollutants using building materials: a)-retention of pollutants in materials with high adsorptive properties; b)-combination of adsorption process with chemical immobilization or chemical degradation of indoor pollutants. The first way is used widely [16, 20-21], but a few questions arise here: the inertness of the material after saturation and possible

desorption of pollutants in the event of a change in external conditions. A major flaw of chemical immobilization (i.e., immobilization of CO_2 and acid gases by calcium oxide, added to the matrix of concrete [22, 23]) is again, inactivity after the chemical reaction. Therefore, such method is recommended if the periodic replacement of the material is possible.

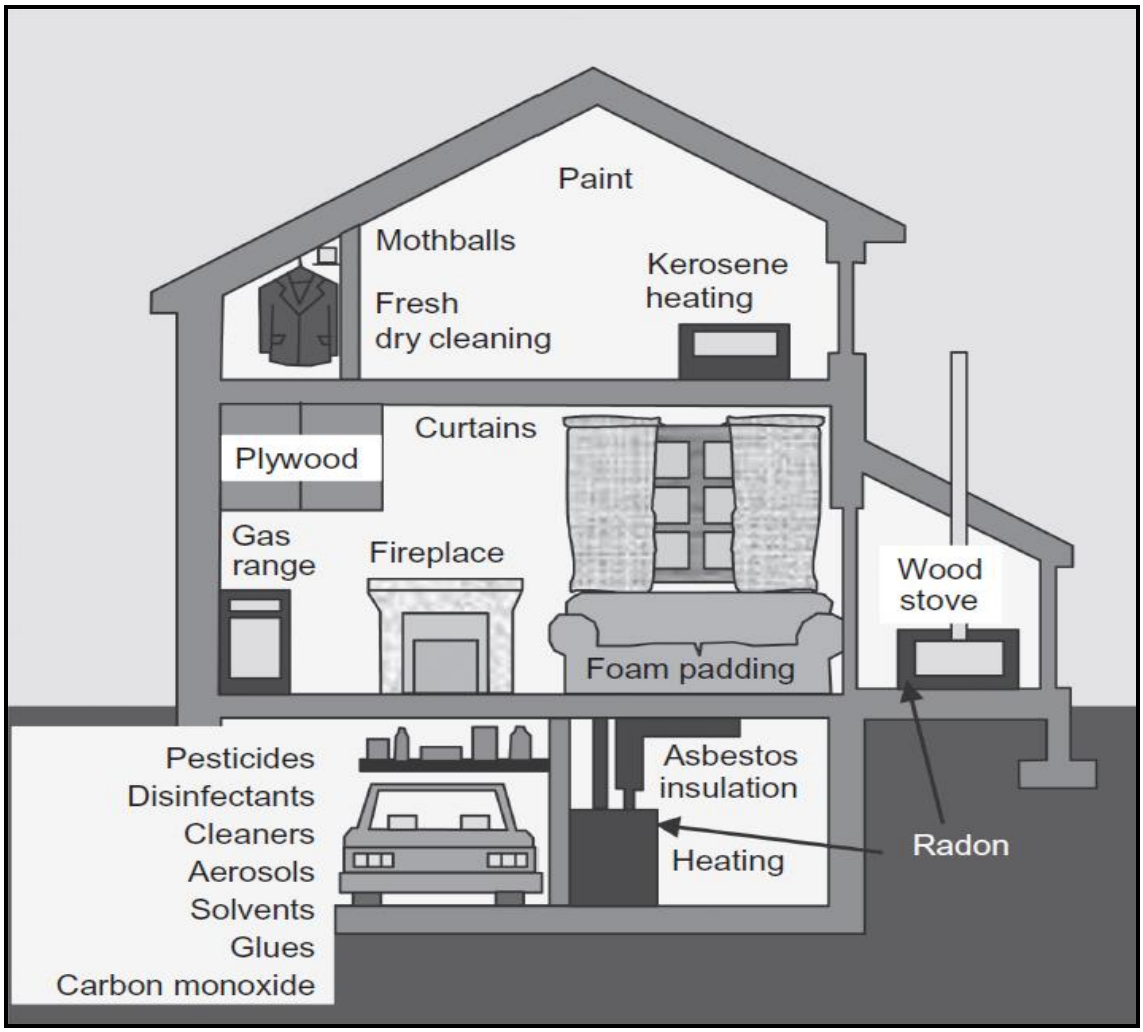

Figure 1.1 Air pollution sources in a house [2]

In order to avoid these disadvantages, more attention is now being focused on the methods of chemical degradation of indoor pollutants, especially on photocatalytic oxidation (PCO) process. This approach includes both the development of devices for air purification and construction materials, containing UV-sensitive components (mostly titanium dioxide). It must be stressed that there are limitations for a wider spread of technology.

The decomposition of organic pollutants (especially volatile and semi-volatile compounds) is a promising area, given that they are the majority of indoor air pollutants. This issue has been addressed since the start of investigating the photocatalytic oxidation process. In addition to paragraph 1.1, the data about decomposition of some organic compounds is represented below.

In 1997 the study [24] was published. The subject of gas-phase photocatalytic destruction of 17 VOCs over illuminated titanium dioxide was investigated using a plug flow reactor. At steady state, high conversion yields were obtained for trichloroethylene (99.9%), isooctane (98.9%), acetone (98.5%), methanol (97.9%), methyl ethyl ketone (97.1%), t-butyl methyl ether (96.1%), dimethoxymethane (93.9%), methylene chloride (90.4%), methyl isopropyl ketone (88.5%), isopropanol (79.7%), chloroform (69.5%) and tetrachloroethylene (66.6%). However, the photodegradation of isopropylbenzene (30.3%), methyl chloroform (20.5%) and pyridine (15.8%) was not so efficient.

The degradation of not only volatile, but also fluid and solid organic compounds, molecular weights of which ranged from 600 to 500.000 was studied on the TiO_2 thin films on glass under UV illumination [25]. The gas-phase photocatalytic decomposition of benzene, toluene, cyclohexane and cyclohexene over TiO_2 was studied in [26]. Catalyst deactivation was ascribed to the formation of carbon deposits on the TiO_2 surface and the formation and decomposition behavior of carbon deposits affected the decomposition rate. Solar photocatalytic degradation of formaldehyde in the gaseous phase has been investigated [27].

The mechanism of PCO process of organic pollutants is still a complex subject for the study. [28,29]. While some authors [30] argue that simple organic compounds can be mineralized completely in multi-stage processes, in the opinion of a majority of researchers, the decomposition of typical compounds produces intermediates which are also called "by-products". These compounds can be as harmful as the original pollutants and they can be desorbed into environment if external conditions will change.

The detailed review of the mechanisms of PCO for the decomposition of typical pollutants (e.g. alcohols, alkoxyalcohols, aldehydes, toluene and benzene) is represented in [31]. Therefore, by-products formation is a function of the PCO reaction mechanisms of contaminant types. It is a challenge to predict the generation of by-products qualitatively and quantitatively in the context of complicated PCO mechanisms involved as well as inconsistent experimental environmental conditions. It is concluded, that formaldehyde and acetaldehyde are two common by-products regardless of the compounds. The concern of the formation of more toxic byproducts during the process of UV-PCO makes it necessary to employ a chemisorbent for by-products immobilization [32], to increase the irradiation time for reducing concentrations of by-products [33,34], and to regulate air humidity [35, 36].

While the intermediates remain valid, a number of publications describing PCO for air purification has increased 15-18 times for the recent 15 years (see Figure 1.2). [17]

The tested photoreactor is made of a borosilicate glass tube with the inner surface coated with the sol–gel TiO_2 thin film.

Photocatalytic oxidation of acetone and methyl isobutyl ketone (MIBK), two ketones with different hydrophilicity, over the TiO_2 thin films supported on glass rings were studied under different relative humidity (RH) conditions [37].

As mentioned above, a large proportion of PCO-technologies for air purification is based on construction materials, containing photocatalytic components. Currently, a number of TiO_2-coated building materials, including silicate, cement, glass, mortar, stone have been

examined as a substrate supporting photocatalysts in the laboratory/field environments [2, 38-45].

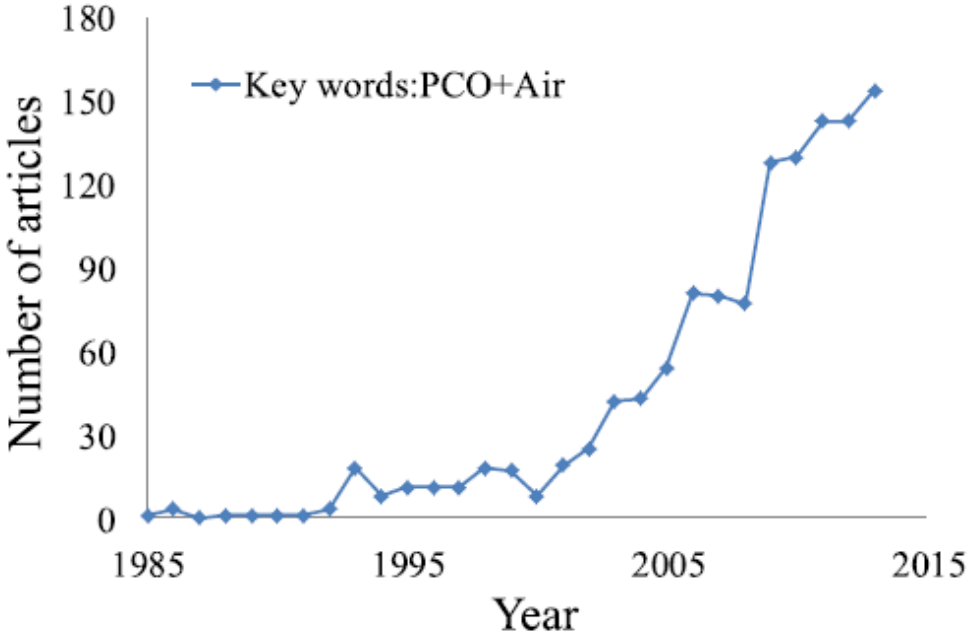

Figure 1.2 A Number of articles published in Compendex from 1985 to 2013 based on the data of the Engineering Village searching engine with key words are photocatalytic oxidation and air [17]

The [2] is the most complete overview of ways of applying TiO_2. The main applications of TiO_2 in construction materials which the authors described included:

Horizontal applications

- Concrete pavements
- Paving blocks and plates
- Roofing tiles
- Roofing panels
- Cement-based tiles

Vertical applications

- Indoor and outdoor paints
- Finishing coatings
- Covering precast panels
- Permanent formworks
- Masonry blocks
- Sound-absorbing elements
- Traffic dividers elements
- Street furniture

Tunnels

- Paints and renderings
- Concrete panels

- Concrete pavements
- Ultra-thin whitetopping

The same work [2] describes the technologies accomplished for production of building materials and devices for air and water purification, including:

- ***Photocatalytic Glass –*** The TiO_2 thin films can also adsorb species and, hence, degrade organic and inorganic (chemically present in a reduced form) pollutants, eventually discharging their oxidation products by easy washing with plain water (even through naturally occurring rain), thus preventing glass from fouling. In addition, a superhydrophilic surface cannot adsorb organic oily liquids but, instead, strongly expels them. Since the TiO_2 films are both photocatalytically active and superhydrophilic, they can work in both ways (a photocatalytic degradation of pollutants on the one hand and the rejection of organic liquid species caused by the superhydrophilic characteristic on the other hand).
- ***TiO_2-modified Cement and Ceramics –*** Concrete materials with TiO_2 can be modified simply by dry adding a certain amount of semiconductor. The TiO_2 weight percentages are in the 0.1–50% range with respect to the binder. The resulting material is commonly used only in an exterior layer with a thickness of about. 1 cm and not in the entire structure. The TiO_2-modified cementitious materials are not used as supporting structural elements, since the inner non-irradiated areas would not work photocatalytically. Thus only an external wearing thin layer should be used, that is why the TiO_2 containing component must be added into the external or laid as a special coating layer, for example, to deposit the TiO_2 sol over it by simple spray-coating. The application of photocatalytic ceramic tiles can ensure a relevant sterilization thanks to their antimicrobial features. A photocatalytic tile can decompose bacteria such as Escherichia coli, once they adsorb on its surface. This effect becomes much stronger when TiO_2 is doped with silver or copper nanoparticles. Doping with silver and copper ensures, moreover, a modest antimicrobial activity even in the absence of light. So it is strongly advised when the bactericidal effect is important even in shadowed surfaces such as in hospitals.
- ***Devices for Water and Air Purification –*** Different devices for Pesticide and Cyanide Degradation in water and different types for air clearing are described.

  At the same time, depending on the application and the area of using a building material the photoactive components may differ in composition, modifications, and the method of obtaining and the presence of doping agents. The present study focuses on the development of TiO_2-based photosensitive components for finishing materials and ceramics. Therefore, the following sections will address the properties, providing photocatalytic activity, the methods of synthesis and possible applications.

1.2 Working principles of heterogeneous photocatalysis

Developed in the 1970s, heterogeneous photocatalytic oxidation has been given considerable attention and in the past two decades, numerous studies have been carried out on the application of a heterogeneous photocatalytic oxidation process with a view to

decomposing and mineralizing recalcitrant organic compounds. It involves the acceleration of photoreaction in the presence of a semiconductor catalyst [46].

According to the IUPAC definition, *photocatalysis* is a change in the rate of chemical reactions or their generation under the action of light in the presence of a substance that absorbs light quanta and is involved in the chemical transformations of the reaction participants. The *photocatalyst* substance is the one, that able to produce by the absorption of light quanta, chemical transformations of the reaction participants, repeatedly coming with them into the intermediate chemical interactions and regenerating its chemical composition after each cycle of such interactions [47]. Fujishima and Honda [48] pioneered the concept of TiO_2-based photocatalysis (also known as "Honda-Fujishima effect"), by studying the possibility of water splitting in a photoelectrochemical cell containing an inert cathode and rutile titania anode. The titanium photo-electrolysis have been focused in environmental applications including water and wastewater treatment [49].

Photocatalysis belongs to photoinduced processes, which are activated by an input of super-band gap energy. Due to a narrow band gap (usually less than 3,5 eV) of semiconductors, the energy required for the initiation of the process can be obtained during the adsorption of a photon. The unique structure allows the formation of the photogenerated electron-hole pairs, where the electron (e^-) is promoted to the conduction band, and the hole (h^+) is generated in the valence band. This is the reason, why all of photocatalysts are invariably semiconductors.

The mechanism of the electron hole-pair by the example of TiO_2 is given in Figure 1.3 [50]. The energy required for the initiation of the process can be obtained after the absorption of radiation of suitable wavelength.

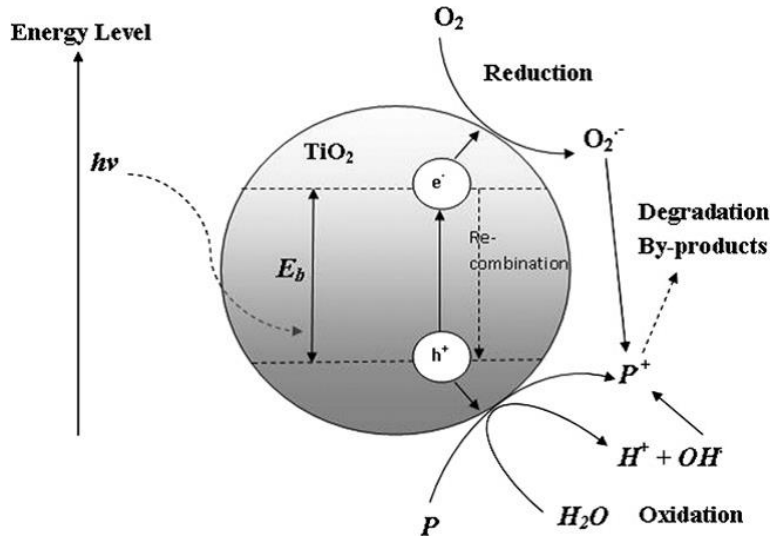

Figure 1.3 The mechanism of electron-hole pair formation in a TiO_2 particle in the presence of pollutant in water [50]

When semi-conductors are irradiated, a great variety of photoinduced chemical reactions able to degrade many organic and inorganic molecules, can occur by means of the

formation of active radical species that are generated in the presence of O_2 and H_2O [2]. The following scheme can summarize the reactions at the semiconductor–water interface when TiO_2 is used as a photocatalyst, where (ads) means adsorbed, (CB) conduction band, and (VB) valence band:

$$TiO_2 + h\nu \rightarrow TiO_2\ (e^-_{(CB)} + h^+_{(VB)}) \quad (1.1)$$

$$H_2O_{(ads)} + h^+_{(VB)} \rightarrow {}^{\cdot}OH + H^+ \quad (1.2)$$

$$e^-_{(CB)} + O_2 \rightarrow {}^{\cdot}O_2^- \quad (1.3)$$

$${}^{\cdot}O_2^- + H^+ \rightarrow {}^{\cdot}HO_2 \quad (1.4)$$

$$2{}^{\cdot}HO_2 \rightarrow O_2 + H_2O_2 \quad (1.5)$$

$$H_2O_2 + {}^{\cdot}O_2^- \rightarrow OH^- + {}^{\cdot}OH + O_2 \quad (1.6)$$

All of the processes (1) - (6) take place simultaneously and form highly reactive oxidants such as O- and, in particular, $OH^{\bullet}$-radicals, which are capable of non-selectively oxidize any adsorbed organic compounds to CO_2, water and mineral acids.

Moreover, the photocatalytic method allows the elimination of many inorganic ionic pollutants present in water by either reducing them to their elemental form on the surface of the catalyst particle:

$$M^{n+}_{(aq)} + e^-_{(CB)} \rightarrow M_{(surf)} \quad (1.8)$$

or transforming them into less noxious species. For example, the reduction of Cr (VI) to Cr (III) allows the elimination of chromium by means of its subsequent precipitation as hydroxide [2].

The decomposition of VOCs plays a special role in the application of PCO for passive degradation of indoor and outdoor pollutants. Paragraph 1.1 describes modern approaches to the mechanisms of decomposition, but the issue is considered in detail in [51]. The general scheme of the VOCs decomposition was shown in [50] (Eq. 1.7).

$$C_xH_pO_qX_y + (x + \frac{p-y-2q}{4})O_2 \xrightarrow{TiO_2, h\nu} xCO_2 + yH^+ + yX^- + \frac{p-y}{2}H_2O \quad (1.9)$$

Where X represents a halogen atom.

1.3 Photocatalytic materials. Titanium dioxide

As it was mentioned above, all of the heterogeneous photocatalysts are semiconductors, including binary, ternary and quaternary compounds. A detailed review of various compounds submitted in [52]. Here is a brief list of photoactive materials according this revew:

- Oxides and sulfides represent *binary compounds*. The first group includes ZnO, Cu_2O, WO_3, V_2O_5, various iron (III) oxides, Bi_2O_3, NiO , ZrO_2 [53]. Among the binary sulfides such compounds as CdS and ZnS are worth noting .
- While *ternary* and *quaternary* oxides were investigated mostly in order to determine their potential to produce H_2 and O_2 by water splitting, these materials were also tested as photocatalysts for the visible light degradation of various types of pollutants. Among them, the following attracted a considerable attention: vanadates (such as $BiVO_4$ [54]), indates, bismutates and single-phase quaternary oxide

materials synthesized by utilization of binary oxides, such us V (Bi_2MVO_7 (M = Ga, Fe, Al, Sb)) or Bi_2YVO_8.

- *Bismuth oxyhalides* (BiOX (X = Cl, Br, I)) are other ternary semiconductors that have been studied as potential candidates for photocatalytic applications. Single-crystalline BiOX samples prepared with the use of $NaBiO_3$ and HX aqueous solutions as raw materials were tested for the photodecomposition of four kinds of typical phenolic endocrine disrupting chemicals.
- Despite a relatively wide band gap, *indium hydroxide* $In(OH)_3$ was tested successfully for the photoinduced oxidation of acetone, benzene, and toluene.
- Among *quaternary oxyhalides*, Bi_4NbO_8Cl showed an excellent visible light efficiency in comparison with Bi_3O_4Cl and anatase TiO_2.

Among other semiconductors with photoactive properties, TiO_2 is characterized by such qualities as photochemical and chemical stability, high activity under natural or artificial light, relatively low cost, availability, absence of chemical and biological toxicity [39]. Given that titanium dioxide is one of the most effective and available photosensitive materials, the further modification of its properties is an essential issue. In order to solve the problem, it is necessary to investigate the impact of various factors on the material.

1.3.1Impact of phase composition of TiO_2

Titanium dioxide occurs in nature as the well-known minerals: rutile, anatase and brookite. The composition of TiO_2 in terms of these phases is a key factor determining photoactivity. In most cases, anatase shows the best efficiency during photoinduced process among the phases [55,56], while pure rutile usually does not demonstrate high activity. Despite this, there are studies, which confirmed that rutile could be more active, especially in aqueous solutions [57-59]. As for brookite, its photosensitivity is mostly negligible [60]. It is worth noting, that the phase content of TiO_2 is correlated with the size of particles. The typical size of rutile particles is around 15 nm or larger [61]. Considering that for particles with the diameter of ~ 10 nm all the volume is involved in the absorption of light, this is possibly one of the reasons of lower activity of rutile.
On the other hand, there are studies that proved that ineffective phases could be more photoactive than anatase. In particular, during the experiment, described in [2], the brookite film was shown to be more efficient for the photodegradation of 2- propanol (see Figure 1.4).

1.3.2 The Effect of particle size on the photocatalytic activity

The primary particle size is often regarded as one of the main parameters that influence the photocatalytic activity, while the same samples show different relative activities in reactions carried out in the gas and liquid phases.
During the reactions in gaseous phase, the samples with high specific surface area and small size of primary particles demonstrated the highest photoactivity. The results obtained during experimental photoinduced oxidation of hexane [62], acetone [63] and toluene [64] demonstrate that the optimal size of the primary particles in the gas phase reactions is 6-15 nm.

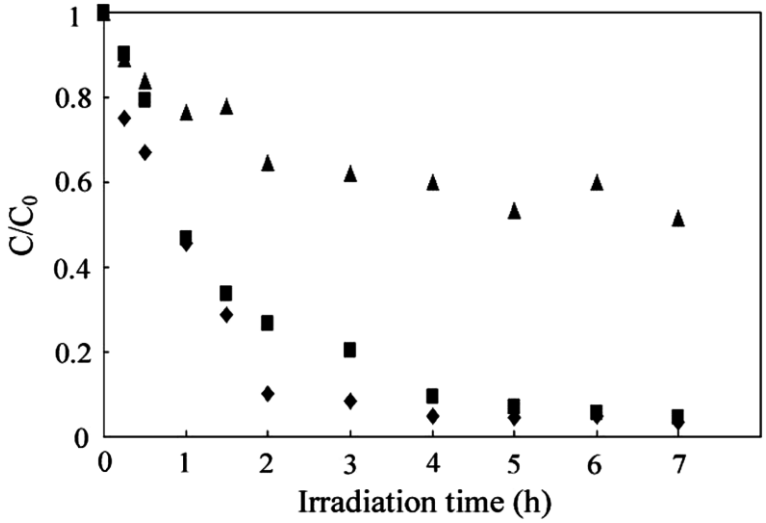

Figure 1.4 2-Propanol degradation versus irradiation time in the presence of ten-step deposited films: (■) pure anatase, (♦) pure brookite and (▲) pure rutile [2]

In the liquid phase, the samples have a large pore size, large particles and a low surface area [58]. The best known highly active photocatalyst for the liquid phase reactions is Degussa P25 having a primary particle size of rutile and anatase about 90 and 37 nm, respectively, and a surface area of 50 m^2/g [64]. Studies of photochemical oxidation of various compounds (including formic acid, acetic acid and benzene) show that the optimal particle size for the liquid phase oxidation reactions is 15-110 nm [65,66].

1.3.3 The impact of surface composition on the properties of TiO_2

The presence of impurities may affect photocatalytic activity.
Initially as confirmed in previous studies [67] the presence of hydroxyl group is beneficial for photoinduced oxidation process, although later it was found this impact has limits [68,69]. Doping with Na decreases photoactivity [70], while the imposition of Be^{2+} [71] ions and lanthanides [72] may enhance the efficiency of the process.
The presence of sulfates is of interest for this study. Sulfating of the TiO_2 surface definitely had a positive impact on the photosensitive properties. There are two ways to provide sulfating: a low-temperature method (adding solution of sulfuric acid to the material with further drying), a high-temperature method (treated samples are subject to calcination) [70-73]. The treatment of both types increased photoactivity of TiO_2, and [70] the correlation between the efficiency of decomposition of acetone and the amount of Brønsted acid sites on the surface of TiO_2 was confirmed. These approve the use of concentrated acid. Other results were described in [74]. The covering of the surface of the photocatalyst has changed the degradation rate of pollutants. Since the change varies with the pollutant species, such modification may be utilized to obtain specificity. Sulfated TiO_2 can be prepared by reacting H_2SO_4 with $Ti(OH)_4$. It was found that the ratio of the mineralization constant rate of heptane was 5.75 for sulfated titanium dioxide, while for non-sulfated TiO_2, made by calcining unsulfated $Ti(OH)_4$, this ratio was only 2.7. This selective

enhancement in the degradation of heptane correlated well with the increased coverage and with the adsorption strength on strong Lewis acid sites produced by sulfation.

1.4 The synthesis of TiO_2 and TiO_2-containing material

TiO_2 can be prepared in the form of powder or thin films. Both powders and films can be built up from crystallites ranging from a few nanometers to several micrometers. It should be noted that nanosized crystallites tend to agglomerate, that is why often a deagglomeration step is necessary. There are a few general approaches of titanium dioxide preparation. These approaches are represented by the methods, which are summarized in [2, 31, 39]. The following brief list includes methods, which were described in [2].

1.4.1 Preparation Methods of Powdered TiO_2

There are many methods of powder preparation. Below there are listed the ones most frequently found in the scientific literature.

- Sulfate Process. This method is interesting for our study because it is the prototype of the proposed technology for preparing TiO_2-containing material
  The sulfate process was the first commercial process for manufacturing powdered TiO_2. The first used raw material was ilmenite ($FeTiO_3$), but subsequently other ores with a much higher TiO_2 content were chosen. The ore is subjected to drying and grinding and then it reacts with concentrated sulfuric acid (exothermic digestion reaction). The experimental conditions are controlled (e.g., the minimum amount of acid should be used) to maximize the conversion of TiO_2 into water-soluble titanyl sulfate. The resultant dry, green-brown cake of metal sulfates is dissolved in a weak acidic aqueous solution, the temperature is lowered to avoid premature hydrolysis and the solution was clarified by settling and chemical flocculation. The resultant clear solution is then further cooled to crystallize the by-product $FeSO_4 \cdot H_2O$, which is separated. The insoluble mud so-obtained is washed to recover the titanyl sulfate liquor, which is filtered to remove the insoluble impurities. The solution is evaporated to a precise composition and hydrolyzed to obtain a pulp consisting mainly of clusters of colloidal hydrous titanium oxide. Precipitation is induced by seeding or nucleation technique. The pulp is then separated from the mother liquor and washed to remove residual traces of metallic impurities, using sometimes chelating agents. The washed pulp is treated with chemicals that adjust physical texture and act as catalysts in the calcination step. This process can produce either anatase or rutile crystal forms depending on the additives used before the calcination process [2].
- Chloride Process. The starting material for the chloride process is generally the mineral rutile containing over 90% TiO_2. As a result, of the contact with hydrochloric acid $TiCl_4$ gas is obtained. After the condensation of the $TiCl_4$ vapor, an extremely pure, colorless, mobile liquid $TiCl_4$ was obtained. The second stage in the chloride process is the oxidation of $TiCl_4$ to TiO_2.
- The flame pyrolysis process was used to prepare the most popular commercial material used in photocatalytic studies (Degussa P25).

- The preparation of powdered and nanocrystalline TiO_2 by the Sol-gel method enables one to synthesize highly pure and homogeneous materials by starting from a colloidal suspension (sol) obtained from liquid solutions of organometallic or inorganic precursors.
- The preparation of nanoparticles, nanorods, nanotubes and nanowires of TiO_2 by the hydrothermal method allows preparing TiO_2 nanoparticles or nanorods, which are carried out in water or in the mixtures of water/ethanol and, generally, steel pressure autoclaves are used.
- The solvothermal method differs from the hydrothermal method in that a nonaqueous solvent is used. Higher temperatures can be achieved because many organic solvents with boiling points higher than that of water can be chosen. Their use allows a better control of size and shape distributions of the TiO_2 nanoparticles, nanorods or nanowires.
- The Sol method is a nonhydrolytic sol-gel process and generally involves the reaction of TiCl4 (or other halides) with different oxygen donor species, such as organic ethers or metal alkoxides.
- The laser pyrolysis method was employed successfully as a single-step reaction route for the synthesis of anatase/rutile mixed nanopowders.
- The microwave method uses microwave radiation to prepare TiO_2 nanomaterials.

1.4.2 The Preparation of Films

The preparation of films allows creating the films of titanium dioxide with thickness ranging from a few nanometers to ca. 100 μm.

- Wet Coating Technologies to prepare TiO_2 films (dip-coating, spin-coating, flow coating, (plasma) spray drying and spray-pyrolysis etc.) were developed for various types of supports, but mainly for glasses. Both the wet coating materials and the equipment are not standardized and therefore they were tested and developed by the users.
- The physical vapor deposition (PVD) includes methods that allow the deposition of thin films by condensation of a vaporized form of the material onto various surfaces.
- Some examples of PVD techniques are vacuum evaporation–deposition, electron beam physical vapor deposition, sputtering deposition, cathode arc (plasma) deposition and pulsed laser deposition.
- The Chemical Vapor Deposition (CVD) is a chemical process used to produce high purity solid materials with high performance. The process is often used in the semiconductor industry to produce thin films.
- The Chemical Bath Deposition (CBD) technique is the cheapest known technique for the preparation of films of various compounds (oxides, sulfides, etc.). It is based on direct deposition onto the chosen support of a compound produced from precursor species by means of chemical reaction(s). It is essential to check the temperature, pH and experimental conditions under which the compound of interest must be produced before its deposition. The films could be subjected to a heating treatment as a second step.

- The Thermal Oxidation and Anodic Oxidation is one way to produce a thin layer of oxide on the surface of water.
- The Electrophoretic Deposition (EDP). Colloidal charged particles suspended in liquid are forced by direct current (DC) in the electric field to move toward an oppositely charged electrode onto which they are deposited.

The technology, proposed in the present study must be designed for the production of building materials, and therefore, should be relatively cheap, available and combinable with the existing methods of producing construction materials. That is why the Sulfate Process combined with deep-coating and further calcination was chosen for the experiment. The list of the literature sources describing the influence of preparation conditions on the properties of the materials is presented below.

The synthesis based on water-soluble compounds allows producing both rutile and anatase TiO_2. Usually, low-temperature methods of titanium dioxide preparation (calcination of materials at 350-600 °C) produce anatase [58, 72], while high-temperature treatment provides the formation of anatase-rutile mixtures at 650-950°C or pure rutile at 950-650°C [75-77].

Furthermore, the presence of chemical supplements significantly changes the temperature of the anatase to rutile phase transformation. In [78] it was proved that the addition of SiO_2 increases the temperature of rutile formation to 700-800 °C. The presence of sulphates [79] and phosphates [80] increases the temperature of the transformation to 800 °C and more, while doping materials with zirconium can raise the temperature up to 1000 °C [81]. From the other hand, the presence of Mg^{2+} lowers the temperature of the phase transition [82].

The choice between the two main forms (powder and thin film) depends on the further use of the material. According to [83] achieving a successful commercial implementation of the photocatalysis technology will require to operate the photocatalyst in a manner consistent with the criteria and constraints of industrial implementation, whether they are the applications in the liquid phase or the gas phase. In the case of liquid-phase applications, TiO_2 suspensions have better efficiency than immobilized catalysts. In the case of photocatalytic applications in the gas phase, the problems can be solved by fixing the semiconductor photocatalyst on an inert support, because it could help to eliminate the costly phase separation process [83]. A lot of studies describes of the methods of deposition, properties of the immobilized semiconductors, various supports and requirements for them (silica gel, quartz optical fibers, glass fiber, glass beads [84], SiC foam, ceramics and ceramic foam [85], cellulose membranes, polymer films, etc [86,87]). In the present case the deposition targeted at the immobilization of TiO_2 on the surface of the support material retaining the photocatalytic properties.

1.4.3 Modified photocatalyst and Composite photocatalysts

The modification of photocatalyst is another method [88], which may take three main forms: bulk modification, surface modification, and the use of composite materials. The term bulk modification refers, for example, to controlling the phase of a photocatalyst or its electronic properties, usually by adding guest chemical species (ions, for most cases) into the bulk of a photocatalyst. Surface modification is manifested by altering the properties of the surface of the photocatalyst, for example, the surface area, affinity toward chemical

species and surface electronic properties. These properties may be altered with or without using chemical species that are removed at some stage of the preparation procedure.

Composite photocatalysts are defined as materials comprising of active titanium dioxide domains in close proximity to domains made of inert compounds or other photoactive compounds. Here, the major difference between composite photocatalysts and bulk-modified photocatalysts is the formation of a segregated phase in the former case.

The latter method is particularly interesting for the study, since it focuses on the obtaining of such modified composites. One of these types consists of composites made of an inert skeleton onto which titanium dioxide is coated, for example, composite membranes made of a porous alumina skeleton onto which mesoporous TiO_2 was grown by the sol–gel method using a mixture of titanium isopropoxide, acetic acid, and a surfactant (Tween 80). Another type of a composite photocatalyst consists of two (or more) domains, both of which are exposed to the outer environment so that the non-TiO2 domains serve as part of the photocatalytic process. The examples include a partial coverage of activated carbon with titanium dioxide (by atomic layer deposition or by physical contact) and structures made from titanium dioxide and inert oxides such as zeolites. Of specific interest are composites made of titanium dioxide substrate, onto which islands of inert materials are grown. In this context, of particular interest are nanoislands of noble metals (such as platinum, gold, and silver). These nanoislands can be easily formed from a variety of metallic complexes, for example, chloroplatinic acid, hexahydroxyplatinic acid, platinum dinitrodiammine, in many cases by the photoassisted reduction process [88]. The mentioned publication is interesting in terms of choosing a method as it presents a review with the analysis of end products of this or that impact. The addition to it may be [39], where the impact of modification on the change of dioxide titanium composite properties is considered.

The Preparation of Composite Photocatalysts The consideration of publications in scientific information points out that composite photocatalyst obtaining is a separate area in the synthesis of photocatalysts. The use of different carriers allows adjusting a porous structure providing molecular sieves to the properties of materials. In [89] it was shown, that selective photocatalysis can be obtained through the use of proper molecular sieves (titanosilicate ETS-10) as shape-selective heterogeneous photocatalysts. This activity is due to the presence of photo-excitable Ti-O-Ti chains in its structure, and of a three-dimensional interconnected system of large 12-membered SiO_4 ring channels, which endow the material with excellent diffusion properties. This regular channel system (not present in bulk metal oxide semiconductors, such as anatase) has a direct effect in determining the shape selectivity of the degradation process, and this has represented the main achievement of our previous studies on the photodegradation of phenols of different sizes. Also, the deposition of titanium dioxide on the porous aluminium foil provided the formation of mesoporous structure [87]. Besides that, carbon nanotube [90], carbon nanofibers [91] or ongraphite rods [92] can be used as supports.

However, the present study focuses on the supports based on SiO_2 and Al_2O_3, as well as the interaction between these oxides and TiO_2. In the 1980s, Anpo et al. investigated TiO_2/SiO_2 and TiO_2/Al_2O_3 composites, obtained by the methods of co-deposition and coating [93-101]. The obtained samples [95-96] were investigated for the reactions of

hydrogenolysis of methylacetylene ($CH_3C{\equiv}CH$) for SiO_2, and propylene ($CH_3HC{=}CH_2$) for Al_2O_3.

The significant increase of photocatalytic activity was proved. Subsequently, the topic was expanded and included the issues of preparation methods, particle sizes, etc. [101]. The interest to this area has remained high over a few decades [102-108].

1.4.4 Clays as carriers of TiO_2

Clay minerals are one of nature nanosystems, containing both SiO_2 and Al_2O_3. The use of some clays for the preparation of composite photocatalysts is studied quite well. For example in [109] the adsorption capacity and photocatalytic removal efficiency of formaldehyde using a hectorite-TiO2 composite in a bench flow reactor was investigated. The same experimental conditions were applied to pure TiO_2 (Degussa P25) as a reference. The catalysts were irradiated with either a UVA lamp (365 nm) or with one of two UVC lamps of 254 nm and 254 + 185 nm, respectively. It was shown that the saturation of catalyst surfaces was achieved after approx. 200 min for P25 and approx. 1000 min for hectorite-TiO_2. In [110] Composite photocatalysts were prepared by incorporating a microfibrous palygorskite clay mineral and nanocrystalline TiO_2 into glass substrates via sol–gel route at 500 ◦C. The synthesis involves a simple chemical method employing nonionic surfactant molecule as a porous directing agent along with the acetic acid-based sol–gel route without a direct addition of water molecules. These materials were tested as new photocatalysts in the photo-discoloration of Basic Blue 41 azo-dye in water and promising results were obtained. In addition, the photodegradation of orange II by TiO_2 supported on three adsorbents namely MCM-41. Montmorillonite and β-Zeolite was studied under different conditions [111]. The surface properties of the catalysts varied with the solution of pH and a strong adsorption of orange II occurred at low pH, while the maximum photodegradation rate occurred at an optimum pH range of 4–5 for the supported catalysts as compared to 2.5 for the unsupported TiO_2 (Degussa P25). Although the adsorption and subsequent photodegradation of orange II were better for the supported catalysts compared to the unsupported TiO_2 , complete mineralization occurred only in the presence of a small amount of ozone, but with lower power consumption as compared to Degussa P25.

In this study, montmorillonite and kaolinite were used as supports. It is a common knowledge that the surface of kaolinite does not have a developed porous structure, but the proposed method combining high-temperature calcination and chemical treatment with concentrated acid allows affecting the structure deeply. This method was proposed in the 1970s and 1980s [112]. Therefore, the properties of carrier materials should be investigated better. There are lot publications of research results of clay modification. The detailed and systematic examination of clays, their composition, properties and methods of the treatment is represented in [113].

F. Bergaya, G. Lagaly [114] basing on the review define clay minerals as:

"The term 'clay mineral' is difficult to define. As a first approximation, the term signifies a class of hydrated phyllosilicates making up fine-grained fraction of rocks, sediments, and soils. The definition that the JNCs proposes is "phyllosilicate minerals and minerals which impart plasticity to clay and which harden upon drying or firing"

The common properties are:
1. a layer structure with one dimension in the nanometer range; the thickness of the 1:1 (TO) layer is about 0.7 nm, and that of the 2:1 (TOT) layer is about 1 nm,
2. the anisotropy of the layers or particles, 3. The existence of several types of surfaces: external basal (planar) and edge surfaces as well as internal (interlayer),
4. the ease with which the external and often also the internal surface can be modified (by adsorption, ion exchange, or grafting),
5. plasticity,
6. hardening on drying or firing ; this applies to most (but not all) clay minerals.
The structures of kaolinite and montmorillonite may be described as follows:

- Kaolinite is a serpentine-kaolin group mineral (structure 1:1 – one tetrahedral sheet for each octahedral sheet); the idealized formulae is $(Si_2)^{IV}(Al_2)^{VI}\ O_5\ (OH)_4$; the layer charge - 0
- Montmorillonite refers to a smectite group (structure 2:1 – two tetrahedral sheets of silica sandwiching a central octahedral sheet of alumina); the idealized formulae is $(Si_4)^{IV}(Al_{2-y}\ Mg_y)^{VI}\ O_{10}\ (OH)_2$, $yM^+.nH_2O$; the layer charge is 0.2-0.6.

See Figure 1.5 for the general appearance of both structures [115, 116].

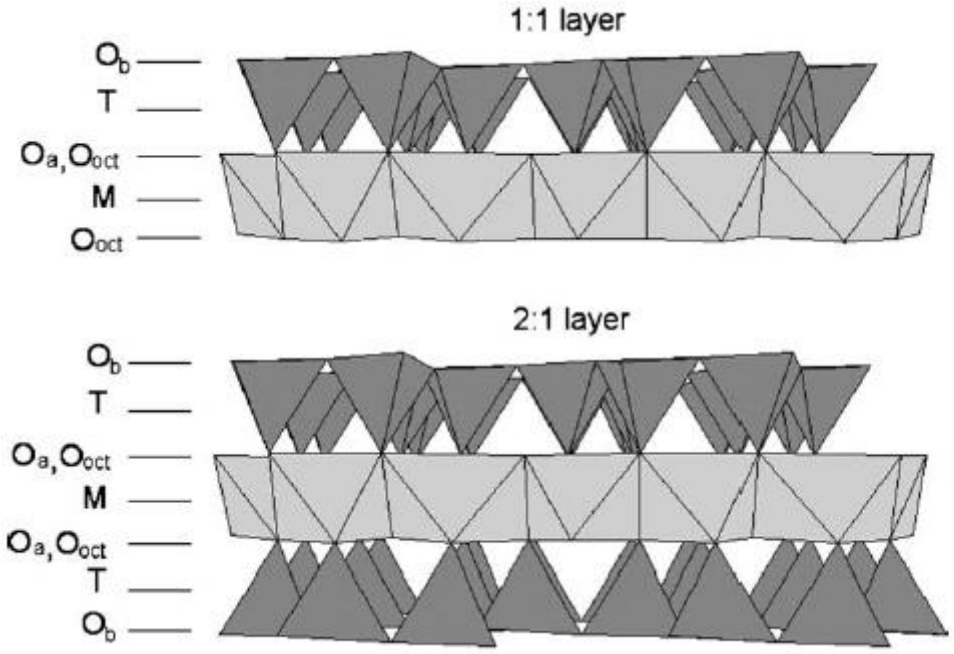

Figure 1.5. The models of the 1:1 and 2:1 layer structure. Oa, Ob, and Ooct refer to a tetrahedral basal, tetrahedral apical, and octahedral anionic position, respectively. M and T indicate the octahedral and tetrahedral cation, respectively [115]

The differences between the structures are responsible for the differences of properties, including adsorption capacity, surface structure, the extent and type of defect sites, layer charge and the type of exchangeable cation(s), and the ability of montmorillonite to adsorb large amounts of water [117].

Another important aspect is the interaction between clays and mineral acids [118, 119.] and thermal treatment [120].

The treatment of clays with strong inorganic acids is frequently called "acid dissolution" or "acid activation" of clays. Depending on the extent of acid activation, the resulting solid product also contains unaltered layers and amorphous three-dimensional cross-linked silica, while the ambient acid solution contains ions according to the chemical composition of smectite and acid used. The above-mentioned review shows the influence of acid treatment on the properties of obtained materials, e.g. specific surface (increasing up to 400 m^2) and dissolution of a material depending of the original structure.

The L. Heller-Kallai [120] includes a detailed analysis of the influence of thermal treatment in the range from 60 °C to 1000 °C (even up to 1500 °C) on the phase contents, porosity and specific surface.

Therefore, the clays were chosen as a carrier material for TiO_2 because of their ability to form porous structure after a thermo-acid treatment. It should be emphasized that there are studies describing photosensitivity of pure and untreated clays.J. Li *and al.* [121] showed that montmorillonite KSF induced the photodegradation of chloroform under a black light lamp (λ= 365 nm) by producing hydroxyl radical (•OH) that oxidized chloroform in heterogeneous clay–water systems. However, this effect was not noticed during these studies.

1.4.5 The using of Fly Ash as TiO_2 carrier for possible waste utilization

In recent years, many studies were dedicated to implementing the concept of removing waste by using another waste. As, for example, these applications are used for water treatment ("green" materials, such as coconut shells, orange peels, sawdust, etc.) [122], producing activated carbon (bio-waste precursors) [123] and other adsorbents (quartz) [124] and the preparation of biodegradable thermal and sound insulation materials (waste wool and recycled polyester fibers) [125]. The studies of the adsorption properties of fly ash and its possible use as a support for active materials describe such innovations.

Energy production based on solid, carbon-based fuels was long ago recognized to pose huge environmental problems through gases released in atmosphere and the solid byproduct - ash. Thus, special attention was devoted to identifying various effective paths to use ash, mainly as construction material, [126] by partially replacing sand in concrete [127]. This attention is due primarily to the fact that fly ash as has to be recycled, given that it is a harmful waste. Since a wide scale coal firing for power generation began in the 1920s, the worldwide production of ash and by-products amounted to hundreds of megatons. The largest part of produced fly ash is disposed to landfill, which is under pressure because of environmental consequences. In fact, the disposal of fly ash will soon be too costly if not forbidden [128].

Fly ash is primarily silicate glass containing silica, alumina, iron, and calcium. Minor constituents are magnesium, sulfur, sodium, potassium, and carbon. Crystalline compounds are present in small amounts. The relative density (specific gravity) of fly ash generally ranges between 1.9 and 2.8 and the color is generally dark to light grey[129].

Ash results as coarse grains are removed from the bottom of the furnace (bottom ash) and as fine particles are captured by the electrofiltre from gaseous exhaust (fly ash, FA). The

more detailed classification of fly ash is based on the activity and cementitious properties ([129]):
Class N Tuffs and volcanic ashes or pumicites;
Class F Fly ash with pozzolanic properties
Class C Fly ash with pozzolanic and cementitious properties
Class F and Class C fly ashes are commonly used as pozzolanic admixtures for general purpose. Concrete Class F materials are generally low-calcium (less than 10% CaO) fly ashes with carbon contents usually less than 5%, but some may be as high as 10%. Class C materials are often high-calcium (10% to 30% CaO) fly ashes with carbon contents less than 2%. Many Class C ashes when exposed to water will hydrate and harden in less than 45 minutes. Some fly ashes meet both Class F and Class C classifications [129].
Nowadays, there are many innovation technologies, determined to re-use fly ash. First, the material is widely used in concrete production [130]. Another possible option is involving fly ash in soil re-cultivation process [131].
Finally, fly ash can be used as a component and raw for adsorptive materials producing.
According to [132] fly ash is a moderate adsorbent and has the disadvantage of a variable composition, depending on the coal composition, the burning process and the burning furnace. Therefore, the goal of many studies is developing fly ash modification as a more reproducible substrate, with increasing the surface area and charge [130]. Fly ash with optimized surface properties was reported as an efficient adsorbent for anionic [133] or organo-reactive dyes [134]. A step forward was done when using fly ash in hydrothermal syntheses for obtaining zeolites or zeolite-type structures, which proved to be highly efficient in dyes adsorption [135]. The addition of various inorganic compounds allowed tailoring the adsorbent properties [136], while the addition of cationic surfactants led to substrates with improved adsorption efficiency [137].
The heterogeneous photocatalysis emerged as promising alternatives to the current wastewater treatment for recalcitrant pollutants removal using modified fly ash [138] and fly-ash grains/cenospheres [139,140.]. These materials use fly ash as an inert substrate for the photocatalysts deposition. Some authors show the results which indicate to an unfortunate experiment of using a substrate from fly ash. [141]. However, there are other more promising experiences where the fly ash – TiO_2 mixture is efficient in simultaneous adsorption and photocatalysis. [142, 143].
Probably, the method of preparing composites will play a significant role.

1.4.6 Nonmetal co-doping as a way of surface sensitization for visible light strategies

The use of UV-irradiation in accommodations is undesirable and often unacceptable which makes it difficult to use the photocatalytic for the passive degradation of indoor pollutants. The large band gap of TiO_2 (~3.2 eV for anatase and brookite and ~3.0 eV for rutile) limits photoabsorption to only the UV region. Even for outdoor conditions where the use of solar light is available, only ~5% of the solar flux incident at the earth's surface lies in this spectral region [144].
Therefore, the development of methods for obtaining composites able to photochemical activity under visible light is an important part of this study. Designing, fabricating and tailoring the physicochemical and optical properties of TiO_2 is of great importance for

utilizing a large fraction of the solar spectrum. For this purpose, TiO_2 is modified by various strategies such as surface sensitization by organic dyes or metal complexes, coupling a narrow-band-gap semiconductor, nonmetal doping or co-doping and noble metal deposition [144].

The mechanisms are described in detail by [145] (Fig. 1.6). The authors cite the following methods of preparing visible-light sensitive semiconductors as examples:

- Narrowing the band-gap metal oxide semiconductor. Since the energy level of VB for metal oxides is governed by that of the O-2p orbital, a narrow-band-gap metal oxide semiconductor, such as WO_3, possesses conduction band energy lower than that of TiO_2.
- Doping with anions. Since the energy level of VB has sufficient oxidation ability, shifting the valence band by doping the N or S anion allows producing the mid-gap level. Photogenerated holes produced on the donor level are expected to have an oxidation ability similar to that of bare TiO_2.
- The deposition of sensitizers. In this case, the deposited compound absorbs visible light and transfers the excited electron to produce a cation radical which can oxidize organic pollutant molecules.
- The interfacial charge transferred absorption originating from the excitation of VB electrons to a deposited (or grafted) metal. The deposited compound has a catalytic ability of O_2 reduction, the efficiency is expected to be increased.

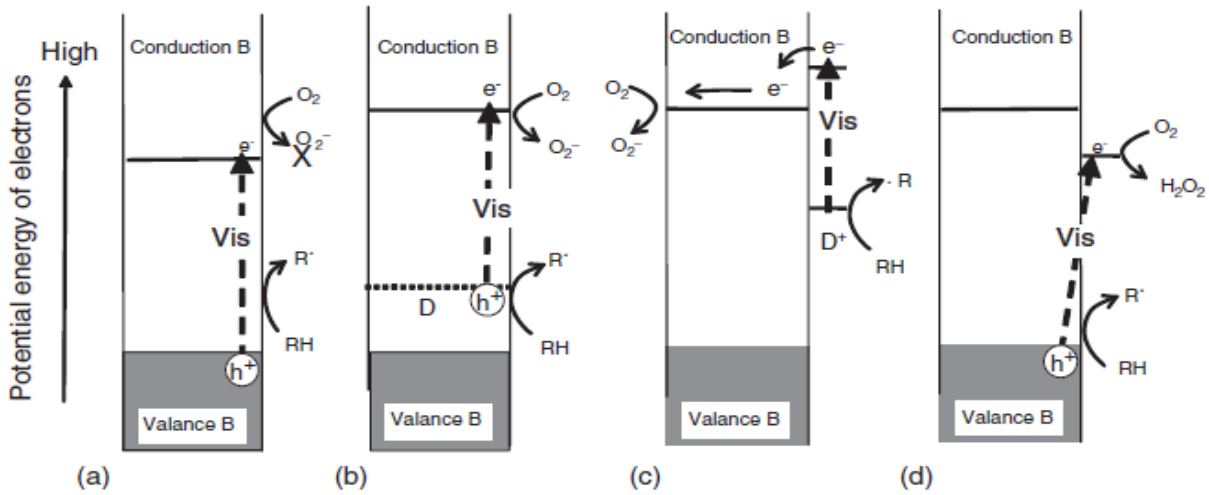

Figure 1.6 The classification of visible-light responsive photocatalysts by the mechanism of reaction: (a) a narrow-band-gap semiconductor such as WO_3, (b) an anion-doped TiO_2 such as nitrogen-doped TiO_2, (c) a sensitizer-deposited TiO_2 such as $PtCl_6^{2-}$-deposited TiO_2, and (d) an interfacial-charge-transfer-type TiO_2 such as Cu(II)-grafted TiO_2 [145]

However, there are different views on strategy for visible light utilizing. For example, the authors [146] analyzed some publications about the sensitivity of modified materials to visible light and expresses doubts about the given results.

The non-metal doping (or co-doping, given the presence of sulfur and silicon in the composites) was chosen for the study. Co-doping is to modify the photocatalyst with two dopants (metal/nonmetal or nonmetal/nonmetal). Co-doping with two or more suitable heteroatoms can achieve substantial synergistic effects.

In principle, the strict requirements for the nonmetal dopant are as follows [144]:

(i) the electronegativity of the selected nonmetal dopant must be lower than that of oxygen and (ii) the nonmetal dopant as a substitutional lattice atom should have a radius commensurate with that of the lattice O atoms so that the dopant atoms can realize a uniform distribution within the whole host matrix.

A lot of studies describe the methods of obtaining nonmetal doping materials, including [147].

There are three different main opinions regarding the modification mechanism of TiO_2 doped with nonmetals: (1) band gap narrowing; (2) impurity energy levels; and (3) oxygen vacancies [148]:

1. Band gap narrowing: N 2p states and O 2p states intersect in anatase TiO_2 doped with nitrogen because their energies are very close, and thus the band gap of N-TiO2 is narrowed and able to absorb visible light.
2. Impurity energy level: It was stated that TiO_2 oxygen sites substituted by nitrogen atom form isolated impurity energy levels above the valence band. Irradiation with UV light excites electrons in both the VB and the impurity energy levels, but illumination with visible light only excites electrons in the impurity energy level.
3. Oxygen vacancies: It was concluded that oxygen-deficient sites formed in the grain boundaries are important for visible light-activity and nitrogen doped in part of oxygen-deficient sites are important as a blocker for reoxidation.

This review [148] surveys methods and practices of non-metal doping. The conclusion is materials are prepared by at least one of the methods comprising substituting anions X for some oxygen sites of titanium oxide crystals, a method comprising doping anions X between lattices of a titanium crystal and a method comprising doping grain boundaries of titanium oxide, or a combination of these methods. Anion X is an element selected from B, C, P, S, Cl, As, Se, Br, Sb, Te, or I, or a molecule containing at least one of these elements.

Three doping agents were chosen for the experiment:

1. Nitrogen. This element was one the first dopants, [149,150] and is still widely used for various goals [151,152]. This element is effective for doping TiO_2 because of such factors, as its atomic size (which is comparable to the size of oxygen), small ionization energy, metastable center formation and stability [153]. The substitution of nitrogen alters both the electronic properties and the surface structure of TiO_2, where the former determines the light response range and redox power of carriers and the latter controls the surface transfer of charge carriers.
2. Chlorine. Chlorine is known as the doping agent almost as well as nitrogen [154,155].
   The results of [156-158] show that the presence of chlorine efficiently decreased the band gap of TiO_2, and extended the absorption spectrum. The doped TiO_2 exhibited strong absorption in visible light range and the doping by Cl recognized as a valid method of the titanium dioxide modification. Xu et al.[159] prepared a Cl-doped rutile

TiO_2 photocatalyst via a soft interface method and found that it has a high potential for environmental pollutant removal as well as in solar cell applications.

3. Phosphorus. Compared with other elements phosphorous can significantly increase the specific surface area of TiO_2 and prevent the phase transformation from anatase to rutile resulting in high photocatalytic activity [148,160]. The change in surface chemistry by the introduction of phosphorous can be used to engineer the properties of titanium for catalytic applications and for organic chemical transformations. P–TiO_2 exhibited excellent thermal stability by retaining anatase phase even at high calcination temperature (500–900°C). The presence of phosphorous species on grain boundary suppressed the particle growth during calcination and stabilized the anatase phase [161]. Anatase formed during hydrolysis acts as crystallization seed leading to the transformation of amorphous titania to anatase at a lower temperature with high resistance to sintering than the amorphous sample. This may be a probable reason for a superior thermal stability of P–TiO_2.

In conclusion, it is worth noting the potential of sulfur as a doping agent.

In [162] chemically modified titanium dioxide photocatalysts in which S (S^{4+}) substitutes for some of the lattice titanium atoms were synthesized. They show strong absorption for visible light and high activities for degradation of methylene blue, 2-propanol in aqueous solution and partial oxidation of adamantane under irradiation at wavelengths longer than 440 nm. The oxidation state of the S atoms incorporated into the TiO_2 particles is determined to be mainly S^{4+} from X-ray photoelectron spectra (XPS) spectra. Also, the biocidal activity of S–N–TiO2 for E. coli inactivation was attributed to interstitial nitrogen doping and substitutional sulphur doping both at Ti4+ and O2− sites [163]. S–N–TiO_2 nanotube array prepared by two - step electrochemical anodization methods showed higher photocurrents and faster MB degradation under visible light compared to undoped TiO2 nanorod array films as a result of improved charge carrier separation [164]

Hence, the development of the composite preparation technology proposed by this study can include the methods for obtaining materials sensitive to visible light.

1.5 The modern applications of TiO_2-containing materials

Photoinduced processes are studied in manifold ways and various applications have been developed since their first description. Despite the differences in the character and utilization, all these processes have the same origin. Semiconductors can be excited by light with higher energy than the band gap, and an energy-rich electron–hole pair originate. This energy can be used electrically (solar cells), chemically (photochemical catalysis), or to change the catalyst surface itself (super hydrophilicity [39]. The photoinduced phenomena is represented in Figure 1.7.

While the importance of each individual area of the photoinduced phenomena application is indicated by an increasing number of publications, a much more importance of photocatalytic reactions is reflected in the increasing number of publications that deal with theoretical aspects and practical applications of these reactions. According to [39] the publications on the investigation of photocatalytic reactions represent approximately one third of those issued on the photoactive materials over the past 20 years. Since the purpose

of this study is the obtaining of components for building materials, able to photoinduced passive degradation of indoor pollutants, only few of a large amount of the publications will be considered in the following section.

Regarding organic synthesis is the application of photocatalysis for Solar Energy Conversion. Interesting publications are represented in the book "New and Future Developments in Catalysis. Solar Photocatalysis", which was published under the editorship of Steven L. Suib. For example, [165] describes integrated solar systems (Figure 1.8), where sunlight is used for obtaining hydrocarbon fuel from CO_2 and water vapor, as well as for obtaining hydrogen (an energy carrier) by water photo-splitting, glycerol or biomass photoconversion. The authors [166-168] also describe this area.

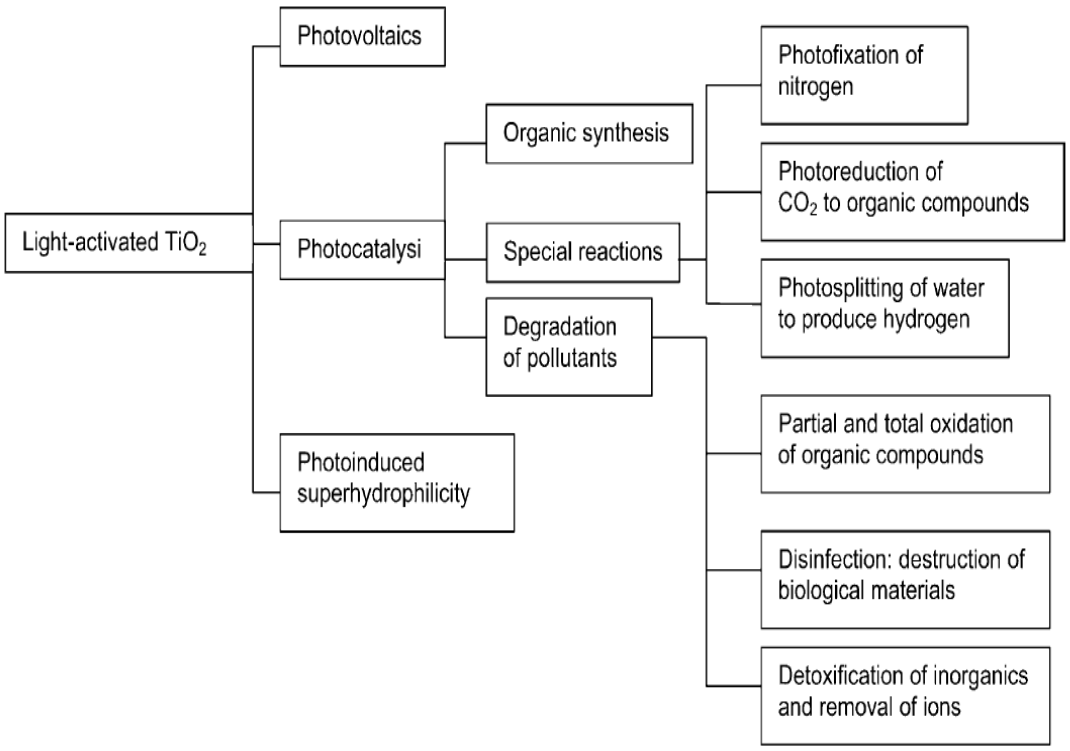

Figure 1.7 The areas of applying titanium dioxide and materials containing it based on the photoinduced phenomena [39]

During the organic synthesis, photocatalytic process can be used both in combination with other processes or independently in the aquatic environment [169]. For example, integration of photocatalysis with a membrane separation process permits the recovery of valuable intermediate compounds (aromatic aldehydes) [170].

At the same time heterogeneous photocatalysis and ozonation allows enhancing synergistically the oxidation capabilities during oxidation processes (AOPs) of waters contaminated by organic pollutants and containing also innocuous bromide ions and avoids the formation of nocuous bromate ions [171].

The area of pollutants degradation is represented by wastewater treatment and air purification. The application of the photocatalysis for wastewater treatment is described in the monography published in 2013 under the editorship of P. Pichat [172], and in the mentioned above New And Future Developments In Catalysis [173,174].
The methods of air purification are described in Paragraph 1.1. At present, the scope of applications extends including such important areas as decomposition of chemical warfare agents [175] and life-support systems of space vehicles [176]. This is the reason why the production of TiO_2-containing photoactive materials is expanding. Among other semiconductors with photoactive properties, TiO_2 ones are characterized by such qualities as photochemical and chemical stability, high activity under natural or artificial light, relatively low cost, availability, absence of chemical and biological toxicity [39].

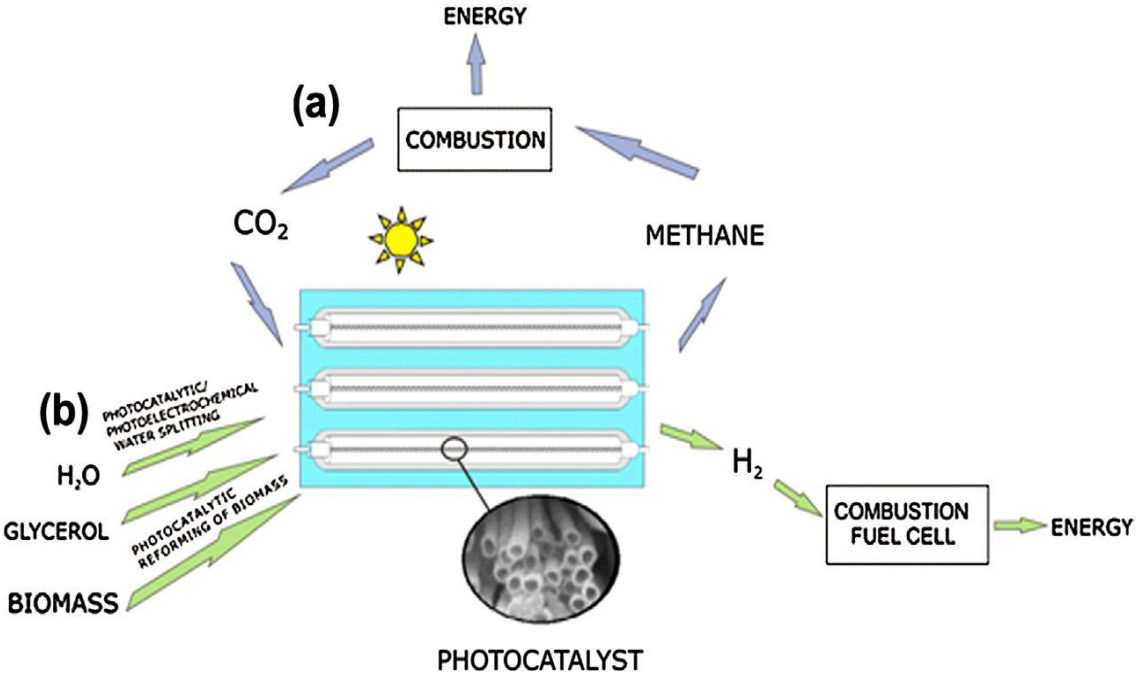

Figure 1.8 The depiction of integrated solar systems where sunlight is used: (a) to convert CO_2 and water vapor into hydrocarbon fuels; and (b) to produce hydrogen (an energy carrier) by water photosplitting, glycerol or biomass photoconversion [165]

At present, many materials based on titanium dioxide are produced on a commercial scale. "Degussa P25" (the specific surface is 50 m^2/g, the composition is 70 % anatase + 30 % rutile) and "Hombifine N" (330 m^2/g, the composition is 100 % anatase) are most used for studies. [177]. Depending on the area of the study and the requirements for the material, methods for preparing, improving and developing, for obtaining of both pure and composite TiO_2-containing materials may differ. These methods are represented in various literature sources. [2, 39, 148, 165].

Such areas as energy and synthesis have stringent requirements in terms of the activity, presence and amount of additives, composition, surface morphology, etc. The requirements for construction materials might be softened.

Environmental malodorous species in air both indoors and outdoors are typically present in very low concentrations, even when human sensitivity feels a very strong smell, [2] and dozens of various compounds are classified as pollutants. Therefore, photoactive components should have a low selectivity, be effective in lower concentrations, retain their properties without deactivation for a long time, and have a UV-sensitivity in normal conditions. It is desirable that their producing could be combined with producing construction materials.

This study offers the method for the composite material synthesis, which is the chemical deposition of TiO_2 on the clay matrix from sulfate solution. Relatively cheap and available materials were used during the preparation: the waste of mechanical processing of titanium (titanium shavings) for obtaining the precursor, montmorillonite and kaolinite as supports. The analysis of the literature sources allows assuming that such method produces the composite with a large specific surface area because of thermo-acid activation and high photoactivity enough for indoor conditions. These properties are confirmed by the experimental data for the obtained samples. The relative simplicity of technology allows organizing industrial production of the materials and possible upgrades of the method. Among the disadvantages of the method is the use of sulfur acid and the need for vapor and sulfate oxide capture.

2. Characterization of materials and definition of methods

2.1. Introduction

The present study was carried out as a part of the research programs of the Department of Materials, Environmental Sciences and Urban Planning of Università Politecnica delle Marche (SIMAU UNIVPM). *The purpose of the project is the development of construction materials able to a passive reduction process thank to adsorption and catalytic process.*
A new method of obtaining TiO_2 with further deposition of photoactive components on clays adsorbents was proposed during the MISE CRUE "CATACLEAN- Catalytic reaction for self-cleaning furniture panel" project (2009-2011) carried out by the Department SIMAU UNIVPM and by the Chemical Technology Department of the Lipetsk State Technical University (LGTU) (the author was involved as an LGTU student).
The first samples were obtained with clay (85% of kaolinite + 15% montmorillonite)/precursor ($Ti+H_2SO_4$ solution) ratio of 1:10 at the temperature of calcination of 600 °C. The titanium content was 30 mg/g, and the composites demonstrated UV-sensitivity [6]. However, such disadvantages as an irritating effect of sulfate dust and a high consumption of sulfuric acid were revealed immediately. Therefore, the aim of the experiment was studying the effect of the reduced amount of the precursor on the properties of the materials.
In the present study, TiO_2-containing materials were prepared under various conditions (different clay matrix/precursor ratios and temperatures of calcination, the addition of doping additives) and tested for UV-sensitivity, given that it is planned to use composites as components for building materials to enhance the effect of passive degradation of pollutants in the air.
Therefore, the study includes the following steps:

1. The preparation of the samples of composite materials;
2. The analysis of the chemical composition;
3. The characterization of surface morphology, average particle size and phase composition of the samples;
4. The examination of water and benzene vapor-phase adsorption, measurement of the specific surface area of the materials and the pore structure parameters;
5. The examination of the material photosensitivity.

The research methodologies of the every step are described in details below.

2.2. The method of producing the titanium-containing materials

The composite TiO_2-containing materials were prepared by hydrolysis of titanium salts with further deposition of titanium dioxide on the surface of the adsorbent (relatively cheap, aluminosilicate materials). The preparation of multi-layered TiO_2-SiO_2 composites on each other [102-104, 178, 179] leads to the formation of a strong bond between the layers due to the similar chemical structure of the oxide surfaces.
In addition, the application of the H_2SO_4 solution of titanium suggests that the effect of acid may improve adsorption properties of the samples (the so-called acid activation), while the residue of sulfur in theTiO_2-layer can serve as a doping agent.

The preparation consists of the following steps:

- The preparation of the precursor (titanium sulfate solution);
- The preparation of the support material with the average particle size <10 μ by sedimentation;
- The mixing of a clay matrix with the precursor and further drying of the sample;
- The calcination of the sample at the 600-750 °C during 30 minutes.

In the ***first stage***, titanium shavings (powder < 1 mm was used in the laboratory, while machining titanium swarf was applied to design the process flow diagram – Figure 2.1, a) were dissolved in concentrated sulfuric acid in the ratio of 1 g of Ti per 6 ml of 95% H_2SO_4. The ratio was chosen in 2010 assuming that sulfuric acid should completely cover titanium shavings while excess acid provides more effective dilution of the metal. After a few hours, the solution turned a blue color, which indicates the occurrence of ion Ti (III). Ions are formed in accordance with the following reaction (Eq. 2.1):

$$2Ti + 6H_2SO_4 \leftrightarrow Ti_2(SO_4)_3 + 3SO_2 + 6H_2O \quad (2.1)$$

The ultra-sonic bath "Bandelin SONOREXTM Super RK 255H" was used for the intensification of the dissolving process. After 4-5 hours of dissolution, the significant amount of titanium (90% for powder, 60% for shavings) dissolves, water is added to the solution resulting in the formation of aqua complex $[(H_2O)_6]^{3+}$ (see Figure 2.1, b), which makes the solution purple (Eq. 2.2, Eq. 2.3):

$$Ti_2(SO_4)_3 + 12H_2O \leftrightarrow 2[Ti(H_2O)_6]^{3+} + 3SO_4^{3-} \quad (2.2)$$

$$Ti_2(SO_4)_3 + 6H_2O \leftrightarrow 2Ti(OH)_3 + 3H_2SO_4 \quad (2.3)$$

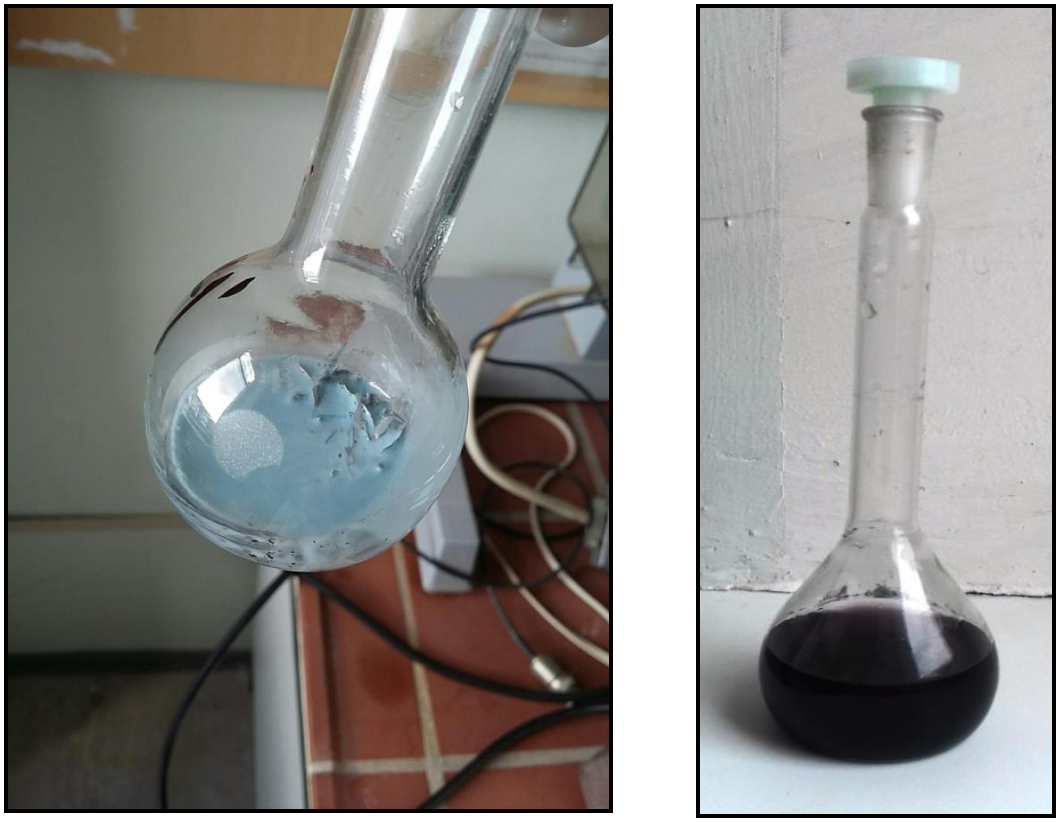

a) b)

Figure 2.1. The stage of the precursor solution preparation: a)- the dissolution of titanium in sulfuric acid; b)- the precursor after hydrolysis

Further, the solution was filtered through acid resistant filters. In order to calculate the amount of the precursor for the mass of the support, the titanium content in the precursor was detected analytically (Sec. 2.3) or was estimated after weighing the undissolved residue.

At the ***second stage***, sedimentation was used for obtaining adsorbent (clay or fly ash) materials [180,181]. The ground samples of montmorillonite (Fluka AG), kaolinite (Industria Chemica Carlo Laviosa), and fly ash (from energy plant burning corn-cobes) were mixed with water and boiled during one hour to provide lump disaggregation. After cooling to ambient temperature, the obtained suspension was placed into graduated cylinders and diluted by water in the ratio 1:15. The temperature of water was 20 °C. The mixtures were intensively mixed, then settled for 18.5 minutes. After that, the upper layers (10 cm from the surface) were decanted and dried in an oven at 115 °C. The clays were ground and sieved through a sieve with the hole size of 0.25 mm. The average particle size of the obtained carrier materials did not exceed 1 μm.

The fly ash sample was sieved through a sieve with the hole size of 0.16 mm and then dried in an oven.

At the ***third stage***, the sample was mixed with acid solution in a ceramic basin. The mixture was dried in a fume cupboard during 2 hours, and then water was evaporated in a sand bath. The matrix/precursor ratio varied for different samples.

The ***fourth (final) stage*** included calcination of the samples in a muffle furnace at various temperatures (600 °C and 750 °C). The specimens were dried at 110 °C (solid sediments had gray-lilac shade), then they were calcined during 30 minutes. At first the temperature of 600 °C was chosen based on the information search, as thermal treatment was to ensure $Ti(OH)_4 \rightarrow TiO_2$ transformation. Sulfuric acid treatment was chosen because this method used to obtain the anatase form of TiO_2, according to the literature [182-184]. The presence of SiO_2 increases the temperature of transforming anatase to rutile up to 700-800 °C [185]. Therefore, the calcination temperature of 750 °C also was chosen for the preparation of materials in order to reduce the content of sulfur.

The processing time also affects the transformation of anatase [186]. The duration of heat-treatment was determined as 10-15 minutes after a complete removal of volatile compounds from the materials and, therefore, 30 minutes for 1-5 g samples. The obtained materials were white or , in case of the samples prepared at 750 °C, yellowish-white. These colors indicate the formation of a TiO_2-film.

During the heat-treatment of the materials, titanium hydroxide of Ti (III) and its salts are gradually oxidized by air (Eq. 2.4, 2.5)

$$2Ti(OH)_3 + O_2 + 2H_2O \leftrightarrow 2Ti(OH)_4 + H_2O_2 \quad (2.4)$$

$$Ti(OH)_4 \rightarrow H_2TiO_3 \rightarrow TiO_2 \quad (2.5)$$

After calcination, the samples were cooled in a desiccator, then ground and sieved through a sieve (the hole size is 0.09 mm). The samples are stored in sealed vials in air-dry conditions.

In order to examine the impact of sulfuric acid on the clay materials, two samples there were prepared without titanium deposition at the second stage. The concentration of acid solution is based on steheometry reactions. It should be noted that concentration is higher during the preparation of titanium-containing samples, given that the additional amount of acid is formed during hydrolysis.

2.3. Materials

For the preparation of the precursor there was used the industrial titanium VT1-00 (BT1-00, national RF standard GOST 19807-91 "Titanium and titanium alloys. Stamps." (Tab.2.1) and sulphuric acid (concentration is 98%, from J.T.Baker®). During the preparation of doped samples, standard solutions of H_3PO_4, HNO_3 and HCl were used.

Table 2.1. The chemical composition of titanium VT1-00 (% wt).

Ti	Fe	Si	C	N	O	H	Impurities
99.58-99.9	0.15	0.08	0.05	0.04	0.1	0.008	0.1

As carrier materials for the preparation of TiO_2-containig samples there were used montmorillonite K-10 from Fluka AG and kaolinite from Industria Chemica Carlo Laviosa and non-commercial fly ash biomass from energy plant burning corn-cobes (USA).
All chemical reagents are analytical (AR) grade and all aqueous solutions are prepared with distilled water.
In order to compare UV-sensitivity of the composites with the known material, Degussa (Evonic) P25 was also used.

2.4 Analytical control devices

The following analyses were performed :

- The analysis of the titanium-containing precursor
- The analysis of the obtained Ti-contained composites
- The analysis of the methyl ethyl ketone (MEK) content in the air of the reactor.

The analysis of the titanium-containing precursor. The composition of the solution was examined by the method of optical emission spectrometry, which was performed by the ICP-OES Spectrometer Optima 8300
The analysis of the obtained Ti-contained composites.
In order to study the composition of the obtained materials, the method of SEM-EDXA was used. These analyses were performed with the Scanning Electron Microscope FESEM ZEISS SUPRA 40. The characteristics of the equipment are the following:
Source – field emission (EGF) Schottky
Acceleration voltage: 0.1-30 kV
Secondary electron detector Everhart-Thornley type
Detector of secondary electrons in the-lens
Detection of backscattered electrons in the solid state at 4 sectors
System for X-ray Microanalysis Bruker Quantax 200-Z10 SDD detector with liquid nitrogen
CCD camera with IR illumination to visualization in the indoor conditions
Magnifications: 12x - 900.000x
This unit allows performing both types of tests, which greatly simplified the study at that stage.
In addition, the amount of titanium dioxide in the samples was determined by emission spectral analysis. For this purpose, the photovoltaic system Emission spectrometer MFS-8 with registration of the spectra on the CCD-lines was used.

The GSO 7177-95 and GSO 7125-94 were used as a standard sample. The characteristics of the spectrometer are represented in Table. 2.2.

Table. 2.2 The characteristics of the spectrometer.

Characteristics of the item	Values
Excitation source	UGE-4
Discharge mode	AC electric arc
Amperage of the discharge	5 A
Material of reference electrode	Graphite, copper
Electrode spacing	1,5 mm
Duration of sparking	5 s
Duration of exposure	10 s
Duration of integration	200 ms

The infrared spectrophotometer IRAFFINITY-1 ("Shimadzu") was applied in order to affirm the presence of doping agents. The samples were preliminarily thermally processed in order to remove water and grounded. After this, the nujol suspension was prepared.

The analysis of the methyl ethyl ketone (MEK) content in the air of the reactor.

MEK content inside the reactor was determined by the chromatograph GC8000 Top (CT instruments) The analysis was performed under under the following conditions: the temperature range – 80-220 °C, the rate of heating 15 °C/min. The method of the internal standard (hexadecane was chosen as a standard substance) was used for the analysis. The analytical column ULTRA 1 (crosslinked Methyl Silicone Gum, 25m x 0,32mm x 0,52μm film thickness, made in USA) and FID detector were applied.

Despite high-sensitivity of the method, the sampling of air using a micro syringe results in deviations of the volume of the probes.

2.5 Surface morphology, average particle size, particle shape

Scanning Electron Microscopy (SEM) and Optical microscopy were used to investigate the structure of the materials. The SUPRA™ 40VP Field Emission Scanning Electron Microscope is described in Paragraph 2.3.

Optical microscope Altami MET C1 300x. (An average particle size was calculated for 5 fields (pictures) of every sample. On each field 5-7 secants were inflicted. The total analyses includes 80-120 values.

The differential thermal analyzer TERMOSCAN-2 was used to perform a thermal analysis of the samples. The test was performed in air atmosphere, while the heating rate was 5 °C/min.

The X-ray diffractometer (Siemens–D500–BRAUN) was used to perform X-ray diffraction analysis. For comparison, Figure 2.2 shows the diffractogram of the sample, obtained in 2009 with the matrix/precursor ratio of 1:10. For this sample, the TiO_2-content is 30,3 wt % [6,7]. The X-ray diffraction showed the presence of aluminum sulfate and quartz. Despite of this, the analysis of the numerical data revealed that the maximum intensity values were achieved at the diffraction angle 2θ of 25.28 degree, which is corresponds to 100% intensity of anatase. The aluminium sulfate peak has the maximum intensity of 2θ=25.413 degrees, therefore the strong reflection makes identification of anatase more

difficult. In addition, there are peaks at 2θ of 48.05° and 37.801°, but low intensity (35% and 20%, respectively) do not make it possible to identify them.

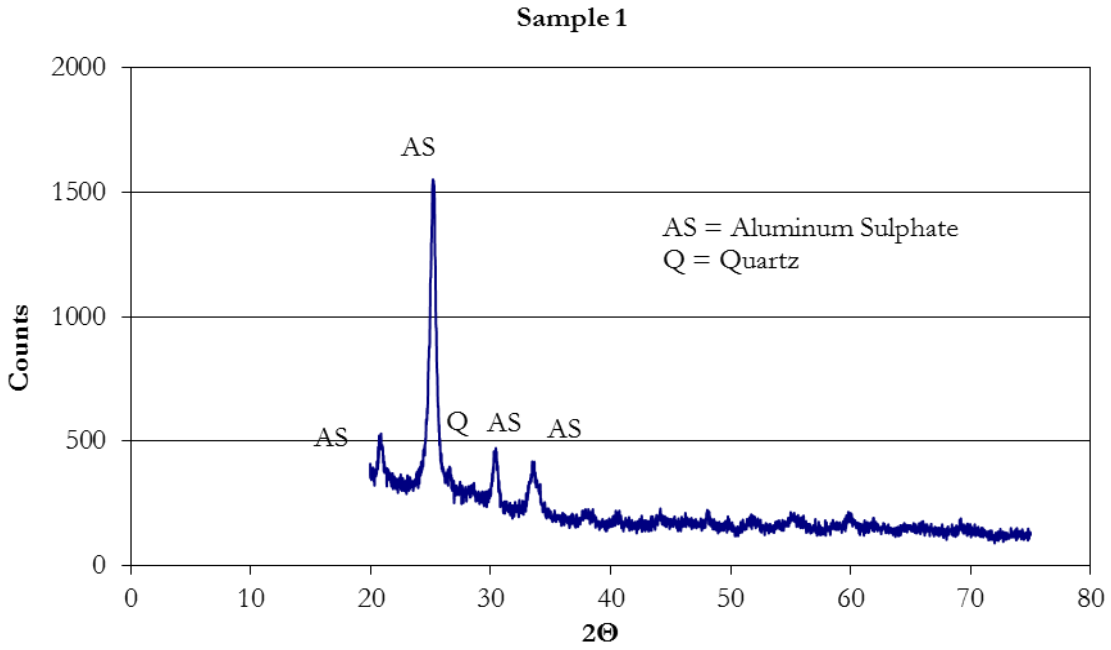

Figure 2.2. The diffractogram of the sample at matrix/precursor ratio of 1:10

2.6 Preparations for the experiment

2.6.1 The preparation of the samples for tests for water vapor and benzene vapor adsorption

The preliminary preparation of TiO_2-containing samples before the investigation of the adsorption isotherm included drying at 250 °C (the temperature was chosen after the differential thermal analysis, see Figure 3.5) to a constant mass and stored in a desiccator in the presence of concentrated sulfuric acid during 24 hours. This scheme was used to study the porosity of the samples.

To study the adsorption of benzene the samples were previously dried to a constant weight at the residual pressure of 10-5 Pa and at the temperature of 180 °C in order to remove air and other gases.

2.6.2 The preparation of the samples for tests of UV-sensitivity

For examining the products of UV-initiated decomposition and the mechanisms of photocatalytic reactions, the surface of titanium dioxide is often processed.. For example, there was conducted sequential heating at the temperatures up to 1000 K (≈727 °C) and under the pressure of 10-100 Pa) for oxide photocatalysts. Heating was performed

alternately in vacuum and in oxygen [187].This alternating preparation takes several tens of hours. To accelerate the process, heating in oxygen is combined with UV irradiation.
The examination of the mechanism and products of the decomposition process was not the purpose of the research. It was necessary to test the effectiveness in the process of disappearance of MEK; therefore, the method was simplified.
To examine the adsorption of MEK, the probes (1 g) of the materials were dried at 120 °C for 5 minutes, cooled to room temperature, and stored in a closed container to prevent excessive wetting. At the same time, UV-irradiation was used to reactivate the surface [31, 188]. The preliminary experiments showed that the maximum effect was achieved after 2 hours of irradiation.
The temperature of heat treatment was chosen considering the effects of residual moisture on the properties of the samples. The attempt of UV pre-activation in a sealed container in the presence of concentrated sulfuric acid led to the fact that the activity of the samples in the process of MEK-disappearance decreased significantly. Therefore, the activity under UV illumination of the materials after this treatment was less than in the dark. Chapter 3 provides the thermograms of the samples (Figure 3.5), where the first endoeffect within 70-250 °C was found. In order to prevent full desorption of water from the sample, drying was performed at the temperature of 120 °C.

2.7 Adsorption activity

2.7.1 Water vapor adsorption

The adsorption of gas or vapor is usually described through isotherms. S. J. Gregg and K. S. W. Sing [189] described specific behavior of water on the TiO_2-surface. However, in constant conditions (first of all, temperature and pressure) for the preparation of the materials the isotherms are replicable. Since adsorbed moisture is important for providing a photocatalytic process for TiO_2-containing materials [30,190] water vapor was chosen as an adsorbate.
The main exact methods of experimental study of isotherms are subdivided into gravimetry and volumetry/manometry [83, 191,192]. The former is based on the measurement of mass of the sorbent, while the later uses the measurement of volume of the adsorbate gas. In addition to these basic methods, impedance spectroscopy, oscillometry and gas chromatography are used. However, these methods are time-consuming and require special equipment and additional processing of the sorbent (e.g. heat-treatment into the inert gas flow) [83, 191,192]. One of such complex methods was used in order to examine benzene vapor adsorption activity.
Another method to obtain water vapor adsorption isotherms was known for several decades. It is a simpler, reasonably accurate technique [191,193], which is currently used for testing materials in the production of aluminosilicates, and in applied research of hydrophilic adsorbents [194-197].
The experiment was performed in a thermostat at 25 °C. Sulfuric acid solutions (50 mL) with specific concentrations (see Table 2.3) were used for regulating the pressure of water vapor. After the preparation (see paragraph 2.5.2), the materials (samples of 1g each) were placed in the desiccator (2 L) for 24 hours in the presence of 90% solution of sulfuric acid. Then the sample was weighed, and a bowl with acid of lower concentration was installed in

the desiccator. Then the sample of the material was weighed, and acid was changed to a less concentrated solution.

The replacement continues until pure water is used, which corresponds to the capacity at $P/P_s = 1$. After that, the tests were performed in the reverse order. Thus, adsorption and desorption lines were obtained.

The adsorption capacity of the materials was determined by the equation:

$$a = \frac{mi - m_1}{m_2 - m_1} \quad (2.6)$$

Where a – adsorption capacity, g/g, m_i - mass after keeping the bottle with the material in the desiccator, m_2 – mass of the dry flask with material, m_1 – mass of the dry empty flask.

Table 2.3. The water vapor pressure over a solution of sulfuric acid at 25°C.

Concentration of H_2SO_4, % mass	Water vapor pressure, mmHg	Relative vapor pressure, P/P_S
0	23.76	1
10	17.24	0.72
20	16.41	0.69
30	14.5	0.61
40	11.29	0.41
50	7.37	0.31
60	3.71	0.16
70	1.09	0.046
90	0.12	0.0021

S. J. Gregg and K. S. W. Sing [189] described the specific behavior of water on the surfaces of silica and metal oxide in terms of Brunauer–Emmett–Teller (BET) theory of polymolecular adsorption. The monolayer capacity a_m, the parameters of the BET-equation (2.7) were determined after the analyses of the isotherms.

$$\frac{p/p_s}{a(1-\frac{p}{p_s})} = \frac{1}{a_m C} + \frac{(C-1)p/p_s}{a_m C} \quad (2.7)$$

Where a – adsorption capacity, mol/g; a_m – monolayer adsorption capacity, mol/g; P/P_S – relative pressure, C – BET constant.

The obtained results are used to estimate the capacity of the materials at a relative pressure corresponded to the monolayer filling. However, the research demonstrates that the formation of crystalline sulfate hydrate occurs in parallel with physical sorption [189]. Therefore, the value is approximate. The maximum adsorption capacity for water vapor (a_s) is another characteristic used to evaluate adsorptive properties of the materials, obtained under different synthesis conditions.

2.7.2 Benzene vapor adsorption, specific surface area and properties of the porous structure

In order to characterize the porous structure of the materials and to determine adsorption capacity towards organic compounds, the adsorption and desorption isotherms were obtained and specific surface area of some samples was examined. These studies were conducted in the Russian Academy of Sciences A.N. Frumkin Institute of Physical Chemistry and Electrochemistry (IPCE RAS) (http://eng.phyche.ac.ru/), in the Laboratory

for Synthesis and Investigation of Sorbents (http://www.phyche.ac. En /? Page id = 2416).

The benzene vapor adsorption and desorption isotherms were obtained at 293 K (≈20 °C) by gravimetric method. The samples were preliminary evacuated (i.e., all gases were removed from the materials) to a constant weight at 180 °C and residual pressure of 10^{-5} Pa. The mass changes were monitored using quartz spring microbalance with the precision of 20 μg.

The Dubinin–Radushkevich equation (Eq.2.8), the mathematical tool of the theory of the volume filling of micropores (TVFM) [198-200] was used to examine the parameters of the microporous structure.

$$a = \frac{W_0}{\upsilon} \exp\left[-\left(A/E_0\beta\right)^2\right] \quad (2.8)$$

Where a – adsorption capacity for benzene vapor, mol/g; W_0 – maximum micropore volume, cm^3/g; v – molar volume of adsorbate, cm^3/mol; A – thermodynamic potential $RT\ ln\ (P/P_S)$, J/mol; E_0 – characteristic energy of benzene vapor adsorption, J/mol; β – scaling coefficient, characteristic energy of benzene per characteristic energy of standard adsorbate (in this case – 1).

The equation is applicable for describing adsorption isotherms in the area of low and middle values of the relative pressure (at $1*10^{-4}$ to 0.2 of P/P_S) for adsorbents with homogeneous microporous structure. The linear form of the equation in semi-logarithmic plot $[ln\ a = f(A)^2]$ is:

$$ln\ a = ln\frac{W0}{v} - \frac{1}{E_0^2}\left(RTln^2\left(\frac{P_S}{P}\right)\right) \quad (2.9)$$

Where W_0 is determined as the segment, cut off from the Y-axis, E_0 by the slope of the curve.

A micropore size is calculated given the slit-like microporous structure. The relation between characteristic energy of benzene vapor adsorption E_0 and a pore high-width x_0 was used (2.10)

$$k = E_0 * x_0, \quad (2.10)$$

where k – micropore characteristic energy constant (10 kJ·nm·mol^{-1}) [201].

Mesopore volume is determined as a difference between the limited sorption volume:

$$V_S = a_s \cdot \upsilon, \quad (2.11)$$

and the maximum micropore volume W_0 (2.12):

$$V_{mes} = V_S - W_0 \quad (2.12)$$

The specific surface of mesopore structure S_{meso} was examined by the γ-method [202,203]. The method is useful, given that it is based on the same adsorption isotherm, which is used to determine the micropore volume, although the polymolecular adsorption in mesopores occurs at the P/P_S range of 0.45 to 0.7. The filling of micropores is virtually complete at the relative pressure of 0.40-0.45, while capillary condensation occurs at $P/P_S>0.7$.

$$\gamma = \left(\frac{9.11}{A^{0.5645}}\right) * 10^3 \quad (2.13)$$

Where γ – adsorption capacity at the given range of relative pressure, mol/m^2; A – thermodynamic potential $A=RT\ ln\ P_s/P$, J·nm·mol^{-1}.
The amount of adsorbate in mesopores:

$$a_{meso} = \gamma * S_{meso} \quad (2.14)$$

In general, adsorption capacity can be calculated as the sum below (2.15)

$$a = a_{micro} + a_{meso} = a_{micro} + \boldsymbol{\gamma} S_{meso} \quad (2.15)$$

The dependence $a = f(\gamma)$ at 0.45-0.7 P/P_S is straight line formula.
Therefore, it can be determined as the tangent of that angle of inclination of the graphic line.
Specific surface area of some samples was determined in IPCE RAS during nitrogen adsorption at −196 ºC and 0.05-0.99 P/P_S, using the automated analyzer TriStar II 3020. Pre drainage of the samples was carried out by the VacPrep™ 061 (Micromeritics Instrument Corp., USA).
The methods that were used to determine porosity, fenestration and density of the material are described below.
True ϱ_{true} and apparent ϱ_{app} density were determined by a pycnometer. Water was used as pycnometer fluid to determine ϱ_{true} and mercury was used to determine ϱ_{app}. (see Fig. 2.3)

a) b)

Figure 2.3. The determination of true and apparent density of the composites: a) – true density, pycnometer fluid is water, b) apparent density, pycnometer fluid is mercury.

The bulk density (Δ) was measured by a volumeter, after processing the samples on the shake table. The other parameters were calculated based on the porosity of the samples. Porosity (%) was calculated by Equation 2.16:

$$P = \frac{\rho_{tr} - \rho_{app}}{\rho_{true}} * 100\% \quad (2.16)$$

The total pore volume, cm^3/g (Eq.2.17):

$$V_{total} = \frac{1}{\rho_{app}} - \frac{1}{\rho_{true}} \quad (2.17)$$

The base layer fenestration, cm^3/g (Eq. 2.18):

$$V_{fr} = \frac{1}{\Delta} - \frac{1}{\rho_{app}} \quad (2.18)$$

2.8 Testing methyl ethyl ketone (MEK) removal of the composite materials

To study the photocatalytic properties of TiO_2-based materials, various VOCs were used [31]. In this study, methyl ethyl ketone (MEK) was used as model pollutant [29].
MEK was chosen due to the fact that oxidation of vapors of oxygen-containing organic substances (i.g. alcohols, aldehydes, ketones and ethers) does not cause significant deactivation of TiO_2 [37, 204].
The experiments on MEK removal were carried out in single chamber batch reactors. The reactor of this type consists of a chamber (where a catalyst should be placed preliminarily), mixing and sampling devices and an analyzer (gas chromatograph). The volumes of the reactors were 0.0436 L, 16 L, 0.45 L.
Humidity affects the maximum rate of pollutant removal. Despite this, the effect varied depending on the type of a test pollutant:

- For ketones and aromatics – at the 17-32% of humidity [30].
- For butyl acetate – at the 75% [190]
- For acetone – at the 28%[37].
- Maximum oxidation rate for toluene removal depends on the concentration of a pollutant: the higher concentration is, the higher humidity is [205].

In order to provide the highest effectiveness of the process, it is desirable to determine the humidity range. However, the applied purpose of the research is the development of photoactive materials for passive degradation of indoor air pollutants in standard conditions. Therefore, the tests were performed in an air-conditioned room to maintain the constant temperature (T = 20 ± 2 °C) and relative humidity (RH = 50 ± 5%) [1].

2.8.1 The photosensitivity of the materials in the absence of UV-irradiation (reactor 43.6 mL)

In order to examine the properties of the composites after three years of storage, MEK removal experiment was carried out in the absence of illumination. The 43.6 mL vial, hermetic was used as a batch reactor, a magnetic stirrer provided convective distribution of the pollutant. The vial was covered with aluminum foil for light insulation (Fig. 2.4).
The sample of each material was tested for 10-30 minutes. The sample (0.2 g) was placed into the vial, and then methyl ethyl ketone (1 μL) was injected. The sampling of air was implemented every 2-3 min. The MEK content in the vial was determined by chromatographic analysis.

Figure 2.4. The reactor (43.6 mL)

2.8.2 The photosensitivity of the materials and MEK removal kinetics in the presence of UV-irradiation (ULTRA-VITALUX E27 lamp, reactor 16 L)

The samples of the materials (1±0.0007 g) were placed in the 16,64 L hermetic test chamber (further this is denoted by 16 A for simplicity) made of borosilicate glass (PYREX®) equipped with a fan to stir the inner air (Fig. 2.5). MEK (100 µl) was used as a modeling pollutant. The analysis was implemented by the gas chromatograph GC 8000, the duration of each experiment was 80-120 minutes, depending on its capabilities. The sampling of air from the test chamber (10 µl) was carried out every 10-15 minutes. The initial concentration of MEK is 5,03 mg/ L. The test box is described [1].
Testing was carried out in two conditions: the analysis of the samples without UV (for comparison) and under UV-irradiation. Besides that, promising kaolinite-based materials were additionally exanimated with an UV pre-irradiation (see Paragraph 2.5.1). The idea of preliminary irradiation of the material is based on the analysis of the main methods of reactivation of TiO_2 after the photocatalytic oxidation of VOCs [31, 206].

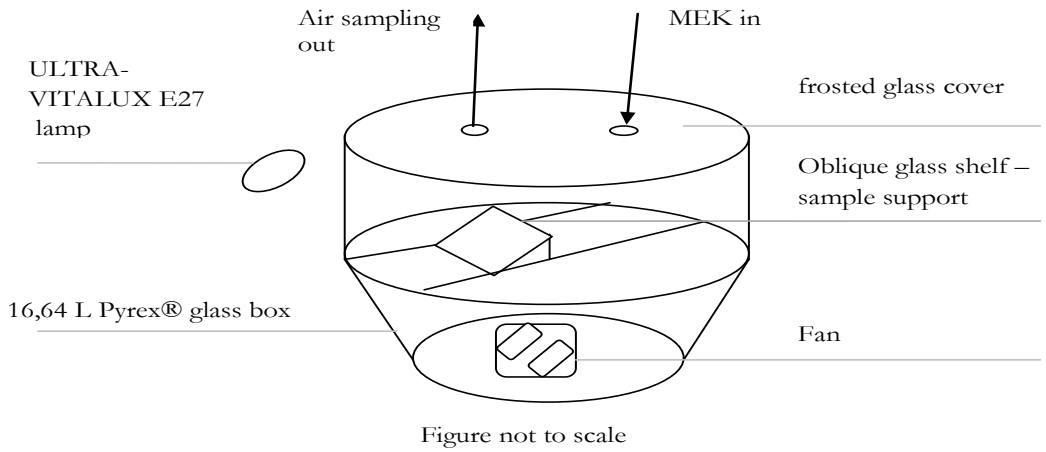

Figure 2.5. The batch reactor (16 L)

The leakproofness of the reactor was examined by the blank test, which was carried out during 130 min (Fig.2.6).

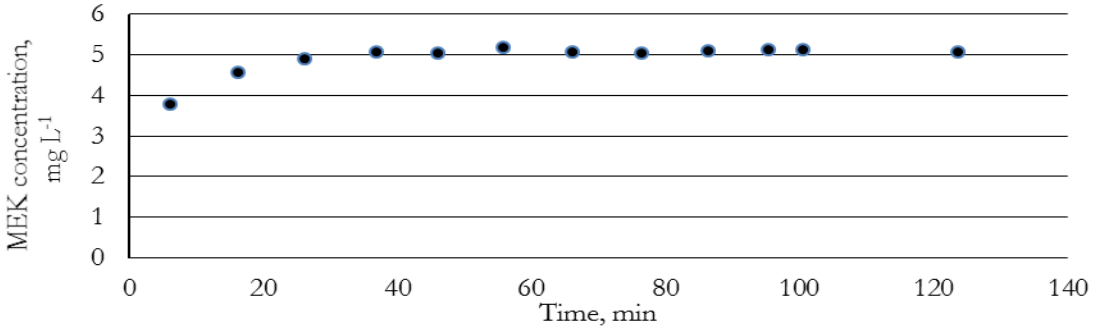

Figure 2.6. The blank test of the reactor

To confirm the reproducibility of the test results, two series of the tests with K158-sample were carried out at two-month interval (Fig. 2.7).

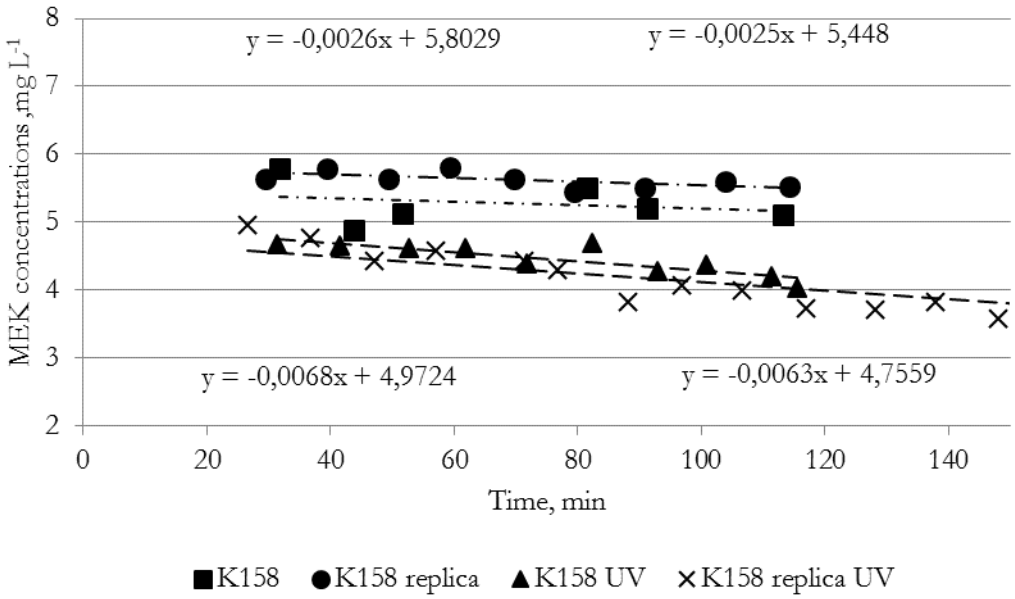

Figure 2.7. The reproducibility of data for the reactor (volume 16 L)

Electrical and spectral characteristics of the ULTRA-VITALUX E27 lamp are represented in Table 2.4 and in Figure 2.8, respectively. [https://www.osram.com/os/].

Table 2.4.The electrical data of the ULTRA-VITALUX E27 lamp.

Parameter	Value
Nominal wattage, W	300
Nominal voltage, V	230
Lamp voltage, V	230
Construction voltage, V	230

As it was confirmed during the calibration of the chromatograph, the stabilization of MEK concentration inside the chamber continued around 30 min, therefore it was impossible to get the results, describing the initial part of the kinetic curve. The slope of the curve was used to estimate the photoactivity of the materials.
After processing the results are represented in the following formulas:

$$Ct = f(t) \text{ or } m_t = f(t)$$

where C_t –concentration of MEK at time t; m_t – the MEK mass adsorbed by material 1 g at time t.
The trend line of this process is linear, given that the initial phase with non-linear reducing of concentration was not considered. Considering that the slope of the line characterized the rate of the process, it is used as an "apparent" kinetic constant $K_{C_t}^{ap}$ (A is formal constant of the regression equation).

$$C_t = -K_{C_t}^{ap} t + A \qquad (2.19)$$

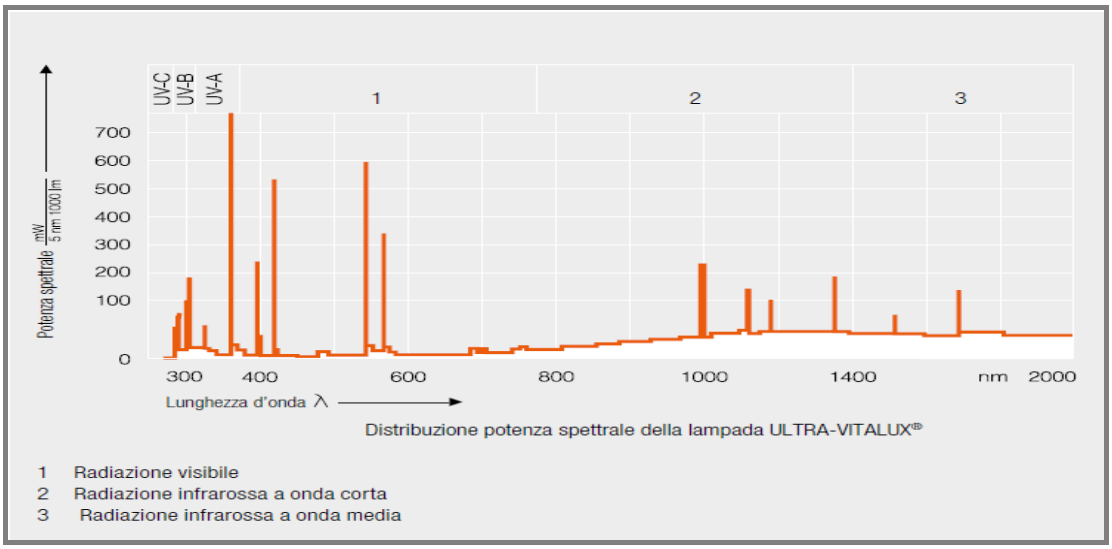

Figure 2.8. Spectral characteristics of the ULTRA-VITALUX E27 lamp

2.8.3 The photosensitivity of the materials and MEK removal kinetics in the presence of UV-irradiation (UV and Daylight LEDs, reactor 0.45 L)

For greater accuracy, it was decided to conduct the experiments in a small volume reactor and under mild UV radiation. For this purpose an experimental installation based on LEDs with given characteristics was prepared. The reactor was used for testing synthesized and doped samples. The common view of installation is shown in Figure 2.9.
To run these experiment the samples of the materials (0.03 g) were placed in the installation (0.45 L), equipped with a magnetic stirrer to stir the inner air. MEK (10 µl) was used as a modeling pollutant. The initial concentration of MEK is 17.90 mg/ L. The analysis was implemented with the gas chromatograph GC 8000, the duration of each experiment was 120 minutes depending on its capabilities. The air sampling from the test chamber (10 µl) was carried out every 5-15 minutes. For UV-radiation tests ultraviolet and daylight LEDs(light-emitting diodes) were applied. Chapter 4 describes 6 DFL-5AP4SC-400, Chapter 5 (co-doped samples) – DFL-5013UVC-380 and L54 PWC.

Table 2.5. The characteristics of the diodes.

Parameter	UV	UV	Daylight (white)
LEDs type	DFL-5AP4SC-400	DFL-5013UVC-380	L54 PWC
Iv, mcd	150	500	500
Forward Voltage (VF), V	2,6	4,5	3,6
Reverse Current (IR), mA	20	20	10
Average wavelength, nm	400	360	-

Spectral characteristics of LEDs were measured with the spectrometer SF-46 (Fig. 2.10). LEDs DFL-5AP4SC-400 and DFL-5013UVC-380 have overlapping intensity. The

intensity at the wavelength of 380 is 90% for DFL-5AP4SC-400 and 93% for DFL-5013UVC-380. There is maximum intensity for L54 PWC in the wavelength of 450 nm.

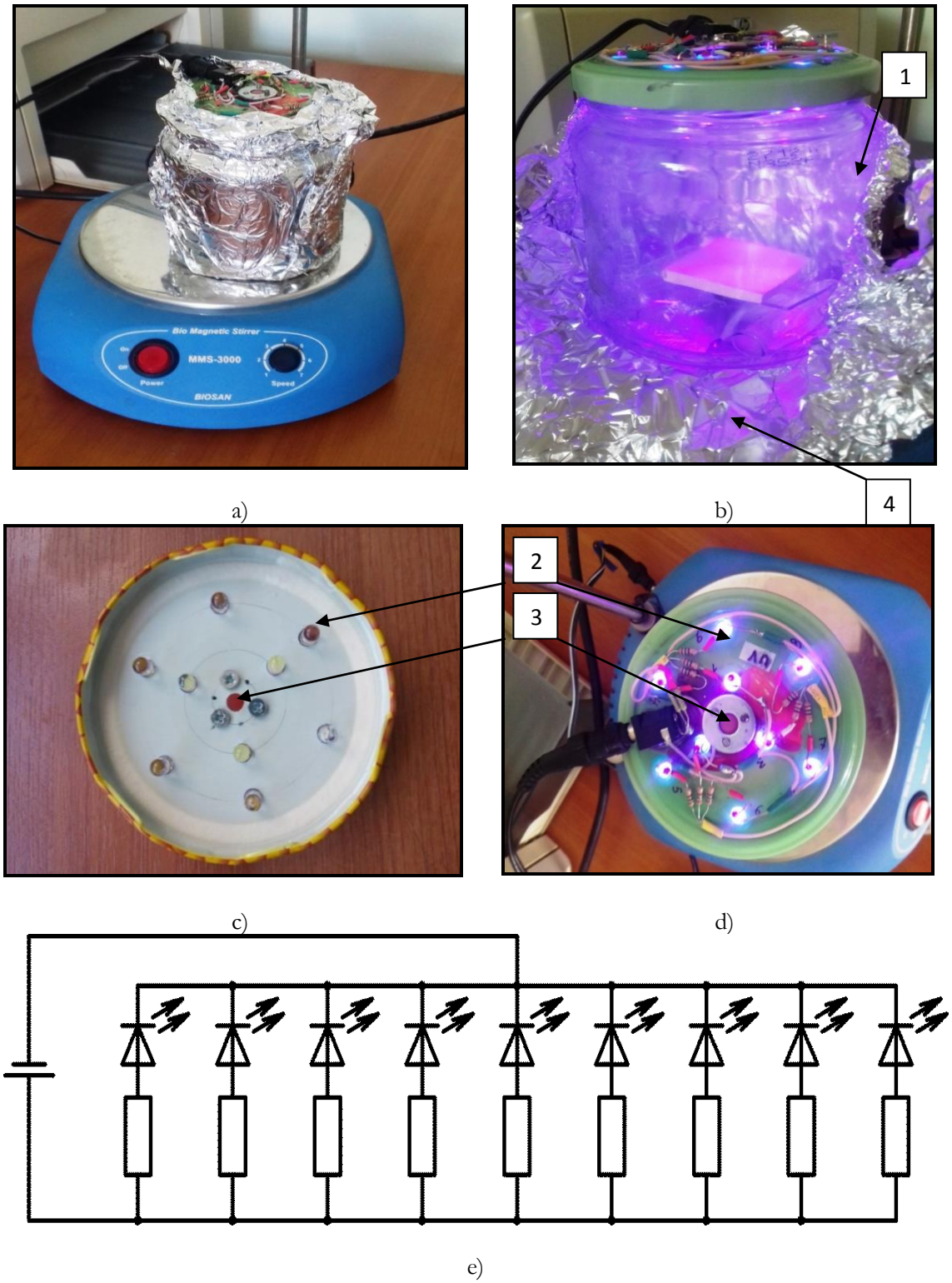

Figure 2.9. The general view of the experimental setup: a, b – the general view; c, d – the cover with LEDs; e- the wiring diagram for LEDs; 1 – the glass container; 2 - LED lamps for UV radiation; 3 – the membrane for injection and sampling; 4- the magnetic bar

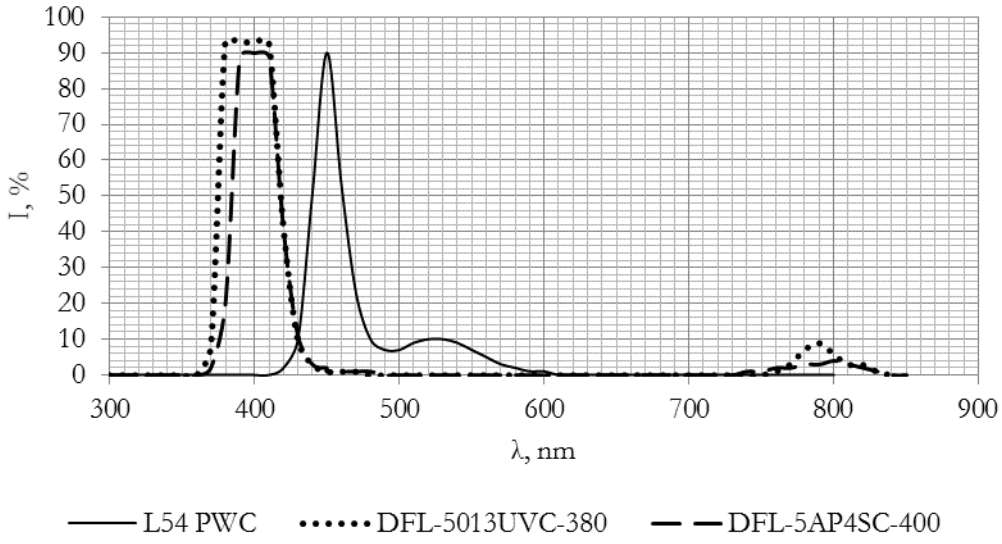

Figure 2.10. Spectral characteristics of LEDs

The angle of light dispersion of the diodes is 30°. The lamps are arranged so as to ensure the illumination of the samples. The Figure 2.11 shows the scheme of irradiation the bottom and the photo of the reactor.

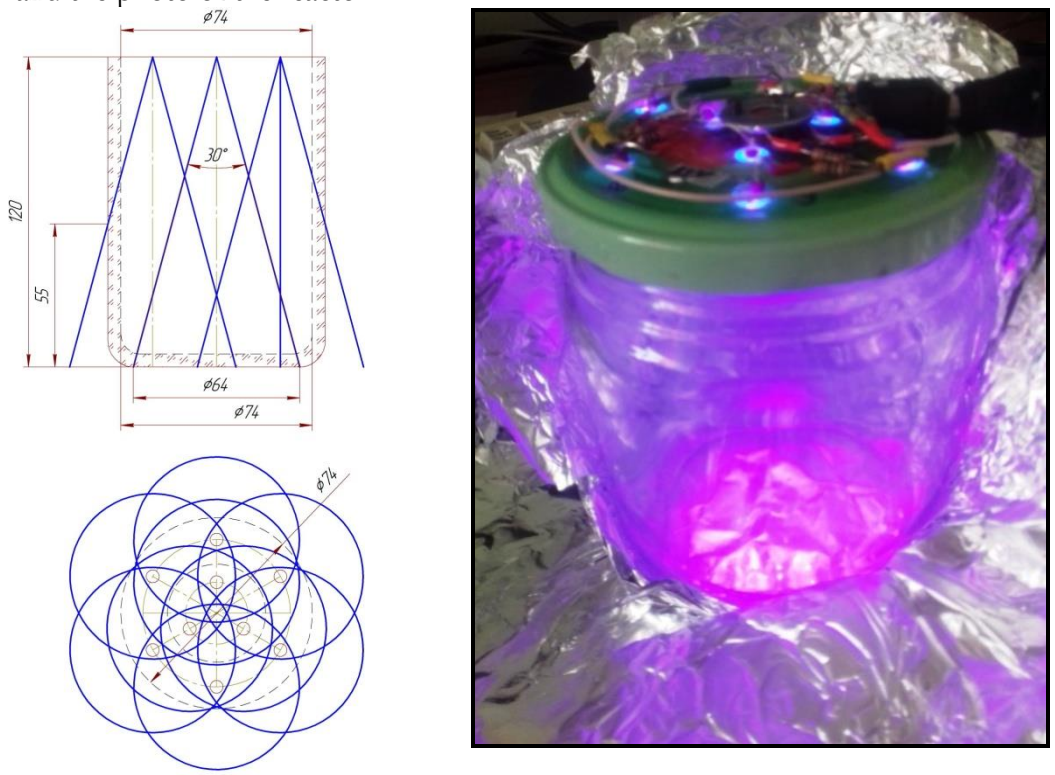

a) b)

Figure 2.11. The scheme of the reactor illumination at the level of 15mm from the bottom (a) and the photo of the reactor (b)

The light dispersion scheme (Figure 2.11, a) demonstrates, that the zones completely overlaps at a distance of at least 55 mm from above the bottom.

Because the co-doping of the samples with non-metals was performed for some specimens for shifting the activity of the samples in the visible light region (that is more suitable for domestic conditions), two types of LEDs DFL-5013UVC-380 and L54 PWC were used for the application (Tab. 2.5).

For a correct comparison of the behaviour of the samples it was necessary to provide similar values of the radiation intensity with different wavelength, so the comparison was carried out on the value of the electromotive force EMF, which is generated by LEDs irradiation. The photodiode tester n-p junction of germanium transistor МП 42 (Figure 2.12, a), b)) was used after cover removing.

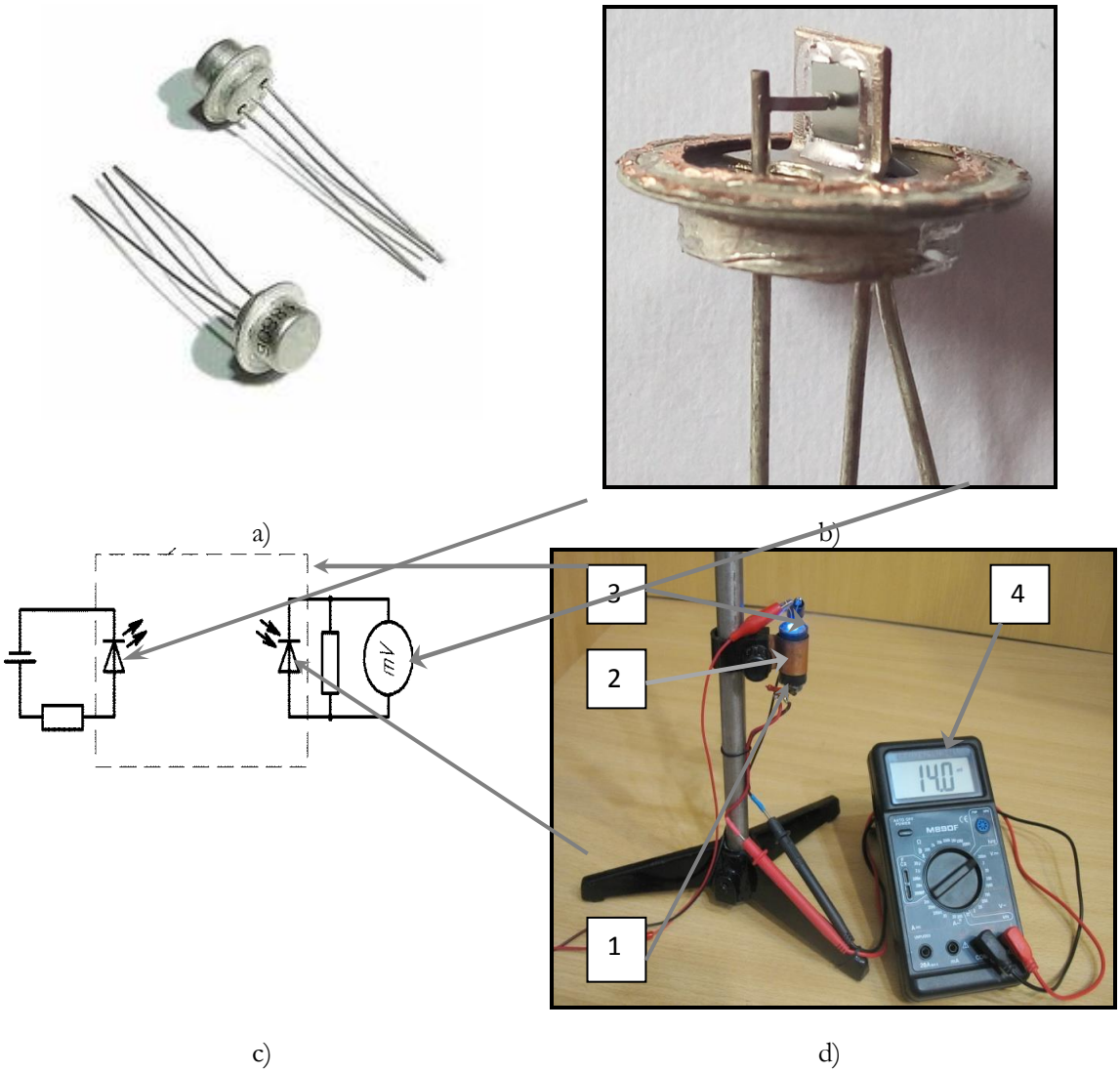

Figure. 2.12. Testing the LEDs (UV and Daylight): a)-Transistor МП42; b)- without cover; c)-a wiring diagram for the testing unit; d)-the testing unit (general view).; 1 – the transistor МП42 without cover, it was connected to the electrical circuit; 2 - a light-tight enclosure; 3 -a port (hole) for LEDs; 4 – millivoltmeter

The choice of LEDs was made according to the total values of EMF for 9 LEDs, which were identical (equal) for both DFL-5013UVC-380 and L54 PWC.
Selecting germanium transistors was approved due to shallow parameters [207] of intensity in the wavelength range of 300-400 nm (Fig.2.13).

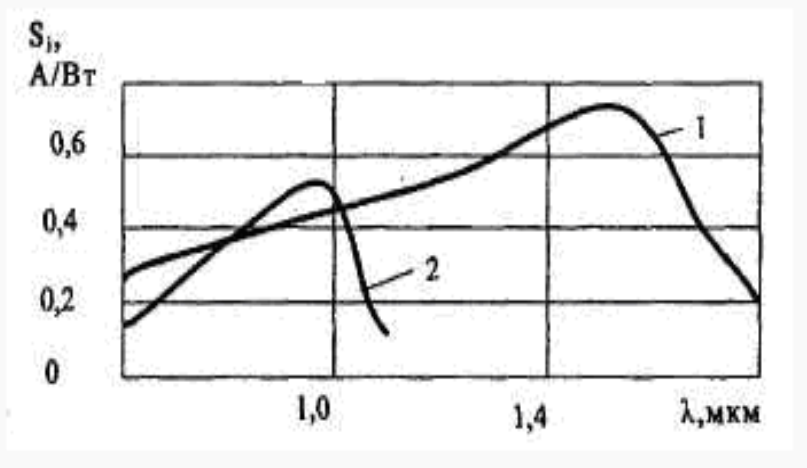

Figure. 2.13. Spectral characteristics of germanium (1) and silicon (2) of photodiodes [207]

The blank test for the reactor (0.45 L) is shown in Figure 2.14. Leakage tests were conducted both in the dark and under UV-irradiation, and leakproofness was confirmed for both conditions.

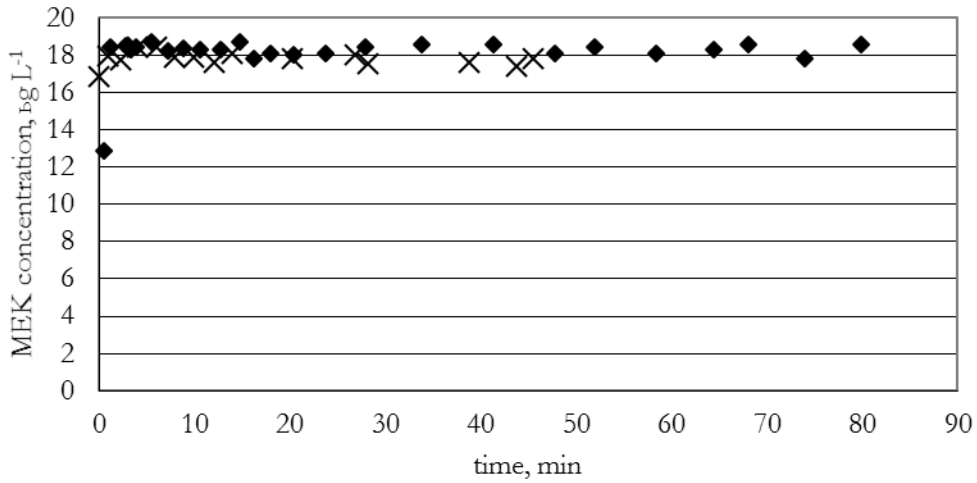

Figure 2.14.The blank test for the reactor (volume 0,45 L) : ♦ -dark condition; ×- UV irradiation

The experiment included successive measurement of the MEK concentration in the dark and under UV-irradiation after the kinetic line becomes flat. The results of such a measurement are shown in Figure 2.15 (the sample weight is 0.08 g, later it was reduced to 0.03 g). The scheme like this was used for testing of the building materials with/without TiO_2-containing materials (Sec. 5.2)

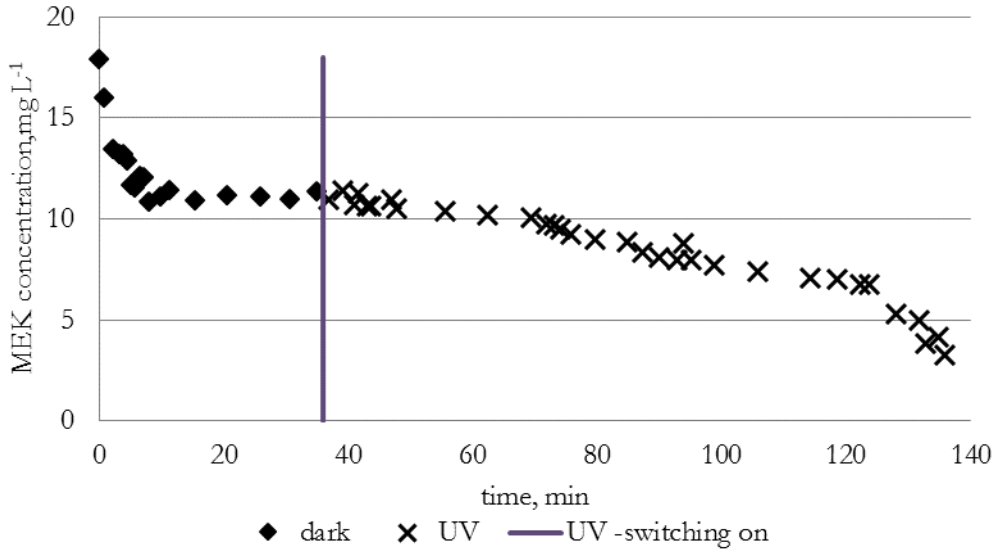

Figure 2.15. The results of continuous measurement of MEK removal in the dark and under UV-radiation

This method made it difficult to interpret the results given that UV-sensitivity of the materials was estimated after adsorption. The purpose of the research is the development of active components for building materials; therefore, of MEK removal by both adsorption and photo-induced decomposition was examined as the characteristic. In addition, there are scientific publications on the correlation between the adsorption properties and the UV-irradiation impact [2, 208, 209].
It was also noted that the process is intensified significantly after preliminary irradiation of the samples during 2 hours.
Therefore, the method was abandoned in favor of the technique of separate tests (in the dark, under UV, and after UV pre-treatment). At the same time, adsorption and photocatalytic degradation were investigated simultaneously, hence it is more correct to call the process "MEK removal" without specifying the mechanism.

2.8.4 Using the parameters of the kinetic equation for estimating UV-sensitivity of the TiO_2-containing materials

In [29] MEK the adsorption kinetics is described using Langmuir-Hinshelwood (LH) model (2.20):

$$-r = -\frac{dC}{dt} = k_{deg}\theta = k_{deg} \times \frac{K_{LH}C}{1+K_{LH}C} \qquad (2.20)$$

Where K_{LH} is the adsorption constant (L mg^{-1}); C - the pollutant concentration in the gas phase (mg L^{-1}); k_{deg} is an apparent kinetic constant (mg min^{-1} L^{-1}).
LH-model describes the kinetics of heterogeneous catalysis and involves the following assumptions [210,2]:
• The rate of the reaction between adsorbed molecules is lower than the adsorption rate. Therefore, Langmuir adsorption equilibrium remains during the process.

• Simple decomposition reactions without the adsorption of products are considered as monomolecular
• In addition, the LH-model adheres to all assumptions of the Langmuir adsorption model (a fixed number of well-defined localized sites; one site holds one adsorbed molecule; energetically equivalent for all sites; no interaction between molecules adsorbed on neighboring sites) [214, 2, 215].
As mentioned above, both constants increase during the photocatalytic process [2, 209, 211] in proportion to irradiation intensity.

$$k^*_{deg} = \frac{aI}{e+dI} \quad (2.21)$$

$$K^*_{LH} = \frac{e+dI}{dI} K_{ads} \quad (2.22)$$

where *I* is the incident light intensity; *K ads* is the dark Langmuir adsorption constant; *a,d,e* are constants.

Therefore, the experimental data processing at the LH-model coordinates and value K^*_{LH} and k^*_{deg} (UV), K_{LH} and k_{deg} (dark) allow assessing photosensitivity of the materials.
The total amount of MEK in the reactor is defined by (2.23) [2]:

$$C_T = C_L + \frac{n_S}{V} \quad (2.23)$$

where C_T - the total concentration of MEK, C_L - the current concentration in the liquid phase, n_S – the amount of the removed pollutant; V – the volume of gas phase on solids.
The assumption was that C_T is in direct relation to C_L, therefore (n_s/v), is negligible. Hence, the equations 2.24-25 were obtained:

$$\left(\frac{1}{C_L} + K_{LH}\right) dC_L = - K_{LH}\, k_{deg}\, dt \quad (2.24)$$

$$\frac{\ln\frac{C_0}{C_L}}{(C_0 - C_L)} = K_{LH} k_{deg} \frac{t}{(C_o - C_L)} - K_{HL} \quad (2.25)$$

However, the application of LH-model did not bring satisfactory results. The results of processing the data obtained for the sample K(1:6)-750 (in 0.45 reactor) are represented in Figure 2.16.
Despite the examples of successful use of LH-model to describe the kinetics of ketone and other VOCs degradation [212, 204], there are results that show limitations of the model. For example, [188] studied the effect of the acetone vapor concentration (C_a) on the oxidation rate of acetone (w). The results show that this dependence on TiO_2 and Pt / TiO_2 is not described by the single-center Langmuir-Hinshelwood equation, but is well described by the two-center model. The adsorption constants on different types of pure and platinized titanium dioxide obtained by selecting the coefficients of Eq. (4) in order to achieve the best coincidence between experimental data and model calculations are by an order of magnitude.
A more complex Langmuir–Hinshelwood–Hougen–Watson model was used in [213]. To describe the kinetics of the MEK degradation process, the authors of [4] applied standard methods; data fitting were obtained by performing the least square minimization with the Levenberg-Marquardt algorithm.

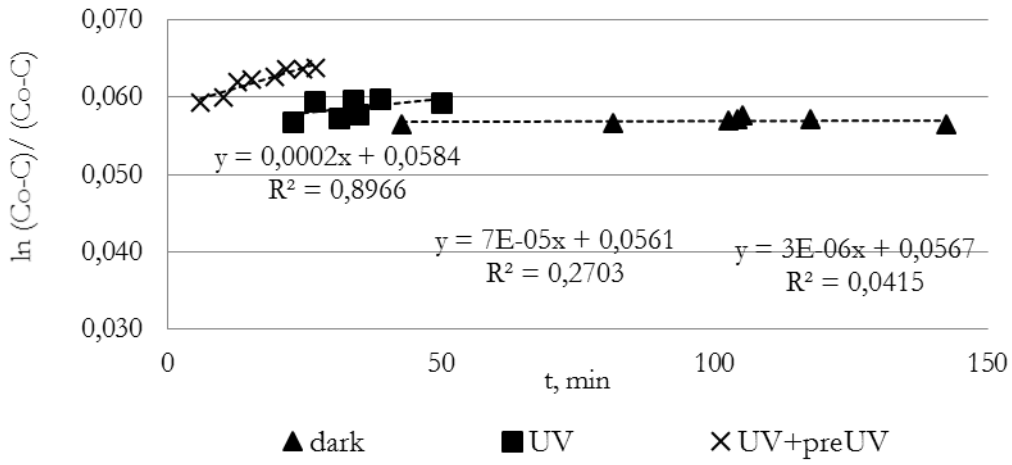

Figure 2.16. The kinetics of MEK removal on the sample K(1:6)-750 in LH-coordinates

Furthermore, MEK decomposition is a fairly complex process [29] and can be described by another equations, especially on a chemically heterogeneous surface.

In the review [215] B. Ohtani describes the LH-model for heterogeneous catalysis: «…original definition, in the field of catalysis, of "LH mechanism" is a bimolecular (two kinds of molecules) reaction proceeding on a surface in which both kinds of molecules are adsorbed at the same surface adsorption sites with the surface reaction being the rate-determining step.

Thus, the general rate equation for the LH mechanism, not shown here, includes two sets of parameters for the two kinds of molecules, and, as an exception, when one set of parameters is neglected for a monomolecular reaction, the equation can be similar to the reaction of a substrate adsorbed in Langmuirian manner. At least in the field of catalysis, however, the term LH mechanism is seldom used for such monomolecular surface reactions, since the LH mechanism has been discussed for a bimolecular surface reaction in comparison with the Rideal–Eley mechanism, in which a surface-adsorbed substrate molecule reacts with a molecule coming from the bulk."

Furthermore, application program packages are not applicable for the current study, due to the lack of variation conditions and a relatively small number of the dots. As mentioned above, the effectiveness of the composites was measured by MEK removal without the division of the adsorption and the decomposition stages. Therefore, the kinetic equation of adsorption was applied for processing the results.

However, another equation [216] was used in order to keep the main approach of LH-model (i.e., the rate is proportional to the surface filling) (Eq. 2.26). And the second order corroborates chemical interactions on a solid surface. The equation was experimentally obtained for the adsorption of ethane and certain organic compounds on metal-containing catalysts with initial and average surface filling [216].

$$\frac{\partial \theta}{\partial t} = k_{ads}(1-\theta)^2 \qquad (2.26)$$

where $\theta = m_t/m_{lim}$, the surface filling rate; m_t – the specific mass MEK adsorbed by 1 g of material at time t; mg/g; m_{lim} – the limit value of adsorbed mass corresponding to

equilibrium monolayer capacity; mg/g; t – the duration of the process, min; k_{ads} –the kinetic constant, mg/(g* min).

Nowadays, the equation is used to describe processes of liquid-phase adsorption [217] in batch reactors. The authors point out that in these conditions adsorption is accompanied by a chemical reaction, leading to the second order of the equation. The linear form of the equation (Eq. 2.27) can be written as following:

$$\frac{t}{m_t} = \frac{1}{k_{ads}} + \frac{1}{m_{lim}} t \quad (2.27)$$

This equation was chosen for the calculations, given that:

1) It shows high values of Pearson coefficient (0.90-0.98, in average);

2) During processing the data, both k_{ads} (kinetic constant rate) and m_{lim} (limit value of adsorbed mass) were examined. The limit value of adsorbed mass is a more obvious parameter for comparing materials.

Beyond this, the linear equation was used to proceed the large-volume reactor results (Sec. 3.5), and the slope was considered as an apparent kinetic constant $K_{C_t}^{ap}$ (Eq. 2.19).

3 Ageing, properties and optimal conditions for the preparation of composite materials

3.1 Introduction

The methods for preparation of titanium-containing materials including the characteristics of substrates and the methods of lamination on a substrate are described in detail in the literature review. Despite the fact that most of them are reliable technologies, possible improvements are still being discussed, considering that properties and characteristics of specific materials must be appropriate to the tasks assigned to them. This chapter focuses on the development of a method for preparing photoactive materials.

The deposition of photoactive components on adsorbents is useful for the process of passive decomposition, providing the transport of pollutants to a photoactive layer.

In 2011, the "Cataclean" project obtained and analyzed the samples of composite materials [6,7], prepared by the method of high-temperature hydrolysis of titanium-containing precursors with the formation of TiO_2 and its deposition on the aluminosilicate matrix (with different precursor/matrix ratio for every sample). Kaolinite (K) and montmorillonite (M) were proposed as carrier materials for the deposition of TiO_2. The water vapor adsorption isotherms and the kinetics of adsorption of MEK without UV-irradiation (see Paragraph 2.7.1) were available based on the results of 2011.

At the first stage of developing the methods for preparing photoactive materials, it was decided to examine the stability of properties of these samples after three years of storage. The research included retesting the materials by the above-mentioned methods and the assessment of the samples' photoactivity (see Chapter 2).

The goal of this experiment was to determine the preferable carrier material and an optimal amount of deposited TiO_2. As obtained results for both matrices are relatively similar, and that kaolinite is one of the most widespread clay materials and an indispensable part of many clays including kaolin [218], this material may be recommended due to its availability and low cost [219, 240].

The possible explanation of ageing includes:

- structural changes of matrix due to the impact of the thermo-chemical treatment,
- structural changes of TiO_2-film, which are caused due to the combined effects of a carrier material and reagents and the impact of environment during storage.

3.2 Synthesis of the samples

In 2011, a number of samples were obtained under the "CATACLEAN" project. The method of preparation is described in Section 2.2, the ratio of matrix and reaction solution is given in Table 3.1. The ID of the samples including first letters of the carrier materials, while the content of TiO_2 is used to define the numerous part.

Regrettably, a full composition analysis of the obtained materials was not carried out in 2011. For the present study, the primary issue is the content of titanium dioxide, which was investigated by the MFS method in 2014 only (see Tab. 3.1). The comparison with the estimated content of TiO_2 showed interesting results: for both types of samples, there is a linear correlation between the amount of titanium dioxide before and after the treatment,

but for K-samples the difference between the estimated and the analytically determined amount is lesser than for the composites obtained on a montmorillonite matrix.

Table 3.1. The characteristics of TiO_2-containing materials prepared in 2011 (project "Cataclean").

Matrix	Conditions of sample preparation				Sample ID
	Material weight, g	The volume of the reaction solution**, ml	TiO_2 content*		
			Introduced with solution, mg / g clay	Determined by MFS, mg / g	
Kaolinite	2	10	255.4	158.5	K158
	4	10	127.7	109.2	K109
	6	10	85.2	97.0	K97
Montmorillonite	1	7	400.5	316.2	M316
	2	7	200.2	167.5	M167
	3	7	133.5	49.0	M49

*the amount of Ti was analytically determined for the solution and the materials, and calculated on the titanium dioxide (hereinafter, it assumes all titanium in form of TiO_2).
**the concentration of the precursor was 30.63 mg Ti/ml for those used for the preparation of kaolinite-based samples, and 34.30 Ti/ml for those used for the preparation montmorillonite-based ones.

The possible explanation of this effect is that sulfuric acid dissolves montmorillonite more than kaolinite. The dissolution caused the formation of incidental aluminium sulfates (as a structural element of clay) and alkali metals. This does not affect kaolinite significantly; therefore, the yield of the materials was lower, while the content of titanium dioxide was higher.
Visually, the color of the samples became darker in comparison with white or grayish white of freshly prepared materials, especially for M-samples (Fig.3.1).

Figure 3.1. The samples K158 (left) and M167 (right)

This is also a sign of ageing of materials. Possible explanations include mechanical damage of the TiO_2-film, the formation of impurities and compounds in the presence of sulfates, the saturation of the surface with components that can hardly be desorbed, etc. However, this issue falls outside the scope of this study, since the major problem is chemical factors, influencing the stability of the materials.

3.3 The analyses of water vapor adsorption isotherms

Since titanium dioxide and clay minerals are hydrophilic materials, and that the process of adsorption of water vapor on them is well researched. [116, 118, 189], vapor was chosen as a testing adsorbate. The presence of water on the surface has a serious impact on the activity of a photocatalyst. Studies describing the influence of air humidity have already been mentioned in Paragraph 2.6.2, while the process of water splitting into H_2 and O_2 is one of the promising applications of a photocatalytic process [220].

At the same time, the classic literature particularly stresses the need for further investigation of water vapor adsorption on TiO_2 and gives useful data for the study of material ageing in a medium containing water vapor [189].

The technical aspects and mathematical tools of the gravimetric method are described in Paragraph 2.7.1.The isotherms are presented in Figures 3.2-3.4 for pure clays, kaolinite-based materials and montmorillonite-based materials, respectively.

A visual comparison of the adsorption-desorption isotherms reveals the following:

- In terms of the form and the values of adsorption capacity, the isotherms of water vapor adsorption are close to typical isotherms for clay materials [116, 221].
- The structural differences between carrier materials (see paragraph 1.4) determine different efficiency of the samples for adsorption processes [222,223] and for industrial application [219].
- The characteristics of kaolinite increased six times after the treatment, while for M-samples the same parameters increased less than 1.2 times. This study showed that the treatment significantly increases the adsorption capacity of K-materials at P/Ps <0.5, and makes them close to the efficiency of M-materials at P/Ps =1.

All samples are characterized by a curve in the isotherm at P/Ps>0.3, which may indicate an increase in the capacity. $P/P_s \approx 0.35$ is a typical value for many materials after which poly-molecular adsorption starts. For this reason, the capacity of the monolayer was determined as an indirect characteristic of changing the specific capacity of surface area (SSA).

A sharp increase in capacity (typical for clay sorbents) starts when $P/P_s > 0.6$ and shows that the surface holds water. This fact has been confirmed by the form of the desorption curves, which do not return to zero even with low values of P/P_s. It is expected that sulfate hydrating is the prevailing process in this area but not physical adsorption. The results of differential-thermal analyses (DTA) (Sec. 2.5) confirm this. Figure 3.5 shows three thermograms for the samples on kaolinite support and one for the montmorillonite-based material. The first endoeffect for all kaolinite samples ends at 250 ° C, which indicates the retaining of crystallized water in crystallohydrate by weak intermolecular bonds, given that the water can be easily removed by heating. The value of ΔT depends on the amount of the reaction solution. With a larger amount of the precursor (for K158) there is the second endoeffect at 250-350 ° C. However, when the clay / precursor ratio decrease, the peak is

not noticeable for K109 and K97. The M47 thermogram is similar to the thermograms of the kaolinite-based samples in terms of temperature range (70-250 ° C), but the peak shape indicates the superimposition of two endoeffects in this area.

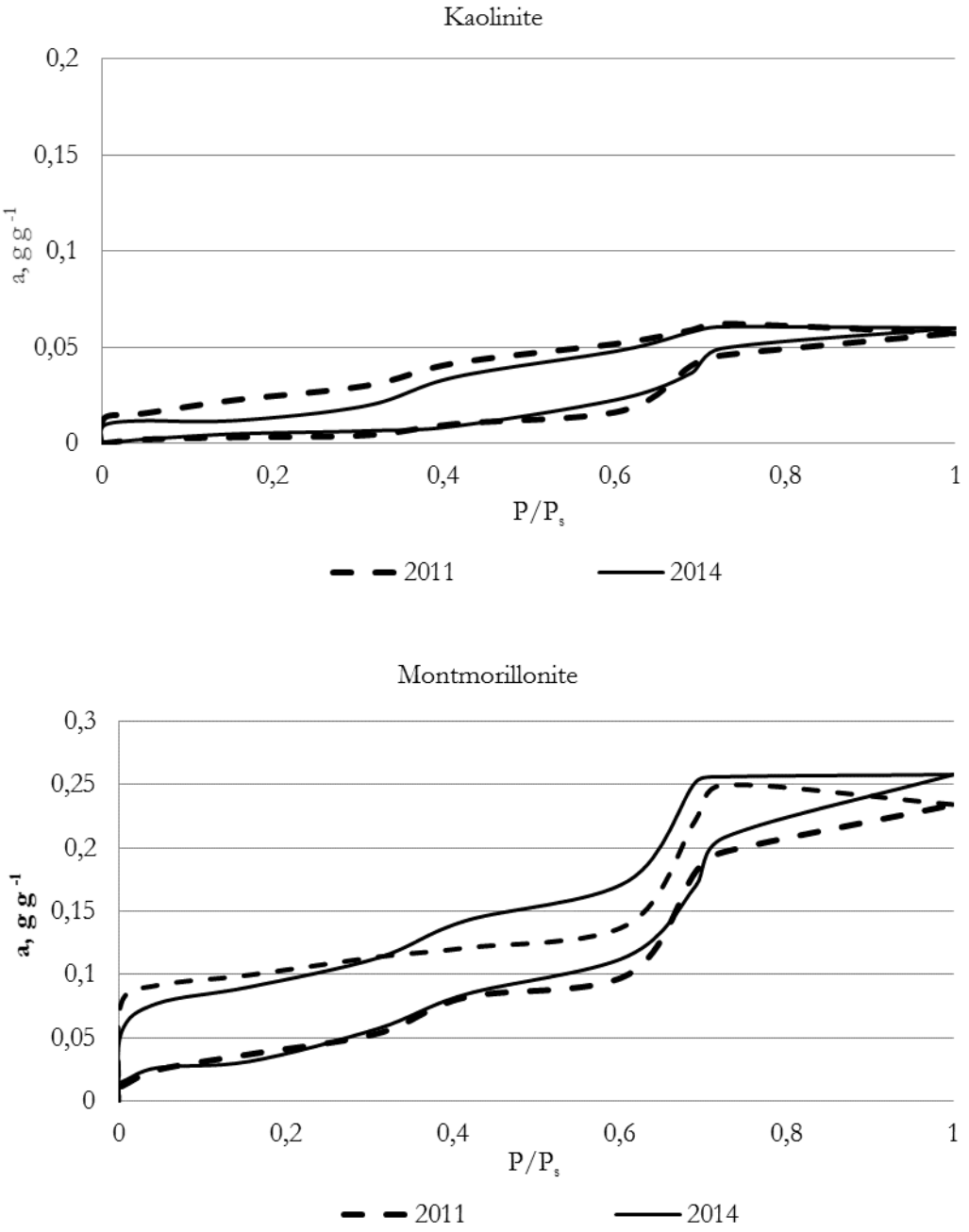

Figure 3.2. The water vapor adsorption isotherms of kaolinite and montmorillonite (2011 and 2014)

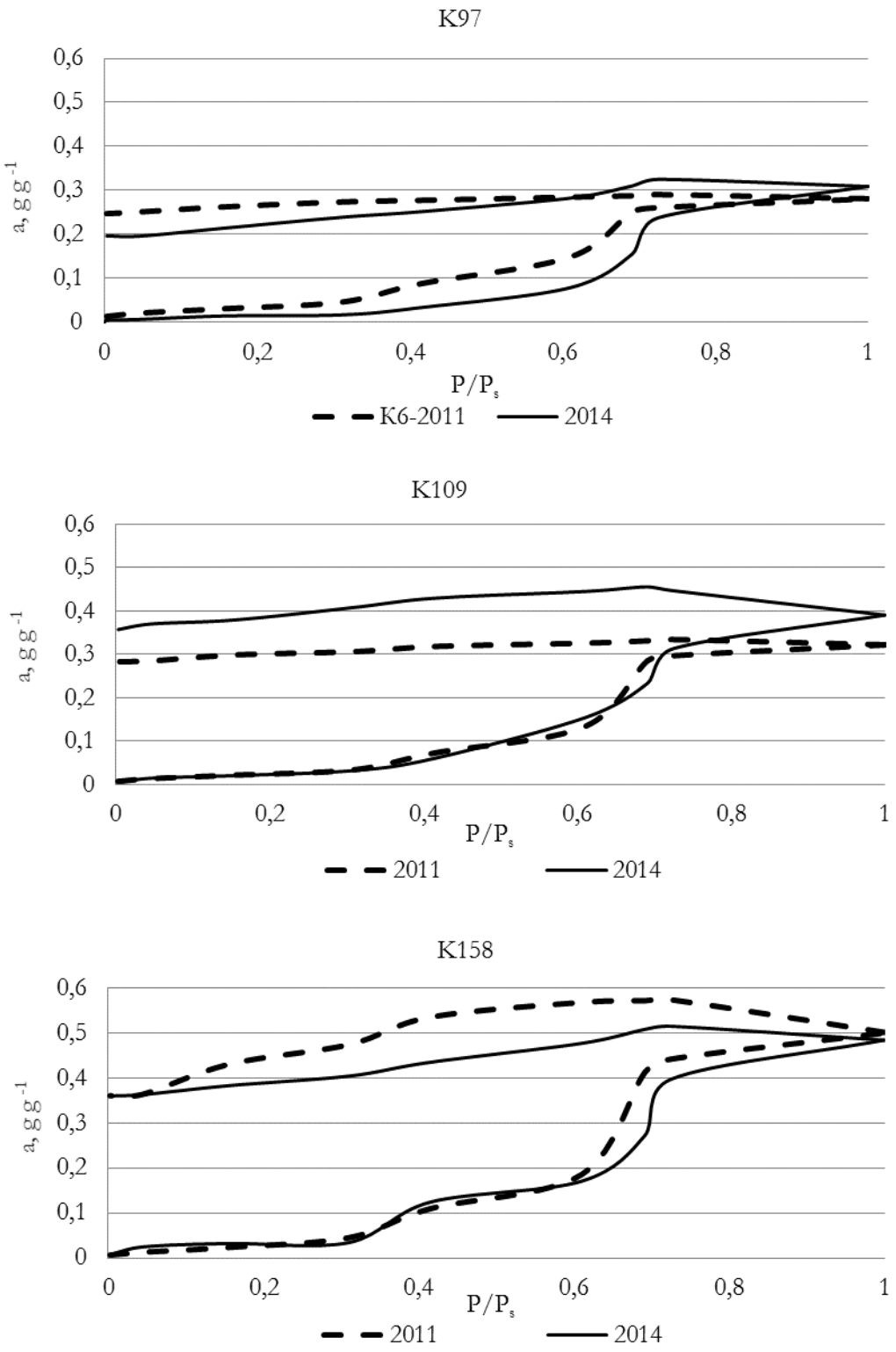

Figure 3.3. The isotherms of water vapor adsorption for kaolinite-based materials (2011 and 2014)

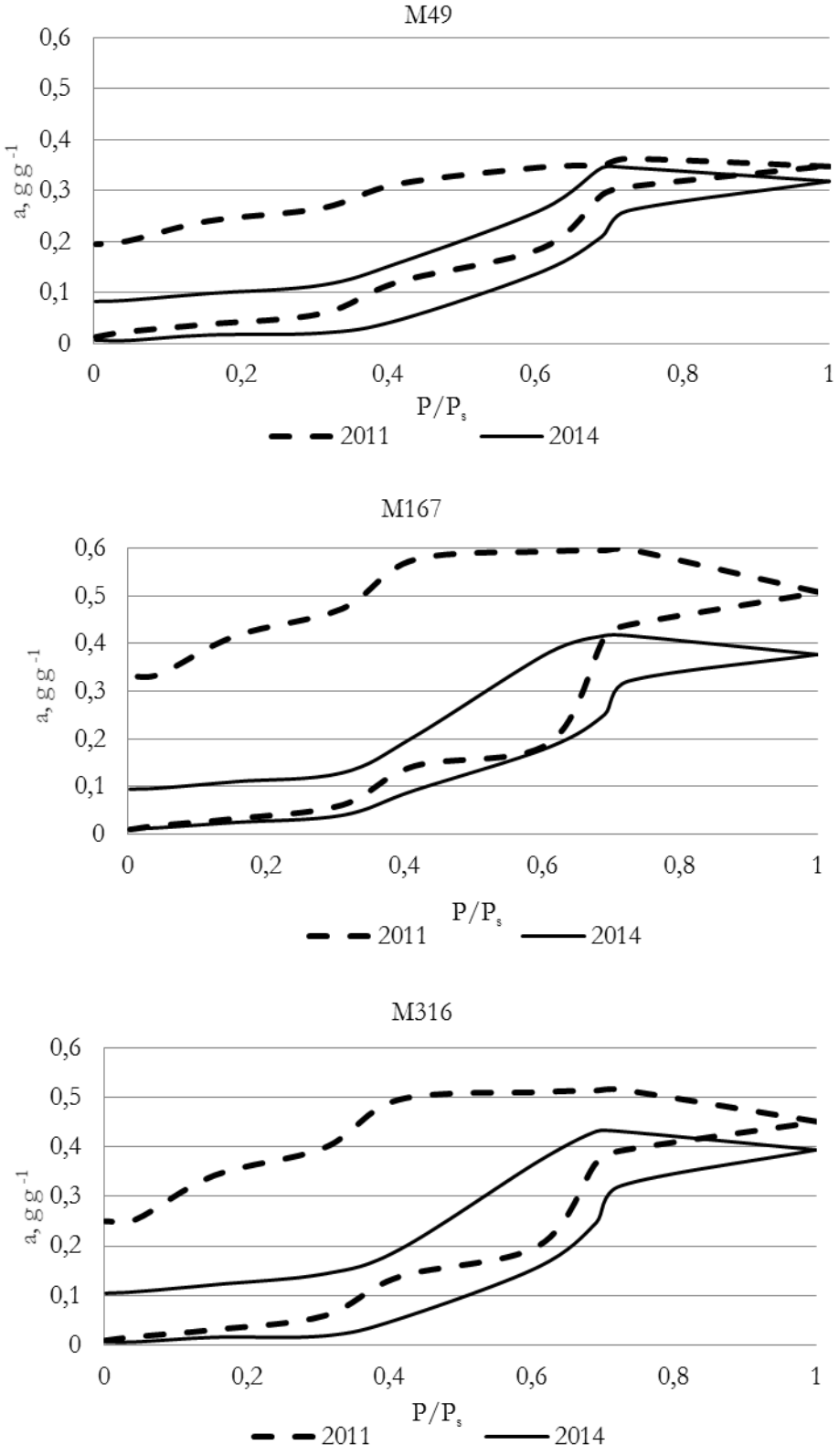

Figure 3.4. The isotherms of water vapor adsorption for montmorillonite-based materials (2011 and 2014)

On the DTA line, endothermic effects are observed in the range from 70 ºC to 250 º C and in the range from 250 to 350 ºC. The dehydration of aluminum sulfate is intensive in a range of 200-300 ºC, while the destruction of sulfates and the formation of sulfur oxides (IV) begin at 650 ºC, and become intense at 700-800 ºC [224]. There is a wide temperature interval of dehydration because temperature is different for various multiplicities of crystalline hydrate.

There arises a question about the influence of sulfate hydration on the titanium dioxide layer.

There are three possible interactions between sulfates and titanium dioxide:

- Sulfates screen saturation of the layer of titanium dioxide with water;
- Sulfates provide a reserve of water in the material;
- After saturation, sulfates do not affect the adsorption of water by titanium dioxide.

In this study, the issue was not considered of paramount importance and has not been explored.

The monolayer capacity and the maximum adsorption capacity at P/Ps=1 were used for a quantitative comparison of properties of the materials after 3 years of storage.

As mentioned above, the form of isotherms' adsorption correspond to the BET-equation at $P/P_s<0.31$. The adsorption of water on TiO_2 was described in [189.]. For experimental isotherms, the reference values of adsorption capacity were determined at 0.046; 0.16 and 0.31P/Ps.

The value of maximum adsorption capacity was found at P/Ps=1, taking into account all types of water retention, such us physical adsorption, specific adsorption on TiO_2 [189] and hydrate water in sulfate (see Tab. 3.2).

The comparison of maximum capacity values showed that these parameters do not change significantly for most of the samples after three years. A difference usually does not exceed 10% (except for K109 and M167 with 20% and 25%, respectively). However, the overall trend shows increasing the capacity for kaolinite-based samples, and reducing for those based on montmorillonite matrix.

The monolayer capacity has decreased for previous years for both montmorillonite (35-65%) and kaolinite (25-45%), which indicates a change in the composition or in the structure of the materials. There is evidence in the scientific literature that acid-activated clays are unstable because of substitution reactions and structural changing in the surface layer [118, 116], which may cause such decrease. Finally, according to the results of 2014, the samples with the similar TiO_2 content (in this instance, K158 and M167) have close values of the monolayer capacity.

The last issue, related to the isotherms, is the kinetics of the desorption process. In 2011, the desorption curves were similar for both K-materials and M-materials, in 2014 their form for montmorillonite-based materials significantly changed. As a_s changed for the samples of both types, it may be assumed that the amount of compounds able to hydration decreased. The chemical mechanism is not clear yet, though sulfates' decomposition or the formation of new compounds due to chemical interactions in solid materials are among possible explanations. Anyway, it can be concluded that kaolinite based materials are less vulnerable to ageing.

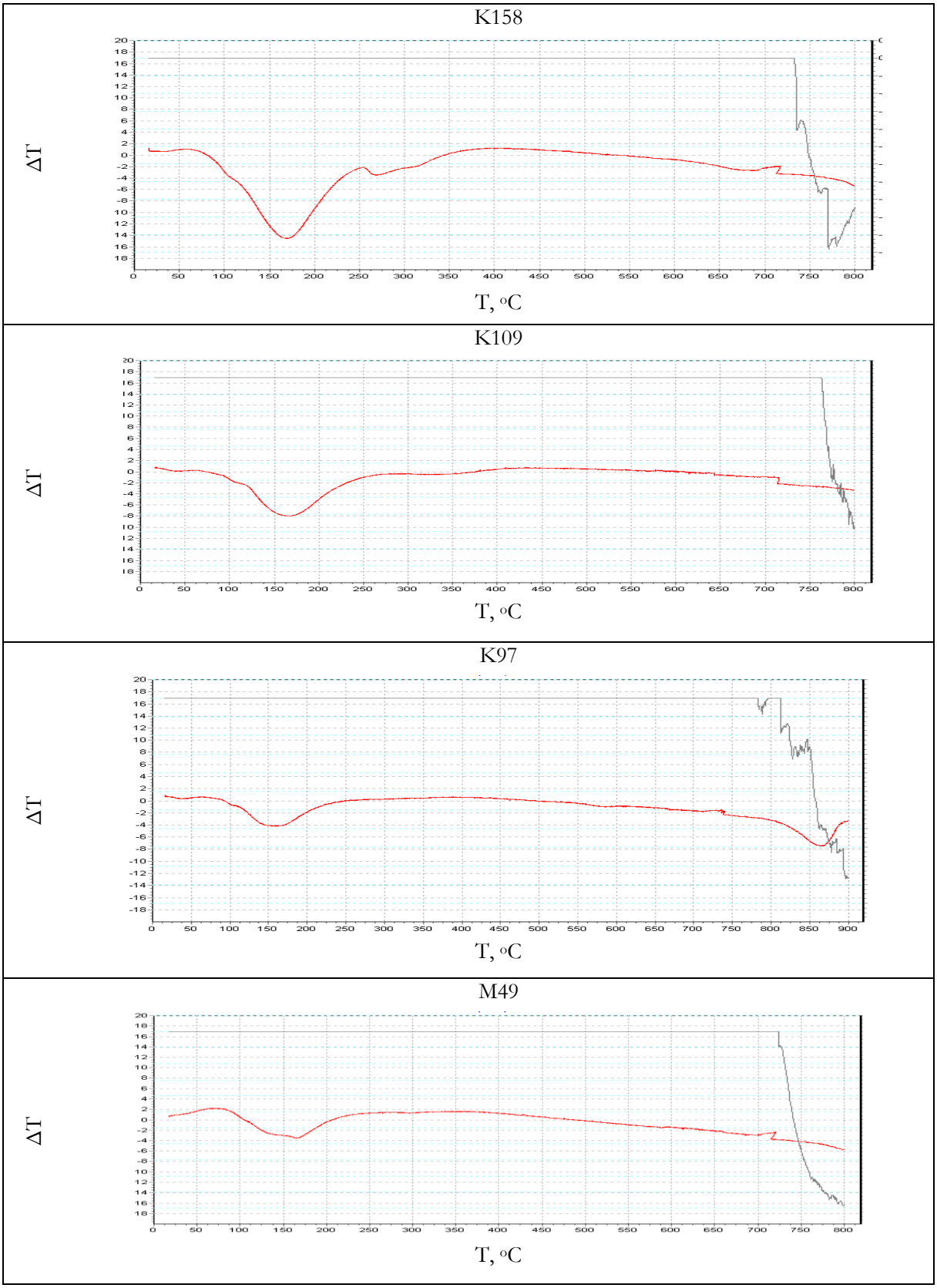

Figure 3.5. Thermograms of the samples

Table 3.2. The value of capacity for water vapor adsorption isotherms.

Samples	Monolayer capacity BET, a_m, mmol/g		Maximum capacity (P/Ps=1), a_s mg/g	
	2011	2014	2011	2014
Kaolinite	0.17	0.25	57	60
K158	1.80	1.34	500	483
K109	1.74	1.23	322	391
K97	1.73	0.96	281	309
Montmorillonite	2.08	2.25	235	258
M316	2.35	0.82	451	394
M167	2.43	1.57	508	377
M49	2.29	1.65	348	318

3.4 The analyses of the kinetics of MEK adsorption

The next area for comparison the montmorillonite-based and kaolinite-based materials are the results for the kinetics of the MEK adsorption. The experiments were carried out precisely according to 2011 year (see Paragraph 2.8.1) in the reactor (43.6 mL). The results are represented in the coordinates of Equation 2.26, 2.27, where m_t – specific mass MEK adsorbed by 1 g of material at time t, mg/g; t – duration of the process, min; (see Figure 3.6–3.7). The further data treatment (see Eq. 2.27) allowed obtaining the parameters of the kinetic equation m_{lim} – limit value of adsorbed mass which is corresponding equilibrium monolayer capacity, mg/g and k_{ads} – adsorption kinetic constant, mg/(g*min) for the kinetic equation (Tab. 3.3).

The heterogeneous reaction was carried out and investigated in a batch reactor. It was necessary to provide the limitation of internal diffusion in comparison with the external one [225].

The alignment of concentrations in the reactor's volume occurs thanks to intense air convection with a magnetic bar inside the reactor. However, the thickness of the diffusion layer on the particle's surface depends on the airflow velocity (other factors are considered equal for the all experiments. That is why, if the external diffusion resistance strongly affected the adsorption kinetic constant; the difference between values must be significant enough. The difference between kinetic constants of titanium containing samples is 4-63 times, while for the untreated clays it is only 1.23-1.24 times, which confirms the significance of changing the kinetics of sorption

Thus, it may be concluded that the adsorption kinetic constant of the composite materials has declined substantially in the last three years: 6-63 times for M-samples, and 4-22 times

for K-samples. Maximal changes were observed for materials K158 and M167, which are similar to each other in terms of the content of titanium dioxide. Despite this, a probable reason for this effect is the influence of H_2SO_4 , taking into account, that the largest amount of acid was added to these samples during the synthesis.

Table 3.3. The value of capacity for water vapor adsorption isotherms.

Sample	Limit value of adsorbed mass m_{lim}, mg/g		Kinetic constant k_{ads}, mg/(g*min)		Pearson coefficients (Eq.2.17) R^2	
	2011	2014	2011	2014	2011	2014
Support - kaolinite						
kaolinite	3.64	3.27	1.12	1.38	0.97	0.99
K158	3.59	3.22	5.25	0.23	0.99	0.91
K109	3.79	4.13	7.46	1.05	1.00	0.98
K97	3.04	4.10	3.67	0.81	1.00	0.93
Support - montmorillonite						
montmorillonite	4.02	3.58	23.22	28.95	1.00	1.00
M316	4.06	1.99	33.90	0.95	1.00	0.99
M167	4.01	2.90	41.43	0.66	1.00	0.95
M49	4.02	3.49	78.34	13.15	1.00	1.00

The values of the m_{lim} for K-based samples changed in the same proportions which was observed for pure kaolinite, while for montmorillonite-based materials these values reduced more than a half (for M316).

Thus, the data provided in paragraphs 3.2 and 3.3 allow making the following conclusions :

- Kaolinite-based materials are less vulnerable to ageing than those based on montmorillonite;
- Despite the fact that the montmorillonite matrix provided some benefits after the preparation of the samples, after a long period of storage the carrier materials of both types possess similar properties;
- The amount of Ti-containing precursor in the matrix/precursor ratio should be reduced) the estimated content of TiO2-content should be no more than 100-120 mg/g), although it must be enough for providing photosensitivity of the material.

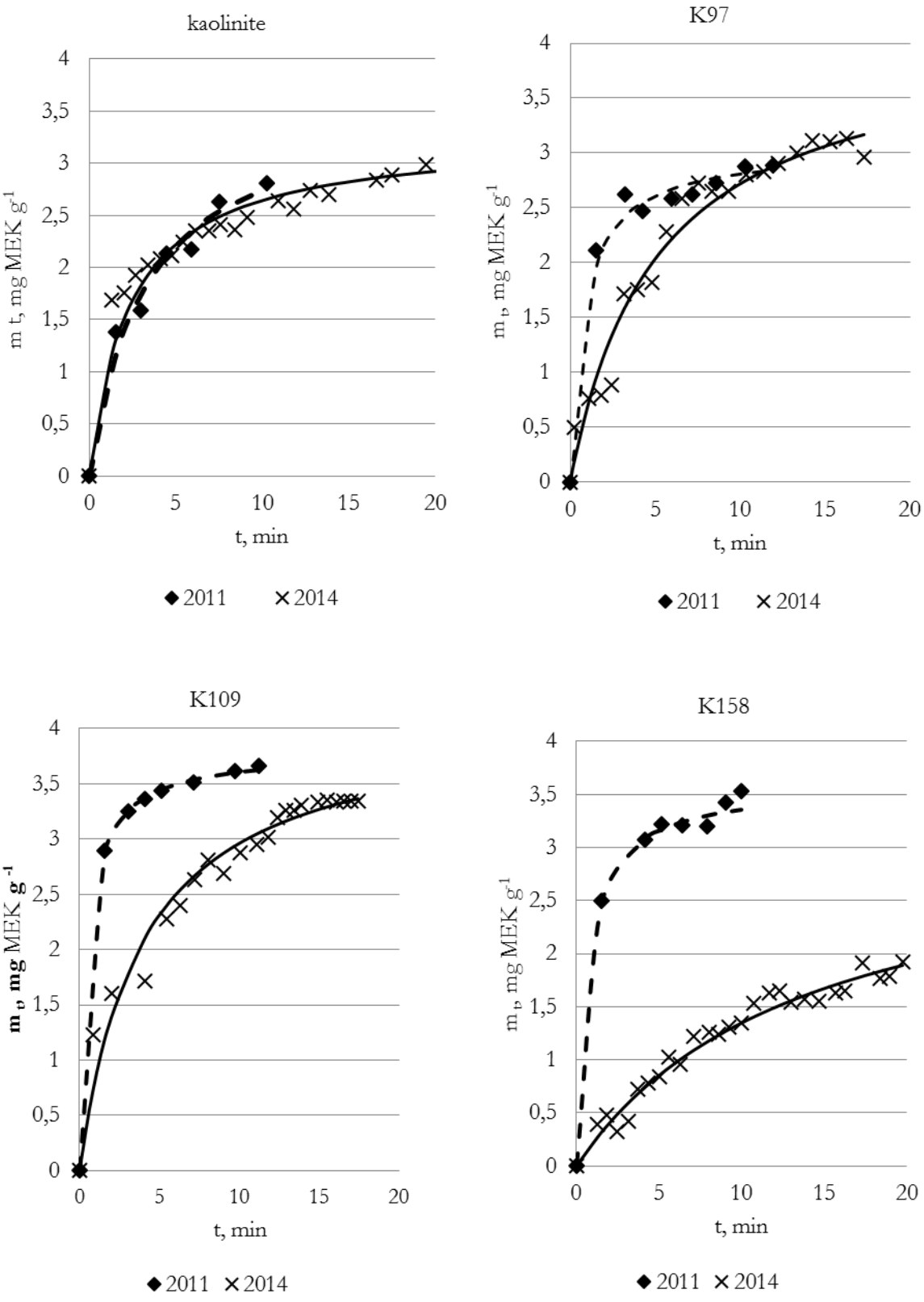

Figure 3.6. The kinetics of MEK adsorption on kaolinite-based materials

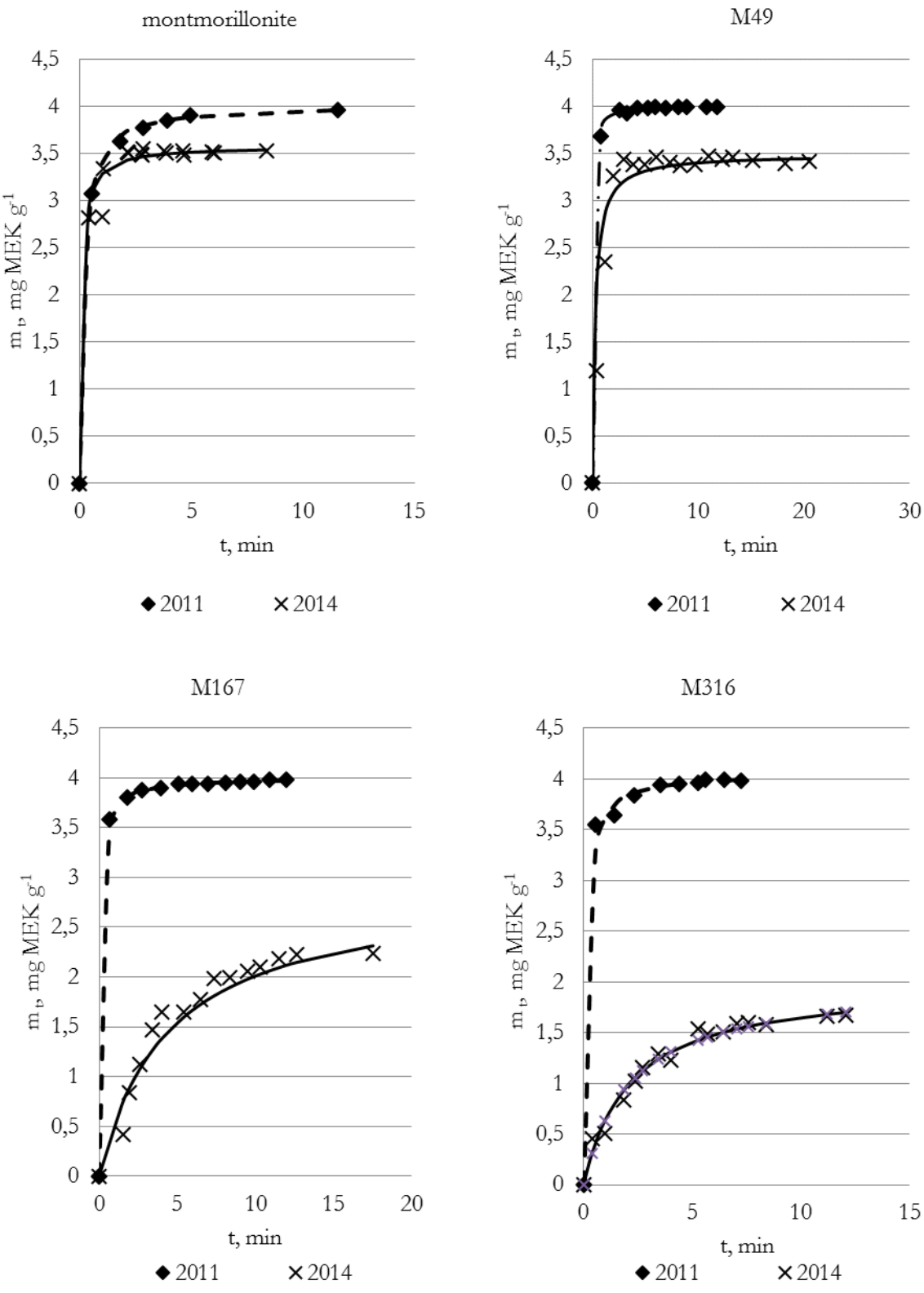

Figure 3.7. The kinetics of MEK adsorption on montmorillonite-based materials

3.5 The effect of UV-radiation on TiO_2-containing materials

The developed materials are planned to be used as finishing materials capable of passive degradation of indoor pollutants. So it is desirable that the materials be stable and keep photoactive properties as long as possible. This paragraph describes the results of testing kaolinite- and montmorillonite-based materials in order to determine their photoactivity. The experiment was performed under various light conditions in the batch reactor with the volume of 16L, which is frequently used in the SIMAU laboratory to test building materials with the effect of passive degradation. The reactor, the characteristics of ULTRA-VITALUX lamp and the data processing methods (Eq. 2.19) are described in detail in Paragraph 2.8.2.

Figures 3.8-3.10 show the reduction of concentrations of MEK in the presence of the samples (1±0.0007 g). As it was mentioned in Paragraph 2.8.2, additional tests were performed for the kaolinite-based samples. They included preliminary activation by keeping samples under UV-irradiation during 2 hours [31, 188]. The results of the first 20-30 min were ignored, taking into account the need for evaporation of MEK, the spread of vapors inside the reactor and mixing with air (see Figure 2.6 for the blank test for reactor).

Apparent kinetic constants $K_{C_t}^{ap}$ were identified based on the linear approximation of reducing the values of the methyl ethyl ketone concentrations (see Tab. 3.4). For illustrating further conclusions, these data were replicated concerning the content of TiO_2 (see Fig. 3.11).

The obtained results definitely show that the materials retain photosensitivity and that montmorillonite-based samples are more active under UV-irradiation than K-samples, while without UV they demonstrated the similar activity. The preliminary activation (reactivation) under UV significantly increased the efficiency of the kaolinite-based samples (Paragraph 2.6.2). The samples with the montmorillonite matrix were not reactivated, considering the greater influence of irradiation on them. It is worth noting, that the most significant increase of kinetic constant values was observed for samples K158 and M167, which contain the similar amount of TiO_2.

Table 3.4. Kinetic constants of MEK disappearance in equation $C_t = -K_{C_t}^{ap} t + A$

Sampels	Apparent kinetic constant $K_{C_t}^{ap}$ of MEK disappearance at different irradiation conditions		
	Dark*	UV**	Pre-UV+ UV***
Kaolinite	1.13	-	-
	1.38	1.32	-
K97	2.05	4.89	19.04
K109	2.67	4.38	24.70
K158	3.10	6.84	30.36
Montmorillonite	1.58	1.99	-
M49	3.76	6.07	-
M167	2.68	11.67	-
M316	2.28	8.36	-

*Dark- light isolation condition;

**UV- irradiation by ULTRA-VITALUX lamp

***Pre-UV+ UV irradiation by ULTRA-VITALUX lamp after preliminary activation (Paragraph 2.6.2).

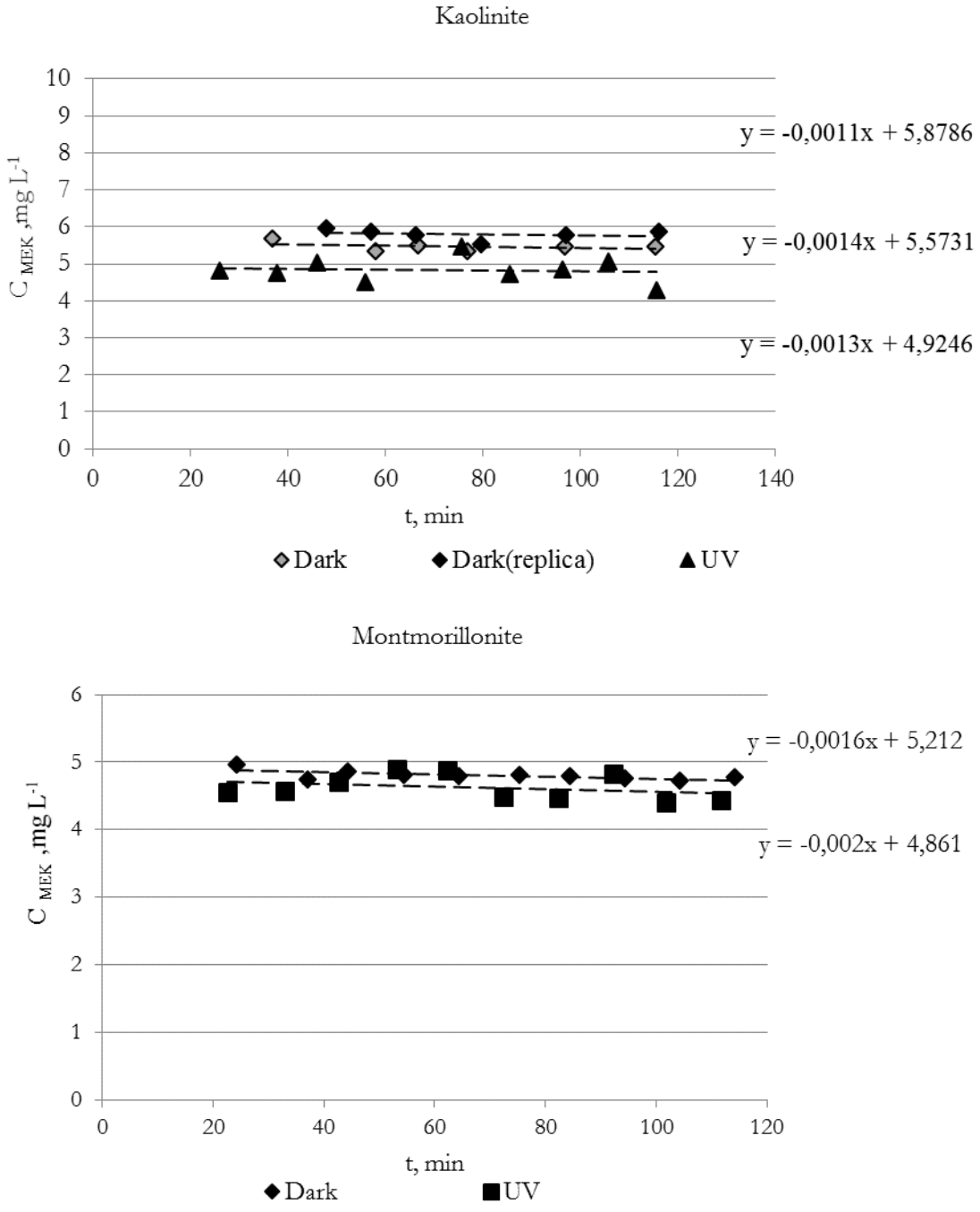

Figure 3.8. The kinetics of MEK concentration reducing on pure clays

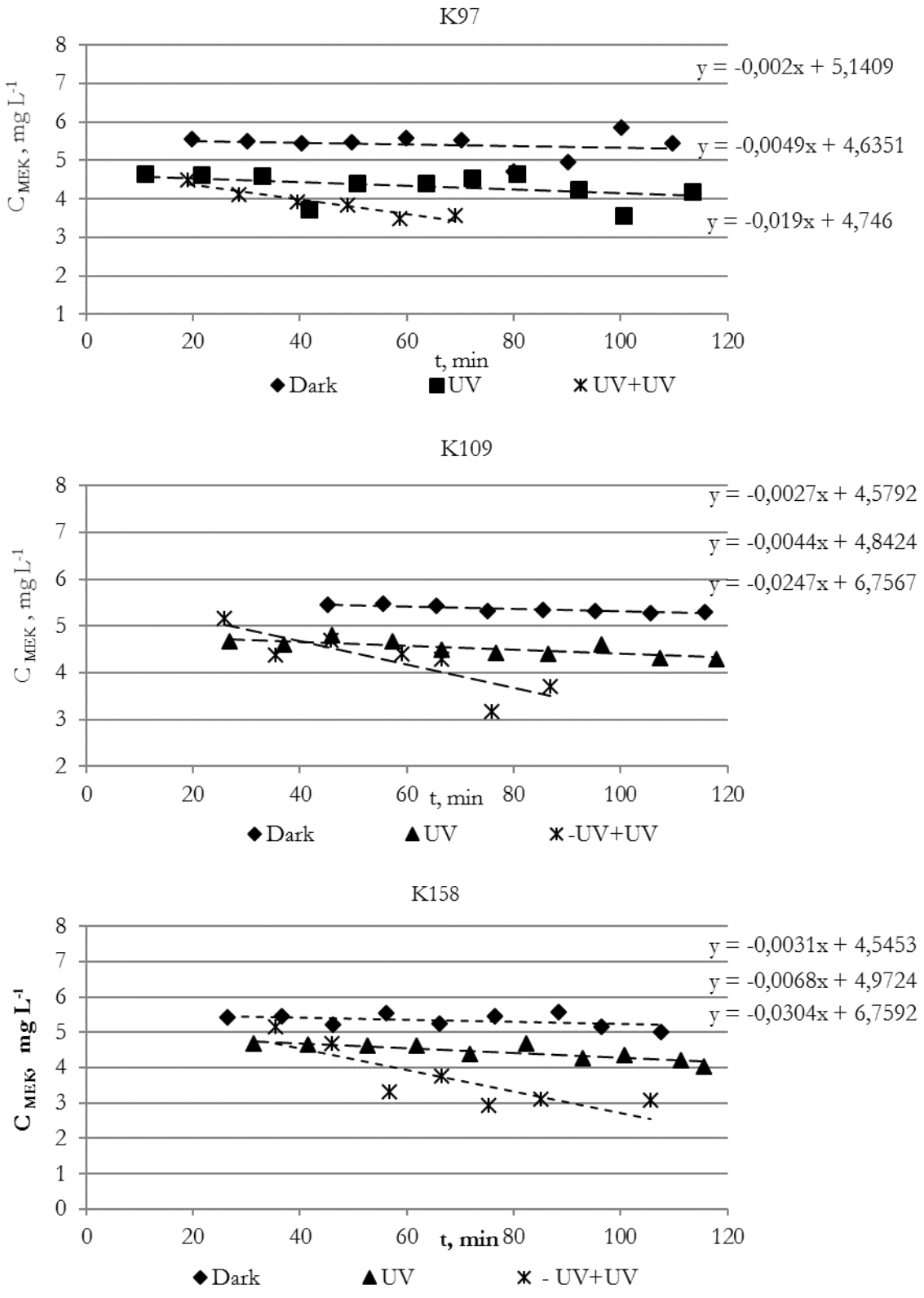

Figure 3.9. The kinetics of MEK concentration reducing on K-based materials: Dark- light isolation condition; UV- irradiation by ULTRA-VITALUX lamp; Pre-UV+ UV irradiation by ULTRA-VITALUX lamp after preliminary activation

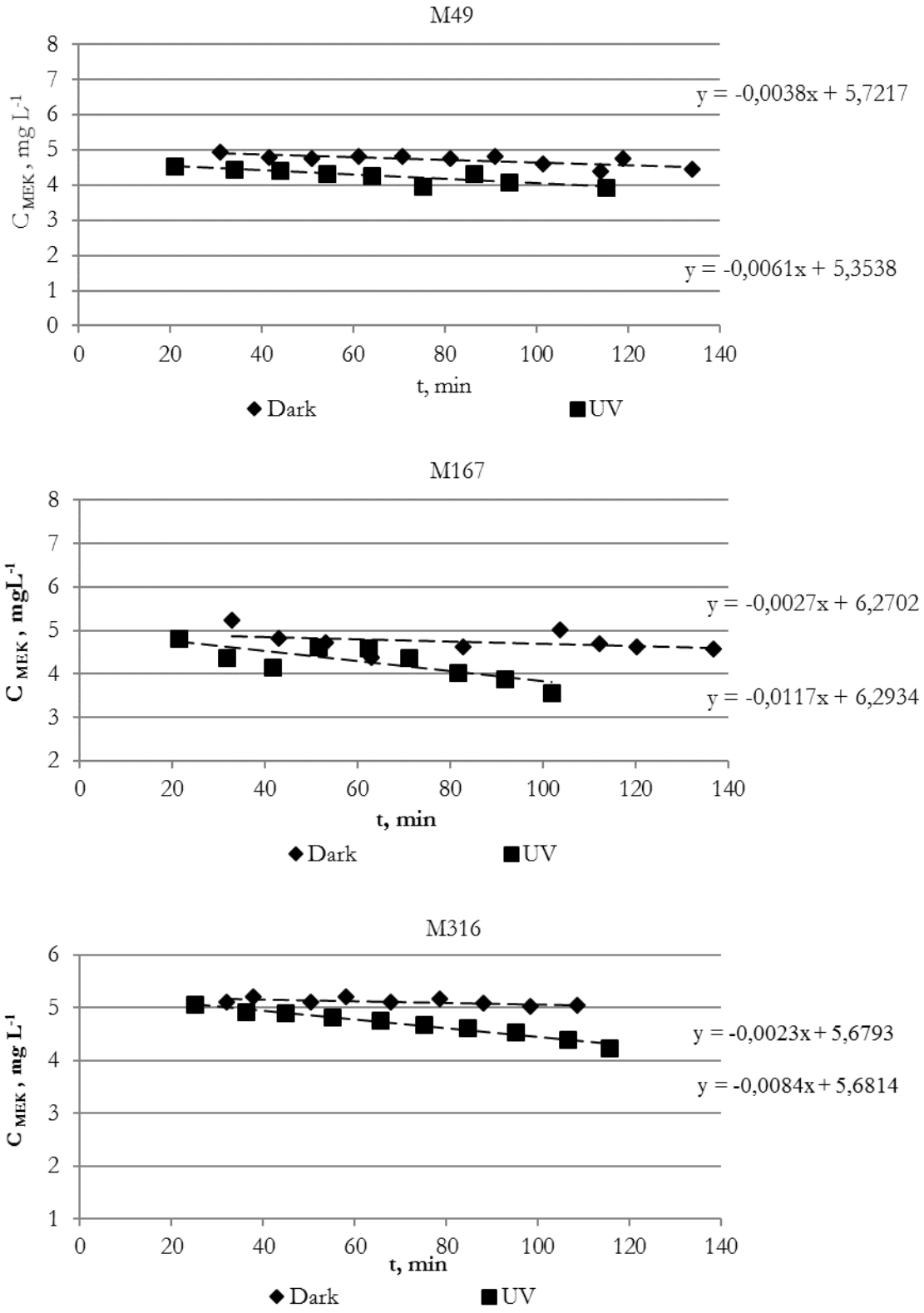

Figure 3.10. The kinetics of MEK disappirance on M-based materials: Dark- light isolation condition; UV- irradiation by ULTRA-VITALUX lamp

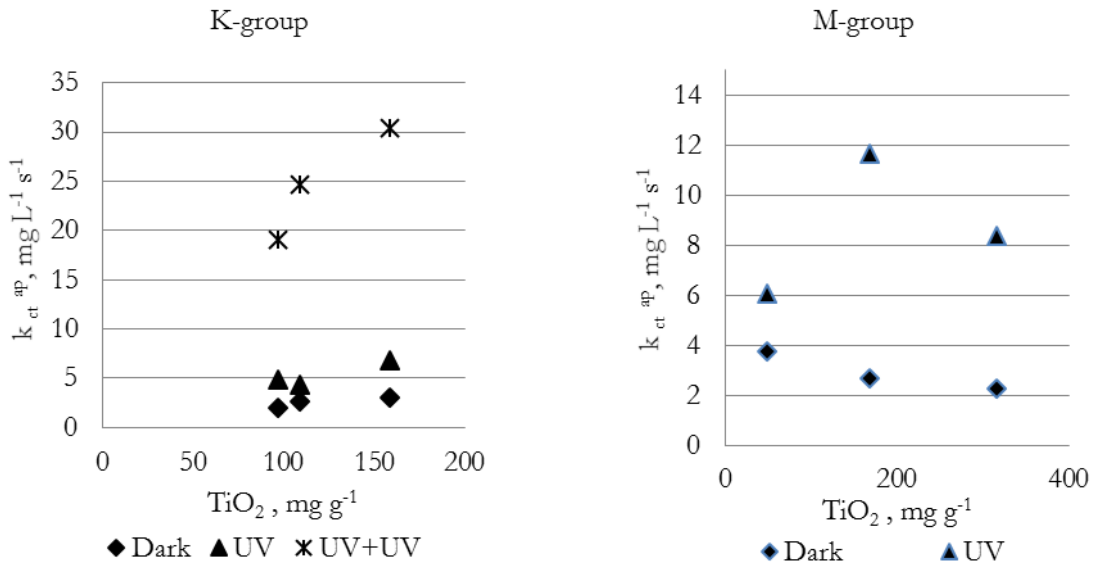

Figure 3.11. The apparent kinetic constant for MEK disappearance under various lighting conditions: Dark- light isolation condition; UV- irradiation by ULTRA-VITALUX lamp; Pre-UV+ UV irradiation by ULTRA-VITALUX lamp after preliminary activation

Based on the results presented above, the following proposals were suggested:

- Preference is given to the kaolinite matrix as more stable and economically advantageous. However, the montmorillonite-based samples also should be prepared for further researches, considering their higher UV-sensitivity.
- Therefore, it was decided to use such matrix/reaction solution ratio, that estimated TiO_2-content was equal to the contents in K97 (85.2 mg/g clay, this ratio was used also for preparing of M-samples) and K158 (191 mg/g clay).

3.6 Conclusions for Chapter 3

1. The section above focuses on the investigation of composite materials, prepared by the method of deposition TiO_2 on the aluminosilicate matrix. After three years of storage, all samples demonstrate the signs of ageing (including changes of properties over time – the monolayer capacity, the maximum adsorption capacity and the forms of adsorption hysteresis).
2. The investigation of the changes includes two groups of experiments, which were carried out in 2011 and repeated in 2014: the analysis of the water vapor adsorption isotherms and the investigation of kinetic parameters of methyl ethyl ketone removal. The examination of water vapor isotherms shows that the processes in the aluminosilicate matrix (the formation of sulfates and their impact on the titanium dioxide layer) can be a possible reason for aging. Kaolinite is more stable as a carrier material than montmorillonite. In order to confirm these conclusions, differential thermal analysis of the samples was carried out. The results showed the area of endothermic effects, typical for aluminum sulfates dehydration. The common trend for the materials of both types is a better reproducibility

for the samples treated with a lesser amount of the precursor solution. In particular, the treatment strongly affected the adsorption properties of the kaolinite-based samples and made them comparable with M-materials.

The kinetics of adsorption processes of MEK was additionally monitored. The results confirmed the data above.

3. The montmorillonite-based materials are more sensitive to ultraviolet irradiation, but reactivation allows accelerating the process of adsorption of MEK by K-samples.

4. For the synthesis of new samples, it was decided to use kaolinite as a carrier material and to prepare two samples with various amounts of TiO_2 – one of them with the matrix/precursor ratio equal to K97, while the second will be treated with a double amount of the precursor. For comparison, one sample on the montmorillonite matrix was also prepared with the ratio equal to K97.

4. The synthesis and testing UV-sensitive materials on clay supports

4.1 Introduction

The present section focuses on the synthesis of photosensitive materials on a kaolinite and montmorillonite matrix. The methods for the preparation were chosen by considering the data given in the previous chapter. Special attention is given to the characteristics of clays used as carrier materials and the influence of thermo-acid treatment on the properties of the supports.
The samples were obtained and analyzed to determine their chemical composition, morphological and adsorption properties and sensitivity to UV-irradiation in the process of MEK adsorption. The results of the experiment formed the basis for creating a pilot plant for producing materials as components of construction materials.

4.2 The clay materials characterization and the investigation of the thermochemical treatment influence

Kaolinite and montmorillonite were selected among other clays as carrier materials for the deposition of TiO_2. During the experiment, the brands of the materials were the same which had been used in 2011. Their properties are represented in Section 2.2., while the behavior of clays during thermal and acid treatment is detailed in paragraph 1.4.4 with references to literature sources.
The basic results of research are given below, including chemical composition, surface morphology images, the results of optical microscopy to determine the particle size. In addition, it was suggested that the increase of the adsorption capacity of the materials (see Sec. 3.2) could be caused by the effect of acid treatment during the preparation of the samples. Therefore, the concentration of free sulfuric acid in the precursor solution was calculated from the stoichiometric balance. The evaluated value is 86.95 g/L, or 7.8% by weight. The samples activated by the solution of H_2SO_4 with aforementioned concentration were prepared under the same conditions as titanium-containing materials. However, the conditions must be considered as "softer" in comparison with the preparation of TiO_2-containing material, considering the influence of acid formed during hydrolysis of titanium sulfate.

4.2.1 Montmorillonite and its activated form

In Chapter 3 it was mentioned, that montmorillonite is not the main carrier material considering both economic factors (e.g. higher cost, lesser availability and a limited application in construction materials producing) and lower stability of the M-samples. Despite this, they seem to be more photosensitive. It was therefore decided to prepare the montmorillonite-based samples, using lesser amount of the precursor in order to provide resistance to aging and investigate their activity.
A fine fraction (the size < 5 micron) of commercial montmorillonite (see Sec. 2.3) was applied as a solid support. The chemical composition of the untreated mineral was examined by EXDA (Sec. 2.4) (see Table 4.1.).

Table 4.1. The chemical composition of montmorillonite.

Analysis	Contents, wt %							
	Al	Si	Fe	O	Mg	K	Ca	Na
1	8.46	29.76	2.91	55.09	1.77	0.59	0.55	0.87
2	8.48	30.26	2.91	54.62	1.64	0.72	0.55	0.82
3	8.57	31.05	3.56	53.28	1.62	0.59	0.57	0.76
average	8.50	30.36	3.13	54.33	1.68	0.63	0.56	0.82

The molar ratio Al_2O_3/SiO_2 of montmorillonite after the separation is 0.25.
To assess the particle form and size, the sample was investigated by the methods (Sec.2.5) of scanning electron microscopy (Figure 4.1) and optical microscopy (Figure 4.2).

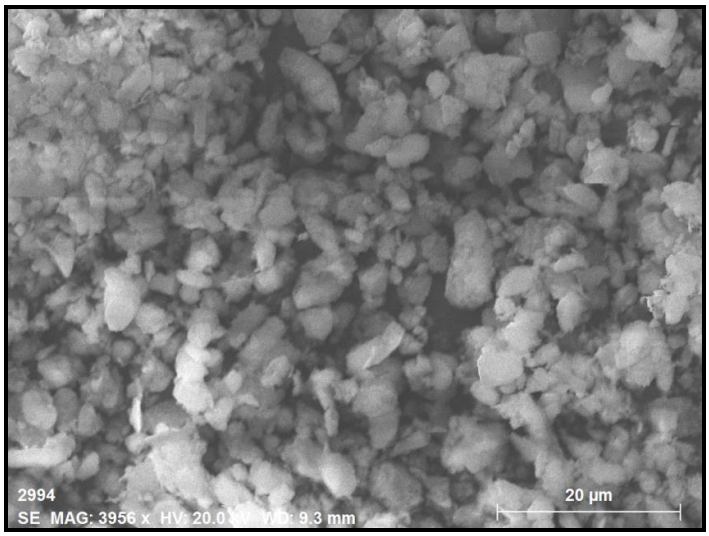

Figure 4.1. The montmorillonite particles (SEM)

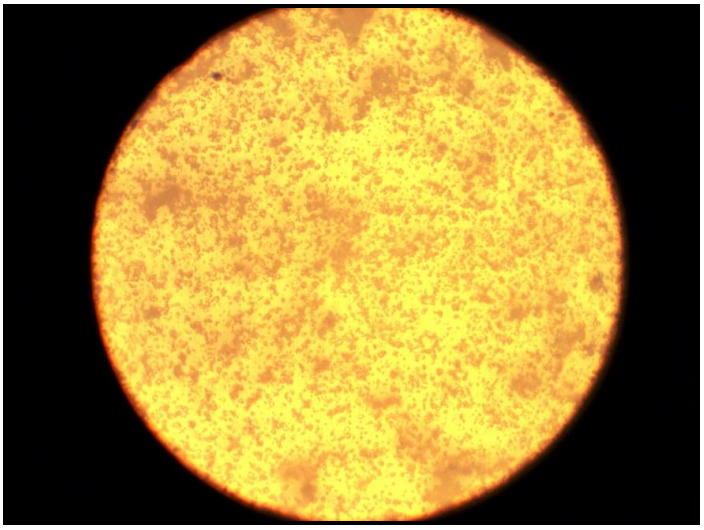

Figure 4.2. The montmorillonite particles (optical microscopy)

According to the results an average particle size is 4.87 ± 0.33 μm.
The isotherms of water vapor adsorption and the UV-sensitivity data are represented in chapter 3. Some publications pointed out that montmorillonite clays are sensitive to ultra-violet irradiation, for example in the process of chloroform [121].
However, this property for the process in gas phase was not observed in the present study.
In addition, differential thermal analysis (Sec.2.4) was performed for the sample of montmorillonite (Fig.4.3). According to the information about thermo-effects for montmorillonite [226] the DTA-curve of montmorillonite shows intense endothermic effect in the temperature range of 120-250°C due to the removal of water adsorbed on the particle surface and inter-packet gaps. The shape, size and temperature of the first endothermic peak and the weight loss, associated with this endothermic reaction depend on the nature of the saturating cation and humidity, whereas a sample is stored before the thermal analysis. Montmorillonite samples saturated with Na^+, K^+, or Cs^+ are characterized by a low-temperature endothermic unimodal shape effect, the maximum of which is observed at 180-190°C. The samples with Li^+, Ba^{2+}, Cr^{2+}, Ca^{2+} or Mg^{2+} lead to a bimodal end effect, whereas the first peak corresponds to a temperature of 160 -180°C, and the second - 210-220°C. The second peak is more noticeable for the samples, saturated with Li^+, while the thermograms of the samples, saturated with divalent cations of the first of the two low-temperature peaks have a greater intensity.

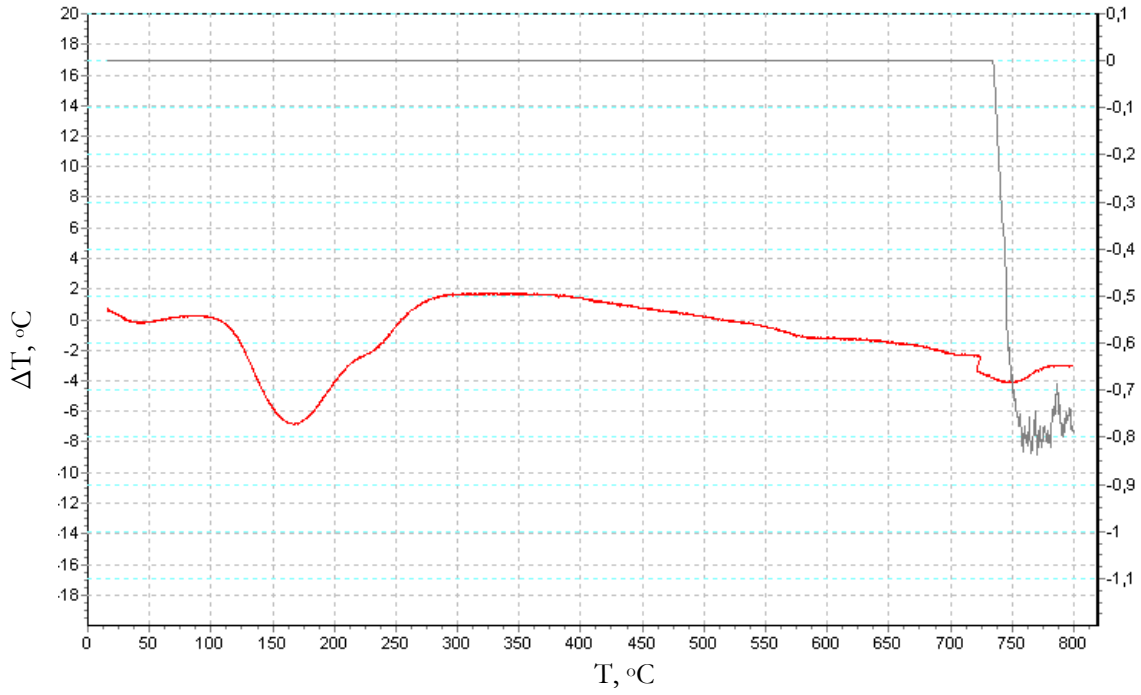

Figure 4.3. The differential thermal analysis of the montmorillonite, range 25-800 °C

The second effect is due to the loss of the OH-groups in the crystal lattice and lead to its complete destruction, respectively. The temperature and intensity of these effects depend on the chemical composition and the position of the charge in the crystal lattice for minerals of the montmorillonite group. For proper montmorillonites, the charge in the octahedron layer characterize the endothermic effects at 700 °C and 900 °C.

The presence of large amounts of iron in the crystal lattice of montmorillonite significantly lowers the temperature of the dihydroxylation reaction. The presence of magnesium in octahedral positions increases the temperature and intensity of the endothermic effect caused by the dihydroxylation reaction. The removal of OH groups in the minerals lead to reducing the mass by 5-6% of the weight of the original sample. The bulk of the constitutional portion of water is removed during the second endothermic effect and is accompanied by a partial amorphization of the material.

Therefore, the thermal properties of the sample are typical for montmorillonite clays with anion exchange complex (including Fe, K, Ma, Ca, and Mg). There were two peaks in the range of 100 to 270 °C, and the next one – in the range over 700 °C.

In order to investigate the influence of H_2SO_4, the montmorillonite samples were prepared by the same method (treatment with sulfuric acid with further hot air drying and calcination at 600 °C), which was used for the preparation of TiO_2-containing materials. The details are described in Section 2.2.

The concentration of the solution and the precursor/matrix ratio were selected on the basis of the following considerations:

- The concentration was calculated by the stoichiometric ratio and amounted to 86.95 g/l, or 7.8% wt (see Sec. 2.2).
- As will be seen below, the content of Ti in the solution was 17.47 g/L. For the preparation of the samples with the content of TiO_2 greater than 85 mg/g, the matrix/precursor ratio should be 1 g per 3 ml, respectively.

The yield of the activated material was 0.881 g/g of montmorillonite, while according EXDA composition analysis (Sec. 2.4) the molar ratio of Al_2O_3/SiO_2 is 0.17. The sample ID is **M (1:3) act**.

Table 4.2. The chemical composition of the montmorillonite-based sample after thermo-acid activation.

Analysis	Contents, wt %									
	Al	Si	Fe	O	Mg	K	Ca	Na	S	Au
1	9.42	39.09	5.12	41.61	1.26	0.40	-	0	3.10	0
2	6.65	22.35	2.61	46.1	1.35	0	-	1.01	2.81	17.10
3	3.02	36.45	1.23	53.66	0.47	0.28	-	0	4.89	0
average	6.36	32.63	2.99	47.12	1.03	0.23	-	0.34	3.60	5.71

It should be clarified that the presence of Au is considered an accidental impurity and this issue will not be touched upon further. The molar ratio decreased from 0.25 to 0.17, which can be indicative of dissolution process of the aluminum oxide structural layer. The content of oxygen also decreased significantly compared with pure montmorillonite, which is possibly caused by the loss of adsorbed and structural water, although the temperature of the treatment was less than 700 °C. The possible explanation is that the simultaneous impact of acid and high-temperature treatment could destroy the material structure.

The reduction of alkali metals and alkaline earth metals concentrations is more difficult to explain, given that the yield of the material is less than 1 g. The compounds and ions could not be leached during the experiment given that the technique did not provide the dilution in water. Perhaps this is due to the entrainment of the solid particles in flowing vapors and SO_2, during drying and calcination.

The results of SEM (Sec. 2.5) showed no significant structural changes after processing the sample (see Fig. 4.4). The surface retained a scaly structure, which is typical for natural clays.

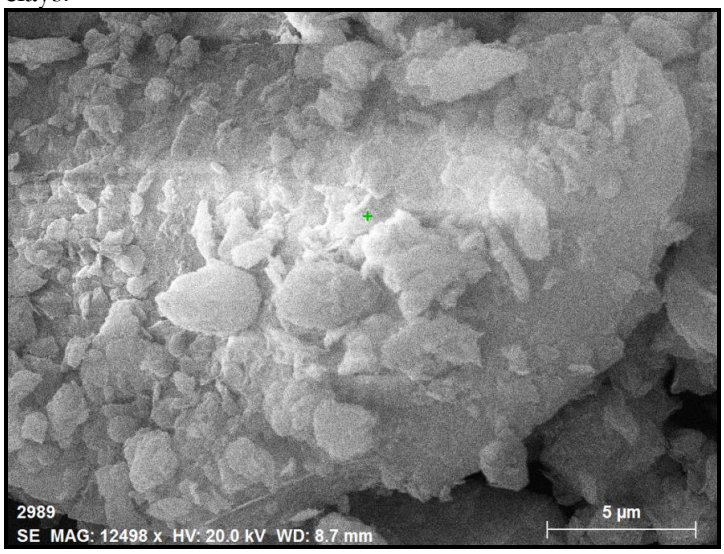

Figure 4.4. The M(1:3)act particles (SEM image)

The isotherm of water vapor adsorption at 25 °C was obtained for the sample (see Figure 4.5 in comparison with the isotherm obtained for pure montmorillonite in 2014).

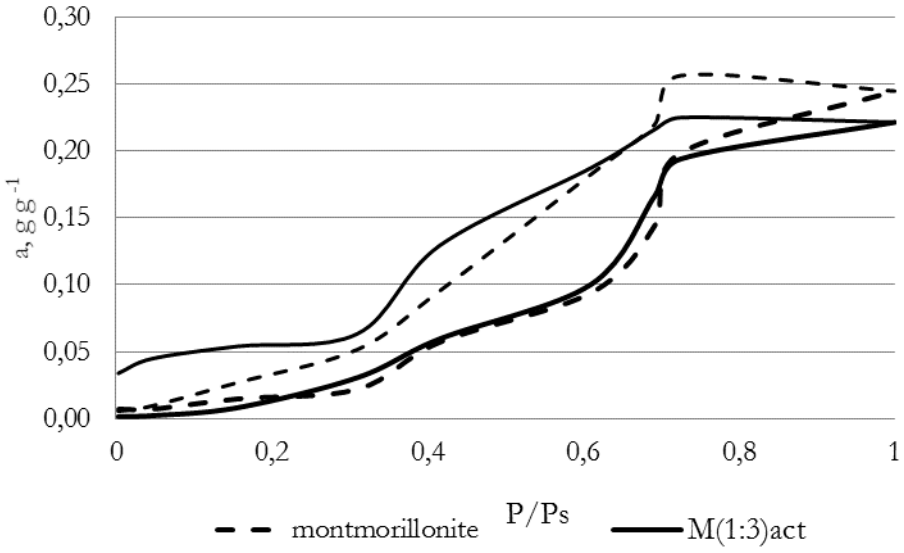

Figure 4.5. The isotherms of water vapor on M (1:3) act samples (comparing with montmorillonite)

The results show that the adsorption capacity of the material did not change significantly after the treatment. However, the large area of the hysteresis loop may be due to the hydration of sulfates, formed during the treatment.
Furthermore, the UV-sensitivity of the samples of the activated clay was investigated in the reactor (0.45 L) based on the analysis of reduction of the MEK concentration (see Paragraph 2.8.2). Kinetic curves are represented in Figure. 4.6.

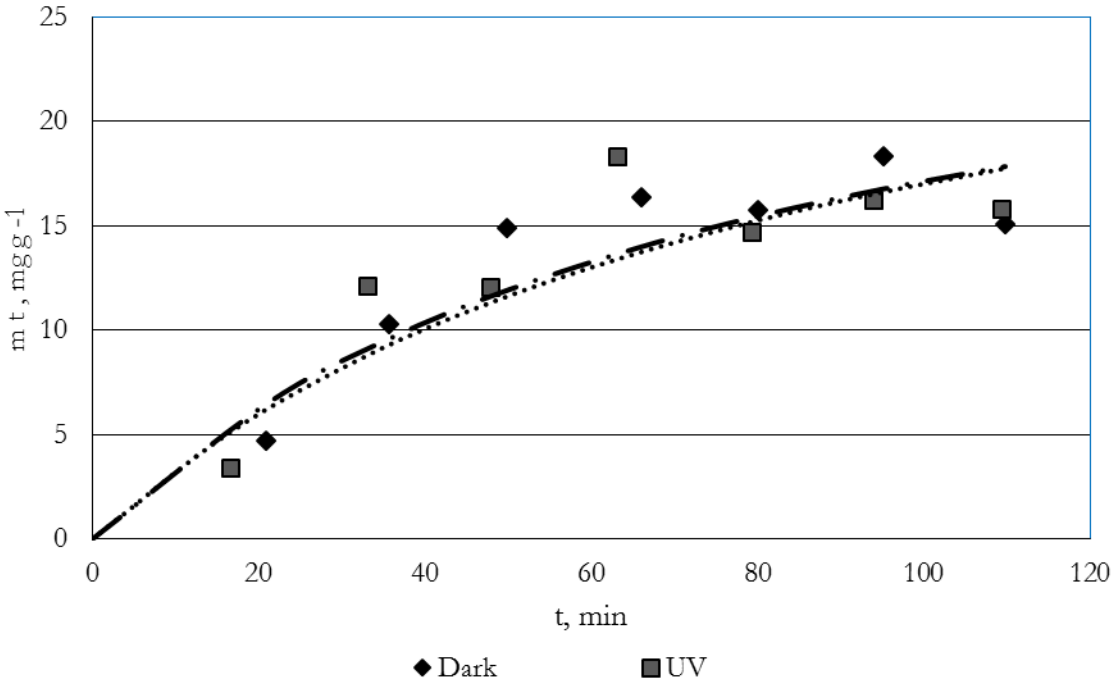

Figure 4.6. The kinetic line of a changing of the disappeared MEK specific mass per 1 g of M(1:3) act material at time (min)

The values of the concentration are all quite similar. Based on this information, it appears that the sample does not have a significant UV-sensibility.

4.2.2 Kaolinite and its activated form

The examination of the samples of activated kaolinite included the same methods, which were used for the investigation of the M-sample, including a chemical composition analysis, SEM and optical microscopy and a differential thermal analysis (Sec.2.4, 2.5). The results are represented in table 4.3 and in Figures 4.7-4.9.
The molar ratio Al_2O_3/SiO_2 for kaolinite after the separation is 0.95.
The presence of titanium was detected and confirmed by using the MFS method. Given that the average layer charge is near zero, kaolinite does not contain such exchange ions as montmorillonite. The structure of the surface is less orderly compared with montmorillonite, while an average particle size is 4.40 ± 0.33 μm (see Sec 2.5).

Table 4.3. The chemical composition of the kaolinite.

Analysis	Contents, % wt (EXDA)					Content TiO_2, mg/g matrix	Content TiO_2 by MFS	
	Al	Si	Fe	O	Ti		T% wt	TiO_2 mg/g $_{mat}$
1	22.4	22.0	1.6	55.2	0.8	16.4	0.6	10.1
2	22.0	21.1	1.8	53.9	1.1			
3	22.21	21	1.7	54.05	1.02			
average	22.2	20.7	1.7	54.4	0.97			

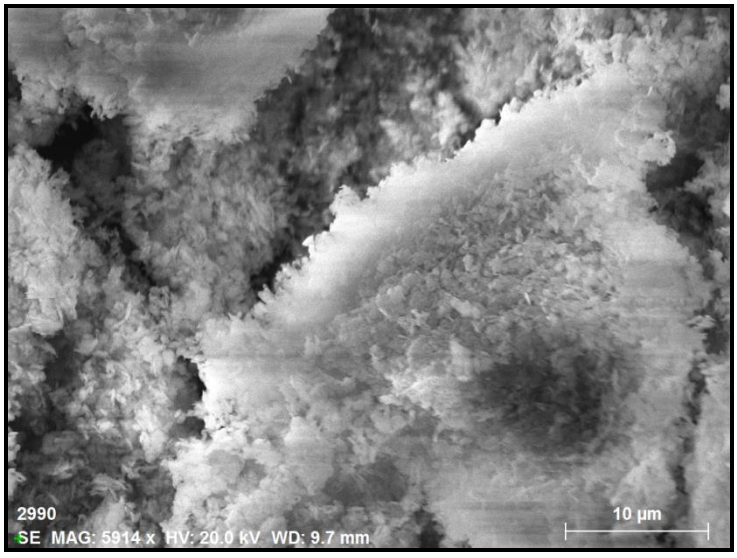

Figure 4.7. The kaolinite particles (SEM image)

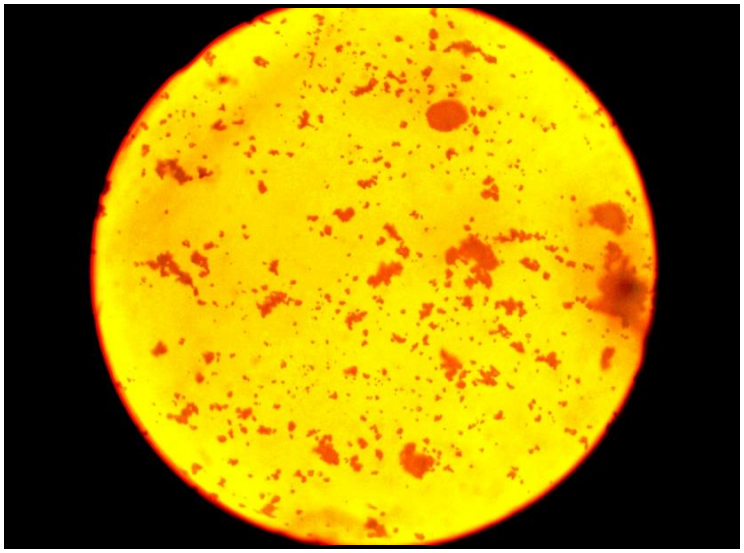

Figure 4.8. The kaolinite particles (optical microscopy)

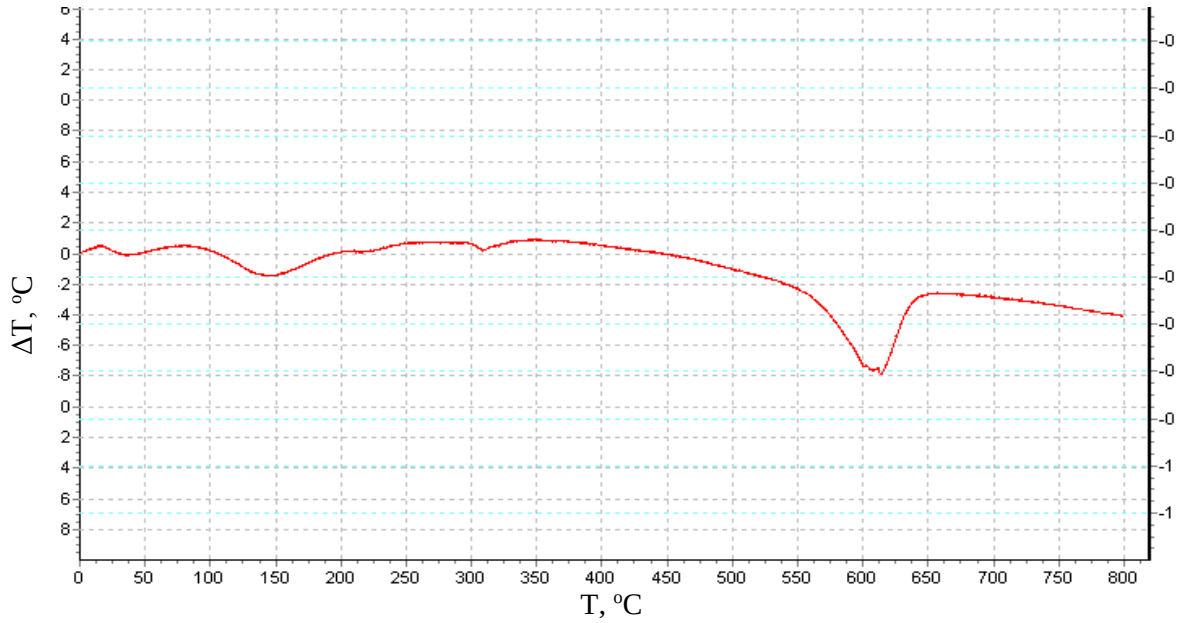

Figure 4.9. The differential thermal analysis of the montmorillonite, range 25-800 °C

According to the information about thermo-effects for kaolinite[226] the DTG-curve shows a weak low-temperature endothermic effect for kaolinite in the temperature range of 120-160 °C which is caused by the removal of adsorbed water. Since kaolinite often is not capable of inter-packet sorption of water, the endothermic effect is an insignificant intensity and it corresponds to a small mass reduction, measured in dozens of percent by the weight of a sample. In the temperature range of 550-650 °C the decay of a crystal lattice is accompanied by the loss of hydroxyl groups without destroying the molecule (dihydroxylation). There is an exothermic peak at about 1000 °C which can be explained by the formation of the allophonic molecule in an admixture with molecules of silica.

Like with montmorillonite, the sample of kaolinite were subjected to thermochemical treatment to identify the reasons for the increase of adsorption activity. The method of preparation of the activated material is described in paragraph 4.2.1. Two samples of kaolinite-based, K(1:3) act and K(1:6) act materials were prepared with the matrix/precursor ratio of 1g per 3ml and 1g per 6ml, respectively. Their chemical compositions are represented in Table 4.4.

The yields of the samples were 0.936 g/g and 1.049 g/g for K (1:3) act and K (1:6) act, respectively. The molar ratio of Al_2O_3/SiO_2 is from 0.95 (for pure kaolinite) to 0.9-0.83, while there is a negative correlation between this ratio and the amount of added acid solution. There is a significant presence of sulfur, which can be an indication of the aluminum sulfates formation. Hence, the assumption of the influence of the sulfate hydration on the drying properties is confirmed. It should be added that for montmorillonite Al_2O_3/SiO_2 the ratio was 0.25 and decreased to 0.17 after the treatment.

Table 4.4. The chemical composition of the kaolinite-based samples after thermo-acid activation

Samples	Contents, wt %						Content TiO_2, mg/g matrix	Molar ratio Al_2O_3/SiO_2
	Al	Si	Fe	O	Ti	S		
K(1:3) act	27.16	23.66	1.76	38.4	1.00	6.70	20.2	0.90
	23.66	22,44	1.63	45.1	1.38	5.80		
	17.73	20.63	2.14	53.15	1.14	5.20		
	average							
	22.85	22.7	1.84	45.54	1.19	5.89		
K(1:6) act	15.55	18.00	1.00	53.20	0.90	15.70	15.56	0.83
	18.0	22.30	1.20	50.10	-	8.33		
	17.1	17.20	0.60	49.10	0.95	13.40		
	average							
	16.9	17.9	0.95	50.80	0.92	12.50		

The content of sulfur for the activated montmorillonite was 3.6%, which is around 1.5 times lesser than for K (1:3) act. However, the presence of other metals (6.82 % wt in total) could lead to the formation of non-aluminum sulfates, which can affect the activity of the water vapor adsorption.

The SEM surface micrograms (Fig. 4.10) did not show significant changes in the structure of the activated kaolinite-based samples.

K(1:3)act K(1:6)act

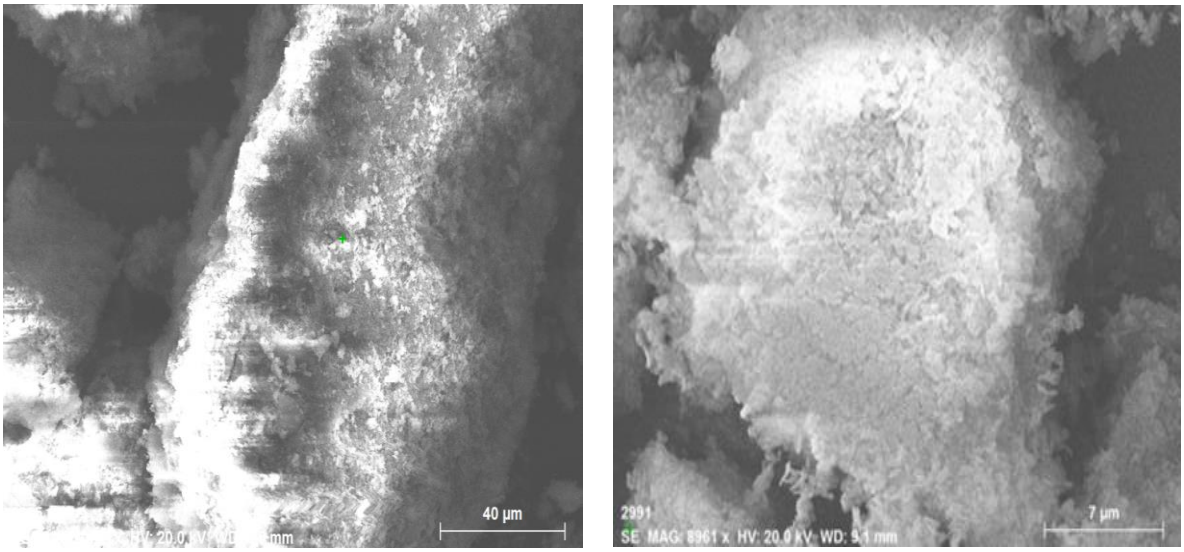

Figure 4.10. The activated kaolinite particles (SEM image):
K (1:3) act (left) and K (1:6) act (right)

The water vapor adsorption isotherms (Paragraph 2.7.1) obtained for the K-materials (see Fig. 4.11) demonstrate a significant increase of the adsorption capacity. Such effect could be caused by the formation of micropores [214], but it is doubtful for the kaolinite matrix.

The hysteresis and the values of the capacity also presuppose the process of hydration of the carrier material. Unlike the titanium-containing samples, the samples of the activated clay, shows relatively high values of the capacity at low P/P_s. The adsorption capacity of the activated materials increases with the amount of sulfuric acid used during the treatment.

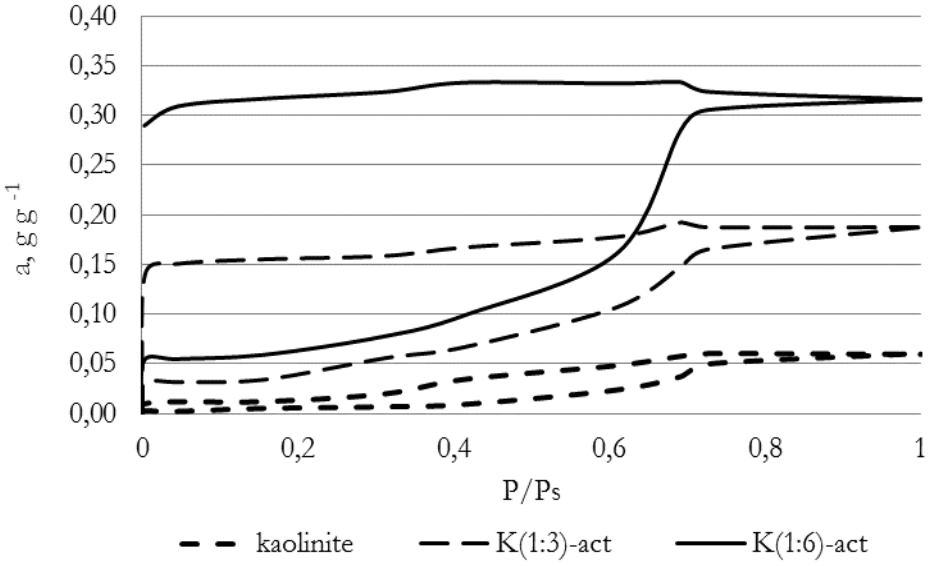

Figure 4.11. The isotherms of water vapor adsorption on activated kaolinite

In this case, the applicability of the BET equation to calculate the monolayer capacity is essentially formal, since it does not correspond to the expected mechanism of adsorption. However, the equation was used to determine the values at $P/P_s<0.35$ (see Tab. 4.5).

Table 4.5. The chemical composition of the kaolinite-based samples after thermo-acid activation

Samples	Monolayer capacity BET, a_m, mmol/g	Maximum capacity P/Ps=1, a_s mg/g
Kaolinite*	0.25	60
K(1:3)act	2.05	187
K(1:6)act	2.92	316
Montmorillonite*	2.25	258
M(1:3)act	2.03	221

*- the data duplicated from Table 3.2

These results confirm the data above. It is worth noting the decrease of the capacity for montmorillonite. Therefore, the treatment method allows activating kaolinite for a subsequent use as a desiccant.

The presence of Ti required the investigation of UV-sensitivity of the samples. For that purpose, the experiment adsorption of MEK adsorption under ultra-violet irradiation was performed (see Paragraph 2.8.2). The results are represented in Figure 4.12.

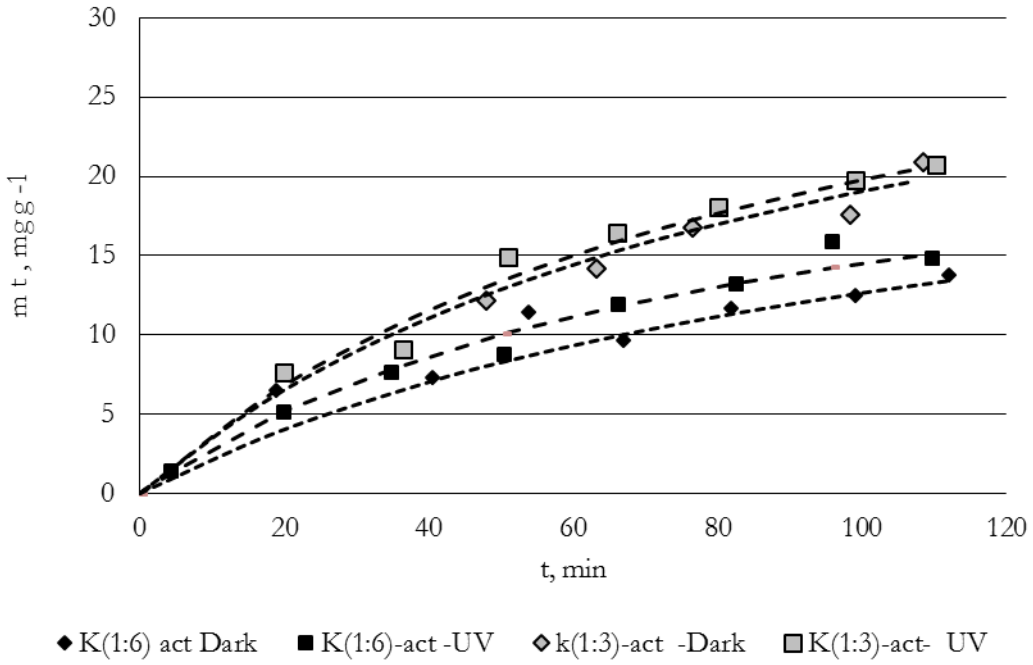

Figure 4.12. The kinetic line of a changing of the disappeared specific MEK mass per 1 g of K-material at time

In this case, the influence of the UV-irradiation was not investigated precisely, given that the results obtained in various conditions are intersected. It is worth noting that the lines of the more hydrophilic material K(1:6) act is at lower values.
Thus, the chemical composition, particle size and thermal behavior were investigated. The influence of thermo-acid treatment on the water vapor adsorption process was examined, and the increase of the activity for the kaolinite-based samples can be observed (possibly, due to the formation of aluminum sulfates). While the activated montmorillonite also contains sulfates, its activity was not affected significantly.
The investigation of UV-sensitivity was performed, but neither material demonstrates the increase of the MEK adsorption rate.

4.3 Composite materials: Synthesis, Structure and Properties

4.3.1 The choice of technology for TiO_2-containing materials preparation

The development of building materials able to passive decomposition of indoor and outdoor pollutants is an important area of research for the department of Materials, Environmental Sciences and Urban Planning - SIMAU Università Politecnica delle Marche.

[1, 3, 5] Paragraph 1.1 describes this in details. Adsorbents and photosensitive components can be used for the preparation of such materials. [17, 41]
Many studies, for instance [41], describe commercial materials applied as supplements.
At the same time, requirements for the materials, used in building industry, can be less strict than for those used in the production of energy, industrial catalysis, wastewater treatment and etc. For these areas, such properties as high degree of selectivity, reproducibility of characteristics and activity are not necessary, while low selectivity, effectiveness in indoor conditions (such as humidity, temperature and low concentrations of pollutants) and activity under domestic light sources (including domestic lamps, LEDs or even daylight) are important for passive degradation process. That is why the proposed method is based on the use of waste from surface treatment of titanium and available supports and can be easily combined with production of construction materials.
The method of obtaining composite is described in detail in Section 2.2. The thermo-acid treatment with sulfuric acid was chosen as a prototype, given that the treatment allows producing anatase crystalline modification, which is more resistant to high-temperature (see paragraph 1.3). Near 30 years ago Anpo [93-97] obtained the samples of TiO_2-SiO_2 [and TiO_2-Al_2O_3 by the method of co-deposition, and tested them in the reactions of hydrocracking of $CH_3C{\equiv}CH$ (for SiO_2) and $CH_3HC = CH_2$ (for Al_2O_3). Later, the information about TiO_2/clay composites was published in [109, 227] The effectiveness of air purification, comparable and even superior to the effectiveness of the material Degussa P25 was confirmed.
Based on the information provided by the literature sources [182, 183] the temperature of 600ºC was chosen for calcination since such treatment allows obtaining anatase modification of TiO_2. However, the studies confirmed the presence of sulfates (including aluminium sulfates), which are undesirable in finishing materials, given that they can affect human health [224]. It was therefore decided to use higher temperature during calcination to decrease the amount of sulfur in the samples. In [77] it was mentioned that thermal treatment at temperatures between 650 ºC and 950 ºC can cause the process of formation of rutile-anatase mix. It is known that for most reactions titanium dioxide shows a higher activity in the anatase phase than other polymorphic modifications [227,228]. It was suggested that anatase has a high photoreactivity due to a higher location of the Fermi level which reduces the ability to absorb oxygen and increases the degree of hydroxylation (i.e., a number of hydroxyl groups on the surface) [229.]. However, there are works the authors of which claim that the mixture of anatase (70-75%) and rutile (30-25%) is more photoactive than pure anatase [61.]. In this case, the minimum upper limit of the temperature was chosen based on the conditions of chemical interaction between kaolinite and sulfuric acid. [230] According to the data, the treatment at more than 750 ºC can cause the formation of metakaolin, which is highly soluble in H_2SO_4. However, the dissolution of the aluminosilicate matrix was not the main goal of this study. Therefore, it was decided to limit the temperature to 750 ºC which could provide the decomposition of aluminium sulfate without destructing the structure of kaolinite matrix. That is why, the preparation of the samples was carried out at 600 ºC and 750 ºC.

4.3.2 The synthesis of composite materials

The composites were obtained by the method described in Section 2.2 but according conclusions of Chapter 3. The precursor was added to the support in the ratio which provided the content of TiO_2 equal to 87.5 mg/g_{clay}. The second was chosen for providing the doubled amount of the catalyst. The conditions are represented in Table 4.6.

Table 4.6. The conditions for the preparation of titanium-containing samples

Support	Conditions				Samples ID	Yield, g/g_{clay}
	Mass of support, g	Volume of reaction solution, ml	Temperature of heat-treatment, °C	TiO_2 inputted with solution*, mg/g_{clay}		
Montmorillonite	1	3	600	87.52	M(1:3)-600	1.46
	1	3	750	87.52	M(1:3)-750	0.88
Kaolinite	1	3	600	87.52	K(1:3)-600	1.31
	1	6	600	175.05	K(1:6)-600	1.61
	1	3	750	87.52	K(1:3)-750	1.08
	1	6	750	175.05	K(1:6)-750	0.76

*The concentration of titanium in the solution is 17.47 mg/ml

The results show that the yields of the materials, obtained at a higher temperature decreased significantly (by 40% for the montmorillonite-based samples and by 18-53% for the kaolinite-based samples), compared with the composites, obtained at 600 °C. This is due to the disposal of sulfur in oxide forms. However, it was also noted that the yields of two samples are lower than the original mass of clays. Along with the insignificant loss of the mass during sieving and shredding of the materials, the possible explanations are the disposal of structural water and the transformation of aluminosilicate layers. The process affects M (1:3)-750 more than K (1:3)-750 despite the similar method of the treatment, perhaps due to the higher amount of water in montmorillonite and lesser resistance of the matrix to sulfuric acid. [112, 116]. The formation of mesopores, which can be indicative for this process, is described below.

Figure 4.13 shows the samples before and after calcination. The samples obtained under a high-temperature treatment have a yellow tint which may be indicative both of the formation of rutile and for the diffusion of iron during the decomposition of the aluminosilicate matrix.

4.3.3 The study of chemical composition and surface morphology of the samples

The chemical composition was determined by the method of EXDA, while MFS was used for investigating the titanium content (see Sec. 2.4, 2.5). The results are represented in Tables 4.7-4.8, while Figure 4.14 shows the images of microprofiles, obtained by scanning electron microscopy. This data allow identifying common trends specific to the thermochemical treatment of montmorillonite and kaolinite at various temperatures. The two different methods were used for analyzing the amount of titanium and the results were significantly different.

Figure 4.13 The samples during the synthesis: a- after drying, b- after calcination (600°C on the left, on the right - 750°C), c - K(1:3)-600, d – K(1:6)-750, e- K (1:3)-750, f- K(1:6)-750.

The analysis of the results leads to the following conclusions:

- The content of titanium dioxide differs significantly from the estimated one. Thus, the amount of TiO_2 in the samples obtained after calcination at 600 °C, was 1.5-2.5 times lower than those, added with the precursor, while for the composites prepared at 750 °C this value is 1.3-2.7 times higher than estimated one. The sample M (1:3)-750 is only one which matched the expected content.
- Despite this, there are some general trends. For example, the amount of titanium is higher for K(1:3)-600 than for K(1:6)-600. The content differs most for kaolinite-based samples obtained at 750 °C. Figure 4.14 demonstrates the surfaces of the samples prepared at different temperatures.
- The influence of the treatment on the aluminosilicate matrix was investigated for the molar ratio Al_2O_3/SiO_2. The ratio did not change significantly for the M-material, compared to pure montmorillonite. In terms of aluminum content, M(1:3)-600 was slightly different, but for the sample obtained by high-temperature calcination, the ratio is equal to the basic value (0.27). As for the K-samples, the Al_2O_3/SiO_2 ratio (which is 0.95 for the untreated clay) insignificantly decreased after the treatment with a big amount of the precursor (it is 0.81 for K(1:3)-600). However, high-temperature calcination increases this characteristic to 1.03 in for K(1:3)-750, and to 1.2 for K(1:6)-750. Given that the method does not include the leaching of the samples, the different values of the rate could be explained only by the loss of particles during calcination, although it was not observed directly. Such process can affect adsorptive properties.
- The content of sulfur is 6-10 times higher for the samples, obtained during the calcination at 600 °C. While the amount of sulfur increased around 2 times, proportionally to the amount of the added precursor, the content of the residual sulfur did not depend on the original clay/precursor ratio and the values are 1.72 and 1.22 for K (1:3)-750 and K (1:6)-750, respectively. Montmorillonite-based samples contain more sulfur than the K-materials under the treatment at different temperatures. Complete sulfur removal is undesirable, given that sulfur has positive effects on the adsorptive characteristics of the materials (see Paragraph 1.3). At the same time, because of the complex chemical composition of montmorillonite, it can be assumed that sulfur is contained in thermo-resistant forms, compared with aluminium sulfate and therefore it does not limit the field of application.
- The SEM results demonstrate that the surface of the samples, obtained at 600 °C is similar to the surfaces of untreated clays. At the same time, materials prepared at 750 °C have a smoother, more geometrically regular surface without scales.
- Optical microscopy was used to determine the form of average particles (Fig. 4.15) and the size (Table 4.9) for obtained materials. The results showed that the treatment of kaolinite allows obtaining particles with the average size < 5 μm, while for the montmorillonite-based samples the same parameter is around 7-10 μm. The finest and most homogeneous particles were obtained for the sample K(1:6)-750.

Table 4.7 The composition of montmorillonite-based samples

Samples		Contents, wt %											TiO2/ Σcomp otents, mg/g	Molar ratio Al_2O_3:SiO_2	Contents (emission-spectral - analysis)		Estimated amount of TiO_2/ Σcompotents, mg/g
		Al	Si	Fe	O	Mg	K	Ca	Na	Au	Ti	S			Ti , % wt	TiO_2, mg/g	
M (1:3)-600	1	6.04	24.83	2.25	54.38	1.21	0	0	1.1	0	1.27	8.92	28.66	0.22	2.10	36.30	63.77
	2	6.2	25.58	1.58	54.82	1.4	0	0	0.82	0	1.54	8.06					
	3	6.85	25.31	1.97	52.65	1.38	0	0	0.85	0	2.2	8.79					
	average	6.36	25.24	1.93	53.95	1.33			0.92		1.67	8.59					
	matrix Al_2O_3;SiO_2, mol/g	0.12	0.54														
M (1:3)-750	1	10.3	28.06	2.09	50.16	1.53	1.4	0	0	0	4.64	1.82	99.88	0.27	6.40	119.51	110.44
	2	7.94	25.87	2.11	54.93	1.68	0.22	0	0	0	4.18	3.07					
	3	7.48	28.7	2.98	49.03	1.39	0.5	0	0	0	7.51	2,41					
	average	8.57	27.54	2.39	51.37	1.53	0.71				5.44	2.43					
	matrix Al_2O_3;SiO_2, mol/g	0.16	0.59														

Table 4.8. The composition of kaolinite-based samples.

Samlpe		Contents, % wt						TiO_2/ Σcompotents, mg/g	Molar ratio Al_2O3/SiO_2	Content (emission-spectral - analysis)		Estimated amount of TiO_2/ Σcompotents, mg/g
		Al	Si	Fe	O	Ti	S			Ti , % wt	TiO_2, mg/g	
K(1:3)-600	1	20.19	18.98	1.65	50.7	2.81	5.67	53.37	0.93	2.50	43.51	71.59
	2	21.71	20.4	1.97	45.73	4.23	5.96					
	3	15.29	14.65	1.47	55.74	2.07	10.8					
	average	19.06	18.01	1.70	50.72	3.04	7.47					
	matrix Al_2O_3;SiO_2, mol/g	0.36	0.39									
K(1:6)-600	1	13.12	13.24	1.49	54.81	2.54	14.8	48.82	0.81	2.30	39.89	121.99
	2	12.32	13.98	0.85	54.25	2.2	16.4					
	3	16,59	18.81	1.37	49.1	3.63	10.5					
	average	14,01	15.34	1.24	52.72	2.79	13.91					
	matrix Al_2O_3;SiO_2, mol/g	0.26	0.33									
K(1:3)-750	1	21.71	17.99	1.85	45.26	11.52	1.67	241.67	1.03	17.70	358.73	88.18
	2	22.66	18.71	2.67	41.05	13	1.91					
	3	20.05	18.62	2.37	46.9	10.48	1.58					
	average	21.47	18.44	2.30	44.40	11.67	1.72					
	matrix Al_2O_3;SiO_2, mol/g	0.41	0.39									
K(1:6)-750	1	23.15	13.75	2.24	44.45	15.19	1.22	386.09	1.20	25.80	755.45	299.25
	2	20.12	17.65	2,23	42.03	16.78	1.19					
	3	20.02	15.23	2.45	42.9	18.12	1.28					
	average	21.10	15.54	2.31	43.13	16.70	1.23					
	matrix Al_2O_3;SiO_2, mol/g	0.40	0.33									

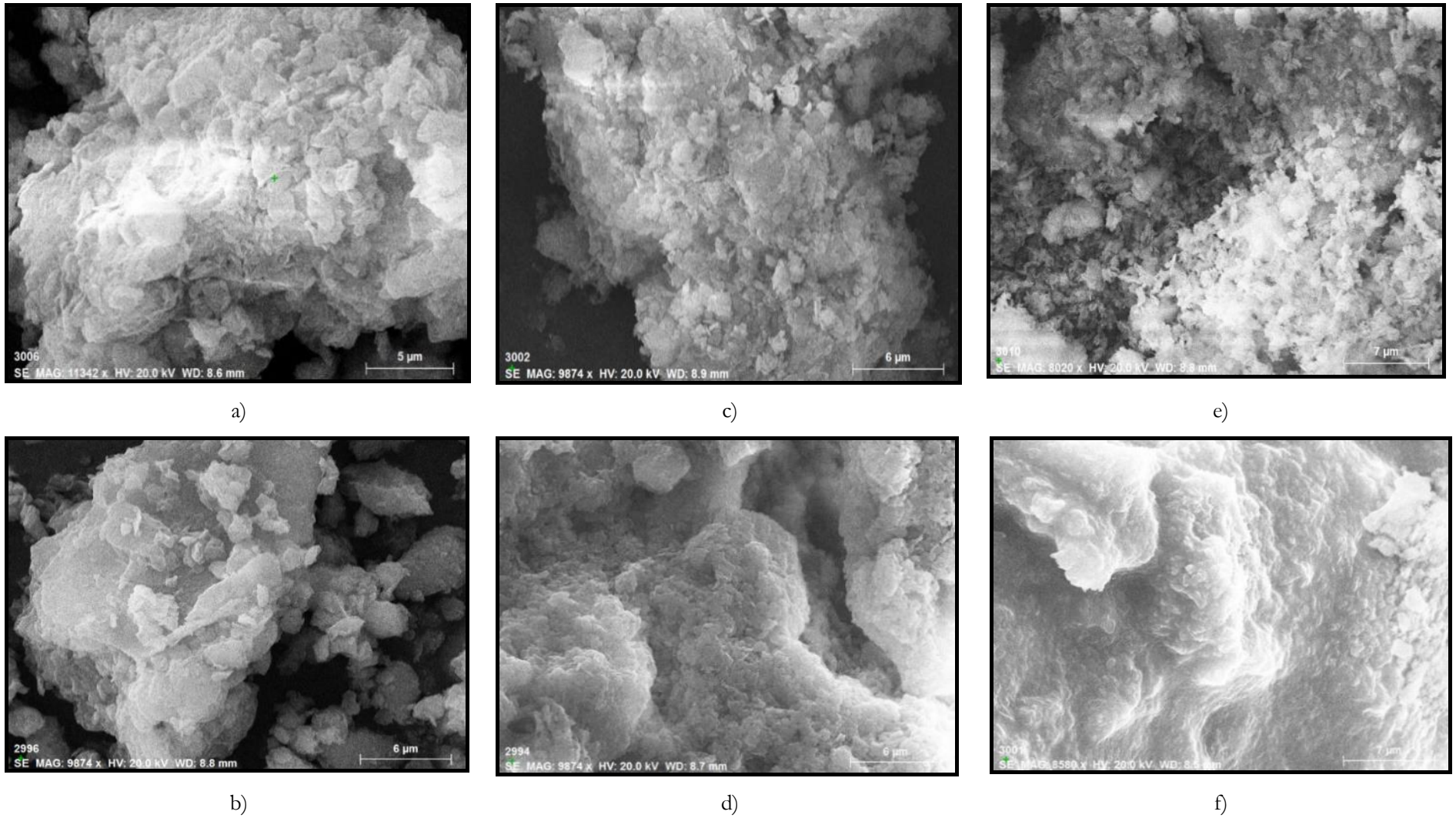

Figure 4.14 The microstructures of the samples: a) M(1:3)-600; b) M(1:3)-750; c) K(1:3)-600; d) K (1:3)-750; e) K(1:6)-600; f) K(1:6)-750

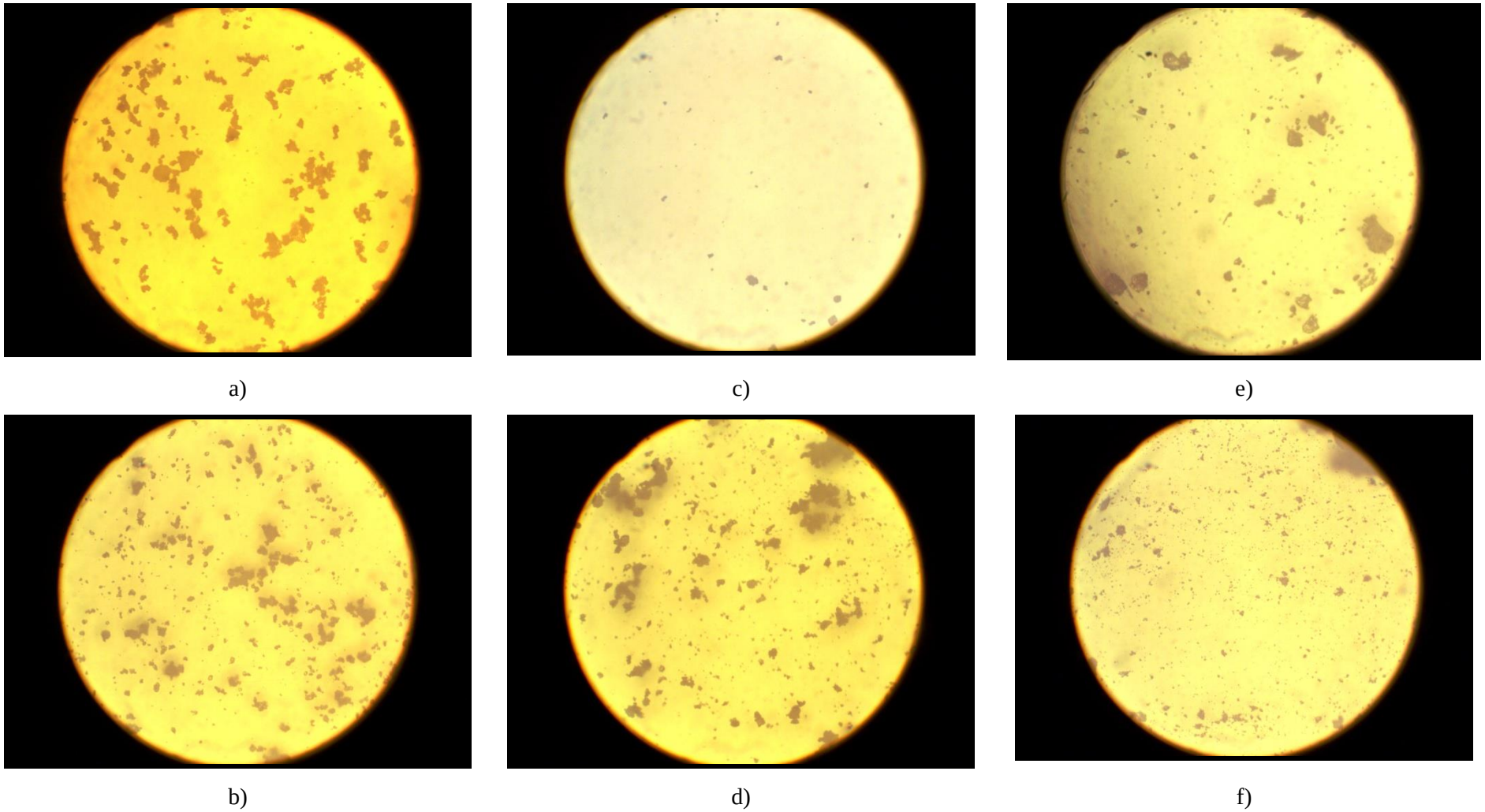

Figure 4.15 The optical microscopy: a) M(1:3)-600; b) M(1:3)-750;c) K(1:3)-600; d) K (1:3)-750; e) K(1:6)-600; f) K(1:6)-750

Table 4.9 Average particle size.

The sample	The particle size, μm
M(1:3)-600	10,07 ± 0,75
M(1:3)-750	7,34 ± 0,58
K(1:3)-600	3,93 ± 0,39
K(1:6)-600	4,18 ± 0,43
K(1:3)-750	4,53 ± 0,25
K(1:6)-750	2,72 ± 0,14

Therefore, the processing of kaolinite makes it possible to obtain particles with the average size lesser than 5 μm, while for the montmorillonite-based material the average particle size is around of 7-10 μm to be obtained.

4.3.4 Water vapor adsorption isotherms for TiO_2-containing material

The influence of the thermo-chemical treatment on the adsorption activity of the samples was examined by the analysis of water vapor and benzene vapor adsorption. As mentioned previously (see Paragraphs 4.1.1 and 4.1.2), the sulfuric acid treatment of a clay support, strengthened by the impact of high temperature, increased the adsorption capacity. During the reactions, the concentration of the used precursor was equal to the excess of sulfuric acid in stoichiometric ratio titanium/acid for the Ti-containing solution. However, the precursor used for obtaining the TiO_2-containing samples has a higher concentration of acid because of the hydrolysis of titanium sulfate, and thus it provides a deeper interaction with the clay matrix. Furthermore, the influence of high-temperature (750 °C) could strongly affect the properties of the samples. That is why the adsorption capacity and monolayer capacity (Paragraph 2.7.1) were obtained for all TiO_2-containing samples based on the water vapor adsorption isotherms (see Fig.4.16).

Table 4.10 The capacity of monolayer and maximum capacity of water vapor for the materials.

Samples	Monolayer capacity BET, a_m, mmol/g	Maximum capacity P/Ps=1, a_s mg/g
M(1:3)-600	4.14	396
M(1:3)-750	1.08	162
K(1:3)-600	3.85	337
K(1:6)-600	2.27	192
K(1:3)-750	3.50	162
K(1:6)-750	1.34	123

The comparison of adsorptive capacity shows that the composites obtained at 600 °C with the matrix/precursor ratio of 1:3 are most hydrophilic, regardless of the type of a support material. The capacity was compared with the results for the samples, activated by the thermos-acid treatment (Fig. 4.5, 4.8). For the kaolinite-based samples, the doubling of clay/precursor ratio results in a lower capacity.

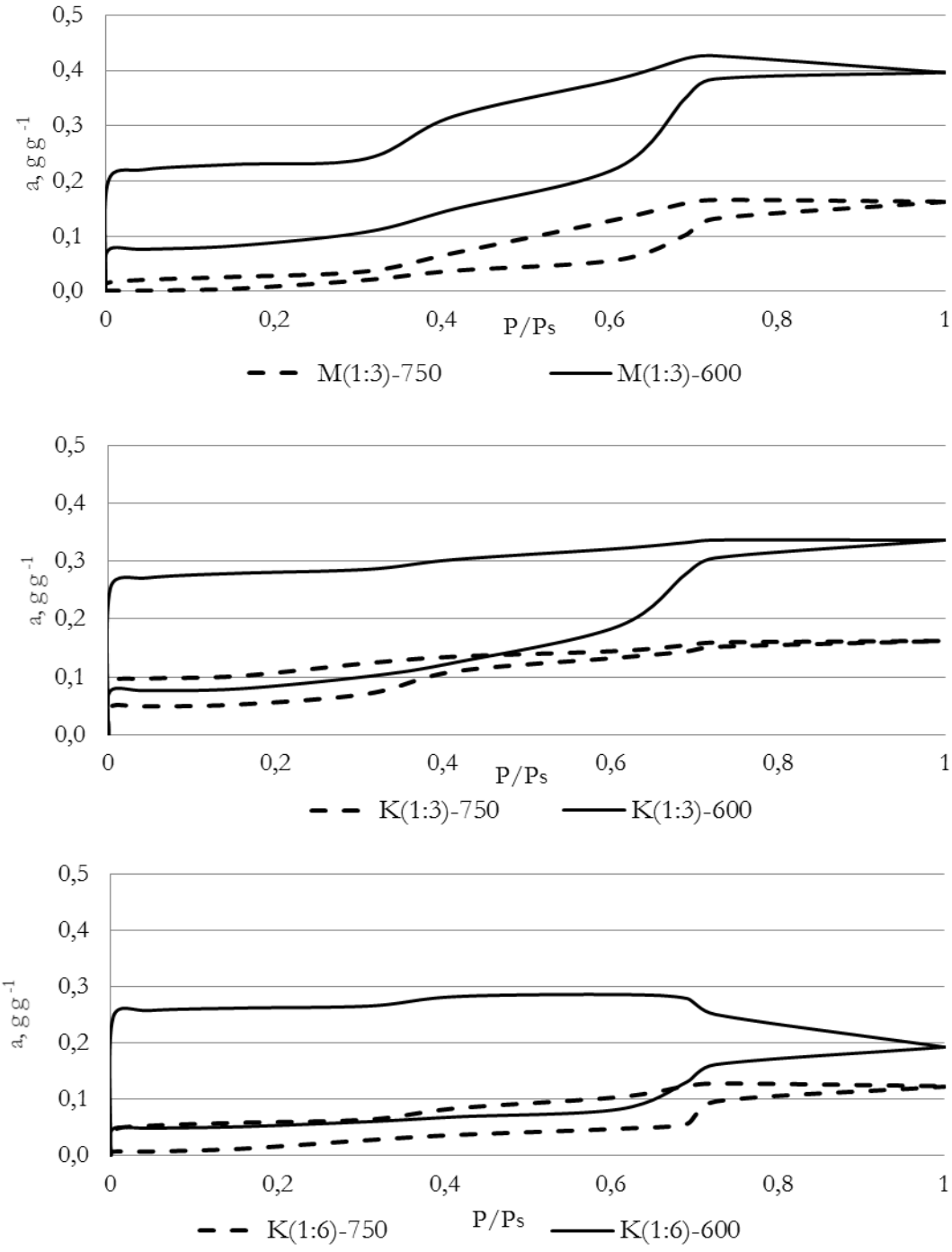

Figure 4.16. The isotherms of water vapor at 25 °C for new titanium-containing samples

The wide hysteresis loop, which expands at lower P/P_S is indicative for a deeper effect on the original matrix, compared to the samples K(1:3)-600 and K(1:6)-600. The X-ray analyses confirmed sulfate-formation process (see paragraph 4.3.6 below). High adsorption capacity, hysteresis loop's form, irreversibility of adsorption for low P/Ps and complete desorption at 250-270 °C (see Fig. 3.5) are specific for semi-chemical adsorption with the formation of crystallohydrates, along with physical adsorption. However, an increase of the heat treatment temperature to 750 °C causes the reduction of the adsorption capacity

values at the initial section of the isotherms. For M(1:3)-750 and K(1:6)-750 the values are close to zero, which is typical for adsorbents with a low micropore volume. At the same time, the adsorption capacity of K(1:3)-750 is high and close to the maximum values for kaolinite (5-7% at P/Ps = 1).

The narrow hysteresis loops and reduction of sulfur content in the samples (see Tables 4.7-4.8) amounted to 2.43 % wt. for M(1:3)-750; 1.72% wt. for K(1:3)-750 and 1.23 % wt. for K(1:6)-750. At the same time, the temperature of the treatment (750 °C) suggests the formation of alumina, the temperature of formation of which is 700-900 °C and which is characterized by low porosity and specific surface [231-233].

Both M (1:3)-750 and K (1:6)-750 have close values of monolayer capacity (see Table 4.10), while for K (1:3)-750 the capacity is only 14% lower than for K(1:6)-750 (see Table 4.10). Despite this, a narrow hysteresis loop and a low sulfur content indicate the decomposition of a significant amount of sulfates. Therefore, the monolayer capacity values may be explained by the formation of microporous structure, which is unlikely, or by differences in the chemical composition of K(1:6)-750 and K(1:3)-750, such as the presence of the surface centers able to collect the molecules of water. The results of X-ray Phase Analysis confirming significant phase differences are represented below.

Therefore, calcination at the temperature of 600 °C makes it possible to obtain a hydrophilic material that adsorbs and irreversibly retains atmospheric water. It should be noted that both montmorillonite and kaolinite have such properties. The capacity of the sample K(1:3)-600 is comparable with the capacity of montmorillonite-based materials. The material is hydrophilic and keeps a high capacity during the desorption when $P/P_s=0$, therefore they composites can be recommended as air-drying components. The increase of the amount of the precursor results in a lower adsorption activity of the material, but the increase of the calcination temperature does not affect it this way. The monolayer capacity of the sample is at least 5 times higher and the limited sorption volume is 2 times higher compared with pure kaolinite. Therefore, this method can be promising from the point of view of increasing the adsorption activity of kaolinites. [116]

However, the presence of irreversible sorption of water vapor does not make it possible to characterize the porous structure of the materials. On the other hand, benzene is used as the standard organics substance to characterize the adsorption activity of materials. [191]. Since kaolinite-based composites are promising materials, the benzene adsorption isotherms were experimentally constructed.

4.3.5 Benzene adsorption isotherms, specific surface area and porous structure

The adsorption isotherms of benzene at 293 °K (Paragraph 2.7.2) were constructed in order to examine the porous structure and the adsorption activity of the composites (see Figure 4.17).

The isotherms are of the type H1, according to the IUPAC nomenclature. [234] The shapes of hysteresis loops have often been identified with specific pore structures. Thus, the type H1 is often associated with porous materials which consist of agglomerates or compacts of approximately uniform spheres in regular array. Hence, these materials have narrow distributions of pore size. Some corpuscular systems (e.g. silica gels) tend to give the type H2 loops, but in these cases the distribution of the pore size and shape is not well-defined. Indeed, the H2 loop is especially difficult to interpret: in the past it was attributed to a difference in the mechanism between condensation and evaporation processes occurring in pores with narrow necks and wide bodies (often referred to as 'ink bottle' pores), but it is now recognised that this provides an over-simplified picture. [243]

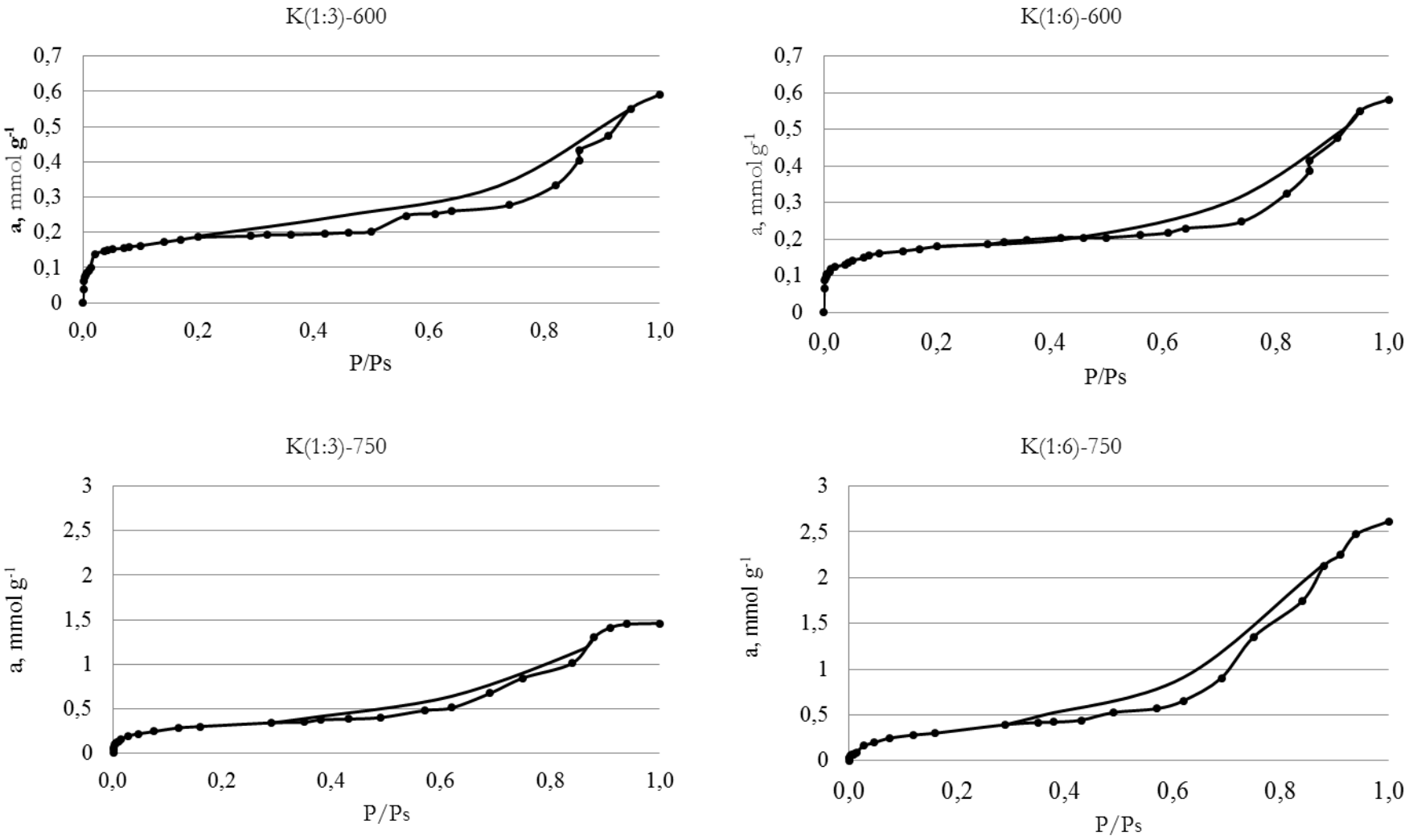

Figure 4.17 The isotherms of benzene vapor sorption-desorption at 20 °C

The comparison of different isotherms with each other is shown in the following way:
The isotherms of benzene vapor on the samples with the calcination temperature of 600 °C have a lower capacity compared with the samples obtained after the calcination at 750 °C in the entire range of relative pressures.
Therefore, the increase in temperature changes the properties of the surface layer, including the reduction of hydrophilicity and the increase in the capacity of organic compounds.
The isotherms of the benzene vapor on the materials K (1:3)-600 and K (1:6)-600 practically coincide. There is a slight excess of the capacity of the sample K (1:3)-600 in the relative pressure range 0.02-0.07 and 0.45-0.7 above the sample capacity of K (1:6)-600. Further, starting with P/Ps = 0.8, the isotherms coincide.
Therefore, the increase in the matrix/precursor ratio affects the micro and mesoporous structure insignificantly, while the volume of pores decreased insignificantly as the amount of the reagent was increased during the synthesis. The maximum capacity for samples K (1:3)-600 and K (1:6)-600 was 0.053 cm^3/g and 0.052 cm^3/g (46 mg/g and 45 mg/g, respectively, for benzene). For comparison, it was 0.337 cm^3/g and 0.192 cm^3/g for water vapor.
The effect of the matrix/precursor reaction is clear for the samples obtained during the calcination temperature of 750 °C. The values of the capacity for the samples K (1:3)-750 and K (1:6)-750 are close each other only in the initial section of the benzene vapor adsorption isotherms (up to P/Ps = 0.2). Further, especially for values correspond to adsorption in mesopores, the capacity of K (1:6)-750 significantly exceeds the capacity of K (1:3)-750. As a result, for P / Ps = 1, the capacity of K (1: 6) -750 is 0.232 cm^3/g (204 mg/g), and for the sample K (1: 3)-750 the capacity was 0.130 cm3 /g (114 mg /g). For water vapor adsorption, the limiting adsorption capacity was 0.123 cm^3/g and 0.162 cm3/g, respectively. The comparison of the capacity of the samples shows that negatively charged adsorption centers form on the surface of the material, especially for the samples with the calcination temperature of 750 °C, as water absorption decreases due to the formation of crystalline hydrates. The molecules of both water and benzene would be adsorbed on the hydroxylated surface due to the dipole moment (for water), or due to the presence of a common electronic "cloud", which is formed by π-bonds of the carbon atoms (both of these molecules are well retained on the positively charged centers). However, benzene, unlike water, cannot be adsorbed specifically on a negatively charged center. [235]. Such an effect of the change in the nature of the surface of clay minerals was previously observed when montmorillonite was treated with concentrated sulfuric acid. [236.] Anion or dehydroxylated oxygen of aluminosilicate layers can be negatively charged canters in this case. The influence of sulfur compounds on specific adsorption is more likely for the examined samples, considering that the samples obtained at 600 °C contain sulfur and show a high water vapor adsorption capacity, but the isotherms for benzene almost coincide. Therefore, it is likely that the adsorption of benzene is provided by the dispersion interaction. As the calcination temperature increases, the amount of sulfur decrease substantially, and the values a_s of the maximum water capacity decrease and become closer. The benzene isotherms for these samples practically are similar in the area of microporous filling (for benzene P / Ps <0.17 according to the theory of micropore bulk filling [203] but are different in the region of the mesopore filling.

The results of the experiment were analyzed according to Dubinin-Radushkevich equation and to Micropore Volume Filling Theory [198, 237] (see Paragraph 2.7.2). This allows determining the characteristic energy of adsorption, size and volume of micropores, limited sorption volume and the volume of mesopores. In addition, a specific surface area was experimentally determined the nitrogen adsorption (see Paragraph 2.7.2). The results are represented in Table 4.x. The mesopore surface area $\mathbf{S_{ме}}^{\gamma}$ was determined for the benzene adsorption isotherms with the area of P/P_S from 0.45 to 0.70 (the γ-method) [202, 203].

Table 4.11 The parameters of the internal structure of kaolinite-based materials.

Samples	Volume of micro pores W_0, cm^3/g	Charac-teristic energy of adsorption E_0, kJ/mol	Micro-pores width x_0, nm	Limit adsorption volume V_S, cm^3/g	Volume of mesopores $V_{ме}$, cm^3/g	SSA S_{BET}, m^2/g	SSA of meso-pores $S_{ме}{}^{\gamma}$, m^2/g
K(1:3)-600	0.018	13.4	0.75	0.053	0.035	37	26
K(1:3)-750	0.026	12.9	0.77	0.130	0.103	74	60
K(1:6)-600	0.014	18.5	0.54	0.052	0.037	36	19
K(1:6)-750	0.027	13.4	0.83	0.232	0.206	122	90

Given that the micropore volume is relatively small (0.01-0.03 cm^3/g), therefore the mesopores are the most significant part of the adsorption space of the samples. It is worth noting that the micropore volume for the samples obtained after the calcination at 750 °C is almost 2 times higher than for the samples prepared at 600 °C. However, the temperature affects the volumes of mesopores more significantly, the values are 2.5-5 times higher for the 750-samples. The characteristic energy is almost the same for the materials of both types and it is normal for mineral sorbents, although K(1:6)-600 has the biggest value (18.5 kJ/mol). While the structural characteristics are very close, this can be indicative for the changes of the chemical composition of the surface layer, despite the fact that the data do not allow saying , exactly which element or a compound provides such interaction with benzene.

The size (width) of micropores is calculated for the sorbent structure with slit-shaped pores [200]. This allowed verifying the correspondence between SSA values $\mathbf{S_{BET}}$ for BET and the mesopore surface [202], given that SSA is the sum of $S_{ме}{}^{\gamma}$ and the volume of micropores divided by twice the width of the micropores ($\boldsymbol{W_0/2\ x_0}$):

K (1: 3)-600: 26 + 12 = 38 m^2/g
K (1: 6) -600: 19 + 13 = 32 m^2/g
K (1: 3)-750: 60 + 17 = 77 m^2/g
K (1: 6) -750: 90 + 16 = 106 m^2/g

Therefore, the results are close to the obtained experimental values $\mathbf{S_{BET}}$.

The results confirmed that increasing the calcination temperature reduces the amount of sulfates in the samples and causes the formation of a mesoporous structure with the specific surface area around 74-122 m^2/g.

According to the results, the method of the synthesis should be reconsidered, given that the porosity of the materials, obtained by using the same amount of the precursor, increases with the increase of the calcination temperature. Chapter 3 concluded that the composites, for which titanium content did not exceed 100 mg/g of the carrier, were less susceptible to aging. The amount introduced in the sample K (1:6)-750 is 1.5 times more. However, it can be assumed that the decrease of sulfate content with increasing the calcination temperature will provide lesser ageing of the materials, compared with the samples obtained at 600 °C.

In order to characterize the total porosity and pore volume for the kaolinite-based samples, the true, apparent and bulk density, porosity, total pore volume, microporous volume and the porosity of the material layer were determined in Paragraph 2.7.2 (see Table 4.12)

Table 4.12 The density and characteristics of the kaolinite-based materials' macrostructure.

Sample	Density, g/cm^3			Total porosity, %	Summary volume of pores, cm^3/g	Macroporous volume, cm^3/g	Fenestration, cm^3/g
	true	**apparent**	**bulk**				
K(1:3)-600	2.793	0.778	0.658	72	0.927	0.874	0.154
K(1:3)-750	2.663	0.696	0.541	74	1.061	0.931	0.223
K(1:6)-600	2.805	0.868	0.590	69	0.795	0.743	0.321
K(1:6)-750	2.739	0.824	0.451	70	0.849	0.617	0.453

The true density values are close to each other, especially for the materials obtained at the same calcination temperature (the difference between the values is 0.011 and 0.075 for the samples obtained at 600 °C and at 700 °C, respectively). In terms of the matrix/precursor ratio, the results show that the composites obtained at 600 °C have a denser structure (the difference is 0.013 g/cm^3 for the samples prepared with the 1:3 ratio, and 0.065 g/cm^3 – for the samples prepared with the 1:6 ratio). The apparent density is minimal for K (1:3)-750, while the porosity of the sample is 74% and the summary volume of pores is 1.061 cm^3/g. The sample K (1:6)-750 has the maximum fenestration due to the minimal average particle size (see Table 4.9).

4.3.6 The results of X-ray crystallography for the kaolinite-based materials

The difference in the adsorption characteristics (SSA and mesopores volumes) of kaolinite-based composites indirectly indicates the difference in the phase composition formed during the synthesis. This effect can be caused both by transformation of titanium dioxide crystalline phases and by changes in the clay support. X-ray (Sec. 2.5) crystallographic analysis was used to clarify these issues. The interpretation of the results is a complicated task, given that the materials are multi-component composites with different crystallinity. The similar method was applied for the studies of TiO_2/SiO_2-composites prepared by

titanium dioxide deposition through the process of hydrolysis of $TiCl_4$, with commercial SiO_2 as supports: Cabot, Axim and Fly Ash [141].

Figure 4.18 represents the diffractogram of kaolinite clay. The results show that the untreated matrix is kaolinite with an insignificant amount of mica. However, the structure of the materials changed substantially after the deposition of TiO_2. Their diffractograms (see Fig. 4.19) demonstrate the formation of the phase composition of different samples and helps compare them with each other. The X-ray crystallography did not indicate any non-completely crystalized phase; therefore, the analysis focuses on the expected reflections specific to anatase, rutile, aluminium sulfate and aluminium oxide, considering the alleged chemical processes that took place during the synthesis. The diffraction angles and peak intensities are represented in Table 4.13.

Table 4.13 The diffraction angles and peak intensities of the crystalline phases.

Compound name	2Θ	Intensity %
TiO_2 anatase	25.28	100
	37.80	20
	48.05	35
TiO_2 rutile	27.45	100
	36.086	50
	41.226	25
$Al_2(SO_4)_3$	15.221	35
	25.413	100
	44.451	40
a'-Al_2O_3*	21.24	74
	25.44	42
	34.96	61
	37.86	74
	43.17	100
s-Al_2O_3*	19.33	56
	31.82	93
	37.50	100
k'-Al_2O_3*	38.10	30
	42.63	100
	48.48	60

*- the presented forms of aluminium oxide show maximum intensity in the range of diffraction angels 2Θ, it is not possible to analyze other forms

The presence of the peaks specific to the original matrix (kaolinite at 2Θ = 12.4 and 2Θ =24.9) was also considered and investigated.

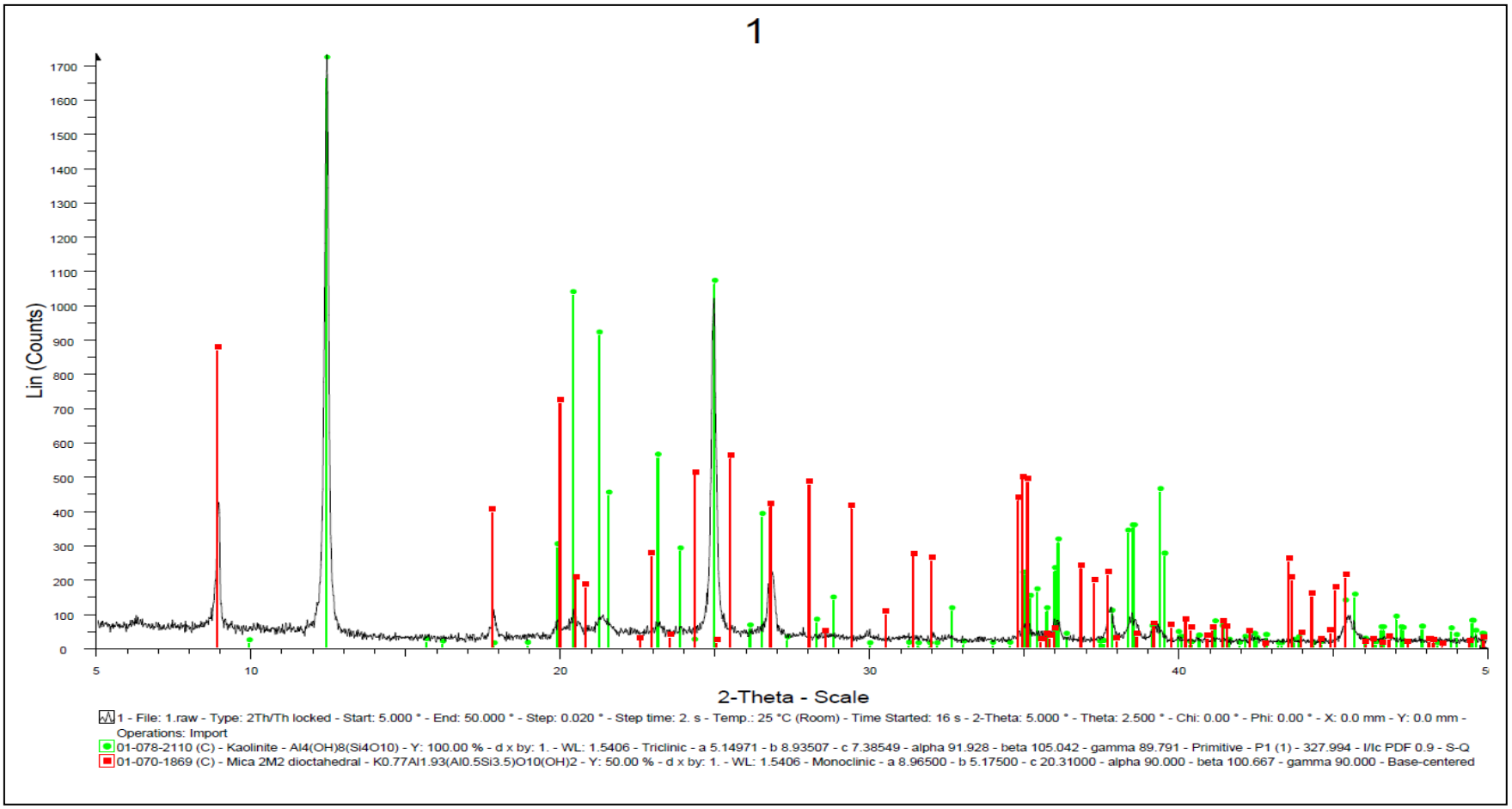

Figure 4.18 The diffractograms of pure kaolinite

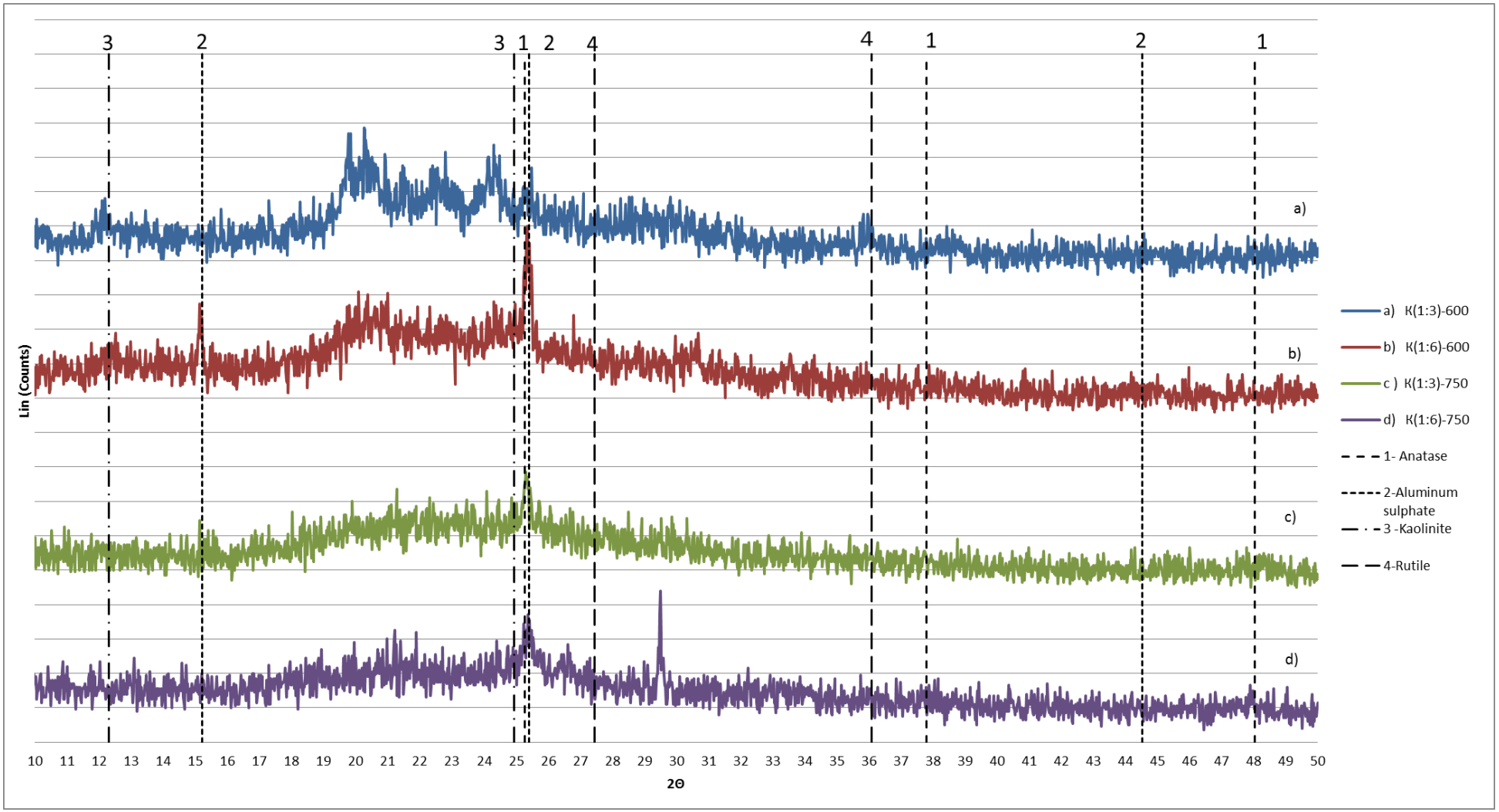

Figure 4.19 The diffractograms of the kaolinite-base samples

The peaks corresponding to 100%-activity for anatase and aluminium sulfate are common for all samples. For the composites obtained at 600 °C, the peaks corresponding to aluminium sulfates are higher, compared to the peaks corresponding to anatase, while for the samples prepared at 700 °C the peaks are close to each other. For K(1:3)-750 the anatase-peak is larger than the peak for aluminium sulfate.

It should also be noted that the peaks for 100% intensity of anatase and aluminum sulfate have similar values of 2Θ, which makes it difficult to interpret the results, (see paragraph 2.4 for the details).

To explain the results, the average thickness of the titanium dioxide layer was calculated. The calculations were done considering the titanium content (see Table 4.8) and SSA of the samples; while the minimal density of titanium dioxide was approximatively equal to 3.82 g/cm^3, and using the assumption that titanium dioxide is uniformly distributed over the surface of the support. The results are:

K (1:3)-600 - 5.2 nm;
K (1:6)-600 - 4.9 nm;
K (1:3)-750 -10.0 nm;
K (1:6)-750 - 8.7 nm.

Therefore, the average thickness of TiO_2-layer is higher for K(1:3)-750 than for K(1:6)-750, while the content of titanium is lesser (19,46 wt. % and 27,85 wt. %, respectively).

The traces of the original clay matrix (aluminum sulfate peaks) are observed only for the sample K (1:3)-600. There are unidentified peaks for this sample in the range of diffraction angles of 19.5-25 degrees. The same peaks with lower intensity are observed for K (1:6)-600, and almost absent in diffractograms of the other samples. Hence, these peaks presumably correspond to sulfates or other sulfur compounds.

As mentioned above, the peak of the anatase is better expressed on the X-ray diffractogram of the sample K (1:3)-750. In addition, there is a peak of aluminum sulfate; other peaks could be interpreted.

On the diffractogram of the sample K (1:6)-750 there is a notable peak at 2Θ = 29.5, in addition to the peaks of anatase and aluminum sulfate. The attempt to identify this peak was unsuccessful; one can only assume from the intensity and width of the peak that it corresponds to a well-crystallized phase. Presumably, due to the formation of this phase, the sample has an increase of the mesopore volume.

All the diffractograms failed to detect the peaks corresponding to rutile and to the forms of alumina, listed in the table.

Therefore, titanium dioxide is deposited on the surface of the samples as anatase. The presence of other forms is possible, but this analysis did not identify that. All the samples contain aluminum sulfate, but the amount decreases with increasing calcination temperature. The increased amount of the precursor (1:6) and the calcination temperature of 750 °C causes the formation of the phase, which is characterized by the peak with the maximum intensity at 2Θ = 29.5 degree. This presumably provides an increased porosity of the material.

4.3.7 UV-sensitivity of the samples (MEK removal)

This paragraph describes the research results on photosensitivity of the TiO_2-composites. The two series of the experiments using two different sources of UV-irradiation (ULTRA-VITALUX E27 lamp и LEDs DFL-5AP4SC-400) were organized.
ULTRA-VITALUX E27 are adapted to generate broad-spectrum radiation (see the spectral characteristics in Paragraph 2.8.2), including UV-A, UV-B and UV-C wave ranges. However, this kind of lamps requires special measures for the use in the presence of a person. LEDs DFL-5AP4SC-400 (Paragraph 2.8.3) has the irradiation range close to visible light and significantly less dangerous (see Fig. 2.8, 2.10). The samples may be sensitive enough for this radiation due to the presence of sulfur [152]. Chapter 2 describes the condition of the experiment (see Paragraph 2.8.2 and 2.8.3). The VITALUX E27 lamp was used to irradiate two batch reactors with the volume of 16 L, while LEDs DFL-5AP4SC-400 was used to irradiate the reactor with the volume of 0.45 L. The principal objective of the experiment was to evaluate the rate of MEK removal under UV-illumination for the materials with different titanium content and structures due to the calcination temperature and the amount of the precursor. The additional test was carried out for the kaolinite-based samples; each K-sample were exposed to UV-irradiation during 2 hours in the small-volume reactor before the experiment (UV pre-treatment) [188]. In order to compare the results of the experiments in the 16 L-reactor and 0.45 L-reactor, the results obtained for the former were processed according to the second-order kinetic equation (see Paragraph 2.8.4, eq. 2.26-2.27). The data are presented in the form of specific mass of MEK adsorbed by 1 g of the material (m_t) plotted as a function of time. Considering the sampling starts after 25-30 minutes after the injection of MEK, the absolute values of the kinetic constant are difficult to interpret and below they will only be discussed in comparison with the results obtained in the small-volume reactor (see Fig.4.20 for the results, and Tab. 4.14 for the equation parameters).

Table 4.14.The parameters of the kinetic equation 2.26 (linear form 2.27) for the process in the large-volume reactor

Samples	Kinetic constant k_{ads}, mg/(g min)		Limit value of adsorbed mass, m_{lim}, mg/g	
	Dark	UV- irradiation	Dark	UV- irradiation
M(1:3)-600	0.383	1.369	32.0	76.1
M(1:3)-750	0.152	1.320	33.7	51.7
K(1:3)-600	0.687	1.066	29.4	62.3
K(1:6)-600	0.721	1.382	28.4	67.6
K(1:3)-750	0.470	1.276	26.7	49.6
K(1:6)-750	0.740	1.432	32.9	92.4

The second series of the experiments was carried out for the small volume (0.45 L) reactor (see Sec. 2.8.3). The equalization of the MEK concentration is faster in the reactor of this size, which provides an opportunity of sampling after 5 minutes from the moment of injecting a test pollutant.

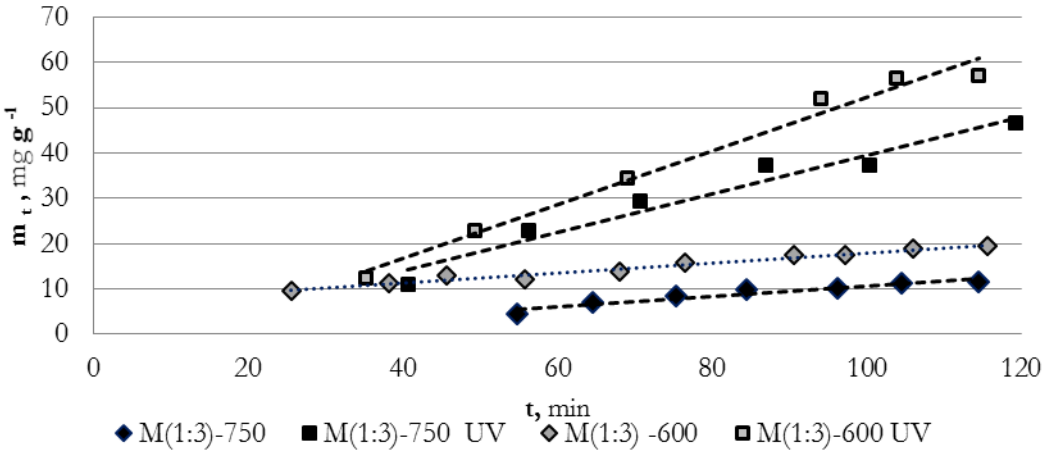

a)

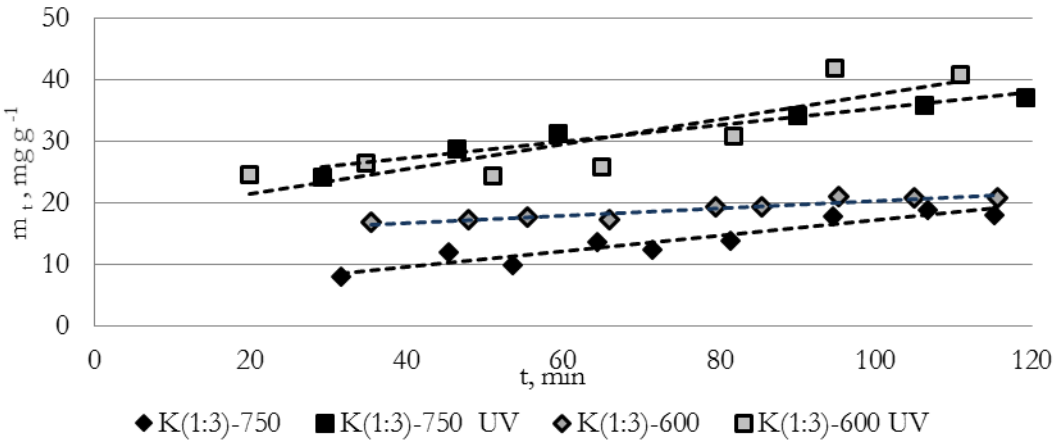

b)

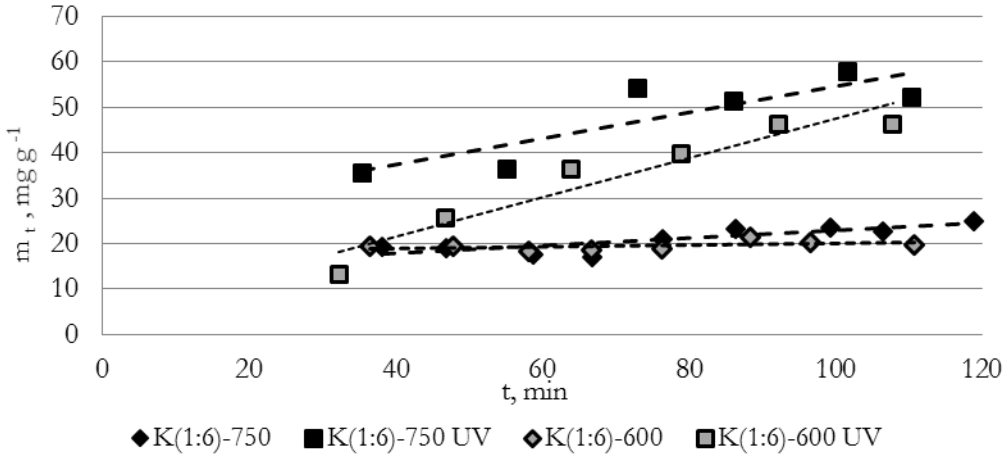

c)

Figure 4.20 Kinetic curves of the MEK concentration reducing process in the large volume reactor: a) - for M(1:3), b) - for K(1:3), c) - for K(1:6)

In addition, photoactivity of Degussa P25-sample was examined to compare the activity of the obtained composites with a commercial material (see Figure 4.21 for the results of Degussa P25 and Figure 4.22 for the results of the synthesized samples.
Further, the results were described by the second-order kinetic equation (Eq. 2.26, 2.27). See Table 4.15 for the equation parameters, while Table 4.16 represents the values of the linear correlation coefficients for both series of the experiments.

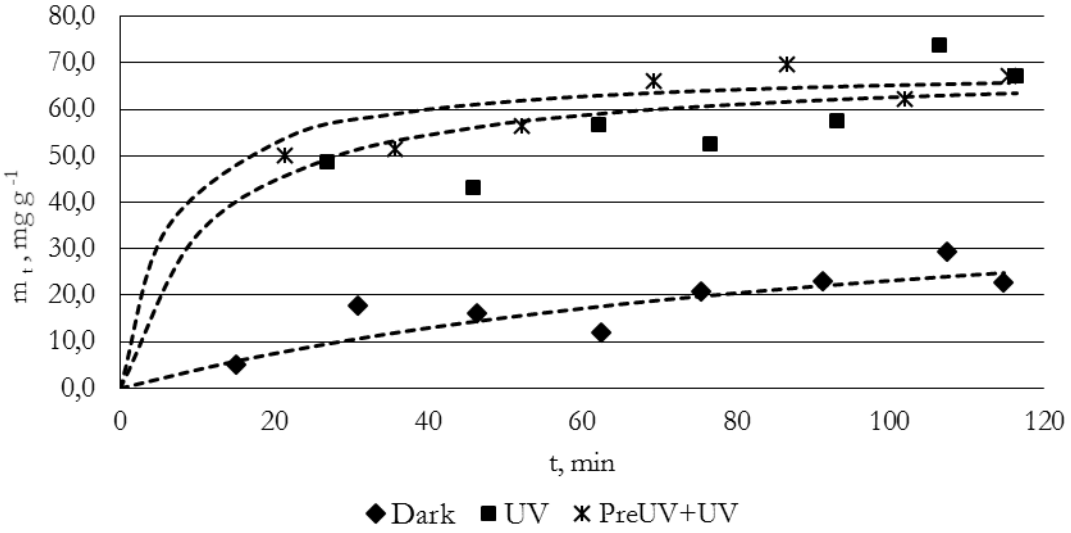

Figure 4.21 The kinetic curves of MEK concentration reducing process for the Degussa P25 (0.45 L reactor)

Table 4.15. The parameters for the kinetic equation (0.45 L batch reactor).

Samples	Kinetic constant k_{ads}, mg/(g min)			Limit value of adsorbed mass, m_{lim}, mg/g		
	Dark	UV-irradiation	UV-pre-treatment + UV- irradiation	Dark	UV-irradiation	UV-pre-treatment + UV- irradiation
Degussa P25	0.444	6.332	11.31	48.5	69.6	69.2
M(1:3)-600	0.448	1.129	-	34.0	44.3	-
M(1:3)-750	0.517	1.929	-	36.9	37.6	-
K(1:3)-600	0.348	0.481	1.016	18.8	53.0	73.3
K(1:6)-600	0.515	0.761	1.34	17.4	43.6	92.5
K(1:3)-750	0.261	0.496	2.52	18.0	58.0	65.1
K(1:6)-750	0.43	0.624	3.729	21.1	73.7	84.5

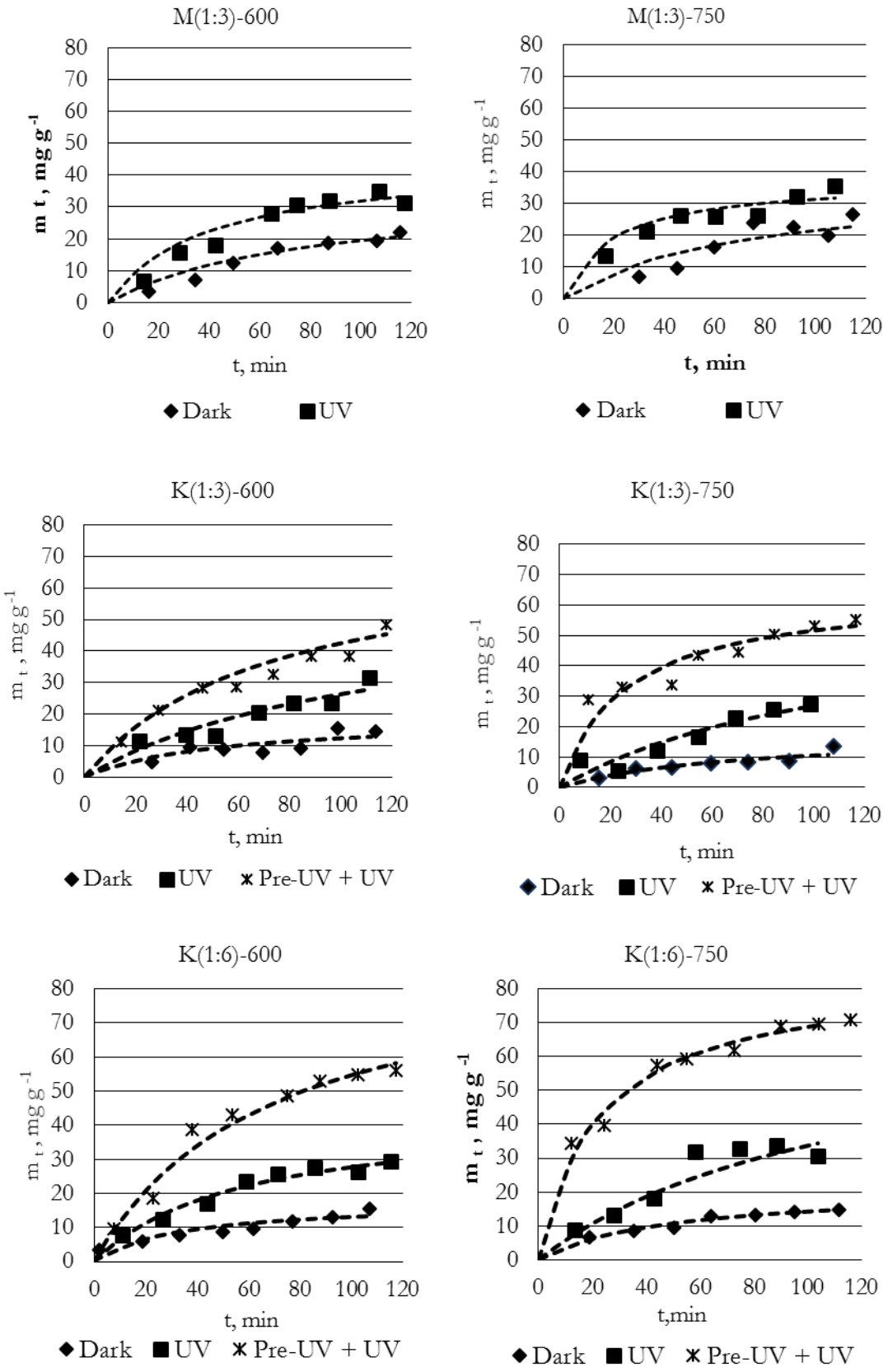

Figure 4.22 The kinetic curves of MEK concentration reducing process for the composites (0.45 L reactor)

Table 4.16. The coefficients of the correlation between values of t/m_t and t.

Sample	Correlation coefficient				
	Reactor (16 L)		Reactor (0.45 L)		
	Dark	UV-irradiation	Dark	UV-irradiation	UV-pre-treatment + UV- irradiation
Degussa P25	-	-	0.77	0.96	0.98
M(1:3)-600	0.96	0.84	0.94	0.91	-
M(1:3)-750	0.92	0.83	0.65	0.72	-
K(1:3)-600	0.98	0.92	0.79	0.83	0.97
K(1:6)-600	0.97	0.96	0.95	0.93	0.95
K(1:3)-750	0.93	0.97	0.87	0.70	0.97
K(1:6)-750	0.95	0.93	0.96	0.93	0.99

The photosensitivity tests are conducted in order to develop the method for the synthesis of photoactive composite materials able to provide VOCs degradation. In addition, it is necessary to take into account the recommendations for ensuring resistance to aging of the material and the technical characteristics of the method.

All samples demonstrated UV-sensitivity to varying degrees, which can be estimated by increasing the specific amount of disappeared MEK under irradiation of various types. The parameters of the equations for both series of the experiments were compared to each other in order to interpret the results (see below).

-*Limit value of adsorbed mass, m_{lim}, mg/g* is the monolayer capacity, and ideally, these values should be close for different series of the experiment. However, the differences in the size and hydrodynamic conditions of the reactors, as well as the influence of different sources of UV radiation should be taken into the consideration.

Without irradiation, the results are similar to each other for the montmorillonite-based samples and differ considerably for the kaolinite-based materials (the difference is about 5% and 30%, respectively). However, the relationship between the value and the synthesis method is the same for the reactors of both types, the difference between m_{lim} values is 8.7-11 mg/g.

The comparison of absolute values is affected by different UV-irradiation sources. For the tests carried out with the ULTRA-VITALUX E27 lamp, which has a wide spectrum of irradiation; the samples show higher m_{lim} values than for the tests with the diodes. However, the difference between values is similar for most of the samples in both series of the experiments. In addition, the results on the same level and even better were achieved for LEDs DFL-5AP4SC-400 after the pre-activation.

The experimental determination of the limit value of the adsorbed mass for the Degussa P25 sample demonstrates that, in the first place, the values do not change considerably after preliminary irradiation; secondly, in the absolute value they are similar to m_{lim} of kaolinite materials with UV pre-activation.

-*Kinetic constant k_{ads}, mg/(g*min)*. The hydrodynamic conditions of the process in the reactors differ significantly, which considerably affects kinetic constants. The values are significantly different from each other for the same samples tested in different reactors. The most likely

cause of this is the effect of kinetic transport and external diffusion on the process in the 16 L-reactor, due to the large volume and local mixing. However, these processes are not discussed in detail because of the large calculation error. The first results were obtained after half an hour from the moment of MEK injection, while the initial section of the kinetic curve is the most informative to determine the kinetic constant. Therefore, the values k_{ads} of the kinetic constant in these series of the experiments were used only to estimate the overall trend of variation for different samples, without considering the absolute value. The values obtained in the reactor of 0.45 L without illumination are similar for all samples, while the tests carried out with UV-irradiation show that the rate for the Degussa P25-sample increases more than 10 times in comparison with K-materials and 4 times in comparison with M-materials. Moreover, the kinetic constant increased almost twice during preliminary irradiation. As for the kaolinite-based materials, the sharp increase in the kinetic constant (5-6 times) was noted for the samples of K(1:3)-750 and K(1:6)-750. Both a higher titanium dioxide content and a larger specific surface area than K(1:3)-600 and K(1:6)-600 can explain this effect, but the comparison with Degussa P25 (SSA = 50 m^2/g) indicates that the content of titanium dioxide has a more significant effect on the rate constant.

The common trends for kaolinite-based materials are almost the same for both series of the experiments (in the small- and the large-volume reactors).

To select the method of synthesizing the photoactive composite materials the following issues should be considered:

- The influence of the Ti-content on photosensitivity of the composites. In this study, the content of the deposited titanium was calculated as the amount deposited with the precursor divided by the yield of the material.
- How does the calcination temperature affect the UV-sensitivity of the material?
- Is it possible to provide UV sensitivity of the material under "softer" LEDs irradiation, which are safer for domestic use?

The discussion and analyses of these questions would allow developing the recommendations for the pilot unit for production of the composites.

Montmorillonite-based materials.

For the materials of this type, the influence of the deposited TiO_2 amount is not considered as a factor, given that the samples were obtained only for one matrix/precursor ratio (1:3).

Under UV-irradiation, k_{ads} increases 2.5-3.7 times, and m_{lim} increases 1.3-2.5 times. The exception is M (1:3)-750, considering that its limit value of the adsorbed mass was not considerably affected by UV-light during the experiment in the 0.45 L reactor.

Under the conditions of the experiments, the sample M (1:3)-600 demonstrates greater photoactivity compared with M (1:3)-750. For example, the experiments in the large-volume reactor show that m_{lim} of the M (1:3)-600 increases 2.7 under the influence of ultra-violet light with the absolute value of 76.1 mg/g, while for M (1:3)-750 the same characteristic increases only 1.5 times, and the absolute value was only 51.7 mg/g. At the

same time in the small-volume (0.45 L) reactor m_{lim} is only 1.3 times and only for M(1:3)-600.

Kaolinite-based materials.

All kaolinite-based samples are affected to varying degrees by UV-irradiation. For both series of the experiments the results are similar, therefore, the study can focus on the questions.

The comparison of the results obtained for the tests under UV-illumination in the 16 L reactor and under UV illumination, and in the 0.45 L reactor after preliminary two-hour exposure shows the increase of the kinetic constant by 1.5-3 times for the samples obtained at 600 °C, and by 8.6-10 times – for the materials obtained at 750 °C. At the same time, the values of the limit value of the adsorbed mass increase 1.8-2.8 times (16 L-reactor) and 3.6-5.3 times (0.45 L-reactor) due to the influence of UV-irradiation.

The materials obtained at the same temperature were compared to determine the effect of the amount of the deposited titanium dioxide. The results show that for the materials prepared with the matrix/precursor ratio of 1:6, both the kinetic constant and the limit value of the adsorbed mass are on average 1.3 higher for both K (1: 6)-600 and K (1: 6)-750. It must be noted that the amount of the solution was doubled during the preparation, while the content of titanium increased with increasing processing temperature, according to EXDA (see Tab. 4.8).

The calcination temperature significantly affects the properties of the surface layer (see the results of scanning electron microscopy in Figure 4.14 d, f), the chemical composition (according to X-ray crystallography) and the capacity toward water vapor and benzene vapor adsorption. However, the *limit values of the adsorbed mass* for the MEK adsorption without UV did not differ much from each other during the same series of the experiments. The possible explanation is that the adsorption occurs in micropores, and the values of micropore volume are relatively small and similar for the samples (see Tab. 4.11).

The results of the experiments with UV-irradiation show inverse relation between the amount of the deposited TiO_2 and m_{lim}. The comparison of the pairs of the samples united by the support/precursor ratio confirmed that the composites obtained at 600 °C have higher *limit values of the adsorbed mass* in comparison with the materials obtained at 750 °C (see Tab. 4.15). The presence of sulfur and the amount of titanium is considered as the factor affecting the properties. The effect of the TiO_2 crystal modification on the properties is possible, but an X-ray analysis did not identify significant differences and, indeed, the samples obtained at 750 °C showed the properties that are characterize the anatase. Therefore, sulfur can be a doping agent for the materials.

On the other hand, a considerable increase of the *kinetic constant* can be caused by increasing the volume of mesopores and the specific surface. The correlation coefficient between the *kinetic constant* and SSA is 0.99 for the experiments carried out under UV irradiation + UV-pre-treatment (see Fig. 4.23). Therefore, the increased calcination temperature provides a high specific surface area and a positive effect for the MEK adsorption rate.

The source of UV-irradiation substantially affects the kaolinite-based composites compared to the montmorillonite-based materials. The *limit value of the adsorbed mass* and *the kinetic*

constants are 1.2-1.5 and 1.8-2.7 higher, respectively, for the tests performed under the ULTRA-VITALUX E27 lamp than for those carried out under LEDs DFL-5AP4SC-400. However, the values of the kinetic constant obtained after the pre-activation are comparable with the results for the large-volume reactor.

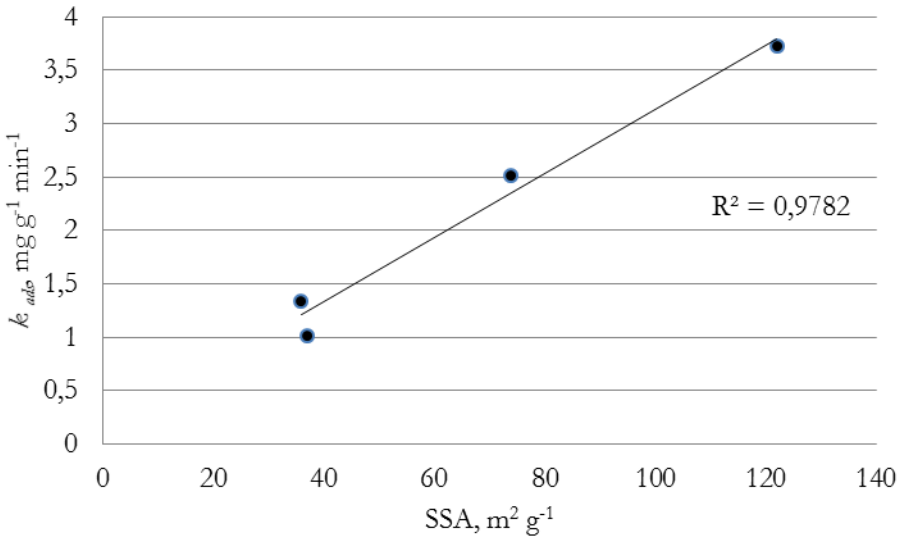

Figure 4.23 The correlation between the kinetic constant and SSA for the MEK adsorption under UV light

Perhaps, the pre-activation by the ULTRA-VITALUX lamp could affect the materials in the similar way, but this experiment was not carried out due to the limited applicability of this powerful UV-lamp. The high *limit value of the adsorbed mass* for the sample K(1:6)-750 obtained during the experiments in the large-volume reactor may be due to the higher titanium dioxide content, as well as due to higher dispersity of the material (see Tab. 4.9).
Therefore, considering the purpose of the production of TiO_2-containing UV-sensitive components for construction materials, the following conclusions and recommendations may be highlighted:

- The preferable support material is kaolinite, due to its stability, resistant to aging, applicability to building and relatively low cost.
- The recommended matrix/precursor ratio is 1:6. The samples of this type demonstrate high UV-sensitivity and adsorption activity towards organic compounds. At the same time, the *limit value of the adsorbed mass* of the materials obtained with the 1:3 ratio is only 30 % lower, while the amount of the precursor used during the preparation was two times higher, which increases the emissions. Hence, the materials with the ratio of 1:3 can be promising due to the less complicated technology, which requires further investigation.
- The recommended calcination temperature is 750 °C. This choice is due to: a) a lower sulfur content, which reduces emissions of dangerous aluminum sulfate dust, if the composite will be used for producing construction materials, b)a higher mesopore volume and specific surface area.

4.4 The pilot plant for producing the TiO_2-containing composite additives for building materials: technological scheme

For testing composites as additives to building materials, it is necessary to produce this product in quantities that enable the experiment to be carried out on a larger scale. For this purpose, a technological scheme of a batch processing pilot plant has been developed. The plant can produce within a few kilograms of the materials, although the larger-scale plants require additional methods for waste management and the integrated pollution prevention. This section gives the technological scheme of the pilot plant for producing the TiO_2-containing composite additives.

4.4.1 The consumption ratios for to produce

Titanium shavings (the metal processing residues) have been proposed as feedstock for producing the precursor (Fig. 4.24). It should be noted that the solubility of such shavings in sulfuric acid is considerably lower than the solubility of the titanium powder, considering the mass of the residue after filtration (11-15% and 40% of the mass of the used titanium for the powder and the shavings, respectively). On the one hand, this increases the consumption of titanium for obtaining the precursor with the concentration of 20 mg Ti/L. On the other hand, it simplifies the question of waste management, given that the residue contains enough titanium for further recycling with other metal waste.

Figure 4.24 The titanium shaving, the raw material for the preparation of the precursor

Table 4.17 shows the costs of raw materials for the production of K(1:6)-750, K(1:3)-750 and K(1:3)-600 composites. The excess of some raw materials (e.g., sulfuric acid and water for dilution) was taken according to the results of the experiment to ensure fluidity and filterability of the precursor. The solubility of the shavings, the yields and the amount of the residue were determined. According to this data, the amounts of the raw material available to produce 100 kg of the photosensitive materials were calculated. However,

during the further research, the amount of titanium can vary due to the difference in kaolinite/precursor ratio.

Table 4.17 The consumption of raw materials for the production of the TiO_2-containing composites

Materials	The cosumption, kg/ 100 kg of the composite		
	K(1:3)-600	K(1:3)-750	K(1:6)-750
Titanium shavings	7.63	9.26	20.83
Sulfuric acid, 95 %	50,39	61,12	137.53
Water	201,53	244,44	550,0
Filter Consumption	3,03	3,68	8,28
Kaolinite (dry, fine fraction)	76,34	92,59	104,17
The yeald of finished product	100	100	100

4.4.2 The Process Flow Diagram

The scheme of the experimental plant for the batch production of composites includes three main units: the matrix preparation, the precursor preparation and the composite material preparation. In addition, the preparation of the precursor, drying and calcination process generate SO_2, SO_3 and water vapor, which requires a gas neutralization unit. The schematic diagram of the process is represented in Figure 4.25.

The matrix preparation unit:

Kaolin clay is milled in the ball mill (BM), mixing in the reactor (R1) with water and the solution of sodium tripolyphosphate (or other liquefying agent for clay slips). A diluent is added in order to ensure the dispersion of aggregates of the clay; the type and concentration of it can be determined by the technology of construction ceramics with which the proposed plant is combined with. The solution heats up and boils for 40 minutes. The clay cools to 40-50 °C, then it is mixed in a settler (ST1) and is diluted with water and cools to the temperature of 25 °C. Then the clay is mixed and in 20-25 minutes, the layer 10 cm high from the surface level of the suspension is decanted into the evaporator (E), in which the main amount of the water is evaporated. After that, a thin slurry is dried in the convective dryer (D) and crushed in the grinder (G).

The precursor preparation unit:

The mix of titanium shavings and concentrated sulfuric acid inside is processed during 6 hours (40 °C) in the reactor equipped with the ultrasonic bath (UBS). Then, the distillate water is added to provide hydrolysis, and after 0.5 hour the solution goes onto the filter FP1 in order to separate undissolved precipitate.

The material preparation unit:

In the reactor (R2), a fine fraction of kaolin clay and the precursor is mixed and heated gradually in order to avoid intensive evaporation of water and sulfuric acid and the emission of sulfur oxides. The diagram does not show the source of heat, given that it can be either electrical heating or heating with flue gases.

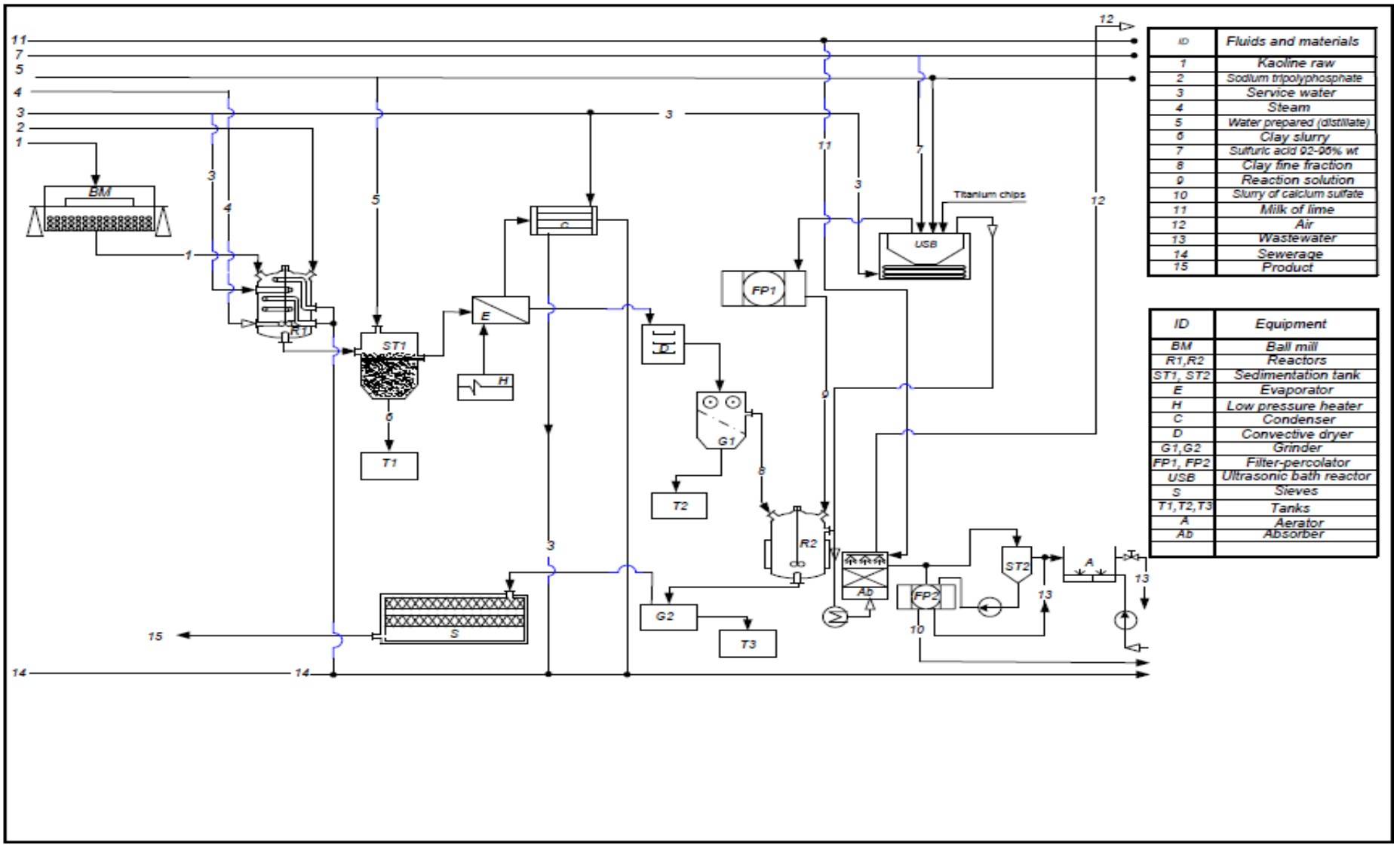

ID	Fluids and materials
1	Kaoline raw
2	Sodium tripolyphosphate
3	Service water
4	Steam
5	Water prepared (distillate)
6	Clay slurry
7	Sulfuric acid 92-96% wt
8	Clay fine fraction
9	Reaction solution
10	Slurry of calcium sulfate
11	Milk of lime
12	Air
13	Wastewater
14	Sewerage
15	Product

ID	Equipment
BM	Ball mill
R1,R2	Reactors
ST1, ST2	Sedimentation tank
E	Evaporator
H	Low pressure heater
C	Condenser
D	Convective dryer
G1,G2	Grinder
FP1, FP2	Filter-percolator
USB	Ultrasonic bath reactor
S	Sieves
T1,T2,T3	Tanks
A	Aerator
Ab	Absorber

Figure 4.25 Schematic diagram of the producing process

The heating finishes at the process temperature (600 or 750 °C) in 10-20 minutes after the release of volatile products has ceased. The product is cooled in the reactor, then the material is ground in the Grinder G2 and sieved on S-screens. Then, packaging and storing of the finished material must be provided.

The gas neutralization unit:

The reactor for preparing the precursor (USB) and the reactor for preparing the material (R2) are localized sources of sulfur oxides. The process of sparging through limewater is suggested as the method of purifying gases from sulfur oxides [238]. This method is considered to be economical, efficient (98% of sulfur oxide is neutralized) and simple in the organization of the process which is important in pilot plants. The main ongoing reactions:

$$Ca(OH)_2 + CO_2 \rightarrow CaCO_3 + H_2O \quad (4.1)$$

$$CaCO_3 + CO_2 + H_2O \rightarrow Ca(HCO_3)_2 \quad (4.2)$$

$$Ca(HCO_3)_2 + SO_2 + H_2O \rightarrow CaSO_3 \cdot 2H_2O + 2CO_2 \quad (4.3)$$

$$CaSO_3 \cdot 2H_2O + 1/2O_2 \rightarrow CaSO_4 \cdot 2H_2O \quad (4.4)$$

As can be seen, in this process the mixture of $CaSO_4 \cdot 2H_2O$ is obtained which is widely used in the production of building materials. However, the use of this product requires further examination, depending on the degree of conversion of calcium hydroxide to calcium sulfate dehydrate and the presence of clay particles or its decomposition products carried away by vapor-gas stream.

The volatile products from these reactors are pre-cooled to the temperature of 110 °C and less (water condensation must occur in the absorber) and then go to the absorber (Ab). External cooling must be provided for the absorber to prevent the lime milk from overheating due to the contact with hot products. When the volume of the liquid phase in the absorber increases, it is taken to the settler (ST2), where the solid phase precipitates. T Sludge from the sump is squeezed out on the FP2 filter and the water from the settler and filter comes to the aerator, where it accumulates and is blown through with air for additional oxidation of possible impurities. Depending on its quality, it can be further processed, used in technology (for example, for the preparation of a reaction solution) or is drained into the sewage system.

4.5 Conclusions for Chapter 4

- The samples of the composite UV-sensitive materials were obtained by the method of deposition of TiO_2 titanium-containing precursor on the surface of the clay supports. The chemical composition, surface state, average particle size, crystal-phase composition, adsorption and structural characteristics of materials were examined. The UV sensitivity for the adsorption of MEK was tested for the two sources: UV ULTRA-VITALUX E27 lamp and DFL-5AP4SC-400 LEDs. The process flow diagram for obtaining an experimental batch of the material is proposed.
- It has been proven that high adsorption activity of the TiO_2-containing materials in water vapor is due to the sulfuric acid treatment of the aluminosilicate matrix coupled with heat treatment. The chemical composition of the samples and the shape of the adsorption-desorption isotherm suggests that the main mechanism of water retention

is chemisorption due to the formation of crystalline hydrated metal sulfates, mainly aluminum. The kaolinite matrix undergoes deeper changes in the interaction with acid than the montmorillonite-matrix. The UV sensitivity of the samples containing no titanium dioxide was not detected.

- The study of the properties of the samples obtained at the calcination temperature of 600 °C confirms the conclusion from Chapter 3 that during the preparation, the matrix/precursor ratio above 100 mg/g is not appropriate, given that the content of titanium dioxide in the composites does not increase while the amount of sulfur increases significantly. The increase in the yield of the material is due to the formation of sulfates, while the content of titanium dioxide remains at the same level as for the lower ratio (e.g. for 1:3 ratio the content is 53.37 mg/g, while for 1:6 ratio the content is 48.82 mg/g of the carrier). In addition, some sulfur compounds including aluminum sulfate are an undesirable component for building materials as it has an irritating effect.
- An increase of the calcination temperature to 750 °C makes it possible to considerably reduce sulfur content in the samples (7-14 wt%. and 1.7-1.3 wt% for 600 °C-samples and 750 °C-samples, respectively). The increase in the temperature ensured a positive change in many characteristics of the materials: despite the general decrease of water vapor adsorption activity, the form of the adsorption-desorption isotherm is typical for clay minerals, and adsorption capacity for kaolinite is 2-2.5 times higher than the of the native mineral. At this temperature, a mesoporous structure is formed in the samples that provides the specific surface area of 74 and 122 m^2 / g for K(1:3)750 and K(1:6)750, respectively. The content of titanium increases in comparison with the samples calcined at 600 °C, from 3 wt% to 11-16 wt% .

  X-ray phase analysis confirmed presence of anatase modification of titanium dioxide the materials of both types (obtained at 600 °C and 750 °C), but the reflexes on the diffractogram corresponding to the anatase were clearer for the 750 °C samples.
- The UV-sensitivity of the samples was tested under the two UV-sources (ULTRA-VITALUX E27 lamp and DFL-5AP4SC-400 LEDs) for the process of MEC disappearance. The comparison of the efficiency in testing under LEDs lighting conditions was carried out with Degussa P25 titanium dioxide as the reference material.

  The results of the samples of the kaolinite-based composites are comparable, and when illuminated with LEDs they exceed the samples in the montmorillonite matrix in terms of the absorption of MEK. Under the LEDs, K-materials demonstrated results of MEK removal, which were lower than the results of Degussa P25 by 40%, but after preliminary UV-activation the activity increase up to the level of Degussa P25 and even more. The kaolinite-based materials synthesized at 750 °C are more active than those calcined at 600 °C.

5. The Development and Application of the Materials

5.1 Introduction

The chapter describes the building materials containing the component K (1:6)-750 and the efficiency of the MEK removal process under UV-irradiation. In addition, the methods for improving the photosensitive materials were examined, including testing the composites co-doped with non-metals in order to implement the visible light strategy, and examining fly ash as a matrix of TiO_2-containing materials.

5.2 The testing of the photosensitive building materials, containing the K (1:6)-750 composite

The overall aim of the study was to develop TiO_2-containing components for construction materials in order to apply the strategy to improve indoor air quality. Therefore, a series of the experiments was carried out to prove UV-sensitivity of the finishing materials containing active composite. The "small-volume" (0.45 L) reactor was used for the experiments. Putty, ceramics and polyurethane varnish were obtained and used as test materials. Materials of two types were obtained for the experiments: with and without the addition of K(1:6)-750 (see Section 4.2 for the properties of the composite). The blank samples (without the addition of the composite) were examined in order to identify its influence on the building materials.
A brief description of the materials and a method of their obtaining are described below:
1. Finishing putty.
The main material is white finishing putty Vetonit LH (by Saint-Gobain S.A.). The putty contains expansive filler and polymer adhesives as a cohesive. The samples (3 g of each) were prepared by depositing the putty on a metal mesh plate (10 cm^2). The composite-containing sample was obtained by rubbing 0.3 g of K(1:6)-750 in the putty before drying (see Fig. 5.1).

Figure 5.1. Vetonit LH: the blank sample (left), the composite-containing sample (right)

2. Ceramic Coating.

White clay plates (9 cm^2) were used as a carrier material for the composite. Untreated sample (Fig, 5.2, a) was used as a blank, while two composite-containing samples were prepared by depositing 0.5 g of K(1:6)-750 and by further calcination, 0.25 g of kaolinite was added to the samples in order to reduce the calcination temperature. The calcination at 900 °C [38] was not sufficient to provide the photoactive layer formation (Fig. 5.2, b). Therefore, the second sample was obtained at 1200 °C (Fig. 5.2, c). Both samples were examined, given that the authors of [38] describe reducing the photoactivity of TiO_2 after heat-treatment at the temperature above 900 °C.

Figure 5.2. Ceramic coating (from left to right): the blank sample (a); the TiO_2-contained sample (900 °C) (b); the TiO_2-sample (1200 °C) (c)

3. Polyurethane Varnish

Glass plates (10 cm^2) were used as supports. Parkettlack (Düfa) based on alkyd and polyurethane resins (0.41 g) was deposited on them. For preparing an active sample, 0.2 g of the composite was applied (Fig. 5.3).

Figure 5.3. Parkettlack Düfa: the blank sample (left), the TiO_2-containing sample (right)

The samples were air dried for several days, then tested in the 0.45 L reactor. Given that the goal of the study was to quantify the activity of the material, the conditions of the experiment were changed compared to the method described in Paragraph 2.8.3 (see Fig. 2.15). Initially after the introduction of MEK, sampling was carried out in dark conditions for 0.5 hours, and then LEDs DFL- 5013UVC-380 were applied.
Figures 5.4-5.6 represent the results of the testing.
The most significant MEK removal was achieved for the finishing putty (Fig. 5.4), in both dark and UV conditions. It is difficult to explain the sharp decrease in MEK concentration immediately after switching on the LEDs, but this effect was observed during several repetitions.

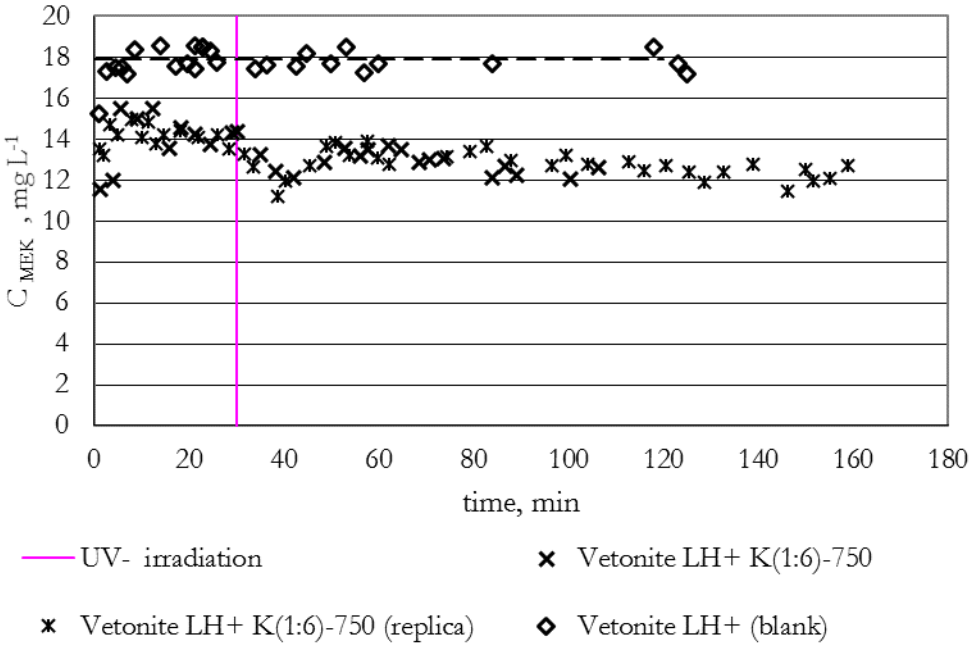

Figure 5.4. MEK-removal of finishing putty

The sample of ceramic coating prepared at 900 °C clearly demonstrated UV-activity. However, the calcination process at this temperature was not effective, considering that the composite layer is very fragile. On the other hand, photosensitivity of the sample obtained at 1200 °C is mostly negligible. The rate of MEK removal under UV is on the same level as in the dark (see Fig. 5.5), though a few tests show an insignificant increase in the rate after 2 hours of irradiation.
The results of testing polyurethane varnish (see Fig. 5.6) are the most controversial. The MEK removal was observed even for the blank sample. The presence of the photoactive material increased the adsorption capacity in the dark, but then the wavelike adsorption-desorption process was observed. A possible explanation is the chemical interaction of the material with the components of the varnish. This effect probably led to stricter standards of the material selection.

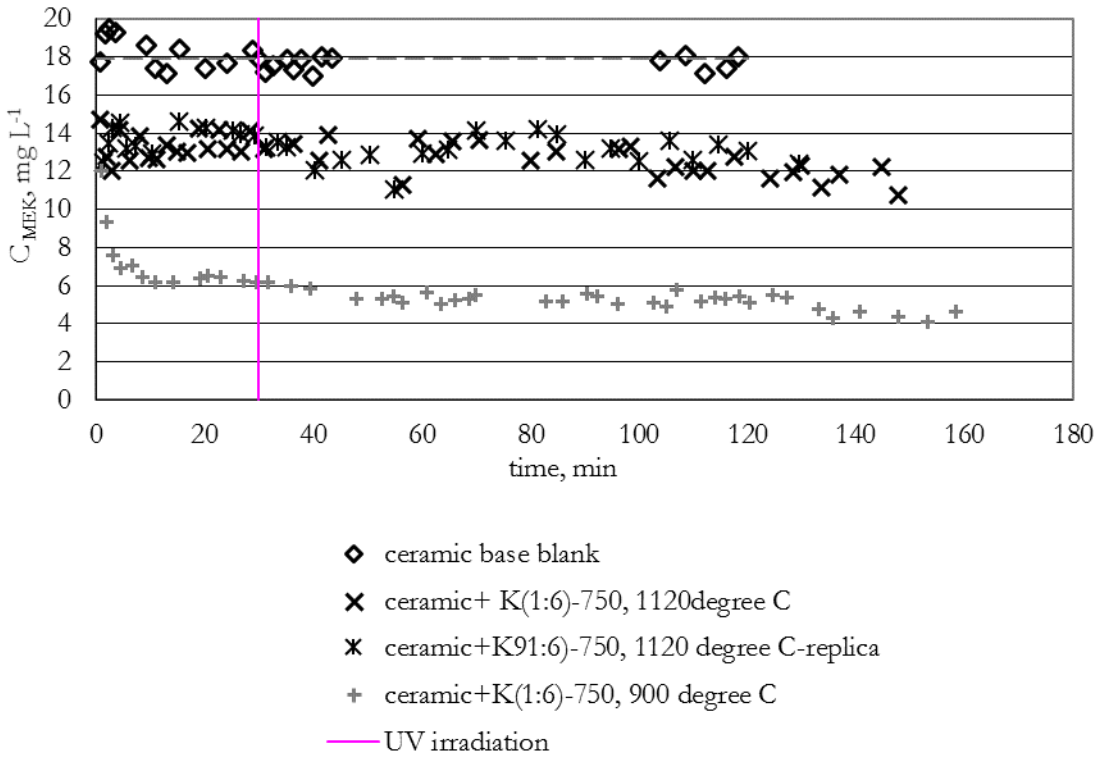

Figure 5.5. The MEK-removal of the ceramic coatings

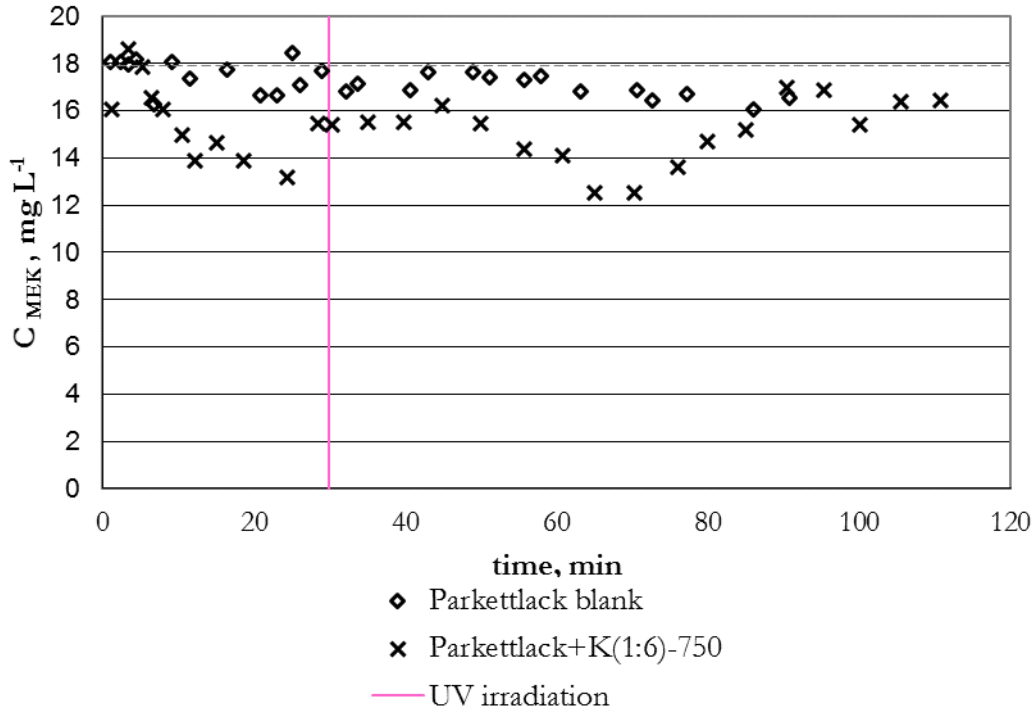

Figure 5.6. MEK-removal of the samples of the polyurethane varnish

Thus, the composites might be used as photoactive component of building materials for the removal of indoor air pollutants. However, further research is needed to determine specific applications and the conditions for use. In addition, the degree of mineralization of VOCs is still the issue (see Sec. 1.1). On the other hand, the last does not displace possible application of the material for air purification.

5.3 The nonmetal co-doped samples

Paragraph 1.4.6 describes in details nonmetal co-doping as a method of surface sensitization providing activity in the conditions of visible light, which is particularly important since the use of UV-irradiation in accommodation is strictly limited due to safety requirements. The method used in this study is based on bandgap arrowing effect. The doping agents were added to the composites in the synthesizing stage. Nitrogen, phosphorus and chlorine (see Paragraph 1.4.6) were chosen as dopants, therefore HCl, HNO_3 and H_3PO_4 were used as components of the precursor. Considering that sulfur may also be regarded as a doping agent, the term 'co-doping' is used hereinafter.
Titanium is resistant to corrosion; therefore, it reacts slowly with mineral acids, usually when heating to high temperature. The reaction with concentrated HCl is:

$$2Ti + 6HCl \rightarrow 2TiCl_3 + 3H_2 \quad (5.1)$$

In the aqueous solution it forms an octahedral aqua complex $[Ti(H_2O)_6]Cl_3$ instead of $TiCl_3$.
The reactions with nitric acid are:

$$Ti + 2HNO_3 = H_2TiO_3 + NO_2 – \text{for concentrate acid} \quad (5.2)$$

$$3Ti + 4\ HNO_3 + H_2O = 3H_2TiO_3 + 4NO – \text{for diluted acid} \quad (5.3)$$

Titanium is relatively more resistant to phosphoric acid. The metal remains stable in the solution with the concentration up to 30%. The reaction rate increases with a higher concentration. White phosphorus P_4 is produced as a product of the reaction (5.4):

$$15Ti+32H_3PO_4 \rightarrow 5Ti_3(PO_4)_4+3P_4+48H_2O \quad (5.4)$$

However, this method involves the use of small dopant acid/H_2SO_4 (0.025:1 M). Therefore, the ratios of 93 mg/g, 37 mg/g and 82 mg/g were applied for the chlorine-, nitrogen- and phosphorous-doped materials, respectively. At the same time, the mixture of dopant acids with H_2SO_4 is more active. Thus, the presence of doping agents in the composites is expected. The materials were prepared at 600 °C in order to avoid the removal of dopants. Besides that, the un-doped material was synthesized for comparison.

5.3.1 Examination of the chemical composition and surfaces

The preparation method was described in Section 2.2, but the dissolved nitric, chlorine and phosphorous acid was added to sulfuric acid during the preparation of the precursor with the molar ratio of the dopant acid/sulfuric acid of 0.025:1 (Tab. 5.1.)
Figure 5.7 shows how the samples look like after calcination. It is worth noting the color difference between the samples. The un-doped one (see Fig. 4.13) is unusually light, given the method of preparation, while both the phosphorus- and chlorine-containing samples have a typical yellowish tint. The materials, treated with HNO_3 demonstrate lilac shade which is also not typical. Such changes look interesting for further research.

Table 5.1.The conditions for the preparation of doped materials.

Matrix	Conditions			Recourse of non-metal	Ratio acid:sulfuric acid, M:M	Samples ID	Yield, g/g kaolinite
	Mass, g	Volume of reaction solution, ml	Temperature of heat-treatment, °C				
kaolinite	2	12	600	H_2SO_4 (base)	-	K-S	1.51
				HNO_3	0.025:1	K-S-N	1.55
				H_3PO_4	0.025:1	K-S-P	1.26
				HCl	0.025:1	K-S-Cl	1.61

Figure 5.7. The samples after synthesis (from the left to right): the test sample, the Cl-doped sample, the N-doped sample, the P-doped sample.

The chemical composition of the samples was determined by EXDA (see Tab. 5.2). The results are unexpected. The sulfur content is comparable with its content in the sample K(1:6)-600, and is even higher for the samples K-S and K-S-P (Tab. 4.8). The lowest sulfur content is found in the sample K-S-Cl, while the highest is in the phosphorus-doped sample (more than 20% wt). In addition, the sample has also the highest content of titanium. Hence, the K-S-P sample contains 4.75 % wt, while the content in other samples is 3.04-3.52 % wt. High titanium content was also detected in the K-S-Cl sample, but only at one point.

Fourier transform infrared spectroscopy or FTIR (Sec.2.4) was used to verify the results above (see Fig. 5.8). The absence of nitrogen in K-S-N and the presence of fluorine and chlorine in the K-S-Cl were checked qualitatively. According to the results, the spectrum band of fluorine was not detected in K-S-Cl. The band at the range of 1300-1000 cm^{-1} corresponds to valence vibrations of the compounds. Chlorine was found in small

amounts, as indicated by small bands of 800-600 cm^{-1}. The nitrogen-related bands were detected for the sample K-S-N, but it is difficult to identify its form.

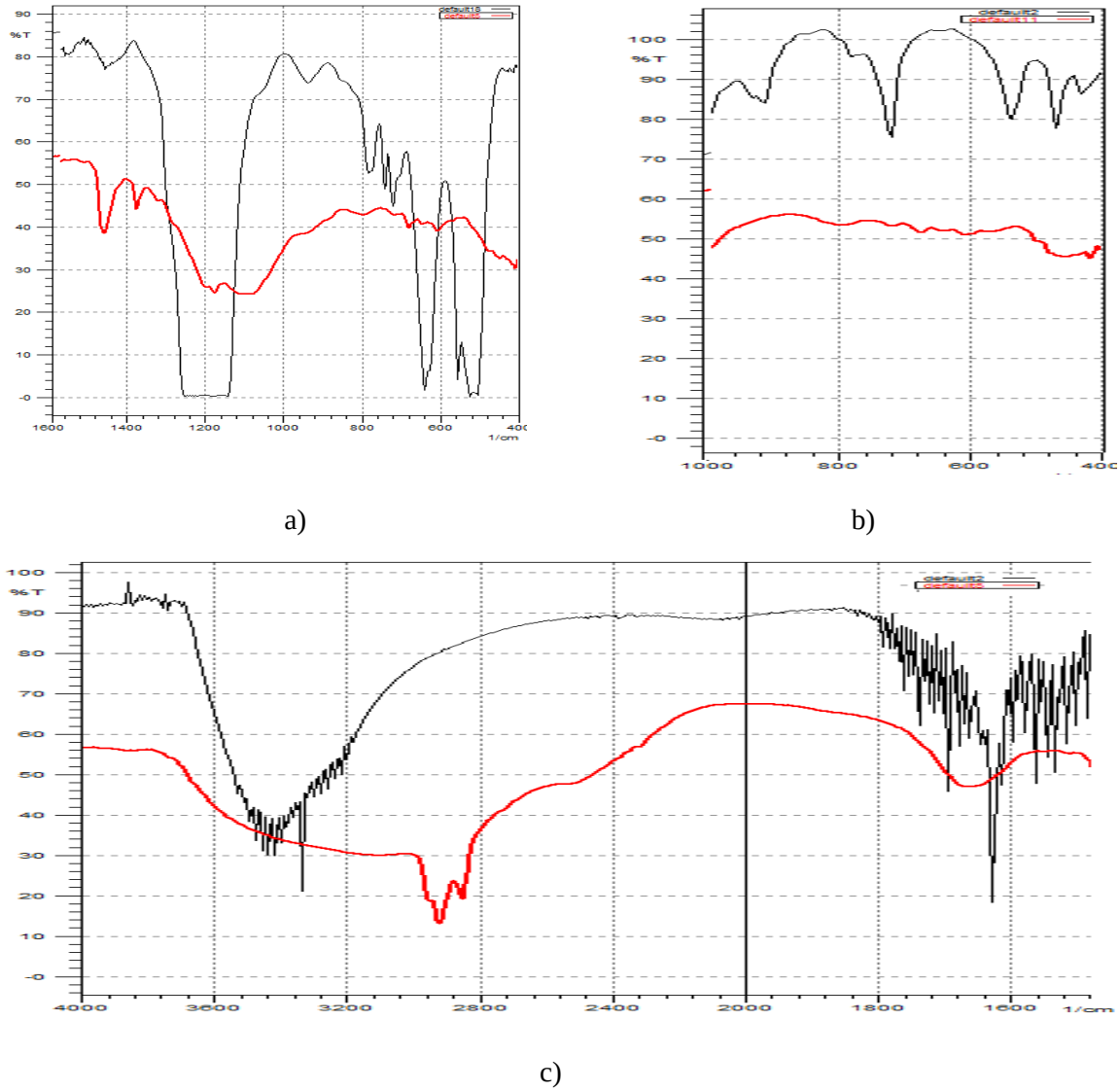

Figure 5.8. The spectrograms (red line) of a) K-S-Cl (compared with fluoropolymer), b) K-S-Cl (compared with NaCl), c) K-S-N (compared with gaseous ammonia)

The scanning electron microscopy (SEM, see Sec. 2.5) confirmed that the method of doping barely affected the micro-profiles of the samples (see Fig. 5.9). All the samples have similar scale-like surface structures.

Table 5.2.The composition of the S-containing and co-doped samples.

Samples		Contents, wt %																TiO_2/ Σ compo-nents, mg/g	Molar ratio Al_2O_3/ SiO_2
		Al	Si	Fe	O	Ti	Mg	N	Ca	S	K	F	P	Cl	Cu	Na	Σ		
K-S	1	13.15	14.70	0.99	43.63	4.86			7..33	15.33							99.99		
	2	15.5	17.69	0.46	40.87	1.40			0.00	23.73							100.00		
	3	12.26	9.40	0.88	50.03	4.31			0.00	23.12							100.00		0.87
	everage	13.75	13.93	078	44.84	3.52			2.44	20.73							100.00	62.45	
	Al_2O_3;SiO_2, mol/g	0.26	0.30																
K-S-N	1	13.22	7.17	0.85	54.99	1.07	0.21	0.00	0.13	22.35	0.00		0.00			0.00	99.99		
	2	3.90	14.80	0.70	54.19	6.92	0.40	0.00	4.64	12.83	0.90		0.11			0.62	100.0		
	3	1.17	42.79	1.32	45.69	1.12	0.49	0.00	1.29	1.56	3.93		0.00			0.63	99.36		0.25
	everage	6.10	21.59	0.96	51.62	3.04	0.37	0.00	2.02	12.25	1.61		0.04			0.42	99.58	53.37	
	Al_2O_3;SiO_2, mol/g g	0.12	0.46																
K-S-P	1	13.27	12.62	0.83	47.99	4.89	0.00		0.23	19.64	0.16		0.38			0.00	100.0		
	2	4.82	1.82	0.77	47.24	3.79	0.45		11.0	22.11	6.62		0.54			0.84	95.18		
	3	2.47	14.24		31.45	5.58	0.00		16.4	23.85	3.89		0.21			0.00	98.13		0.63
	everage	6.85	9.56	0.80	42.23	4.75	0.15		9.22	21.87	3.56		0.38			0.28	99.37	86.13	
	Al_2O_3;SiO_2, mol/g	0.13	0.20																
K-S-Cl	1	0.23	1.60	0.07	51.35	8.76			5.47	1.38	5.19	19.79	0.00	0.55	5.61	0.00	100.00		
	2	5.24	14.72	3.82	45.89	1.16	1.51		3.25	17.34	5.62	0.65	0.00	0.00	0.00	0.79	99.99		
	3	2.58	33.30	0.69	53.20	0.14	0.76		0.77	2.79	3.07	0.80	0.13	0.00	0.00	1.78	98.23		0.14
	everage	2.68	16.54	1.53	50.15	3.35	1.14		3.16	7.17	4.63	7.08	0.04	0.18	1.87	0.86	99.52	59.26	
	Al_2O_3;SiO_2, mol/g	0.05	0.35																

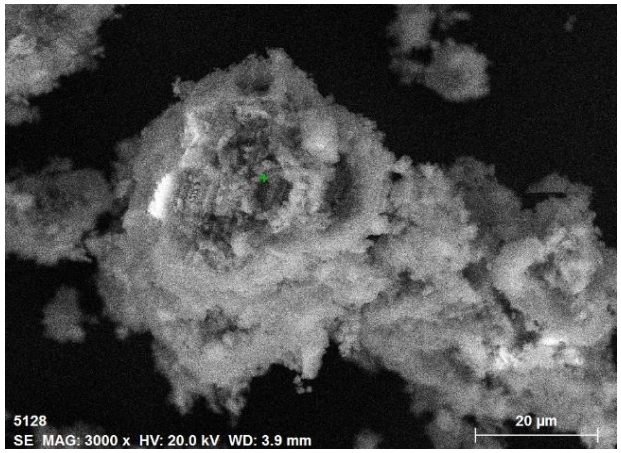

a)K-S

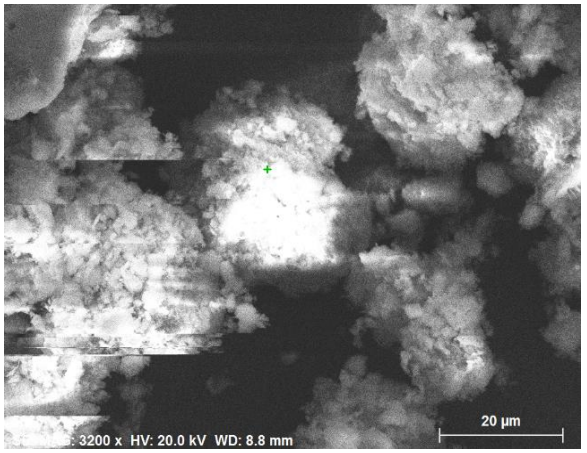

b) K-S-N

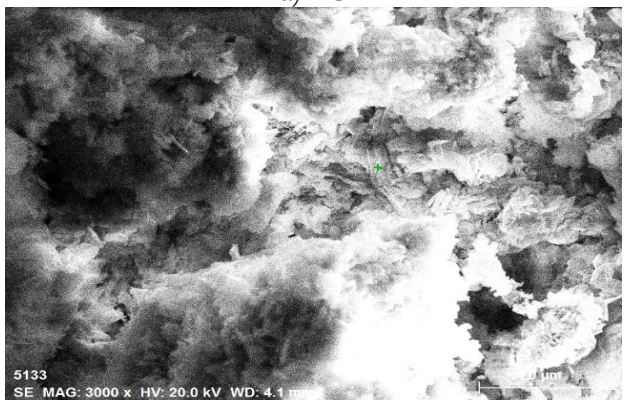

c) K-S-P

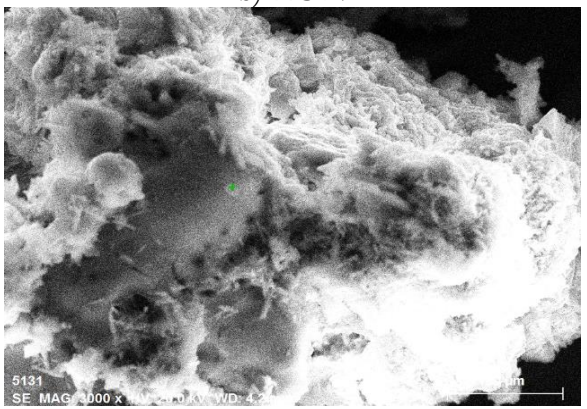

d)K-S-Cl

Figure 5.9 The morphology of the samples: a) the test S-doped material, b) the S-co-doped material, c) the P –co-doped material, d) the Cl-co-doped material

Optical microscopy (300x) was used to determine average particle size of the materials (see Figure 5.10 and Table 5.3). The size is similar for all materials, except for K-S-N (4.6-5.8 μm), which is slightly larger than the remaining materials.

Table 5.3.The average particle size according to optical microscopy.

The sample	The particle size, μm
K-S	3,97 ± 0,46
K-S-N	5,20 ± 0,60
K-S-P	3,81 ± 0,43
K-S-Cl	4,50 ± 0,36

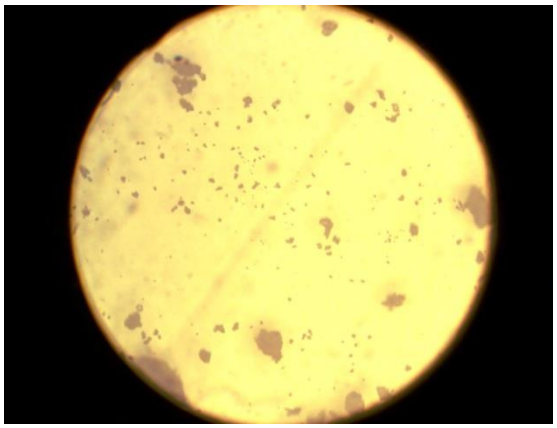

a) K-S

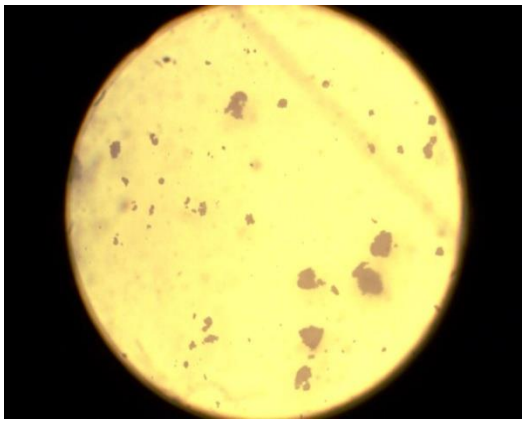

b) K-S-N

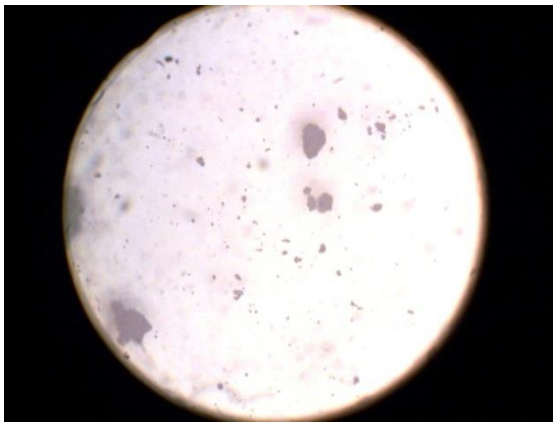

c) K-S-P

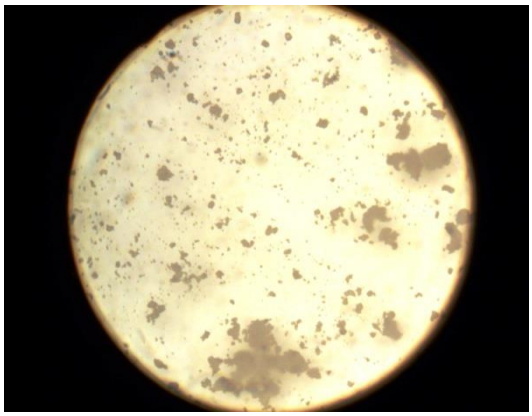

d) K-S-Cl

Figure 5.10 The optical microscopy of a)-the test S-doped material, b)-the S-co-doped material, c) the P –co-doped material, d) the Cl-co-doped material

5.3.2 The study of photo-catalytic activity of the samples

After conducting the tests above, the presence of co-dopant elements for Cl- , N- and P-samples was confirmed. A significant amount of sulfur was found for all samples, especially for K-S and K-S-P (more than 20% wt). Thus, the investigation of the activity of the

materials under ultra-violet (UV) and day light (DL) irradiation could be performed. To study the sensitivity of the materials, it was necessary to compare the irradiation energy for UV and DL. For this, two reactors (0.45 L) with LEDs irradiation sources were used, but the sources UV LEDs and DL LEDs were chosen so that the EMF generated by them in the germanium crystal in the sum for all 9 sources had similar values for both of them. The detailed scheme for testing the sources of irradiation is described in Paragraph 2.8.3.
Degussa P25 was used during the tests as a sample for comparison.
The kinetic lines of Degussa P25 are represented in Figure 5.11; the line of the co-doped sample is shown in Figure 5.12.

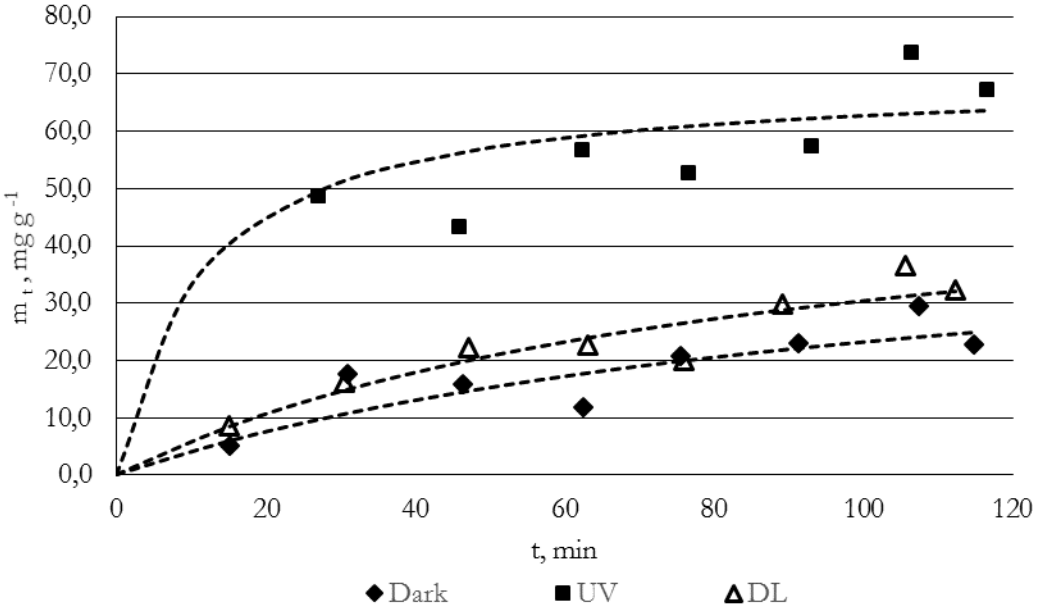

Figure 5.11 The kinetic lines of MEK disappearance over for Degussa P 25 in different irradiations: dark condition (♦ - Dark), UV- irradiation (■ - UV) and day light irradiation (Δ - DL)

The visual comparison of the kinetic curves shows that the Degussa P25 sample practically does not respond to daylight illumination: the of values m_t of the specific mass of MEK, adsorbed by 1 g of material at a time are similar both in dark conditions and under day light irradiation. At the same time, co-doped samples and the S-containing sample react to daylight, and MEK removal values obtained in the presence of daylight are only slightly lesser or even greater than the results obtained under UV. The sample of K-S-Cl, co-doped with chlorine was found to be most effective.
The results were mathematically processed in the linear form (Eq. 2.27) of the kinetic equation of adsorption (Eq. 2.26); Table 5.4 presents the parameters of the equation. Although the K-S-N sample was more active under daylight irradiation, in general, the material demonstrates the lowest efficiency. This behavior was unexpected, since the presence of HNO_3 was supposed to increase the intensity of titanium dissolution and affect the silicate matrix. However, it negatively affected the interaction of sulfuric acid with kaolinite, which may be indicated by a lower sulfur content in the samples and the largest

average particle size. A change in the parameters of the porous structure can be assumed, but the study did not intend to study this. The content of titanium dioxide is also the smallest of all samples.

Table 5.4. The parameters of the kinetic equations for co-doping materials and Degussa P25 at different irradiations.

Parameters	Irradiaton					
	Dark	UV	DL*	Dark	UV	DL*
Sample		K-S			K-S-P	
TiO_2 content , mg/g		62.45			86.13	
m_{lim} ,mg/g	39.47	97.86	96.56	43.60	83.88	92.36
k_{ads} , mg/(g min)	0.60	1.59	2.70	1.76	7.24	4.47
Pearson koefficient R^2	0.89	0.87	0.95	0.91	0.93	0.92
Sample		K-S-N			K-S-Cl	
TiO_2 content , mg/g		53.37			59.26	
m_{lim} ,mg/g	24.86	47.74	74.78	59.30	71.66	113.84
k_{ads} ,mg/(g min)	0.37	3.58	2.41	1.49	7.09	5.99
Pearson koefficient R^2	0.80	0.96	0.93	0.91	0.93	0.94
Sample		Degussa P25				
m_{lim} ,mg/g	48.52	57.13	69.57			
k_{ads} , mg/(g min)	0.44	6.33	0.65			
Pearson koefficient R^2	0.77	0.95	0.86			

DL* - day light irradiation

While the K-S and K-S-P samples demonstrated similar results, the kinetic constant of the phosphorus-doped sample is significantly higher, which can be caused by a higher content of titanium dioxide and/or a different porous structure of the samples.

The most promising results were obtained for the sample co-doped with chlorine. It should be noted that hydrochloric acid, along with sulfuric acid, is an activating agent for the acid treatment of clays [118], and their mixture is more active than individual acids. This fact is confirmed by a higher rate of dissolution of titanium in a mixture of hydrochloric and sulfuric acid compared with dissolution in sulfuric acid. However, upon a prolonged (>5 hours) contact of the mixture with metallic titanium, a light residue was observed. Therefore, the formation of $TiCl_3$ or aqua complex $[Ti(H_2O)_6]Cl_3$ can be assumed. The high kinetic constant rate in dark conditions and high value of $Al2O_3$:SiO_2 may indicate a change of the kaolinite matrix towards the formation of a transitional porous structure. That is attested by high Al_2O_3/SiO_2 (see Tab. 5.2) and the high kinetic constant rate. Furthermore, the best result of MEK-removal (the highest limit value of adsorbed mass m_{lim}) under daylight was achieved for the chlorine-doped sample. Therefore, chlorine co-doping is the most promising method for further researches, aimed to obtain UV/visible light-sensitive building material components for IAQ strategy implementation.

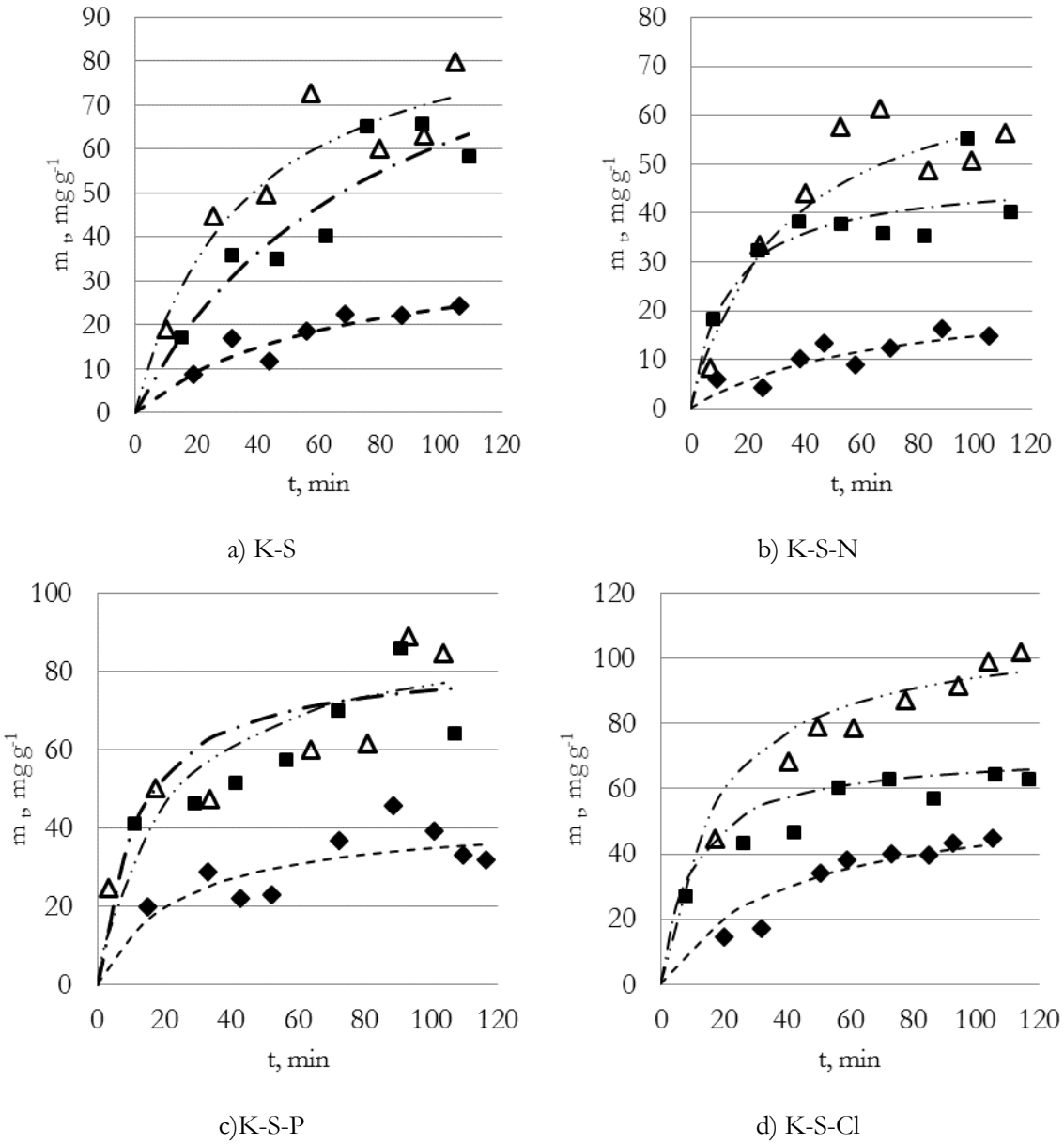

Figure 5.12. MEK-removal kinetic curves: a) K-S, b) K-S-N, c) K-S-P, d) K-S-Cl. Conditions of irradiations: dark condition (♦ - Dark), UV-irradiation (■ - UV) and daylight irradiation (Δ - DL)

Another promising method is doping of composites with pigments, providing colored materials. However, this technique is more complicated, considering the corrosive environment of the precursor and its effect on a doping agent.

5.3.3. Conclusion for Section 5.3

The analysis of the data allowed the following conclusions:
-During the experiment, the TiO_2-containig materials co-doped by non-metals were obtained and examined to study their photo-activity under ultraviolet and daylight irradiation. The un-co-doped sample (sulfur-containing) showed similar capacity values for

both ultra-violet and daylight irradiation. Such result is encouraging, since the use of UV light is limited by safety regulations.
-The difference between the chemical properties of non-metals and their activities in the solution caused different contents of nonmetals in the samples, despite the fact that the content in the precursor was the same.
-All samples demonstrated the increase of adsorption capacity both under UV and daylight irradiation. However, significant activity under irradiation by light with a greater wavelength was observed only for the chlorinated sample.
-For all the samples, the adsorption kinetic constant increased especially in comparison with data in Table 4.12. However, the results obtained under the daylights-results was 15.5-38.2% lower than UV-results. Moreover, higher values of maximum adsorption m_{lim} was obtained. This can be explained by two independent factors: a) the effect of non-metals on the formation of the porous structure of materials; b) the effect of non-metals on the formation of titanium dioxide layer and band gap narrowing in the materials.
-To investigate of the synthesis conditions and properties of the materials, the chlorine doping method is recommended.

5.4. The study of the properties of fly ash as a matrix for photoactive component

The use of solid carbon-based fuels in energy industry results in the production of solid byproduct, ash. Ash results as coarse grains removed from the bottom of the furnace (bottom ash) and as fine particles captured by the filter from gaseous exhaust (fly ash, FA).The more detailed classification of fly ash, its cementitious properties and some methods of its utilization are represented in paragraph 1.4.5.
Fly ash is primarily silicate glass containing silica, alumina, iron, and calcium. Minor constituents are magnesium, sulfur, sodium, potassium, and carbon. Crystalline compounds are present in small amounts. The relative density (specific gravity) of fly ash generally ranges between 1.9 and 2.8 and the colour is generally dark, grey or light grey.
The particle sizes in fly ash vary from less than 1 μm (micrometer) to more than 100 μm with the typical particle size under 20 μm. Only 10-30% wt of the particles are larger than 45 μm. The surface area is typically 300 to 500 m^2/kg, although some fly ashes can have surface areas as low (200 m^2/kg) and as high (700 m^2/kg). For fly ash without close compaction, the bulk density (mass per unit volume including air between particles) can vary from 540 to 860 kg/m^3, whereas with close packed storage or vibration, the range can be from 1120 to 1500 kg/m^3. [129].
Paragraph 1.4.5 describes the use of fly ash as raw material for the production of adsorbents among other methods of FA utilization [130], basic [239]. The experience of using fly ash as a matrix for titanium-containing material was described a number of scientific sources [141-143], although the efficiency is questionable. Since the proposed method involves a strong effect on the mineral matrix, the present study has explored the possibility of using FA as a carrier of titanium dioxide. Professor Tarun R. Naik, Ph.D., P.E. Research Professor and Academic Program Director UWM Center provided fly ash for By-Products Utilization (Department of Civil Engineering and Mechanics, College of Engineering & Applied Science, University of Wisconsin).

5.4.1 The study of the composition and adsorption characteristics of fly ash

Fly ash is a heterogeneous material; aluminosilicates, Fe_2O_3, CaO, a significant amount of carbon dust and occasionally other minerals are the main chemical components present in fly ashes. Mineral components often lose adsorption activity under the influence of high-temperature treatment (the combustion). Therefore, in the first phase of the study the chemical composition and adsorption properties of the material should be examined. The chemical composition (Sec. 2.4) was determined by the method of emission spectrometry (Tab. 5.5).

Table 5.5.The chemical composition of fly ash (FA).

Components	Contents, % wt
SiO_2	50
Al_2O_3	25
Fe_2O_3+FeO	7
CaO	4
C	11,4
ZnO	0,8
TiO_2	0,8
Cu, Cd, B, P, Cr, Mg, Pb, Mn, Ni, V, Na, Ag	> 1 sum.

According to the results, the base material is silica and alumina (75 % wt). However, there is a considerable amount of carbon, probably in the form of soot blown during coal combustion. Titanium and zinc oxides are also present in the composition of the material. In spite of the high content of silicon and aluminum, SEM (Sec. 2.5) showed a significant difference in surface morphology (Fig. 5.13): FA has a more friable and fibrous structure. This may affect the adsorption properties of the FA.

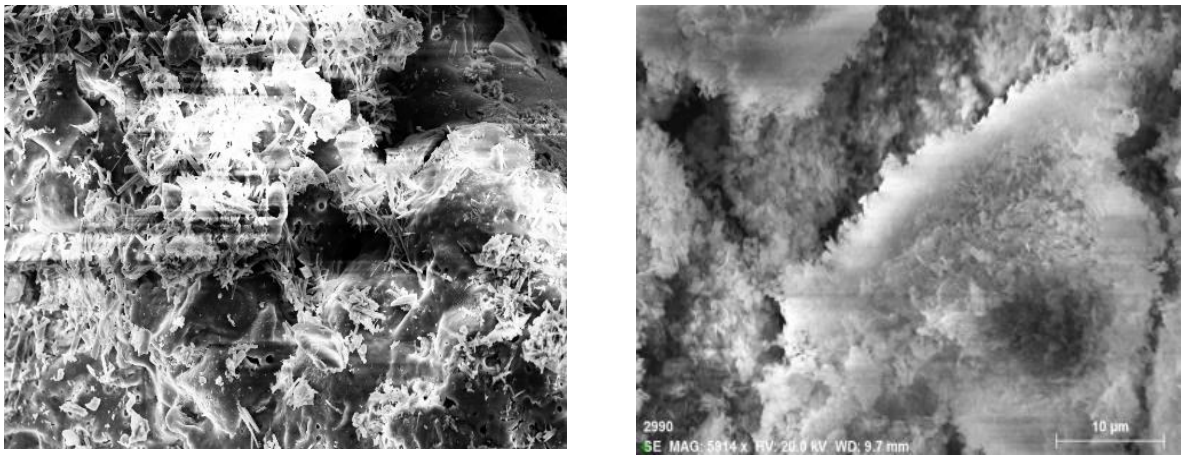

a) b)

Figure 5.13.The micro-profiles of untreated fly ash (a) and kaolinite (b) obtained by SEM method

The study of the adsorption properties was performed by the method described in Section 2.2: for the ash in the original state and for the samples treated by 7.8 % solution of sulfuric acid in the same manner as for the reaction solution, the scheme of treatment was shown in Table 5.6.

Table 5.6.The conditions of the thermo-acid treatment.

Type	Conditions			Samples ID	Yield, g/g
	Mass of FA, g	Volume of reaction solution, ml	Temperature of heat-treatment, °C		
Acid-treated	1	3	600	FA (1:3) Act	0.75
	1	6	600	FA(1:6) Act	0.67

The composition of the samples (Tab. 5.7), identified by EXDA (see Sec. 2.4)), was changed toward the increasing the molar ratio of Al_2O_3/SiO_2; while for the original material this ratio is equal to 0.39, for the samples after thermo-acid treatment it is close to one. An increase in the titanium content of the ash is worth noting as well, since after the treatment it increased roughly up to 1.5% wt for the sample FA (1:3) Act and to 5% wt – for FA (1:3) Act. However, it must be taken into account that the impact of the modification on the aluminosilicate matrix remains unpredictable, given that the material could be obtained in the high-temperature zone of the flame, which radically changes its structure.

The Figure 5.14 demonstrates the surfaces of the samples after chemical processing and heat-treatment. In contrast to the sample of untreated ash, the surface becomes more relief, but local fragments become smoother.

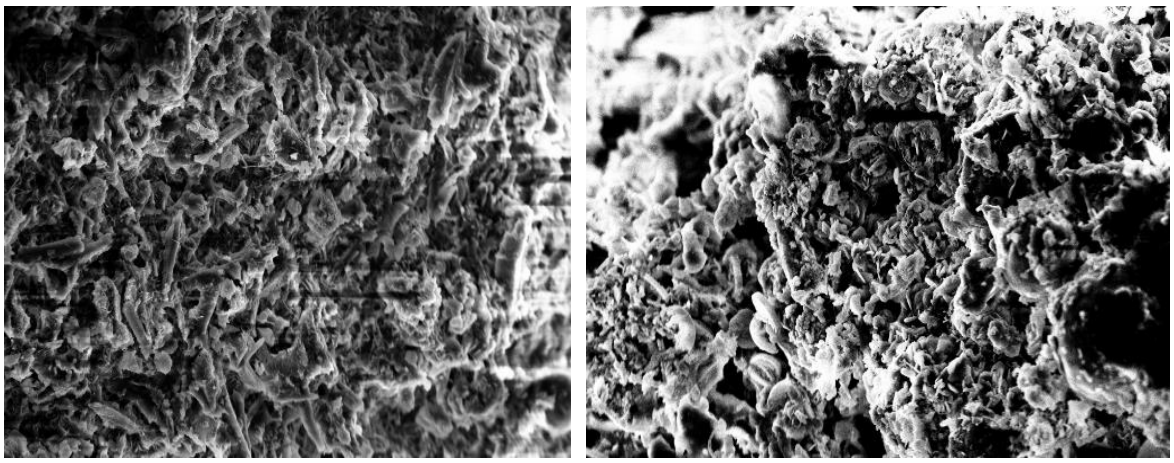

a) b)

Figure 5.14 The microstructure of the samples: a)- FA (1:3) Act, b)- and FA (1:6) Act

Figure 5.7 The chemical composition of the activated ash.

Samples		Contents, wt %											Σ	TiO_2/ Σ components, mg/g	Molar ratio Al_2O_3/SiO_2
		Al	Si	Fe	O	Ti	Mg	K	Ca	S	Na	P			
FA (1:3) Act	1	0.37	3.1	0.16	53.37	0.43	0.37	0.12	23.79	17.74	0.34	0	99.8	25.4	0.82
	2	14.6	14.45	0.53	56.61	1.03	0	0	0	12.27	0	0.03	99.5		
	3	11,59	10.92	0.63	58.62	2.99	0.53	0.10	0.45	13.36	0.65	0.16	100		
	everage	8.85	9.49	0.44	56.20	1.48	0.30	0.07	8.08	14.46	0.33	0.06	99.8		
	Al_2O_3,SiO_2, mol/g	0.17	0.20												
FA (1:6) Act	1	3.33	1.94	2.10	37.29	0	5.79	3.38	3.68	42.48	0	0	100	89.4	0.99
	2	15.7	17.2	1.49	31.79	11.24	0	0	0.62	20.7	0	1.27	100		
	3	13.14	9.53	0.66	55.91	3.52	0.40	0.19	0.24	15.44	0.40	0.56	100		
	everage	10.72	9.56	1.42	41.66	4.92	2.06	1.19	1.51	26.21	0.13	0.61	100		
	Al_2O_3,SiO_2, mol/g	0.19	0.20												

The analysis of water vapor adsorption-desorption isotherms at 25 °C (Fig. 5.15) did not reveal any significant increase of the adsorption activity in the initial section. At the range from P/Ps = 0.45 (microspores filling) to P/Ps=1 (maximum adsorption activity), the capacity increases 2.3-3 times (Tab. 5.8), but the values still were too little and could not be indicative of a significant microspore structure.

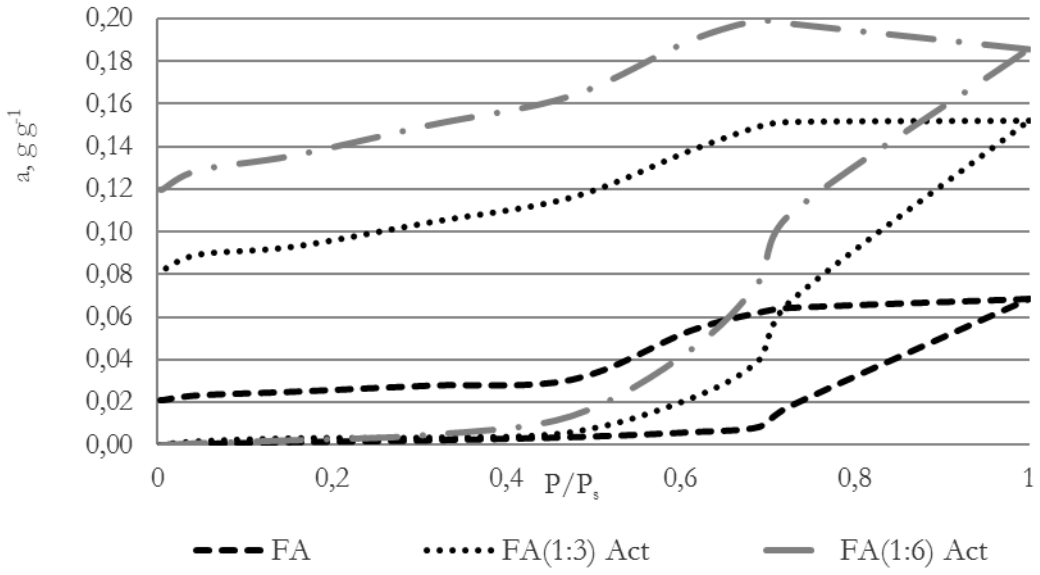

Figure 5.15 The water vapour isotherms at 25°C for activated ash

Table 5.8 The adsorption capacity of acid-treated FA materials.

Samples	Capacity, mg/g,	
	P/P_s=0,45	P/P_s=1
FA	3.8	68.6
FA(1:3) Act	6.1	151.9
FA(1:6) Act	13.7	185.7

The shape of desorption lines and abnormal hysteresis suggests that the materials contain sulphates and formation of crystal hydrates at P/Ps >0.6, as was the case with kaolinite.

5.4.2 The preparation of TiO_2-contaned materials and investigation of their compositions

To study the possibility of using fly ash as a matrix material, titanium-containing samples were obtained. For this purpose, the same precursor and methods were used for processing clays (see Sec. 2.2). The condition of the preparation and the ID of the samples were shown in Table 5.8. The titanium content in the solution was 17.47 mg/ml.

Table 5.8.The conditions of TiO_2–FA material preparation.

Mass of the flay asf, g	Volume of solution, ml	Calcination temperature, °C	Amount of the added titanium, mg/g		Samples ID
			Ti	TiO_2	
1	3	600	52,41	87,52	FA-(1:3)
1	6	600	104,82	175,05	FA-(1:6)

The results of SEM-EXDA are represented in Table 5.9 and Figure 5.16. It is worth noting, that the composition of the samples is significantly more diverse, than for the clay-based materials.

The results are represented in Table 5.9, and can be summarized in the following conclusions:

- Al/Si ratio is for the samples based on clay, especially kaolinite, matrix (see Chapter 4), as it was expected. Despite that, the aluminum content of the sample FA 3 is significantly lower and close to montmorillonite-based materials;
- The amount of sulfur for the ash-based samples is a noticeably (at 1.1 – 1.8 times) higher in comparison with the clay-based materials prepared under the same temperature, while aluminum content is relatively low;
- It is worth noting, that the composition of fly ash is significantly more diverse, than for the clay-based materials. Perhaps this is due to a relatively high content of impurities in the original fuel. This factor may have to be considered in the future in order to avoid the presence of hazardous contaminants.

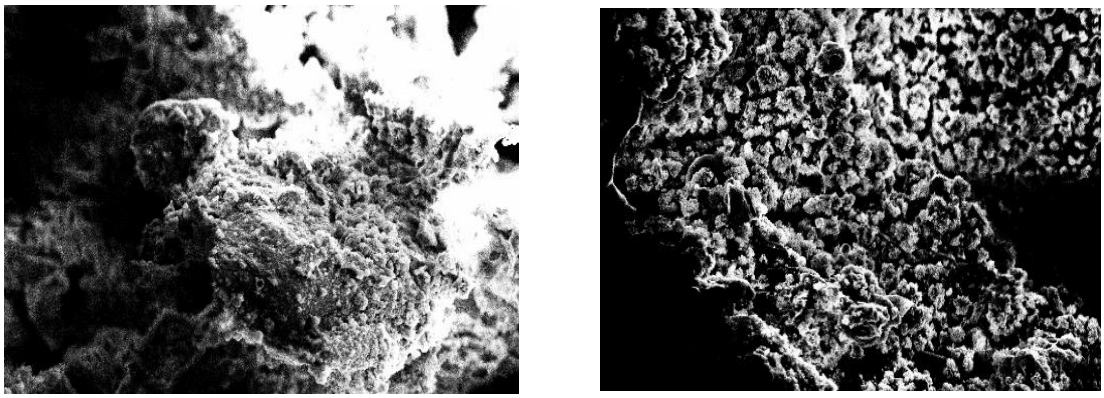

a) b)

Figure 5.16. The microstructure of the samples: a) - FA (1:3), b) - FA (1:6)

Figure 5.16 demonstrates the presence of the titanium dioxide layer. In this case, the content of TiO_2 is higher for the sample FA-(1:3) (see Tab. 5.9), but the surface of this one is more similar to the pure ash (Fig. 5.13, a) than for the sample FA-(1:6), which is more similar to the activated FA. Probably, this effect is due to the use of a higher amount of sulfuric acid for obtaining FA-(1:6).

Table 5.9.The composition of the TiO_2-FA samples.

Samples		Contents, wt %											Σ	TiO_2/ Σ components, mg/g	Molar ratio Al/Si
		Al	Si	Fe	O	Ti	Mg	K	Ca	S	Na	P			
FA-(1:3)	1	4.81	3.77	1.81	58.44	2.21	1.45	2.06	3.76	18.96	2,73	0	100	253.1	0.17
	2	1.95	20.83	3.49	20.81	26.89	0	4.42	11.14	10.06	0	0	99.6		
	3	1.35	17.53	8.42	11.33	7.22	0	8.69	15.08	29.27	0	0,35	99.3		
	everage	2.70	14.04	4.57	30.19	12.11	0.48	5.06	9.99	19.43	0,91	0,12	99.6		
	Al_2O_3,SiO_2, mol/g	0.05	0.30												
FA-(1:6)	1	2.98	30.92	3.75	39.4	7.76	0.00	1.99	3.20	10.00	0.00	0.00	100	191.5	0.54
	2	29.39	20.89	2.82	19.46	15.21	0.98	0.36	1.23	9.62	0.00	1.27	71.8		
	3	16.84	27.95	0.89	37.62	5.93	0.00	0	0.71	9.78	0.29	0.00	100		
	everage	16.40	26.59	2.49	32.16	9.63	0.33	0.78	1.71	9.80	0.10	0.42	100		
	Al_2O_3,SiO_2, mol/g	0.31	0.57												

Optical microscopy (Sec. 2.5) was used to determine an average particle size of the FA-based materials (Fig. 5.17).

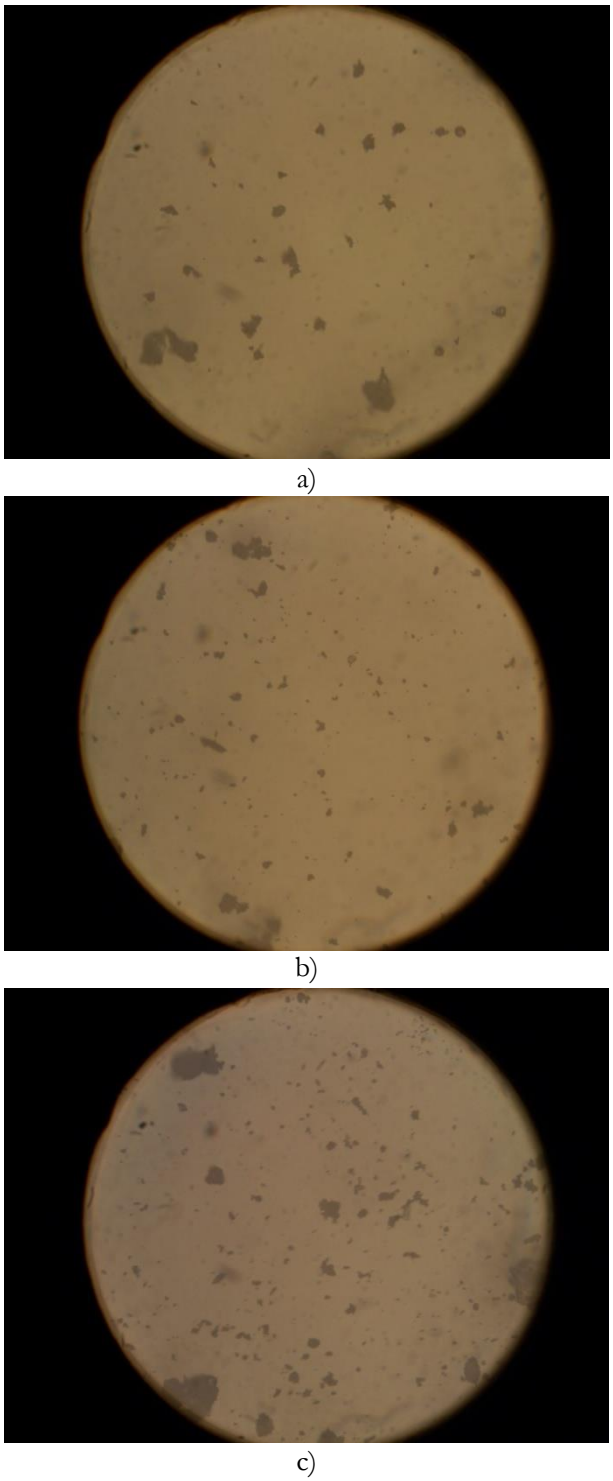

a)

b)

c)

Figure 5.17. The optical microscopy results (300x): a) FA, b) FA-(1:3), c) FA-(1:6)

The average particle sizes of the composites were 9.572±1.154 μm for FA, 7.057±0.717 μm for FA-(1:3) and 8.114±1.060 μm for FA-(1:6), respectively. These values are more

than two times higher than the results obtained for the kaolinite-based samples. In addition, the confidence ranges are significant (from few to few dozens of μm).

5.4.3 The adsorption of water vapor by the TiO_2–FA materials

The adsorption isotherms (Fig. 5.18) show, that the capacity of the samples with deposited TiO_2 increased around 2.3 times in comparison with the adsorbents after a simple thermo-acid treatment, and more than 6 times in comparison with a "pure" ash.

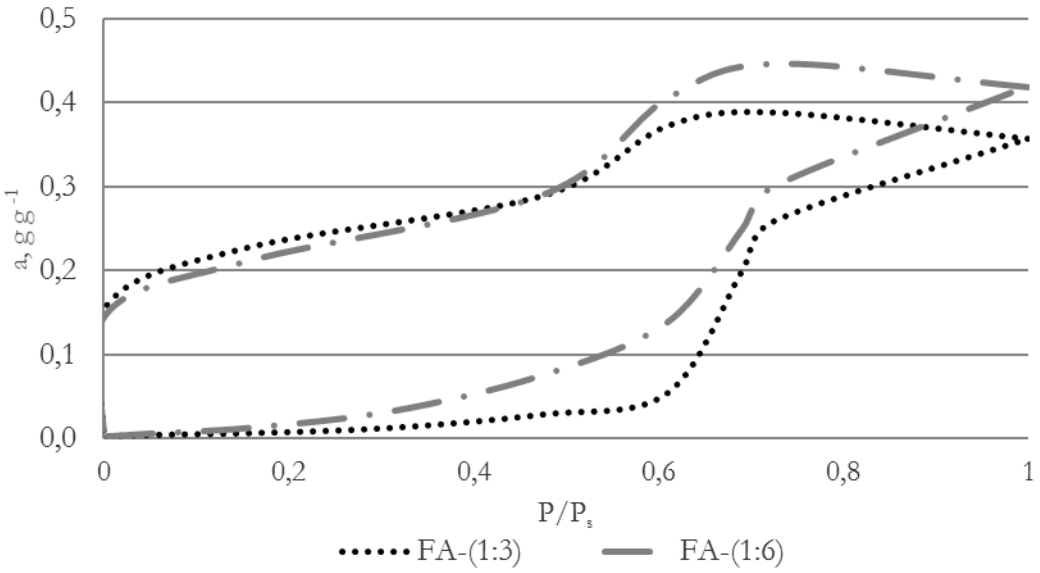

Figure 5.18. The water vapor isotherms at 25 °C for the TiO_2-FA materials

The adsorptive capacities of the samples are given in Table 5.10. Most noteworthy is the fact that both values of capacity at both P/Ps = 0.45 and P/Ps = 1 increased significantly (more than seven times for the former and more than five times for the later). However, the last values of capacity are not enough to confirm formation of the microporous structure.

Table 5.10.The capacity value of theTiO_2-FA samples

Samples	Capacity, mg/g	
	P/P_s=0.45	P/P_s=1
FA-(1:3)	27.8	356.5
FA-(1:6)	75.2	418.7

After the investigation, it can be concluded, that the thermo-acid treatment and deposition of titanium dioxide have a positive impact on the adsorption properties of the samples. However, the FA-based composites are less efficient than the materials obtained on the clay matrix.

5.4.4 The kinetics of MEK-removal under UV-irradiation

The photosensitivity testing was performed using the batch reactor 0.45 L equipped by LEDs DFL-5AP4SC-400 in the conditions according to Paragragh 2.8.3. The results are presented in Figure 5.19 as the parameters of the kinetic equation 2.26.

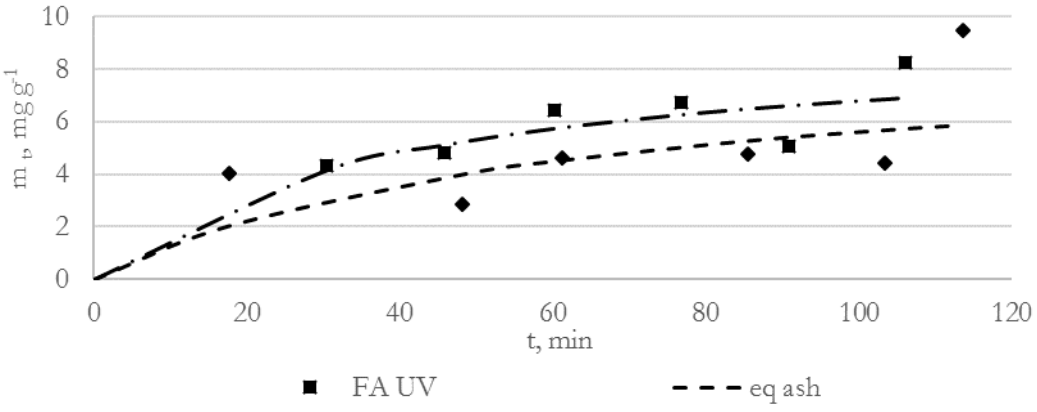

a)

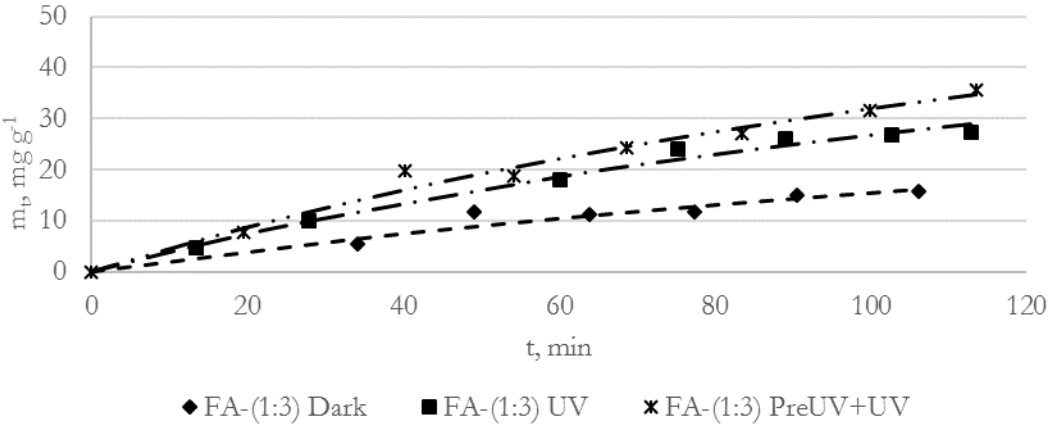

b)

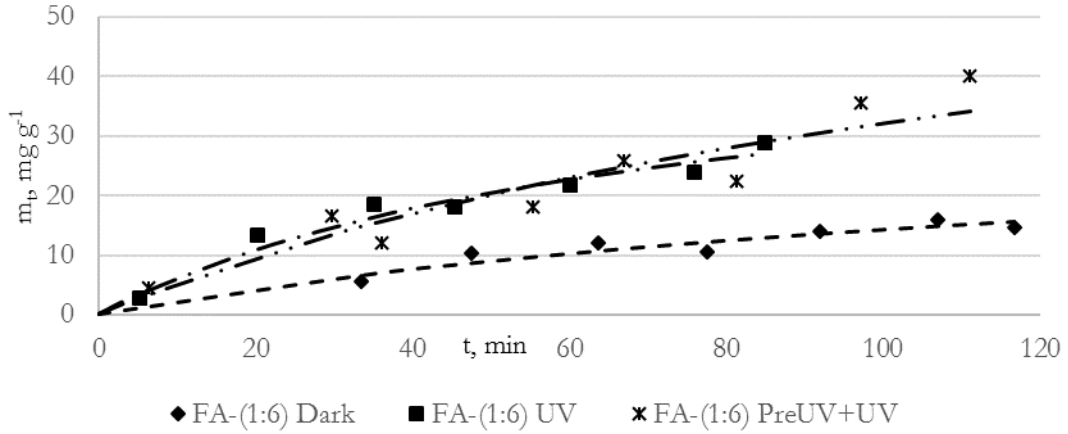

c)

Figure 5.19. The removal of the MEK kinetics: a) for the untreated FA material, b) for FA -(1:3), c) for FA-(1:6)

The calculations show the dispersion of test results due to a relatively low adsorption capacity and the MEK removal rate and deviations within the confidence interval. The relatively high content of Ti (near 0.8% wt) was mentioned above, but there was not any significant difference between the results obtained in dark conditions and under UV-irradiation. In addition, the sample FA-(1:3) demonstrates better results despite the lower content of titanium.

Considering that the goal of the experiment is not only to identify the reaction of the materials to ultra-violet irradiation but examine their potential as adsorbents and UV-sensitive material, the capacity dynamics was calculated (Fig. 5.17) and the parameters of the second order of the kinetic equation for the MEK degradation was determined (see Tab. 5.11).

The thermochemical treatment and deposition of titanium allows a higher degree of the MEK removal. UV-irradiation increases the efficiency of the FA-based samples. However, the results are low, and the materials do not react to preliminary UV-activation. The calculations show that, despite the high values of the limited adsorbed mass m_{lim}, the rate constant does not exceed 0.54 mg/(g min) and UV-irradiation does not increase this parameter significantly.

Therefore, the equilibrium cannot be attained rapidly; e.g. the process requires from 1957 to 5190 hours to achieve the rate m_t/m_{lim}=0.95. Considering this low rate of the process, the applicability of the material is questionable.

Table 5.11.The parameters of the kinetic equation for the MEK removal process

Parameters	Irradiaton		
	Dark	UV-irradiation	UV-pre-treatment + UV-irradiation
Sample	FA		
Ti , %wt	0.8		
m_{lim} ,mg/g	9.0	9.4	-
k_{ads} , mg/(g min)	0.15	0.24	-
Pearson koefficient R^2	0.39	0.62	-
Sample	FA –(1:3)		
Ti , %wt	12.1		
m_{lim} ,mg/g	57.36	79.01	95.97
k_{ads} ,mg/(g min)	0.21	0.41	0.48
Pearson koefficient R^2	0.35	0.87	0.68
Sample	FA –(1:6)		
Ti , %wt	9.63		
m_{lim} ,mg/g	35.48	50.47	79.43
k_{ads} ,	0.24	0.49	0.54
Pearson koefficient R^2	0.74	0.74	0.40

5.4.5 Conclusions for Section 5.4

The results can be summarized in the following conclusions:

The features of the composition of fly ash and the properties of the components allow obtaining the samples with a higher titanium content on the surface layer than that of the samples on the kaolin matrix with the same treatment. This makes it possible to obtain the samples of materials comparable to the clay-based composites in terms of the MEK absorption efficiency, but with lesser speed of the process.

The use of this technology of depositing titanium dioxide made it possible to obtain a material that has some UV sensitivity, but its activity is much lower than that of the samples on the kaolinite matrix.

After processing the data of water vapor sorption experiment, it was confirmed that the thermo-acid treatment has positive effects on the adsorption activity of fly ash. However, the treatment does not significantly increase the adsorption capacity at the stage of micropore and transition pore filling. The increase in capacity comes mostly because of the increase of the mesoporous volume at P/P_s=0.6-1.0.

The deposition of TiO_2 improves efficiency of the MEK removal process. The UV-irradiation increases the activity of the TiO_2-contained samples, although the results still significantly lower compared with clay-based composites, influences the pre-activation was not observed.

Therefore, the use of fly ash to produce a low-active UV-sensitive material can be realized only if the economic efficiency will be determined by the need to recycle the material.

Conclusions

1. The method of the synthesis of photoactive TiO_2/aluminosilicate composites based on high-temperature hydrolysis of titanium-containing precursors with further deposition on matrix surface was developed and examined. In particular, this included:

- Research of the ageing process of the composites in terms of their adsorption properties and photoactivity after three years of storage.
- Synthesis of the materials under different conditions (i.e. different type of carrier material, matrix/precursor ratio, method of calcination, presence and type of doping agents);
- Materials characterization, including chemical composition, surface morphology, average particle size, phase composition, water- and benzene vapor adsorption activity, specific surface area and photosensitivity;
- Development of recommendations regarding method and materials for the synthesis of the photoactive TiO_2/aluminosilicate composites (visible-light sensitive materials), possible applications of the materials, and their industrial production.

The method is promising and with interesting economic and environmental aspects due to the fact it uses available and relatively low-cost raw materials, including aluminosilicates (e.g., kaolinite and montmorillonite clays) and wastes of other industries (e.g., titanium shavings and fly ash).

2. The first materials synthesized with the proposed method were obtained in 2011, which offered an opportunity to examine the effect of ageing on the properties and to determine optimal conditions for preparing a stable material. The isotherms of water vapor and the kinetics of MEK removal were used for comparison. It was found that the increase of the amount of the precursor leads to getting material, more vulnerable to the effects of ageing, and the content of titanium for the samples obtained at 600 °C is disproportionate to the one added with the solution during the synthesis. The kaolinite-based materials demonstrate a better stability of the adsorptive properties over time. Furthermore, the optimal titanium content should not exceed 100 mg per gram of matrix.

A typical adsorption-desorption hysteresis showed that the hydrophilicity of the material can be explained by the formation of crystalline hydrates. Therefore, it was decided to synthesize the new materials at a higher calcination temperature in order to provide the destruction of sulphates.

All tested samples demonstrated photoactivity. The best results were obtained by the samples with the TiO_2-content about 150 mg/g.

Based on the data obtained, the following conditions for the synthesis of the new samples were suggested:

- Preference is given to the kaolinite matrix (although the montmorillonite based samples should be prepared for comparison);
- The estimated TiO_2-contents are 85.2 mg/g (the matrix/precursor ratio is 1:3) and 191 mg/g (the matrix/precursor ratio is 1:6);
- The calcination temperatures are 600 °C and 750 °C.

3. The study of the properties of the synthesized materials confirmed the right choice of the calcination temperature as the sulfur content decreased significantly and despite the general decrease of water vapor adsorption activity, the TiO_2-content of the samples is proportional to the estimated one. At the same time, the treatment at this temperature

leads to the formation of transitional porous structure. The maximum specific surface area is 122 m2/g, of which 95 m2/g is the area of transitional pores. X-ray crystallography also confirmed the reduction of sulfates and the presence of anatase in the samples. At the same time, the prevailing matrix structure could not be identified because of the multicomponent nature of the material.

4. All the synthesized materials demonstrated UV-sensitivity during the process of MEK removal. For comparison, the commercial photocatalyst Degussa P25 was used as a reference material and examined under LED-induced irradiation with the average wavelength of 380 nm. In terms of UV-sensitivity, kaolinite-based materials synthesized at 750 °C are more active than those calcined at 600 °C. In comparison with the commercial photocatalytic material Degussa P25, the K-based composites demonstrated significantly lower results in terms of MEK removal, but preliminary UV-activation improved the activity up to the comparable level of Degussa P25.

5. A pilot scheme for the material industrial production was proposed.

6. The composite which was obtained at the ratio kaolinite/precursor 1 : 6 and the temperature of calcinations 750 °C, than it was examined as component of finishing materials, such us finishing putty, ceramic coating and polyurethane varnish. The testing of the building materials confirmed that the TiO_2-containing composites can be applied as photoactive components, providing the removal of indoor and outdoor air pollutants. However, further research is needed to determine specific applications and the conditions for application.

7. The ways of developing photosensitive materials included:

- TiO_2-containig materials co-doped by non-metals (chlorine, nitrogen and phosphorus). These materials were obtained and examined to study their photo-activity under ultraviolet (λ=380…400 nm) and daylight irradiation (λ=450 nm) by LEDs. The content of doping agents was different for the material due to the difference between the chemical properties of non-metals and their activities in the solution. The MEK adsorption kinetic constant increased significantly for all the samples, although the results obtained under the daylight were 15.5-38.2% lower than the UV-results. The chlorine doped composite demonstrated the best results and therefore, it is recommended for further researches.
- Fly ash was studied as another potentially promising support material. While thermo-acid treatment has positive effects on the adsorption activity of fly ash, the treatment does not significantly increase the adsorption capacity at the stage of micropore and transition pore filling. The deposition of TiO_2 improves the efficiency of the MEK removal process, although the results are still significantly lower compared with the clay-based composites, the influence of the pre-activation was not observed. Therefore, the use of fly ash to produce UV-sensitive material can be realized only if economic efficiency will be determined by the need to recycle the material.

References

[1] F. Tittarelli , C. Giosuи, A. Mobili, M.L. Ruello. *Influence of binders and aggregates on VOCs adsorption and moisture buffering activity of mortars for indoor applications*. Cement & Concrete Composites, vol. 57, pp. 75–83, 2015.

[2] V. Augugliaro, V. Loddo, M. Pagliaro, G. Palmisano, L. Palmisano. *Clean by Light Irradiation: Practical Applications of Supported TiO_2.* The Royal Society of Chemistry, Cambridge CB4 0WF, UK, 2010.

[3] G. Fava, M. Pierpaoli. *A hybrid photocatalytic-electrostatic reactor for nitrogen oxides removal* American Journal of Environmental Engineering and Science, vol. 2(1), pp. 7-13, 2015.

[4] G. Fava, M. Pierpaoli. *Volatile Organic Compounds Removal in a Hybrid Photocatalytic-Electrostatic Reacto*r American Journal of Environmental Engineering and Science, vol. 2(2), pp. 14-17, 2015.

[5] C. Giosuè, M. Pierpaoli, A. Mobili, F. Tittarelli, M.L. Ruello. *Photocatalytic Cement-based Mortars with Unconventional Aggregates for the Improvement of Indoor Air Quality* 9-th European Meeting on Solar Chemistry and Photocatalysis: Environmental Application, Strasbourg-France, June 13-17, 2016.

[6] V. Bondarenko, M.L. Ruello, E. Prokofyeva. *Microscopic analysis of the composite of the catalytic-active material "CATACLEAN – T"*. Ecology of Central Black Earth Region, vol. 1, pp. 26-32, 2011.

[7] M.L. Ruello, E. Prokofyeva, V. Bondarenko, A. Bondarenko, D. Sani. *Adsorption properties of composites prepared by precipitation of the catalytically active materials to the clay*. Sorbents as a factor in a quality of life and health: Proceedings of the IV International Conference, Belgorod-Russia, pp. 138-143, September 24-28, 2012.

[8] V. Bondarenko, M.L. Ruello, A. Bondarenko. *Ageing of photocatalytic materials: investigation, assessment and possible solving*. Chemical Engineering Transactions, vol. 47, pp. 133-138, 2016.

[9] M.L. Ruello, V. Bondarenko, A.V. Bondarenko, N. Sklyarenko, E. Gorlova. Photocatalytic and adsorptive properties of the materials obtained by depositing of titanium dioxide on the silicate matrix. V International conference on chemical technology: collected articles from XX Mendeleev congress on general and applied chemistry, 16-20 may, 2016 – Volgograd: VSTU, vol. 1, pp. 328-330, 2016.

[10] M.L. Ruello, V. Bondarenko, E.A . Gorlova. *Study of fly ash properties for using as a catalyst carrier*. Modern Metallurgy of the Beginning of the New Millennium: Proceedings of 11th International Conference, Lipetsk-Russia, pp. 227-231, 18-21 November 2014.

[11] S.E. Frey, H. Destaillats, S. Cohn, S. Ahrentzen, M.P. Fraser. *The effects of an energy efficiency retrofit on indoor air quality*. Indoor Air, vol. 25, pp. 210–219, 2015.

[12] Y. Sekine, A. Nishimura*, Removal of formaldehyde from indoor air by passive type air-cleaning materials*. Atmos. Environ, vol. 35. Pp. 2001–2007, 2001.

[13] *Environmental Health Criteria 128 (Hexachlorobenzene) International Programme on Chemical Safety*, WHO, Geneva, 1991.

[14] S.K. Brown, M.R. Sim, M.J. Abramson, C.N. Gray. *Concentrations of volatile organic compounds in indoor air–a review*. Indoor Air, vol. 4 , pp.123-134, 1994.

[15] H. Matsumoto, M. Shimizu, H. Sato. *The contaminant removal efficiency of an air cleaner using the adsorption/desorption effect*. Build. Environ, vol. 44, pp. 1371–1377, 2009.

[16] Ch. J. Weschler, W. W. Nazaroff. *Semivolatile organic compounds in indoor environments*. Atmospheric Environment, vol. 42, pp. 9018–9040, 2008.

[17] L. Zhong, F.Haghighat. *Photocatalytic air cleaners and materials technologies*. Abilities and limitations. Building and Environment, vol. 91, pp. 191-203, 2015.

[18] Kunkel D., E. Gall, J.A. Siegel, A. Novoselac, G.C. Morrison, R.L. Corsi. *Passive reduction of human exposure to indoor ozone*. Build. Environ, vol. 45, pp. 445–452, 2010.

[19] L. Senff, D.M. Tobaldi, S. Lucas, D. Hotza, V.M. Ferreira, J.A. Labrincha. *Formulation of mortars with nano-SiO_2 and nano-TiO_2 for degradation of pollutants in buildings*. Compos. Part B, vol. 44, pp. 40–47, 2013.

[20] Y. Liu, X. Zhou, D. Wang, C. Song, J. Liu. *A prediction model of VOC partition coefficient in porous building materials based on adsorption potential theory* . Building and Environmen, vol. 93, pp. 221-233, 2015.

[21] R. Meininghaus, L. Gunnarsen, H.N. Knudsen. *Diffusion and Sorption of Volatile Organic Compounds in Building Materials−Impact on Indoor Air Quality*. Environ. Sci. Technol., vol. 34 pp. 3101–3108, 2000.

[22] Tarun R. Naik, Timir C. Shah, Rudolph N. Kraus, Fethullah Canpolat, Yoon-moon Chun *CO_2 sequestration in no-fines concrete* Report No. CBU-2005-15 August 2005 REP-586 Available: http://www4.uwm.edu/cbu/Papers/2005%20CBU%20Reports/REP-586.pdf

[23] Tarun R. Naik, Rakesh Kumar, and Rudolph N. Kraus. *Carbon dioxide sequestration in cementitious products.* By Report No. CBU-2009-12 August 2009 REP-650 Available: https://www4.uwm.edu/cbu/Papers/2009%20CBU%20Reports/REP-650.pdf

[24] R. M. Alberici, W. F. Jardim. *Photocatalytic destruction of VOCs in the gas-phase using titanium dioxide.* Applied Catalysis B: Environmental, vol. 14, pp. 55-68, 1997.

[25] T.Minabe , D. A. Tryk, P. Sawunyamab, Y. Kikuchi, K. Hashimoto, A. Fujishima. *TiO_2-mediated photodegradation of liquid and solid organic compounds* Journal of Photochemistry and Photobiology A: Chemistry, vol. 137, pp. 53–62, 2000.

[26] H. Einaga, S. Futamura, T. Ibusuki *Heterogeneous photocatalytic oxidation of benzene, toluene, cyclohexene and cyclohexane in humidified air: comparison of decomposition behavior on photoirradiated TiO_2 catalyst*. Applied Catalysis B: Environmental, vol. 38, pp. 215–225, 2002.

[27] W.H. Ching, Michael Leung, Dennis Y.C. Leung. *Solar photocatalytic degradation of gaseous formaldehyde by sol–gel TiO_2 thin film for enhancement of indoor air quality*. Solar Energy, vol. 77, pp. 129–135, pp. 2004.

[28] E. Pellizzetti, C. Minero *Mechanism of the photo-oxidative degradation of organic pollutants over TiO_2 particles.* Electoghimica Acta, vol. 38, No. 1, pp. 47-55, 1993.

[29] G. Vincent, A. Queffeulou, P.M. Marquaire, O. Zahraa. *Remediation of olfactory pollution by photocatalytic degradation process: Study of methyl ethyl ketone (MEK*). Journal of Photochemistry and Photobiology A: Chemistry, vol. 191, pp. 42–50, 2007.

[30] A.V.Vorontsov , D.V.Kozlov, P.G. Smirniotis , V.N. Parmon. *TiO_2 Photocatalytic Oxidation: II. Gas-Phase Processes* . Kinetics and Catalysis, vol.46 (3), pp. 450-465, 2005.

[31] J. Mo, Y. Zhang , Q. Xu, J. J. Lamson, R. *Zhao Photocatalytic purification of volatile organic compounds in indoor air: A literature review*. Atmospheric Environment, vol. 43, pp. 2229–2246, 2009.

[32] A.T. Hodgson, H. Destaillats, T. Hotchi, W.J. Fisk. *Evaluation of a combined ultraviolet photocatalytic oxidation (UVPCO) chemisorbing air cleaner for indoor air applications: Technical Report.* Lawrence Berkeley National Laboratory, pp. 1-74, 2007.

[33] J. Shang, Y.G. Du, Z.L. Xu. *Photocatalytic oxidation of heptane in the gas-phase over TiO_2*. Chemosphere, vol 46, pp. 93- 99, 2002.

[34] G. Vincent, P.M. Marquaire, O. Zahraa. *Photocatalytic degradation of gaseous 1- propanol using an annular reactor: kinetic modeling and pathways*. J Hazard Mater, vol. 161(11), pp. 73-81, 2009.

[35] J. Mo, Y. Zhang, Q. Xu. *Effect of water vapor on the by-products and decomposition rate of ppb-level toluene by photocatalytic oxidation*. Applied Catalysis B: Environmental, vol. 132-133,pp. 212-218, 2013.

[36] S.O. Hay, T.N. Obee, C. Thibaud-Erkey. *The deactivation of photocatalytic based air purifiers by ambient siloxanes*. Applied Catalysis B: Environmental, vol. 99, pp. 435-41, 2010.

[37] J.M. Coronado, M.E. Zorn, I. Tejedor-Tejedor, M.A. *Anderson Photocatalytic oxidation of ketones in the gas phase over TiO_2 thin films: a kinetic study on the influence of water vapor*. Applied Catalysis B: Environmental, vol. 43, pp. 329–344, 2003.

[38] Tobaldi DM, Tucci A, Camera-Roda G, Baldi G, Esposito L. *Photocatalytic activity for exposed building materials*. Journal of the European Ceramic Society, vol. 28, pp. 2645–2652, 2008.

[39] O. Carp, C.L. Huisman, A. Reller *Photoinduced reactivity of titanium dioxide*. Progress in Solid State Chemistry, vol. 32, pp. 33–177, 2004.

[40] C. Cardenas C, J.I. Tob_on, C. García, J. Vila. *Functionalized building materials: photocatalytic abatement of NOx by cement pastes blended with TiO_2 nanoparticles*. Constr Build Mater, vol. 36, pp. 820-825, 2012.

[41] J. Chen, Sh.Kou, Ch. Poon *Photocatalytic cement-based materials: Comparison of nitrogen oxides and toluene removal potentials and evaluation of self-cleaning performance*. Building and Environment, vol 46, pp. 1827-1833, 2011.

[42] P. Krishnan, M.-H. Zhang, L. Yu, H. Feng. *Photocatalytic degradation of particulate pollutants and self-cleaning performance of TiO_2-containing silicate coating and mortar*. Constr Build Mater, vol. 44, pp. 309-316, 2013.

[43] L. Pinho, M.J, Mosquera. *Photocatalytic activity of TiO_2/SiO_2 nanocomposites applied to buildings: Influence of particle size and loading.* Applied Catalysis B: Environmental, vol. 134-135, pp. 205-221, 2013.

[44] M.-Z. Guo, T.-C. Ling, C.-S. Poon. *TiO_2-based self-compacting glass mortar: comparison of photocatalytic nitrogen oxide removal and bacteria inactivation.* Build Environ., vol. 53, pp. 1-6, 2012.

[45] M. Smits, Ck. Chan, T. Tytgat, B. Craeye, N. Costarramone, S. Lacombe, et al. *Photocatalytic degradation of soot deposition: self-cleaning effect on titanium dioxide coated cementitious materials.* Chemical Engineering Journal, vol. 222, pp. 411-418, 2013.

[46] U.I. Gaya, A.H. Abdullah. *Heterogeneous Photocatalytic Degradation of Organic Contaminants over Titanium Dioxide: A Review of Fundamentals, Progress and Problems*. Journal of Photochemistry and Photobiology C: Photochemistry Reviews, vol. 9, pp. 1-12, 2008.

[47] *Glossary of Terms in Photocatalysis and Radiation Catalysis.* Available: http://old.iupac.org/projects/posters01/parmon01.pdf

[48] A. Fujishima, K. Honda. *Electrochemical Photolysis of Water at a Semiconductor Electrode*. Nature, vol. 238, pp. 37-38, 1972.

[49] M.N. Chong, B. Jin, C.W. K. Chow, C. Saint. *Recent Developments in Photocatalytic Water Treatment Technology: A Review.* Water Resources, vol. 44, pp. 2997-3027, 2010.

[50] E. Pelizzetti, C. Minero. *Role of oxidative and reductive pathways in the photocatalytic degradation of organic compounds.* Colloids and Surfaces A: Physicochemical and Engineering Aspects, vol. 151, pp. 321–327, 1999.

[51] W. S. Jenks. *Photocatalytic Reaction Pathways – Effects of Molecular Structure, Catalyst, and Wavelength* in book: Photocatalysis and Water Purification. Edited by Pierre Pichat. Wiley-VCH Verlag GmbH & Co.KGaA, pp. 25-52, 2013.

[52] A.D. Paola, E. García-López, G. Marcì, L. Palmisano. *A survey of photocatalytic materials for environmental remediation.* Journal of Hazardous Materials, vol. 211-212, pp. 3-29, 2012.

[53] K. Sayarna, H.Arakawa. *Effect of carbonate addition on the photocatalytic decomposition of liquid water over a ZrO_2 catalyst.* Journal of Photochemistry and Photobiology A: Chemistry, vol. 94, pp. 67-76, 1996.

[54] H.Jiang, H. Endo, H. Natori, M. Nagai, K. Kobayashi *Fabrication and photoactivities of spherical-shaped $BiVO_4$ photocatalysts through solution combustion synthesis method.* Journal of the European Ceramic Society, vol. 28, pp. 2955-2962, 2008.

[55] I. Sopyan. *Kinetic analysis on photocatalytic degradation of gaseous acetaldehyde, ammonia and hydrogen sulfide on nanosized porous TO_2 films.* Sci. Technol Adv. Mater., vol. 8, pp. 33-39, 2007.

[56] T. Ohno, K. Sarukawa, M. Matsumura. *Photocatalytic activity of pure rutile particles isolated from TiO_2 powder by dissolving the anatase component in HF solution*. Journal of Physical Chemistry *B,* vol. 105, pp. 2417-2420, 2001.

[57] S.Yurdakal, G. Palmisano, V. Loddo, V. Augugliaro, L. Palmisano. *Nanostructured Rutile TiO2 for Selective Photocatalytic Oxidation of Aromatic Alcohols to Aldehydes in Water*. Journal of the American Chemical Society, vol. 130, pp. 1568-1569, 2008.

[58] A. Sclafani, L. Palmisano, M. Schiavello. *Influence of the preparation methods of TiO_2 on the photocatalytic degradation of phenol in aqueous dispersion*. Journal of Physical Chemistry, vol. 94, pp. 829 - 832, 1990.

[59] J. Wang, G. Zhang, Z. Zhangb, X. Zhang, G. Zhao, F. Wen, Z. Pan, Y. Li, P. Zhang, P. Kang. *Investigation on photocatalytic degradation of ethyl violet dyestuff using visible light in the presence of ordinary rutile TiO2 catalyst doped with upconversion luminescence agent*. Water research, vol. 40, pp. 2143-2150, 2006.

[60] A. Testino, I.R. Bellobono, V. Buscaglia, C Canevali, M. D'Arienzo, S. Polizzi, R. Scotti, F. Morazzoni. *Optimizing the photocatalytic properties of hydrothermal TiO_2 by the control of phase composition and particle morphology. A systematic approach*. Journal of the American Chemical Society, Soc., vol. 129, pp. 3564-3575, 2007.

[61] X. Deng, Y. Yue, Z. Gao. *Gas-phase photo-oxidation of organic compounds over nanosized TiO_2 photocatalysts by various preparations*. Applied Catalysis B: Environmental, vol. 39, pp. 135-147, 2002.

[62] A.V. Vorontsov, A.A. Altyrmikov, E.N. Savinov, E.N. Kurkin. *Correlation of TiO_2photocatalytic activity and diffuse reflectance spectra*. J. Photochem. Photobiol. A: Chem., vol. 144, pp. 193-196, 2001.

[63] A.J. Maira, K.L. Yeung, J, Soria, J.M. Coronado, C. Belver, C.Y. Lee, V. Augugliaro. *Gasphase photo-oxidation of toluene using nanometer-size TiOa catalysts*. Applied Catalysis B: Environmental, vol. 29, pp. 327-336, 2001.

[64] Z. Zhang, C.-C. Wang, R. Zakaria, J. Y. Ying. *Role of particle size in nanocrystalline TiOi-based photocatalysts*. Journal of Physical Chemistry B, vol. 102, no. 52, pp. 10871–10878, 1998.

[65] C.B. Almquist, P. Biswas. *Role of synthesis method and particle size of nanostructured TiO_2 on its photoactivity*. Journal of Catalysis, vol. 212, pp. 145-156, 2002.

[66] J. Liqiang, X. Sun, W, Cai, X. Zili, Y. Du, H. Fu. *The preparation and characterization of nanoparticle TiOa/Ti films and their photocatalytic activity*. Journal of Physics and Chemistry of Solids, vol. 64, pp.615-623, 2003.

[67] A.H. Boonstra, C.A.H.A. Mutsaers. *Relation between the photoadsorption of oxygen and the number of hydroxyl groups on a titanium dioxide surface*. Journal of Physical Chemistry, vol. 79, pp. 1694-1698, 1975.

[68] K. Kobayakawa, Y. Nakazawa, M. Ikeda, Y. Sato, A. Fujishima. *Influence of the density of surface hydroxyl-groups on TiOa photocatalytic activities*. Berichte der Bunsen-Gesellschaft für Physikalische Chemie, vol. 94, pp. 1439 – 1443, 1990.

[69] Y. Paz, A. Heller. *Photo-oxidatively self-cleaning transparent titanium dioxide films on soda lime glass: the deleterious effect of sodium contamination and its prevention*. Journal of Materials Research, vol. 12, pp. 2759-2766, 1997.

[70] D. Kozlov, D. Bavykin, E. Savinov. Effect of the acidity of TiO_2 on its photocatalytic activity in acetone gas - phase oxidation. Catalysis Letters, vol. 86, pp. 169-172, 2003.

[71] N. Keller, E. Barraud, F. Bosc, D. Edwards, V. Keller. *On the modification of photocatalysts for improving visible light and UV degradation of gas-phase toluene over TiO_2.* Applied Catalysis B: Environmental, vol. 70, pp. 423-430, 2007.

[72] Q. Zhang, L. Gao, J, Guo. *Effects of calcination on the photocatalytic properties of nanosized TiO_2 powders prepared by TiCU hydrolysis*. Applied Catalysis B: Environmental, vol. 26, pp. 207 -215, 2000.

[73] X. Wang, J.C. Yu, P. Liu, X. Wang, W. Su, X. Fu. *Probing of photocatalytic surface sites of SO_4^{2-}/TiO_2 solid acids by in situ FTIR spectroscopy and pyridine adsorption.* Journal of Photochemistry and Photobiology A: Chemistry, vol. 179, pp. 339-347, 2006.

[74] N. Shaham-Waldmann, Y. Paz *Modified Photocatalysts*. In: New And Future Developments In Catalysis. Solar Photocatalysis Edited by Steven L. Suib, Elsevier, pp. 103-144, 2013.

[75] V.A. Yasir, P.N. Mohandas, K.K.M. Yusuff. *Preparation of high surface area TiO_2 (anatase) by thermal hydrolysis of titanyl sulphate solution*. International Journal of Inorganic Materials, vol. 3, pp. 593-596, 2001.

[76] N.R.C.F. MacHado, V.S. Santana. *Influence of thermal treatment on the structure and photocatalytic activity of TiO_2 P25*. Catalysis Today, vol. 107-108, pp. 595-601, 2005.

[77] M. Johnsson, P. Pemilla, M. Nygren. *Thermal decomposition of fibrous $TiOSO_4$-$2H_2O$ to TiO_2.* ThermoChimica Acta, vol. 298, pp. 47-54, 1997.

[78] K.Y. Jung, S.B. Park. *Anatase-phase titania: preparation by embedding silica and photocatalytic activity for the decomposition of trichloroethylene.* Journal of Photochemistry and Photobiology A: Chemistry, vol. 127, pp. 117-122, 1999.

[79] M. Inagaki, Y. Nakazawa, M. Ilirano, Y. Kobayashi, M. Toyoda. *Preparation of stable anatase type TiO_2 and its photocatalytic performance.* International Journal of Inorganic Materials, vol. 3, pp. 809-811, 2001.

[80] G. Colon, J.M. Sanchez-Espana, M.C. Hidalgo, J.A. Navio. *Effect of TiO_2 acidic pretreatment on the photocatalytic properties for phenol degradation*. Journal of Photochemistry and Photobiology A: Chemistry, vol. 179, pp. 20-27, 2006.

[81] M. Hirano, C. Nakahara, K. Ota, O. Tanaike, M. Inagaki. *Photoactivity and phase stability of ZrO_2-doped anatase-type TiO_2 directly formed as nanometer-sized particles by hydrothermal conditions*. Journal of Solid State Chemistry, vol. 170, pp. 39-47, 2003.

[82] L.F. Mei, K.M. Liang. *Preparation of Mg^{+2}-doped TiO_2 thin film and its photocatalytic activity.* Rare Metal Materials and Engineering, vol. 36, pp. 496-498, 2007.

[83] D. Robert, V. Keller, N. Keller. *Immobilization of a Semiconductor Photocatalyst on Solid Suppors: Methods, Materials, and Applications*. In: Photocatalysis and Water Purification; Pichat, P., Ed.; Wiley-VCH: Weinheim, Germany, pp. 145–178, 2013.

[84] I.M. Arabatzis, S. Antonaraki, T. Stergiopoulos, A. Hiskia, E. Papaconstantinou, M.C. Bernard, P. Falaras. *Preparation, characterization and photocatalytic activity of nanocrystalline thin film TiO2 catalysts towards 3,5 -dichlorophenol degradation*. Journal of Photochemistry and Photobiology A: Chemistry, vol. 149, pp. 237-245, 2002.

[85] E.C. Bucharsky, G. Schell, R. Oberacker, M.J. Hoffmann. *Anatase–rutile transformation in TiO_2–V_2O_5 catalyst coatings for ceramic foams*. Journal of the European Ceramic Society, vol. 29, pp. 1955 – 1961, 2009.

[86] I. Sopyan, M. Watanabe, S. Murasawa, K. Hashimoto, A. Fujishima *A film-type photocatalyst incorporating highly active TiO_2, powder and fluororesin binder: photocatalytic activity and long-term stability*. Journal of Electroanalytical Chemistry, vol. 415, pp. 183-186, 1996.

[87] S.Kang, Z. Gu, D. Gu, J. Mu. *Immobilization and Photocatalytic Activity of TiO_2 Nanoparticles on Porous Aluminium Foil*. Journal of Dispersion Science and Technology, vol. 26, No 2, pp. 169-171, 2005.

[88] N. Shaham-Waldmann, Y. Paz *Modified Photocatalysts* . In: Photocatalysis and Water Purification; Pichat, P., Ed.; Wiley-VCH: Weinheim, Germany, pp. 103-144, 2013.

[89] F. X. Llabre´s i Xamena, P. Calza, C. Lamberti, C. Prestipino, A. Damin, S. Bordiga, E. Pelizzetti, A. Zecchina. *Enhancement of the ETS-10 Titanosilicate Activity in the Shape-Selective Photocatalytic Degradation of Large Aromatic Molecules by Controlled Defect Production*. Journal American Chemical Society, vol. 125, pp. 2264 – 2271, 2003.

[90] K. Zhang, F. J. Zhang, M. L. Chen, W. C. Oh. *Comparison of catalytic activities for photocatalytic and sonocatalytic degradation of methylene blue in present of anatase TiO_2-CNT catalysts*. Ultrasonics Sonochemistry, vol. 18, No 3, pp, 765 – 772, 2011.

[91] N. Hammer, I. Kvande, X. Xu, V. Gunnarsson, B. Tøtdal, D. Chen, M. Rønning , Au. *TiO_2 catalysts on carbon nanofibres prepared by deposition-precipitation and from colloid solutions*. Catalysis Today, vol. 123, pp. 245–256, 2007.

[92] G. Palmisano, V. Loddo, H. Hamed El Nazer, S. Yurdakal, V. Augugliaro, R. Ciriminna, M. Pagliaro. *Graphite-supported TiO2 for 4-nitrophenol degradation in a photoelectrocatalytic reactor*. Chemical Engineering Journal, vol. 155, pp. 339–346, 2009.

[93] M. Anpo, N. Aikawa, S. Kodama., Y. Kubokawa. *Photocatalytic Hydrogenation of Alkynes and Alkenes with Water over TiO2: Hydrogenation Accompanied by Bond Fission*. Journal of Physical Chemistry, vol.88, pp. 2569-2572, 1984.

[94] M. Anpo, N. Aikawa, Y. Kubokawa. *Photocatalytic Hydrogenation of Alkynes and Alkenes with Water over TiO2: Pt-Loading Effect on the Primary Processes*. Journal of Physical Chemistry, vol.88, pp. 3998-4000, 1984.

[95] M. Anpo., T. Shima., S. Kodama, Y. Kubokawa. *Photocatalytic Hydrogenation of CH_3CCH with H_2O on Small-Particle TiO_2: Size Quantization Effects and Reaction Intermediates*. Journal of Physical Chemistry, vol. 91, pp. 4305-4310, 1987.

[96] M. Anpo, T. Kawamura, S. Kodama, K. Maruya, T. Onishi. *Photocatalysis on titanium-aluminum binary metal oxides: enhancement of the photocatalytic activity of titania species*. Journal of Physical Chemistry, vol. 92, No 2, pp. 438–440, 1988.

[97] Anpo M, Nakaya H, Kodama S, Kubokawa Y, Domen K, Onishi T. *Photocatalysis over Binary Metal Oxides: Enhancement of the Photocatalytic Activity of TiO2 in Titanium-Silicon Oxides*. . Journal of Physical Chemistry, vol. 90, pp. 1633-1636, 1986.

[98] Yamashita, H.; Honda, M.; Harada, M.; Ichihashi, Y.; Anpo, M.; Hirao, T.; Itoh, N.; Iwamoto, N. *Preparation of Titanium Oxide Photocatalysts Anchored on Porous Silica Glass by a*

Metal Ion-Implantation Method. . Journal of Physical Chemistry B, vol. 102, pp. 10707–10711, 1998.

[99] M. Anpo, N. Aikawa, Y. Kubokawa. *Photoluminescence and photocatalytic activity of highly dispersed titanium oxide anchored onto porous Vycor glass.* Journal of Physical Chemistry, vol. 89, pp. 5017–5021, 1985.

[100] H. Yamashita, M. Honda, M. Harada, Y. Ichihashi, M. Anpo, T. Hirao, N. Itoh, N. Iwamoto. *Preparation of Titanium Oxide Photocatalysts Anchored on Porous Silica Glass by a Metal Ion-Implantation Method.* Journal of Physical Chemistry B, vol. 102, pp. 10707-10711, 1998.

[101] M. Anpo, S. Dohshi, M. Kitano, Y. Hu, M. Takeuchi, M. Matsuoka. *The preparation and characterization of highly efficient titanium oxide–based photofunctional materials.* Annual Review of Materials Research, vol. 35, pp. 1-27, 2005.

[102] M. Kobayashi, R. Kuma, S. Masaki, N. Sugishima. *TiO_2-SiO_2 and V_2O_5/TiO_2-SiO_2 catalyst: Physico-chemical characteristics and catalytic behavior in selective catalytic reduction of NO by NH_3* Applied Catalysis B: Environmental, vol. 60, pp. 173–179, 2005.

[103] X. Wang1, S. Zhong, X. Xiao. *Photo-catalysis of ethane and carbon dioxide to produce hydrocarbon oxygenates over ZnO-TiO_2/SiO_2 catalyst.* Journal of Molecular Catalysis A: Chemical, vol. 229, pp. 87–93, 2005.

[104] Y. Ishikawa, Y. Hayashi, Y. Matsumoto. *Preparation of titanium(IV) oxide film on a hard alumite substrate.* Journal of Materials research, vol. 17, No 9, pp. 2373-2378, 2002.

[105] L. Yan, S. De-zhi, C. Lin, L. Yan-ping. *Preparation and characterization of Fe_2O_3-CeO_2-TiO_2/Al_2O_3 catalyst for degradation dye wastewater.* Journal of Environmental Sciences, vol. 18, No. 6, pp. 1189- 1192, 2006.

[106] F. J. Beltrán, F. J. Rivas, R. Montero-de-Espinosa. *A TiO_2/Al_2O_3 catalyst to improve the ozonation of oxalic acid in water.* Applied Catalysis B: Environmental, vol. 47, pp. 101–109, 2004.

[107] M. Bellardita, M. Addamo, A. Di Paola, G. Marcм, L. Palmisano, L. Cassar, M. Borsa. *Photocatalytic activity of TiO_2/SiO_2 systems.* Journal of Hazardous Materials, vol. 174, pp. 707–713, 2010.

[108] M. Polat, A. M. Soylua, D. A. Erdogana, H. Erguvena, E. I. Vovka,b, E.Ozensoya. *Influence of the sol–gel preparation method on the photocatalytic NO oxidation performance of TiO_2/Al_2O_3 binary oxides.* Catalysis Today, vol. 241, pp. 25–32, 2015.

[109] D. Kibanova, M. Sleiman, J. Cervini-Silva, H. Destaillats. *Adsorption and photocatalytic oxidation of formaldehyde on a clay-TiO_2 composite* . Journal of Hazardous Materials, vol. 211–212, pp. 233– 239, 2012.

[110] E. Stathatos, D. Papoulis, C.A. Aggelopoulos, D. Panagiotaras, A. Nikolopoulou. *TiO_2/palygorskite composite nanocrystalline films prepared by surfactant templating route: Synergistic effect to the photocatalytic degradation of an azo-dye in water.* Journal of Hazardous Materials, vol. 211–212, pp. 68– 76, 2012.

[111] G. Li, X.S. Zhao, Madhumita B. Ray. *Advanced oxidation of orange II using TiO_2 supported on porous adsorbents: The role of pH, H_2O_2 and O_3.* Separation and purification technology, vol. 55, pp. 91–97, 2007.

[112] Komarov V.S. *New in the activation of natural alumosilicates.* In: The investigation of adsorption processes and adsorbents. FAN, Tashkent, pp.. 186-193, 1979. (Комаров В.С. Новое в активации природных алюмосиликатов . In: Исследование адсорбционных процессов и адсорбентов. – Ташкент: ФАН, 1979. – С. 186-193.

[113] *Handbook of Clay Science.* Edited by F. Bergaya, B.K.G. Theng, G. Lagaly. Developments in Clay Science, Elsevier Ltd, Vol. 1, 2006.

[114] F. Bergaya, G. Lagaly *General introduction: clays, clay minerals, and clay science* In: Handbook of Clay Science Edited by F. Bergaya, B.K.G. Theng and G. Lagaly. Developments in Clay Science, Vol. 1. Elsevier Ltd., pp. 1-18, 2006.

[115] M.F. Brigatti, E. Galan B.K.G. Theng *Structures and mineralogy of clay minerals.* In: Handbook of Clay Science Edited by F. Bergaya, B.K.G. Theng and G. Lagaly. Developments in Clay Science, Vol. 1, Elsevier Ltd., pp. 19-86, 2006.

[116] Y.I. Tarasevich, *Structure and surface chemistry of layered silicates*/Kiev;Naukova Dumka, 1988 - pp. 246. (Тарасевич Ю.И. *Строение и химия поверхности слоистых силикатов*- Киев : Наукова думка, 1988. – 246 с)

[117] R.A. Schoonheydt, C.T. Johnston. *Surface And Interface Chemistry Of Clay Minerals.* In: Handbook of Clay Science Edited by F. Bergaya, B.K.G. Theng and G. Lagaly. Developments in Clay Science, Vol. 1, Elsevier Ltd, pp. 87-114, 2006.

[118] P. Komadel, J. Madejova. *Acid Activation Of Clay Minerals* In: Handbook of Clay Science Edited by F. Bergaya, B.K.G. Theng and G. Lagaly. Developments in Clay Science, Vol. 1, Elsevier Ltd., pp. 263-288, 2006.

[119] Vasil'ev N.G. Goncharuk V.V. Active centers of a surface of layered silicates. In: Synthesis and physical and chemical properties of inorganic and carbon sorbents. Naukova dumka, Kiev, pp. 58–7, 1986. (Васильев Н.Г., Гончарук В.В. *Активные центры поверхности слоистых силикатов* In: Синтез и физико-химические свойства неорганических и углеродных сорбентов. – Киев: Наукова думка, 1986. – С. 58-72.)

[120] L. Heller-Kallai. *Thermally modified clay minerals* In: Handbook of Clay Science Edited by F. Bergaya, B.K.G. Theng and G. Lagaly. Developments in Clay Science, Vol. 1, Elsevier Ltd, pp. 289-308, 2006.

[121] J. Li, F. Wu, G. Mailhot, N. Deng. *Photodegradation of chloroform in aqueous solution: Impact of montmorillonite KSF particles.* Journal of Hazardous Materials, vol. 174, pp. 368–374, 2010.

[122] Sapna N. Nandeshwar, Anjali S. Mahakalakar, Rashmi R. Gupta, George Z. Kyzas. *Green activated carbons from different waste materials for the removal of iron from real wastewater samples of Nag River, India.* Journal of Molecular Liquids, vol. 216, pp. 688–692, 2016.

[123] M. A. Yahya, Z. Al-Qodah , C.W. Zanariah Ngah. *Agricultural bio-waste materials as potential sustainable precursors used for activated carbon production: A review.* Renewable and Sustainable Energy Reviews, vol. 46, pp. 218–235, 2015.

[124] J.-M. Honga, B. Lin, J.-S. Jiang, B.-Y. Chen, C.-T. Chang. *Synthesis of pore-expanded mesoporous materials using waste quartz sand and the adsorption effects of methylene blue*. Journal of Industrial and Engineering Chemistry, vol. 20, No 5, pp. 3667–3671, 2014.

[125] A. Patnaika, M. Mvubu, S. Muniyasamy, A. Botha, R. D. Anandjiwala. *Thermal and sound insulation materials from waste wool and recycled polyester fibers and their biodegradation studies.* Energy and Buildings, vol. 92, pp. 161–169, 2015.

[126] M.J.R. Hinojosa, A.P, Galvín, F. Area, M. Perianes, A. Barbudo. *Potential use of biomass bottom ash as alternative construction material: Conflictive chemical parameters according to technical regulations.* Fuel, vol. 128, pp. 248-259, 2014.

[127] M. Singh, R. Siddique. *Effect of coal bottom ash as partial replacement of sand on properties of concrete.* Resources, Conservation and Recycling, vol. 72, pp. 20-32, 2013.

[128] Shaobin Wang, Hongwei Wu. *Environmental-benign utilization of fly ash as low-cost adsorbents*. Journal of Hazardous Materials, vol. 136, No 3, pp. 482–501, 2006.

[129] Bruce A. Dockter, Diana M. Jagiella. *Engineering and enviromental specifications of state agencies for utilization and disposal of coal combustion products*. World of coal ash, Lexington, Kentucky, USA, 2005.

[130] M. Ahmaruzzaman. *A review on the utilization of fly ash.* Progress in Energy and Combustion Science, vol. 36, No 3, pp. 327-363, 2010.

[131] G. Bidara, C. Waterlota, A. Verdin, N. Proixc, D. Courcotb, S. Détrichéa, H. Fourriera, A. Richardc, F. Douay. *Sustainability of an in situ aided phytostabilisation on highly contaminated soils using fly ashes: Effects on the vertical distribution of physicochemical parameters and trace elements.* Journal of Environmental Management, vol.171, pp. 204-216, 2016.

[132] M. Visa, F. Pricop, A. Duta. *Sustainable treatment of wastewaters resulted in the textile dyeing industry.* Clean Technologies and Environmental Policy, vol. 13, pp. 855-861, 2011.

[133] D. Sun, X. Zhang, Y. Wu, X. Liu. *Adsorption of anionic dyes from aqueous solution on fly ash.* Journal of Hazardous Materials, vol.181, pp. 335–342, 2010.

[134] Z. Eren, F.N. Acar. *Adsorption of Reactive Black 5 from an aqueous solution: equilibrium and kinetic studies*. Desalination, vol. 194, No 1-3, pp. 1-10, 2006.

[135] N.M. Musyoka., L.F. Petrik, O. Fatoba, E. Hums. *Synthesis of zeolites from coal fly ash using mine waters*. Minerals Engin, 53 (2013) 9–15

[136] C. Li, Y. Dong, D. Wu, L. Peng, H. Kong. *Surfactant modified zeolite as adsorbent for removal of humic acid from water.* Applied Clay Science, vol. 52, No 4, pp. 353-357, 2011.

[137] D. Wu, B. Zhang, L. Yan, H. Kong, X. Wang. *Effect of some additives on synthesis of zeolite from coal fly ash.* International Journal of Mineral Processing, vol. 80, pp. 266-272, 2006.

[138] V. Vimonses, B. Jin, C.W.K. Chow, C. Saint. *An adsorption - photocatalysis hybrid processusing multi-functional-nanoporous materials for wastewater reclamation.* Water Research, vol. 44, pp. 5385 – 5397, 2010.

[139] D. Wu, P. Huo, Z. Lu, X. Gao, X. Liu, W. Shi, Y. Yan. *Preparation of heteropolyacid/TiO_2/fly-ash-cenosphere photocatalyst for the degradation of ciprofloxacin from aqueous solutions.* Applied Surface Science, vol. 258, pp. 7008–7015, 2012.

[140] B. Wang, C. Li, J. Pang, X. Qing, J. Zhai, Q. Li. *Novel polypyrrole-sensitized hollow TiO_2/fly ash cenospheres: Synthesis, characterization, and photocatalytic ability under visible light.* Applied Surface Science, vol. 258, pp. 9989 – 9996, 2012.

[141] M. Bellardita, M. Addamo, A. Di Paola, G. Marcм, L. Palmisano, L. Cassar, M. Borsa *Photocatalytic activity of TiO_2/SiO_2 systems.* Journal of Hazardous Materials, vol. 174, pp. 707–713, 2010.

[142] M. Visa, L. Andronic, D. Lucaci, A. Duta. *Concurrent dyes adsorption and photodegradation on fly ash based substrates*. Adsorption, vol. 17, pp. 101-108, 2011.

[143] A. Duta, M. Visa. *Simultaneous removal of two industrial dyes by adsorption and photocatalysis on a fly-ash-TiO_2 composite.* Journal of Photochemistry and Photobiology A: Chemistry, vol. 306, pp. 21-30, 2015.

[144] Z. Wang, C. Chen, W.Ma, J. Zhao. *Sensitization of Titania Semiconductor: A Promising Strategy to Utilize Visible Light* . In: Photocatalysis and Water Purification; Pichat, P., Ed.; Wiley-VCH: Weinheim, Germany, pp. 199–240, 2013.

[145] Y. Nosaka, A.Y. Nosaka. *Identification and Roles of the Active Species Generated on Various Photocatalysts.* In: Photocatalysis and Water Purification; Pichat, P., Ed.; Wiley-VCH: Weinheim, Germany, pp. 3-24, 2013.

[146] B. Ohtani. *Principle of Photocatalysis and Design of Active Photocatalysts. In: New And Future Developments*. In: Catalysis. Solar Photocatalysis , *Edited by* St. L. Suib. .Elsevier, pp.121-144, 2013.

[147] L. Gomathi Devi, R. Kavitha. *A review on non metal ion doped titania for the photocatalytic degradation of organic pollutants under UV/solar light: Role of photogenerated charge carrier dynamics in enhancing the activity.* Applied Catalysis B: Environmental, vol. 140– 141, pp. 559– 587, 2013.

[148] A. Zaleska *Doped-TiO_2: A Review Recent Patents on Engineering,* vol. 2, pp. 157-164, 2008.

[149] S.Sato. *Photocatalytic activity of NOx-doped TiO2 in the visible light region.* Chemical Physics Letters, vol. 1123, pp. 126-128, 1986.

[150] R. Asahi, T. Morikawa, T. Ohwaki, K. Aoki, Y. Taga *Visible-light photocatalysis in nitrogen-doped titanium dioxide.* Science, vol. 293, 269-271, 2001.

[151] X. Zhou, F. Peng, H. Wang, H. Yu, J. Yang. *Preparation of nitrogen doped TiO_2 photocatalyst by oxidation of titanium nitride with H_2O_2.* Materials Research Bulletin, vol. 46, pp. 840–844, 2011.

[152] A. Rengifo-Herrera, C. Pulgarin. *Photocatalytic activity of N, S co-doped and N-doped commercial anatase TiO_2 powders towards phenol oxidation and E. coli inactivation under simulated solar light irradiation*. Solar Energy, vol. 84, pp. 37–43, 2010.

[153] Burda C., El-Sayed M.A. *High-density femtosecond transient absorption spectroscopy of semiconductor nanoparticles. A tool to investigate surface quality.* Pure and Applied Chemistry, vol. 72, pp. 165–177, 2000.

[154] J. M. Herrmann, J. Disdier and P. Pichet. *Effect of chromium doping on the electrical and catalytic properties of powder titania under UV and visible illumination*. Chemical Physics Letters, vol. 108, pp. 618–622, 1984.

[155] L. Palmisano, V. Augugliaro, A. Sclafani and M. Schiavello. *Activity of chromium ions doped titania for the dinitrogen photoreduction to ammonia and for the phenol photodegradation.* Journal of Physical Chemistry, vol. 92, pp. 6710–6713, 1988.

[156] M. Long, W.Cai, H. Chen, J. Xu. Preparation, characterization and photocatalytic activity of visible light driven chlorine-doped TiO2 . Frontiers of Chemistry in China, vol. 2, No 3, pp. 278-282, 2007.

[157] C Chen, M Long, H Zeng, W Cai, B Zhou, J Zhang, Y Wu, D Ding, D Wu. *Preparation, characterization and photocatalytic activity of visible light driven chlorine-doped TiO_2.* Journal of Molecular Catalysis A: Chemical, vol. 314, No 1, pp. 35-41, 2009.

[158] Xi-Kui Wanga, Chen Wanga, Wen-Qiang Jiang, Wei-Lin Guo, Jing-Gang Wang. *Sonochemical synthesis and characterization of Cl-doped TiO_2 and its application in the photodegradation of phthalate ester under visible light irradiation.* Chemical Engineering Journal, vol. 189–190, pp. 288–294, 2012.

[159] H. Xu, Z. Zheng, L. Zhang, H. Zhang, F. Deng. *Hierarchical chlorine-doped rutile TiO2 spherical clusters of nanorods: large-scale synthesis and high photocatalytic activity.* Journal of Solid State Chemistry, vol. 181, pp. 2516–3252, 2008.

[160] L. Korosi, S. Papp, I. Bertoti, I Dekany. *Surface and Bulk Composition, Structure, and Photocatalytic Activity of Phosphate-Modified TiO_2.* Applied Catalysis A: General, vol. 265, pp. 115–121, 2004.

[161] L. Korosi, S. Papp, I. Bertoti, I. Dekany. *Surface and bulk composition, structure, and photocatalytic activity of phosphate-modified TiO_2.* Chemistry of Materials, vol. 19, pp. 4811–4819, 2007.

[162] B T. Ohno, M. Akiyoshi , T. Umebayashi , K Asai, T Mitsui, M. Matsumura. *Preparation of S-doped TiO_2 photocatalysts and their photocatalytic activities under visible light.* Applied Catalysis A: General, vol. 265, pp. 115–121, 2004.

[163] J.A. Rengifo-Herrera, C. Pulgarin. *Photocatalytic activity of N, S co-doped and N-doped commercial anatase TiO_2 powders towards phenol oxidation and E. coli inactivation under simulated solar light irradiation.* Solar Energy, vol. 84, pp. 37–43, 2010.

[164] L. Gomathi Devi, R. Kavitha. *A review on non metal ion doped titania for the photocatalytic degradation of organic pollutants under UV/solar light: Role of photogenerated charge carrier dynamics in enhancing the activity.* Applied Catalysis B: Environmental, vol. 140– 141, pp. 559– 587, 2013.

[165] A. Zaleska, M.Nischka, A. Cybula. *Photocatalysts for Solar Energy Conversion* In: New And Future Developments In Catalysis. Solar Photocatalysis. Edited by S. L. Suib. Elsevier, pp. 63-102, 2013.

[166] K. D. Dubois , G. Li Innovative. *Photocatalysts for Solar Fuel Generation by CO_2 Reduction* .In: New And Future Developments In Catalysis. Solar Photocatalysis. Edited by S. L. Suib. Elsevier, pp.218-214, 2013.

[167] J. M. Thornton, D. *Raftery Photocatalysts for Solar Hydrogen Conversion.* In: New And Future Developments In Catalysis. Solar Photocatalysis. Edited by S. L. Suib. Elsevier, pp.191- 217, 2013.

[168] W. Wei, J. S. DuChene, B, C. Sweeny, J. Wang, W. Niu. *Current Development of Photocatalysts for Solar Energy Conversion.* In: New And Future Developments In Catalysis. Solar Photocatalysis. Edited by S. L. Suib. Elsevier, pp. 279-309, 2013.

[169] V. Augugliaro, Gi. Camera-Rodab, V. Loddo, G. Palmisano, L. Palmisano, F. Parrino, M. A. Puma. *Synthesis of vanillin in water by TiO_2 photocatalysis.* Applied Catalysis B: Environmental, vol. 111– 112, pp. 555– 561, 2012.

[170] G. Camera-Roda, F. Santarelli, V. Augugliaro, V. Loddo, G. Palmisano, L. Palmisano, S. Yurdakal. *Photocatalytic process intensification by coupling with pervaporation* . Catalysis Today, vol. 161, pp. 209–213, 2011.

[171] F. Parrino, G. Camera-Roda, V. Loddo, G. Palmisano, V. Augugliaro. *Combination of ozonation and photocatalysis for purification of aqueous effluents containing formic acid as probe pollutant and bromide ion.* Water research, vol. 50, pp. 189-199, 2014.

[172] *Photocatalysis and Water Purification From Fundamentals to Recent Applications*. Edited by P. Pichat. Wiley-VCH Verlag GmbH & Co, 2013

[173] M. Mao, J. Wang, J. He, Z. Yan. *Mesoporous Materials Catalysts for Photodegradation of Water Pollutants: From Chemical Templates to Biotemplates* In: New And Future Developments In Catalysis. Solar Photocatalysis. Edited by S. L. Suib. Elsevier, pp. 442- 469, 2013.

[174] D. W. Bahnemann, L. A. Lawton, P. K.J. Robertson. *The Application of Semiconductor Photocatalysis for the Removal of Cyanotoxins from Water and Design Concepts for Solar Photocatalytic Reactors for Large Scale Water Treatment.* In: New And Future Developments In Catalysis. Solar Photocatalysis. Edited by S. L. Suib. Elsevier, pp. 392-415, 2013.

[175] A.V. Vorontsov., D.V. Kozlov, V.N. Parmon, P.G. Smirniotis. *TiO_2 photocatalytic oxidation: I. Photocatalysts for liquid-phase and gas-phase processes and the photocatalytic degradation of chemical warfare agent simulants in a liquid phase.* Kinetics and Catalysis, vol. 46, No 2, pp. 189-203, 2005.

[176] E. A. Kurmazenko, D. G. Gromov, A. E. Korobkov, A. A. Kochetkov, A. S. Tsygankov, D. V. Kozlov, P.A. Kalinko, O.V. Kiryushin , O. D. Pushkar. *Photocatalytic System for Decontamination and Purification of Atmosphere of Manned Spacecraft Modules*. Manned Spaceflight scientific periodical, vol. 3, No 20, pp. 88-100, 2016. (Курмазенко Э.А., Громов Д.Г., Коробков А.Е., Кочетков А.А., Цыганков А.С., Козлов Д.В., Калинько П.А., Кирюшин О.В., Пушкарь О.*Д. Фотокаталитическая система обеззараживания и очистки атмосферы обитаемых модулей космических аппаратов от микропримесей* . Пилотируемые полеты в космос. 2016. №3 (20). С. 88-100.)

[177] A.V. Vorontsov, E.A. Kozlova, A.S. Besov, D.V. Kozlov, S.A. Kiselev, A.S. Safatovc *Photocatalysis: Light energy conversion for the oxidation, disinfection, and decomposition of water.* Kinetics and Catalysis, vol. 51, No 6, pp. 801-808, 2010.

[178] Kaishu Guan. *Relationship between photocatalytic activity, hydrophilicity and self-cleaning effect of TiO_2/SiO_2 films*. Surface & Coatings Technology, vol. 191, pp. 155 – 160, 2005.

[179] X. Zhang, A. Fujishima, M. Jin, Al.V. Emeline, and T.i Murakami. *Double-Layered TiO_2-SiO_2 Nanostructured Films with Self-Cleaning and Antireflective Properties*. The Journal of Physical Chemistry B, vol. 110 No 50, pp. 25142-25148, 2006.

[180] K.A. Carrado, A. Decarreau, S. Petit, F. Bergaya G. Lagaly. *Synthetic Clay Minerals And Purification Of Natural Clays* . In: Handbook of Clay Science Edited by F. Bergaya, B.K.G. Theng and G. Lagaly. Developments in Clay Science, Vol. 1 , Elsevier Ltd, pp. 115-140, 2006.

[181] Ivanova A.V., Mikhailova N.A., Technological tests clays. Uhta: Guidelines USTU, 2005. (Иванова А.В., Михайлова Н.А. *Технологические испытания глин*. Екатеринбург ГОУ ВПО УГТУ−УПИ 2005)

[182] M.A.K. Ahmed, H. Fjellvag, A. Kjekshus. *Synthesis and crystal structures of titanium oxide sulfates.* Acta Chemica Scandinavica, vol. 50, pp. 275-283, 1996.

[183] A.V. Vorontsov, E.N. Savinov, E.N. Kurkin, O.D. Torbova, V.N. Parmon. *Kinetic features of the steady state photocatalytic CO oxidation by air on TiO_2, React.* Reaction Kinetics and Catalysis Letters, vol. 62, pp. 83-88, 1997.

[184] A. Kudo, K. Domen, K. Maruya, T. Onishi. *Photocatalytic reduction of NO_2 - to form NH_3 over Pt-TiO_2.* Chemistry Letters, pp. 1019-1022, 1987.

[185] S.L. Zhang, J.F. Zhou, Z.J. Zhang, Z.L. Du, A.V. Vorontsov, Z.S. Jin. *Morphological structure and physicochemical properties of nanotube TiO_2.* Chinese Science Bulletin, vol. 45, pp. 1533 – 1536, 2000.

[186] J. Yu, H. Yu, B. Cheng, M. Zhou, X. Zhao. *Enhanced photocatalyfic activity of TiO_2 powder (P25) by hydrothermal treatment.* Journal of Molecular Catalysis A: Chemical, vol. 253, pp. 112-118, 2006.

[187] Yu. M. Artemiev, V.K. Ryuabchuc. *Introduction to Heterogeneous Photocatalysis*. Saint-Petersburg, Saint-Petersburg State university; 1999. 303 c. (Ю. А. Артемьев, В.К. Рябчик. Введение в гетерогенный катализ. – СПб: СПб ГУ, 1999. – 303 с.)

[188] Kozlov D. *Titanium Dioxide in gas-Phase Photocatalytic Oxidation of Aromatic and Heteroatom Organic Substances: Deactivation and Reactivation of Photocatalyst*. Theoretical and Experimental Chemistry, vol. 50, No 3, 133-154, 2014.

[189] S. J. Gregg, K. S. W. Sing. *Adsorption, Surface Area and Porosity*. 2. Auflage, Academic Press, London, 1982.]

[190] V. Keller, P. Bernhardt, F. Garin. *Photocatalytic oxidation of butyl acetate in vapor phase on TiO_2, Pt/ TiO_2 and WO_3/ TiO_2.* Journal of Catalysis, vol. 215, pp. 129-138, 2003.

[191] N.V. Kel'tsev. *Fundamentals of Adsorption Technique.* Moscow: Khimiya, 1984. (Н. В. Кельцев. Основы адсорбционной техники. - М.: Химия, 1984. - 591 с.)

[192] Y.S. Nikitin, R.S. Petrova (ed) *Experimental methods in adsorption and molecular chromatography* Moscow: MSU Press, p.315, 1990. (Экспериментальные методы в адсорбции и хроматографии. Под ред. Ю.С.Никитина, Р.С.Петровой. - М. : Изд-во МГУ, 1990. - 315 с.)

[193] E.L. Pace. *Thermodynamics of adsorption and experimental measurements*. In: The Solid-Gas Interface ed E. A. Flood. Vol.1 . New York, Marcel Dekker, pp. 105-126, 1967.

[194] T.D. Khokhlova, N.K. Shonija, O.B. Popovicheva. *Kinetics of saturated water vapor sorption on soot particles.* Russian Journal of Physical Chemistry A, vol. 86., No. 1, pp. 120-126, 2012.

[195] V.V. Samonin, V.Yu. Nikonova, E.A. Spiridonova. *The influence of the preliminary adsorption of water on the adsorption of organic solvent vapors on fullerene materials.* Russian Journal of Physical Chemistry A, vol. 81, No 8, pp. 1442-1446, 2007.

[196] L.I. Bel'chinskaya, N.A. Khodosova, L.A. Bityutskaya. *Adsorption of formaldehyde at mineral nanoporous sorbents exposed to a pulse magnetic field.* Protection of Metals and Physical Chemistry of Surfaces, vol. 45, No 2, pp. 203-206, 2009.

[197] T.V..Kon'Kova, M.B. Alekhina, A.I..Mikhailichenko, G.I..Kandelaki, A.N. Morozov *Adsorption properties of pillared clays.* Protection of Metals and Physical Chemistry of Surfaces, vol. 50, No 3, pp. 326-330, 2014.

[198] M.M. Dubinin *Fundamentals of the theory of adsorption in micropores of carbon adsorbents: characteristics of their adsorption properties and microporous structures*. Carbon, vol. 27, No. 3, pp. 457 – 467, 1989.

[199] F.Stoeckli, A. Slasli, D.Hugi-Cleary, A. Guillot. *Microporous carbons and their characterization*. The present state of the art Carbon, vol. 28, No 1, pp. 1-6, 1990.

[200] F. Kraehenbuehl, H.F. Stoeckli, F. Brunner, G. Kahr M, Mueller-Vonmoos. *Study of the water-bentonite system by vapor adsorption , immersion calorimetry and X-Ray techniques: I. Micropore volumes and internal surface areas, following Dubinin's theory.* Clay Minerals, vol. 22, pp. 1-9, 1987.

[201] N. S. Polyakov, M. M. Dubinin, L.I. Kataeva, G. I. Petukhova *Porous structure and adsorbption proporties for active carbons.* Pure and Applied Chemistry, vol. 65, pp. 2189-2193, 1990.

[202] M. M. Dubinin, O. Kadlets, L. I. Kataeva, G. Okampo, N. S. Polyakov *Inhomogeneous microporous structures and adsorption properties of carbon adsorbents. Communication 8*. Bulletin of the Academy of Sciences of the USSR, Chemical Science, vol. 11, pp 1453-1458, 1987. (Дубинин М.М., Катаева Л.И., Поляков Н.С., Суровикин В.Ф. *Неоднородные микропористые структуры и адсорбционные свойства углеродных адсорбентов*. Сообщение 8. Изв. АН СССР. Сер. хим. -1987. № 11.-С. 1453-1458)

[203] N. S. Polyakov G. A. Petukhova *Current State of the Theory of Volume Filling of Micropores.* Russian Journal of General Chemistry, vol. 36, No 6, pp.7-14, 1995. (Поляков Н.С., Петухова Г.А. *Современное состояние теории объемного заполнения микропор.* Журнал российского химического общества им. Д.И. Менделеева-1995 Т.39, №6 - С. 7-14)

[204] R. M. Alberici, W. F. Jardim. *Photocatalytic destruction of VOCs in the gas-phase using titanium dioxide.* Applied Catalysis B: Environmental, vol. 14, pp. 55-68, 1997.

[205] T.N. Obee, R.T. Brown. *TiO_2. Photocatalysis for Indoor Air Applications: Effects of Humidity and Trace Contaminant Levels on the Oxidation Rates of Formaldehyde, Toluene, and 1,3-Butadiene, Environ.* SciTechnol, vol. 29, pp. 1223-1231, 1995.

[206] Kozlov D. *Titanium Dioxide in gas-Phase Photocatalytic Oxidation of Aromatic and Heteroatom Organic Substances: Deactivation and Reactivation of Photocatalyst Theoretical and Experimental Chemistry*. Theoretical and Experimental Chemistry, vol. 50, No 3, pp. 133-154, 2014.

[207] R. A. Beilina, Y.G. Grosberg, D.A. Dovgialo. *Microelectronic sensors.* Novopolotsk, Publishing House of the PSU, pp. 280, 2001. (Белинина Р.А., Гросберг Ю.Г., Довгьяло Д.А. Микроэлектронные сенсоры. – Новополоцк: Издательский дом ПГУ, 2001. – 280 с.)

[208] A. D. Emeline, V. Ryabchuk and N. Serpone. *Factors affecting the efficiency of a photocatalyzed process in aqueous metal-oxide dispersions. Prospect of distinguishing between two kinetic models,* Journal of Photochemistry and Photobiology A: Chemistry, vol. 133, pp. 89–97, 2000.

[209] Y. Xu ,C. H. Langford. *Variation of Langmuir adsorption constant determined for TiO_2-photocatalyzed degradation of acetophenone under different light intensity.* Journal of Photochemistry and Photobiology A: Chemistry, vol. 133, pp. 67–71, 2000.

[210] C. N. Satterfield. *Heterogeneous Catalysis in Practice.* New York, McGraw-Hill Book Company, 416 pp., 1980. (русская версия Сеттерфилд Ч. Практический курс гетерогенного катализа: Пер. с анг. – М.: Мир, 1984.- 520 с., ил.)

[211] A. D. Emeline, V. Ryabchuk, N. Serpone. *Factors affecting the efficiency of a photocatalyzed process in aqueous metal-oxide dispersions. Prospect of distinguishing between two kinetic models*. J. Journal of Photochemistry and Photobiology A: Chemistry, vol. 133, pp. 89–97, 2000.

[212] N. Doucet, F. Bocquillon, O. Zahraa, M. Bouchy. *Kinetics of photocatalytic VOCs abatement in a standardized reactor* . Chemosphere, vol. 65, pp. 1188–1196, 2006.

[213] J. M. Coronado, M. E. Zorn1, I.l Tejedor-Tejedor, M. A. Anderson. *Photocatalytic oxidation of ketones in the gas phase over TiO_2 thin films: a kinetic study on the influence of water vapor.* Applied Catalysis B: Environmental, vol. 43, pp. 329–344, 2003.

[214] D.M. Ruthven. *Principles of adsorption and adsorption processes* A Wiley Interscience Publication John Wiley & Sons. New York, 433 pp, 1984.

[215] B. Ohtani. *Design and Development of Active Titania and Related Photocatalysts* . In: Photocatalysis and Water Purification; Pichat, P., Ed.; Wiley-VCH: Weinheim, Germany, pp.75-102, 2013.

[216] B.B. Damaskin, O.A. Petri, V.V. Batrakov. *Adsorption of Organic Compounds.* Moscow, Science, pp.333, 1968. (Б.Б. Дамаскин, О.А. Петрий, В.В. Батраков *Адсорбция органических соединений.* – Москва:Наука, 1968. 333 с)

[217] W.T. Tsai , C.W. Lai, K.J. Hsien. *The effects of pH and salinity on kinetics of paraquat sorption onto activated clay*. Colloids and Surfaces A: Physicochem. Eng. Aspects, vol. 224, pp. 99-105, 2003.

[218] C. Du, H. Yang, *Investigation of the physicochemical aspects from natural kaolin to Al-MCM 41 mesoporous materials.* Journal of Colloid and Interface Science, vol. 369, No 1, pp. 216–222, 2012.

[219] Swapna Mukherjee *The Science of Clays: Applications in Industry, Engineering and Environment.* Capital Publishing Company, 335 p, 2013. (e-book)

[220] R. Abe. *Z-Scheme Type Water Splitting into H_2 and O_2 Under Visible Light Through Two-Step Photoexcitation Between Two Different Photocatalysts* . In: New And Future Developments In Catalysis. Solar Photocatalysis Edited by Steven L. Suib. Elsevier, pp. 341-370, 2013.

[221] Yu. I. Tarasevich., F.D. Ovcharenko *Adsorption on clay minerals.* Kiev: Naukova Dumka, pp. 351, 1975.(Тарасевич Ю.И., Овчаренко Ф.Д. *Адсорбция на глинистых минералах*. Киев: Наук. думка, 1975. 351 с)

[222] P.C. Mishra, R.K. Patel. *Removal of lead and zinc ions from water by low cost adsorbents* Journal of Hazardous Materials, vol. 168, pp. 319–325, 2009.

[223] K. G. Bhattacharyya, S. Sen Gupta. *Kaolinite and montmorillonite as adsorbents for Fe(III), Co(II) and Ni(II) in aqueous medium*. Applied Clay Science, vol. 41, pp. 1-9, 2008.

[224] A. K. Zapol'skiy, A.A. Baran, *Coagulantsand Flocculants in Water Treatment Processes: Properties. Getting, Application.* L.: Chemistry, 208 p, 1987. (Запольский А.К., Баран А.А. *Коагулянты и флокулянты в процессах очистки воды: Свойства. Получение. Применени*е. – Ленинград: Химия, 1987. – 208 с.)

[225] Romankov P.G., Rashkovskaya N.B., Frolov V.F. *The processes of mass changing in chemical technology(the systems with a solid phase*). Chemistry, Leningrad, 336 p., 1989. (Романков П.Г., Рашковская Н.Б. Фролов В.Ф. Массобменные процессы химической технологии (системы с твердой фазой) . –Ленинград : Химия, 1989 . – 336 с.)

[226] *Characteristics of the main groups of clay materials.* Available:(http://polyera.ru/glinistye-mineraly/2150-harakteristiki-osnovnyh-grupp-glinistyh-mineralov-chast-1.html

[227] D. Kibanova, M. Trejo, H. Destaillats, J. Cervini-Silva. *Synthesis of hectorite- TiO_2 and kaolinite–TiO_2 nanocomposites with photocatalytic activity for the degradation of model air pollutants.* Applied Clay Science, vol. 42, pp. 563–568, 2009.

227 A. Mills, S. L. Hunte. *An overview of semiconductor photocatalysis.* Journal of Photochemistry and Photobiology A: Chemistry, vol. 108, pp. 1-35, 1997.

[228] A. L. Linsebigler, G. Lu., J. T. Yates. *Photocatalysis on TiO_2 Surfaces: Principles, Mechanisms, and Selected Results.* Chemical Reviews. vol. 95, No 3, pp 735–758, 1995.

[229] Tanaka K., Mario F.V. Capule, Hisanaga T. *Effect of crystallinity of TiO2 on its photocatalytic action.* Chemical Physics Letters, vol. 187, No 1, pp. 73-76, 1991.

[230] D. Altenpohl. *Aluminium und Aluminiumlegierungen*. - Spinger-Verlag Berlin Heidelberg GmbH, 899 p., 1965.

[231] B.C. Gates, J.R. Katzer , G.C.A. Schultz. *Chemistry of catalytic processes.* Chemical Engineering Series McGraw-Hill Book Company, New York , 150 p., 1979.

[232] B.C. Lippens, J.J. Steggerda. *Active alumina.* In: Physical and Chemical Aspects of Adsorbents and Catalysts. Edited by B. G Linsen,. Academic Press, New York, pp. 171–211, 1970.

[233] S. Goldberg, J. A. Davis, J. D. Hem. *The Surface Chemistry of Aluminum Oxides and Hydroxides*. In: The Environmental Chemistry of Aluminum. Edited by G. Sposito, Lewis Publishers is an imprint of CRC Press, pp. 271-331, 1996.

[234] *Reporting physisorption data for gas/solid systems with Special* tion by K. S. W. SING. Pure & Appl.Chem.., Vol.54, No.11, pp.22OI—22l8, 1982. https://www.iupac.org/publications/pac-2007/1982/pdf/5411x2201.pdf

[235] A. V. Kiselev, *Intermolecular Interactions in Adsorption and Chromatography*. Moscow: Vysshaya Shkola, 360 p., 1986. (Киселев А.В. *Межмолекулярные взаимодействия в адсорбции и хроматографии*. М.: Высшая школа, 1986. - 360 с.)

[236] A.V. Bondarenko, Yu.Ya. Filonenko, L.I. Belchinskaya, M.L. Gubkina, N.S. Polyakov *Modifying the composition and adsorption properties of a montmorillonite surface layer by acidic activation* . Russian Journal of Physical Chemistry A. , vol. 79, No. 7, pp. 1126-1130, 2005.

[237] U. Huber, Fr. Stoeckli, J.-Ph. Houriet *A generalization of the Dubinin-Radushkevich equation for the filling of heterogeneous micropore systems in strongly activated carbons* . Journal of Colloid and Interface Science, vol. 67, No 2, pp.195-203, 1978.

[238] V.P. Bubnov, D.A. Dovnar *Study of ecological and economic indicators of systems for cleaning gas emissions from sulfur dioxide.* News of higher educational institutions and energy associations of the CIS .Energetics., vol. 1, pp. 65-72, 2013. (Бубнов В.П., Довнар Д.А *Исследование эколого-экономических показателей систем очистки газовых выбросов от диоксида серы.* Известия высших учебных заведений и энергетических объединений СНГ .Энергетика. - 2013. - №1. - С. 65-72.)

[239] J.X. Liu, S.L. Zhan, M.H. Fang, X. Q. Qian, H. Yang. Adsorption of basic dye from aqueous solution onto fly ash. Journal of Environmental Management, vol. 87, pp. 193–200, 2008.

[240] Carter C.B., Norton M.G. Ceramic Materials: Science and Engineering. 2nd Edition, Springer, 775 p., 2013.